CAPITAL REGION HEAT POLLUTION REDUCTION

Atmospheric Modeling for the Development of a Regional Heat Pollution Reduction Plan

Technical Project Report

Prepared for

Shelley Jiang
Sacramento Metropolitan Air Quality Management District
777 12th Street
Sacramento, CA 95814

Julia Kim and Helena Rhim
Local Government Commission
980 9th Street
Sacramento, CA 95814

Prepared by

Haider Taha
Altostratus Inc.
940 Toulouse Way
Martinez, CA 94553
haider@altostratus.com

February 26, 2020

Altostratus Inc.

ACKNOWLEDGEMENTS

This work was funded by the Sacramento Metropolitan Air Quality Management District (SMAQMD) and the Local Government Commission (LGC) with an SB-1 grant from Caltrans. The support we received from Caltrans is acknowledged and appreciated.

Prime investigators and project managers Shelley Jiang (SMAQMD), Julia Kim (LGC), Helena Rhim (LGC), and Joseph Santiago (SMAQMD), are acknowledged for their leadership in this project and for the guidance and directives they provided throughout the study.

The project Technical Advisory Committee (TAC) members are acknowledged for their support, providing direction and feedback to the project, and defining priorities of mitigation measures and actions. They are, in alphabetical order by last name:

Meg Arnold – Valley Vision; Kathleen Ave – SMUD; Alberto Ayala – SMAQMD; Jerry Barton – EDC; Adam Baughman – EDC; Larry Brohman – DOT; Rick Carter – Sacramento County; Matthew Darrow – Sacramento County; William Dean – Cal/EPA; Torin Dunnavant – SacTree; Taro Echiburu – Yolo County; Jenna Hahn – City of Sacramento; Alison Hodgkin – EDC; Kathryn Jeanfreau – EDC; Matt Jones – YSAQMD; Donna Keeler – EDC; Kerry Loux – City of Davis; John Lane – Teichert; Karen Olson – Sacramento County; Lynnea Ormiston – SACOG; Robert Peters – EDC; Sarah Poe – SacRT; Raef Porter – SACOG; Uzma Rehman – DOT; Judy Robinson – Sacramento County; Dan Shoeman – Sacramento County; Sondra Spaethe – FRAQMD; Elena Torres – SMAQMD; Jason Vargo – CDPH; Jennifer Venema – City of Sacramento; Kimberly Villa – Yolo County; Erik White – Placer County; Carrie Whitlock – City of Elk Grove; and Kevin Yount – DOT.

TABLE OF CONTENTS

LIST OF TABLES

ACRONYMS AND ABBREVIATIONS

AGL	Above ground level
Cal/EPA	California Environmental Protection Agency
CCSM4	Community Climate System Model (fourth generation)
CES 3.0	CalEnviroScreen version 3.0
DAC	Disadvantaged communities
DH	Degree-hours
DH hr^{-1}	Degree-hour per hour
DOT	Department of Transportation
EDC	El Dorado County
EDCAQMD	El Dorado County Air Quality Management District
FDDA	Four-dimensional data assimilation
FRAQMD	Feather River Air Quality Management District
JJAS	June, July, August, and September
LGC	Local Government Commission
MJJAS	May, June, July, August, and September
modUCM	An Altostratus Inc.-modified version of an urban canopy model
MTP	Metropolitan transportation plan
NNRP	NCEP-NCAR Reanalysis Project
NO_2	Nitrogen dioxide
O_3	Ozone
PAN	Peroxyacetyl nitrate
PCAPCD	Placer County Air Pollution Control District
RCP	Representative concentration pathway
SACOG	Sacramento Area Council of Governments
SacRT	Sacramento regional transit district
SMAQMD	Sacramento Metropolitan Air Quality Management District
SMUD	Sacramento Municipal Utility District
SoCAB	South Coast Air Basin
TAC	Technical Advisory Committee
UCM	Urban canopy model
UHI	Urban heat island (also see the Glossary)
UHII	Urban heat island index (also see the Glossary)
MPE	Model performance evaluation
WRF	Weather Research and Forecasting model
WSP	WSP Global Inc.
YSAQMD	Yolo-Solano Air Quality Management District
ZEV	Zero emissions vehicles

GLOSSARY

Albedo: Reflectivity integrated over a range of wavelengths and over the hemisphere

DH: Degree-hours

DH hr^{-1}: Degree-hour per hour (temperature equivalent of UHII)

DH/15 days: Total number of degree-hours summed up over a period of 15 days

Heat wave:
A period of time during which the National Weather Service Heat Index (NWS HI) is within or exceeds the values of 105 – 110 ºF on at least two consecutive days.

Probing points:
Points of interest added to the analysis in locations where there are no weather stations – the goal is to increase the spatial data coverage and bridge the gap in areas with sparse monitoring networks

RCP: Representative concentration pathway (defined in detail in the report) is an indicator to the effects of emissions on future climates. Two scenarios (RCP 4.5 and RCP 8.5) are used in this study. Units are W m^{-2} in radiative forcing, e.g., 4.5 or 8.5 W m^{-2}.

UHI: Urban heat island: instantaneous temperature difference between an urban location and a non-urban reference point (e.g., at a single hour). Units are ºC.

UHII Urban heat island index: a cumulative (total) temperature difference between an urban location and a non-urban reference point calculated over a determined time interval, e.g., several hours or several days, etc. Units are ºC · hr.

Time-varying upwind non-urban temperature reference points:
In the approach applied in this study, the upwind non-urban temperatures needed to calculate the UHI or UHII are obtained from reference points that are dynamically identified at each hourly or sub-hourly interval (time-dependent) based on wind approach direction at that hour or interval.

EXECUTIVE SUMMARY

E.0 PREAMBLE

Detailed atmospheric modeling was undertaken in this study with the goal of informing and prioritizing the development of a heat mitigation plan for the Capital region, including the counties of Sacramento, El Dorado, Placer, Yuba, Sutter, and Yolo. The study, funded by SB-1 (Caltrans), was carried out to evaluate the effects of various mitigation measures on urban heat in these six counties.

The modeling was carried out to characterize and rank several proposed heat-mitigation measures in terms of their effectiveness in modifying local microclimates, i.e., in producing urban cooling. The study also addressed the potential negative impacts, albeit smaller, that could arise from implementation of these measures and the factors to consider in order to prevent or minimize any such effects.

An important consideration in this study was to design strategies of urban-heat mitigation that are reasonable and realistic, i.e., measures that are readily found and applied in the region, not hypothetical or extreme levels of modifications. These mitigation levels and characterizations of the interactions with the heat island effect were also designed as a refinement to the California UHI Index developed by Altostratus Inc. for the California Environmental Protection Agency (https://calepa.ca.gov/2015/09/16/urbanheat/).

The mitigation strategies (whether in standalone fashion or in combinations) evaluated in this effort were also based on feedback received from the participating counties, cities, and communities in the region. The main measures were:

- Cool roofs;
- Cool pavements;
- Vegetation canopy cover;
- Vehicles electrification / EV ownership;
- Solar PV; and
- Cool walls.

Six major tasks, each with several subtasks, were completed in this study:

1. Land-use and land-cover analysis (current conditions and future projections);
2. Observational meteorological data analysis (mesonet weather data);
3. Base modeling and model performance evaluation;
4. Modeling of mitigation measures in current climates and land use;
5. Modeling of mitigation measures in future climates and land use; and
6. Reporting and dissemination of results.

Two aspects are discussed in this report. The first is how practices in and modifications to the transportation system, e.g., pavements, roadways, and heat emissions, can affect the microclimate of surrounding areas and communities. The second is how practices in urban areas, e.g., implementation of cool surfaces, vegetation cover, fleet electrification, and other measures, can affect the transportation sector, including impacts on roadways and pavements temperatures.

This Executive Summary provides brief pointers to characterizations and findings from the modeling and analysis tasks. Details on all tasks can be found in the Project Technical Report which follows this summary.

E.1 THE UHI INDEX

To begin this discussion of heat mitigation, a distinction between the terms "urban heat" and "urban heat island" (UHI) or "urban heat island index" (UHII) needs to be made and the concepts clarified (see the Glossary). To re-state the obvious, the goal of this and similar studies is to design and implement measures that reduce urban heat, not urban heat islands per se. In other words, the goal is to cool down the ambient air in any hot urban area, regardless of how much hotter or cooler it may be compared to some other urban areas or some non-urban reference points (the latter being the definition of the urban heat island). Thus, if so, what is the purpose of characterizing urban heat islands (or the UHII) in this study? The simple answer is that the UHI and UHII are just quantitative indicators or yardsticks that tell us how much cooling we can reasonably expect to achieve at a certain urban location. In other words, the UHI (or UHII) simply is an indicator as to how much cooling is needed to bring the temperature at a certain urban location down to that of a nearby non-urban area. This, by definition, is the amount of cooling that could realistically be expected at that location (of course the actual cooling that is achievable could be smaller or larger than the UHI or UHII, as will be shown later in this report).

Having established this general understanding of urban heat and the purpose of computing the UHI or UHII, we can now proceed with the characterization of urban heat in the Capital region.

Based on the definition of time-varying upwind non-urban temperature reference points for each area (see the Glossary) and the hourly calculations of temperatures at each model grid cell per coincident wind direction, the urban heat island index (UHII) was computed for years (2013 – 2016), periods (May through September), and regions of interest in this study. The UHII was calculated for all hours, specific hours, as well as for a range of hours. A graphical example for the all-hours UHII is shown in Figure EX-1a where, additionally, several AB617 communities defined by the Sacramento Metropolitan AQMD are highlighted.

In this example, the UHII is for the period July 16 – 31, 2015 for which the all-hours averaged temperature equivalent (DH hr^{-1}) is as follows (shown with bold numbers on the figure for selected AB617 communities): A: 3.3 °C; B: 3.6 °C; C: 2.1 °C; D: 3.9 °C; E: 2.1 °C; G: 1.5 °C; and H: 2.7 °C. Other UHII temperature equivalents during this period are Davis: 2.1 °C; Woodland: 1.5 °C;

Yuba City: 2.2 °C; Placerville: 1.8 °C; Auburn: 4.5 °C; and Roseville-Lincoln: 4.7 °C, as seen in the figure.

In Figure EX-1a, the UHII in each of the six tiles (rectangles) is calculated independently from the others based on wind direction and different upwind reference points, even though all tiles are shown together as a mosaic on the same map. It is to be emphasized that this is a UHII map, not an absolute temperature field. Thus, in areas such as Auburn and Lincoln, the UHII can be elevated at times because of day/night variations in temperature of the natural surroundings, higher elevations, or heat transport from upwind urban areas.

The same UHII information is provided again in Figure EX-1b, but with urban and city boundaries outlined (with a black line) to provide a visual reference to areas of interest.

Figure EX-1a: Composite of UHII tiles, July 16-31, 2015 for all-hours averages in six tiles in the Capital region (A – H are some of the AB617 communities in this region). The UHII range in this example is 0 to 2176 °C·hr/15 days and each step change in color is equivalent to 155 °C·hr/15 days. The numbers in bold are the all-hours temperature equivalents (ºC) of the UHII at the selected AB617 communities.

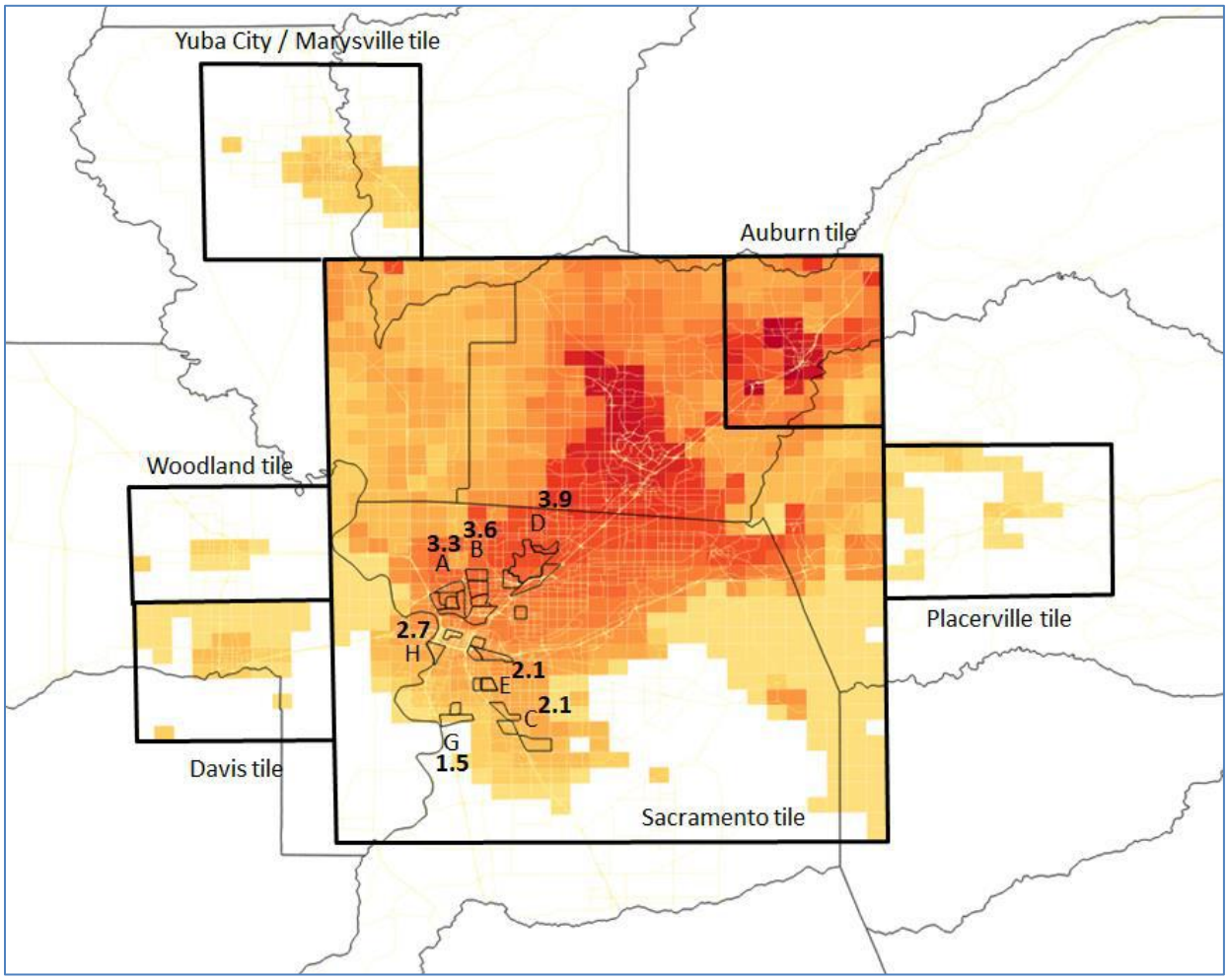

Figure EX-1b: As in Figure EX-1a, above, but with urban / city boundaries outlined.

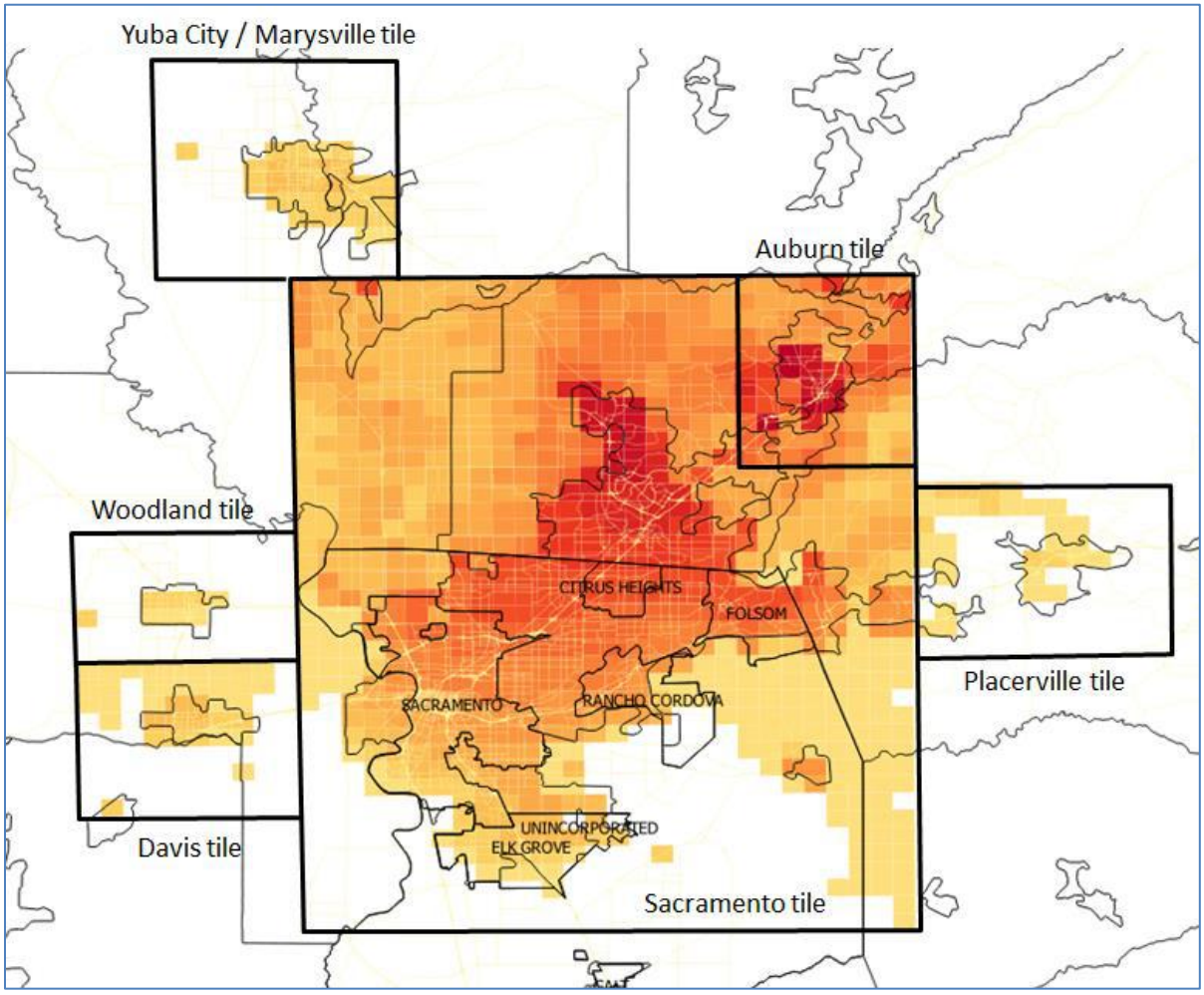

E.2 CHARACTERIZING URBAN HEAT IN RELATION TO CALTRANS PROJECTS

Some attributes of the current-climate urban heat and the UHII may be of interest to Caltrans, local jurisdictions, cities, transit providers, and communities as they can affect various aspects of paving, maintenance of roadways, aging of materials, and the transportation infrastructure in general. The impacts of UHI-mitigation measures on surface temperature (that can provide benefits to pavements' initial construction and long-term maintenance and aging) are discussed in the technical report. Here, a qualitative assessment of Caltrans's facilities and roadway projects locations in relation to the UHII is provided as an initial characterization of areas where urban-cooling measures might need to be introduced first (among other considerations). Those facilities and roadways that fall within the boundaries of the study domains are superimposed on the UHII and shown in Figure EX-2, including locations of airports, Amtrak stations, and state highways within the UHII tiles modeled in this region.

An important point to keep in mind, one that is re-iterated throughout this report, is that urban heat indicators (e.g., UHI and UHII) addressed and calculated in this study are air-temperature-based, not derived from skin surface temperature such as shown in many "urban hot-spot" studies or assessments based on satellite / remote-sensing data or imagery. Hence, the spatial patterns of urban heat analyzed in this study and presented in this report differ significantly from those seen in satellite imagery.

In Figure EX-2, the all-hours UHII for July 16 – 31, 2015, is shown in the background (other years and intervals provide similar information). The UHII range in this example is from 0 to 2176 °C·hr per 15 days and each step change in color is equivalent to 155 °C·hr per 15 days. Considering the information shown in this figure, a rough, initial ranking of Caltrans facilities can be formulated based on the UHII, from highest (most severe) to lowest (less severe):

- Airports rankings (highest to lowest UHII):
  - Auburn Municipal (AUN), Lincoln Regional (LHM), Sacramento McClellan (MCC), Rio Linda (L36), Sacramento International (SMF), Sacramento Executive (SAC), Sutter County (O52), Yuba County (MYV), Rancho Murieta (RIU), UC Davis (EDU), Yolo County (DWA), Placerville (PFV), and Woodland (O41);
- Amtrak stations rankings (highest to lowest UHII):
  - Auburn (ARN), Rocklin (RLN), Roseville (RSV), Marysville (MRV), Sacramento (SAC), State Capitol (SCS), Davis (DAV), Placerville (PCV), and Elk Grove (EKG);
- State highways rankings (highest to lowest UHII):
  - 65, 80, 244, 50, and 51; and
- Rankings based on traffic volume versus the UHII and the main routes in the region.

Figure EX-2: All-hours average UHII (July 16-31, 2015) versus Caltrans roadways and facilities locations. Data source for facilities and roadways: Caltrans (2019).

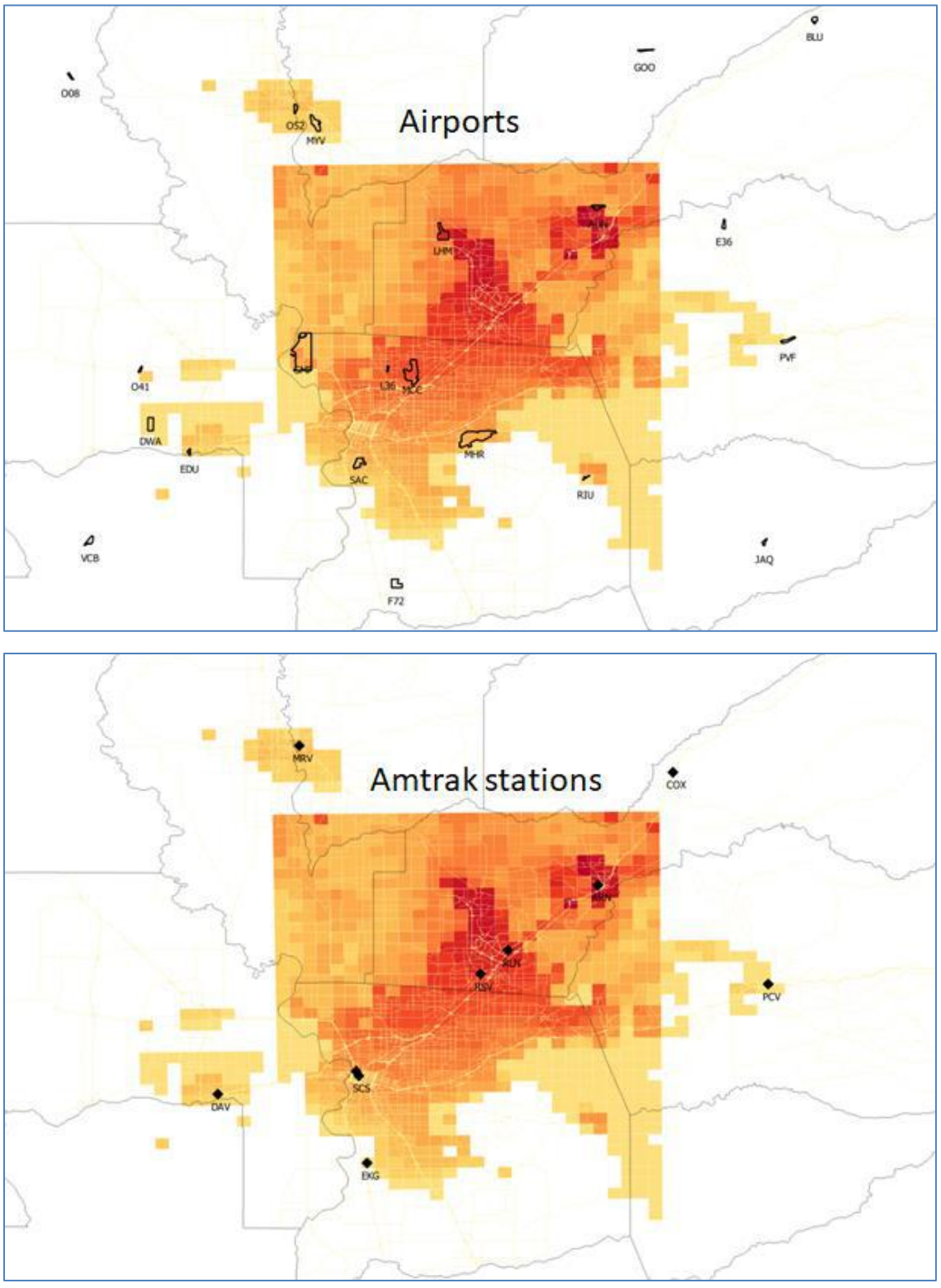

Figure EX-2, continued.

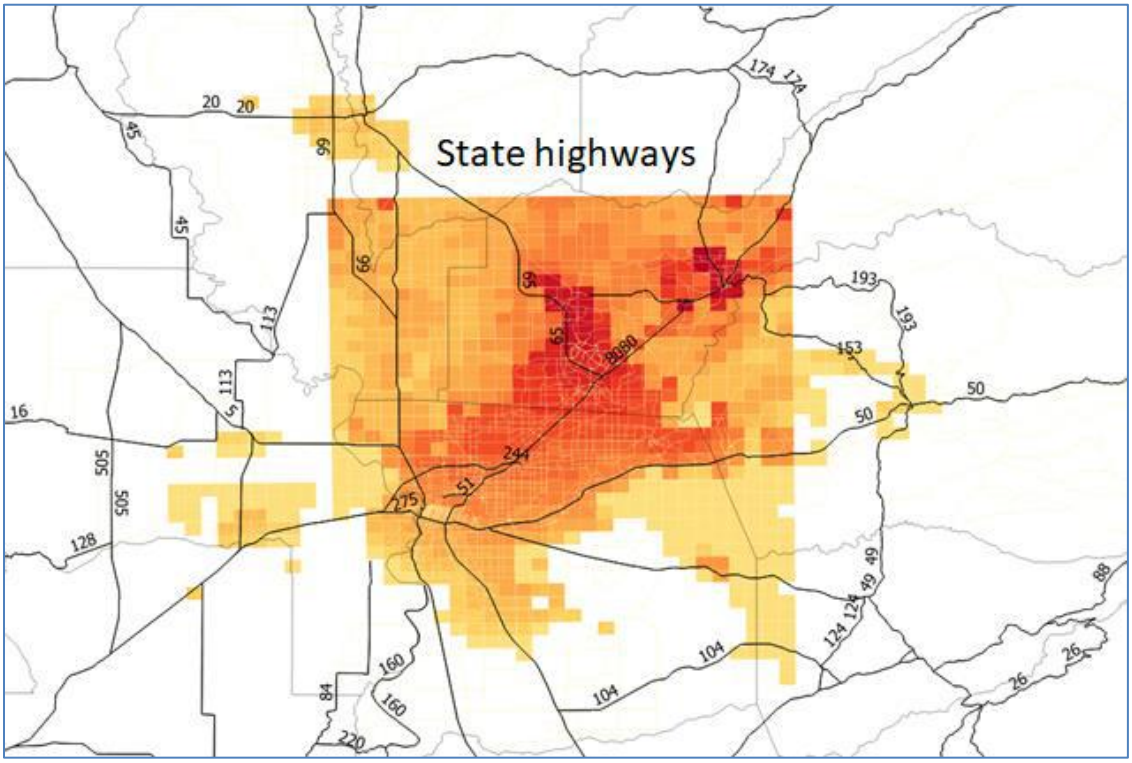

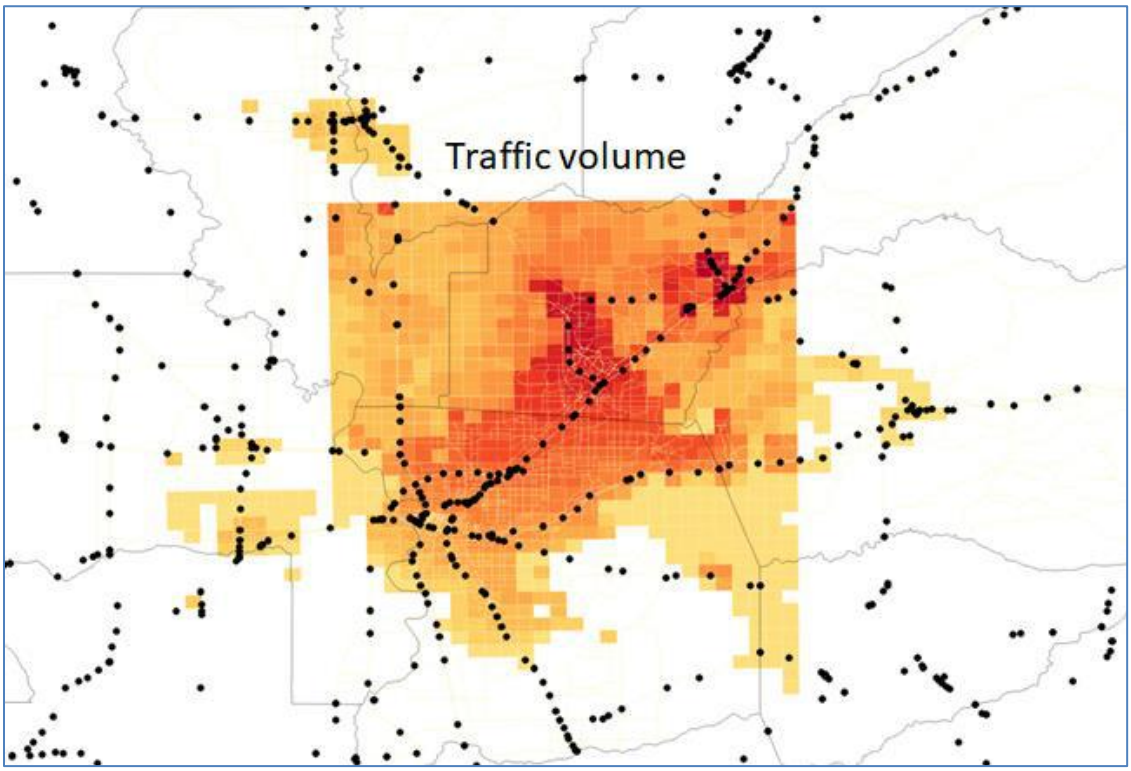

E.3 CALCULATING A TEMPERATURE-WEIGHTED UHII SCORE

The goal of this analysis is to provide additional layers of information, e.g., microclimate data, that could be used in conjunction with other datasets, such as CES 3.0, to help prioritize geographical areas for deployment of UHI mitigation measures, i.e., to offset the UHII. For this purpose, an initial scoring of areas was developed based on the modeled UHII at the regional scale, i.e., the 6-counties Capital region. The first set of scores (Figure EX-3a) is based solely on the UHII regardless of air temperature. In other words, this scoring may be used, for example, by Caltrans and urban planners to develop regional action plans. However, the reductions in absolute temperature, regardless of the UHII, are equally welcomed in all areas.

Thus, the purpose of scoring various geographical areas, such as shown in Figure EX-3a, is to provide additional information to cities and communities when allocating resources. The figure shows five tiers based on UHII intervals of 1 °C including for non-urban areas (heat transport). As with CES 3.0, the higher the UHII score (or tier), the worse the conditions are, i.e., larger urban heat. To reiterate, this scoring is based on climate as the sole criterion, no socio-economic factors are taken into account. If, for example, the UHII score is compared to CES 3.0 scores (last graph in Figure EX-3a), then the UHII score shifts relatively more towards central and south Sacramento, in areas where AB617 communities A, B, and D are located (which occur in UHII Tiers 3 and 4) as well as community C and it surroundings (which occur in UHII Tier 2). Areas near Auburn and Yuba City / Marysville also have high CES 3.0 scores.

With UHII as the sole basis for scoring, the areas including Yuba City / Marysville, Woodland, Davis, and Placerville occur in Tiers 1 and 2 (the lowest and second-to-lowest scores). Most of north and south Sacramento and AB617 communities C, E, and G and others nearby occur in Tier 2 (second score). Central Sacramento, AB617 communities A, B, and D, through Folsom and El Dorado Hills occur in Tiers 3 and 4. Northeast Sacramento, Roseville, Rocklin, Granite Bay, Lincoln, parts of Folsom, and areas west of Auburn occur in Tier 4. Finally, an area from Roseville to Lincoln and a small area over Auburn fall into Tier 5 (the highest score).

However, using only the UHII as an indicator to mitigation priorities and scoring various areas can provide an overall picture that may be counter-intuitive. Thus, the scoring discussed above and shown in Figure EX-3a can be done differently, per data users' specific application or considerations. For example, the above can be repeated but this time using both UHII and absolute air temperature as basis (Figure EX-3b). The goal is to provide relatively more intuitive rankings or scoring, ones that also take into account how hot an area is, not just how large its UHII. This is discussed in detail in the report but it is briefly mentioned here that areas with both large UHII and high temperatures get a higher score than areas with small UHII and lower temperatures. Of course, a range of various combinations exists in-between these two ends.

Figure EX-3b shows an example of urban-area scoring based on both all-hour UHII and all-hour temperature averages for the years and intervals modeled in this study. As can be seen, the pattern differs from that of UHII-only basis (in Figure EX-3a). The lowest score (Tier 1) includes AB617

communities D, G, H and surroundings, peripheral areas in Woodland and Davis, small areas in Marysville, Placerville, and parts of El Dorado Hills.

The second score (Tier 2) includes south and southeast Sacramento, some western parts of downtown Sacramento and surroundings, areas to the south of the American River, peripheral areas in Yuba City / Marysville, northwest Woodland, and central Davis. Some areas in Granite Bay are also included in this tier.

The next-to-top score (Tier 3) includes AB617 communities A, B, D, north Sacramento and parts of downtown, and an area extending east to include south Folsom and El Dorado Hills. Also included in this tier are parts of Lincoln and Auburn.

The top score (Tier 4) includes parts of AB617 community "D", parts of northeast Sacramento, Folsom, El Dorado Hills, Roseville, Rocklin, Lincoln, central parts of Yuba City / Marysville, and parts of Auburn.

Appendix D-2 provides a larger version of these maps.

Figure EX-3a: UHII score for implementing UHI-reduction measures at the regional scale: Tiers 1 through 5 (lowest to highest scores) using UHII as the sole criterion. The CES 3.0 score (last graph) is such that areas with higher score are more vulnerable to various environmental factors.

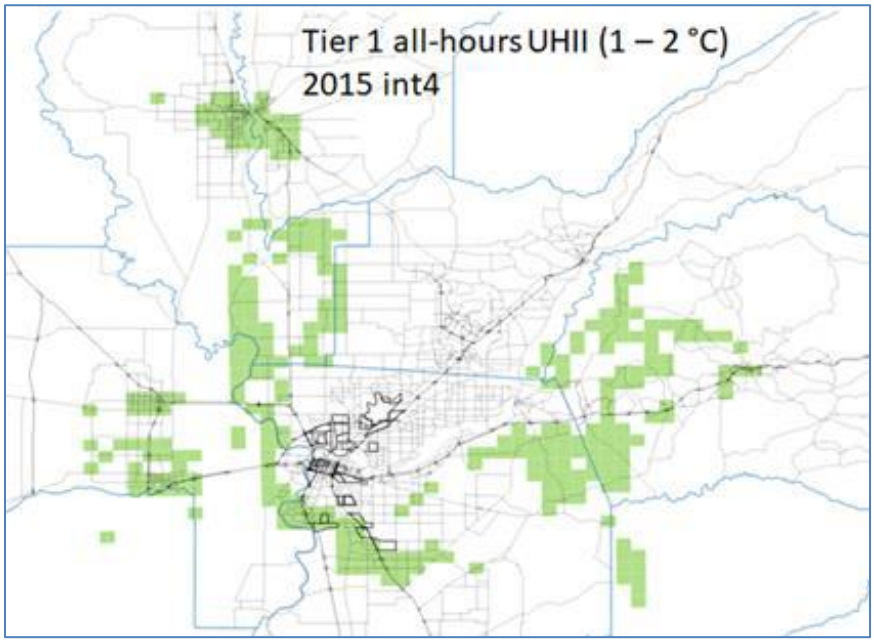

Figure EX-3a, continued.

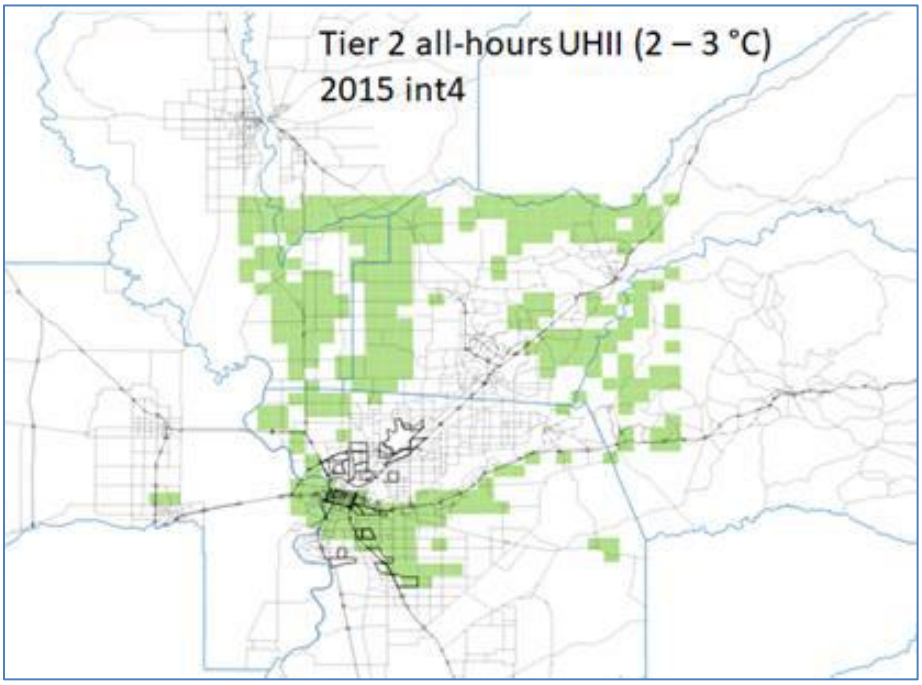

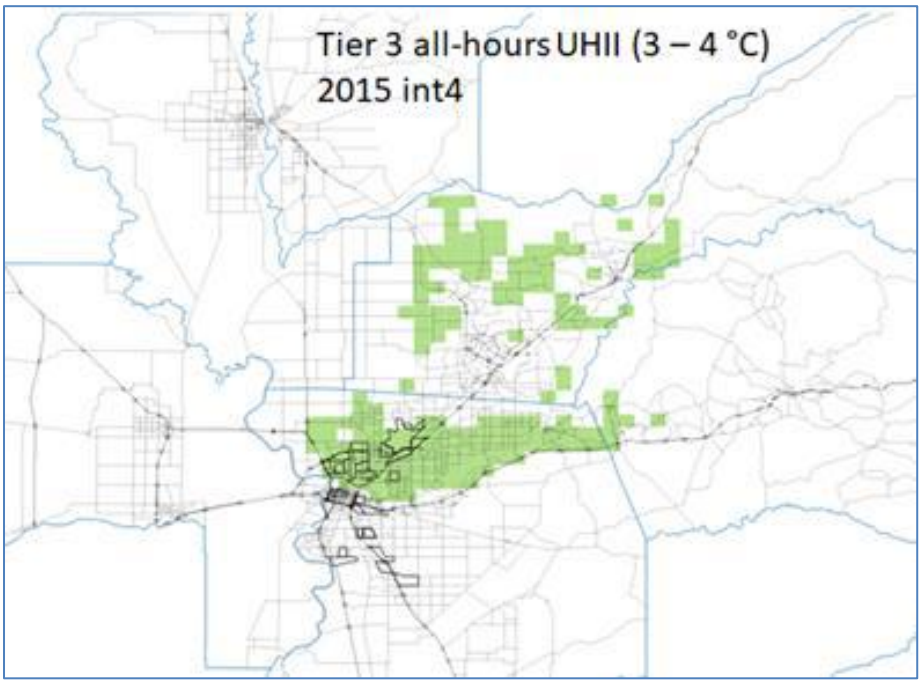

Figure EX-3a, continued.

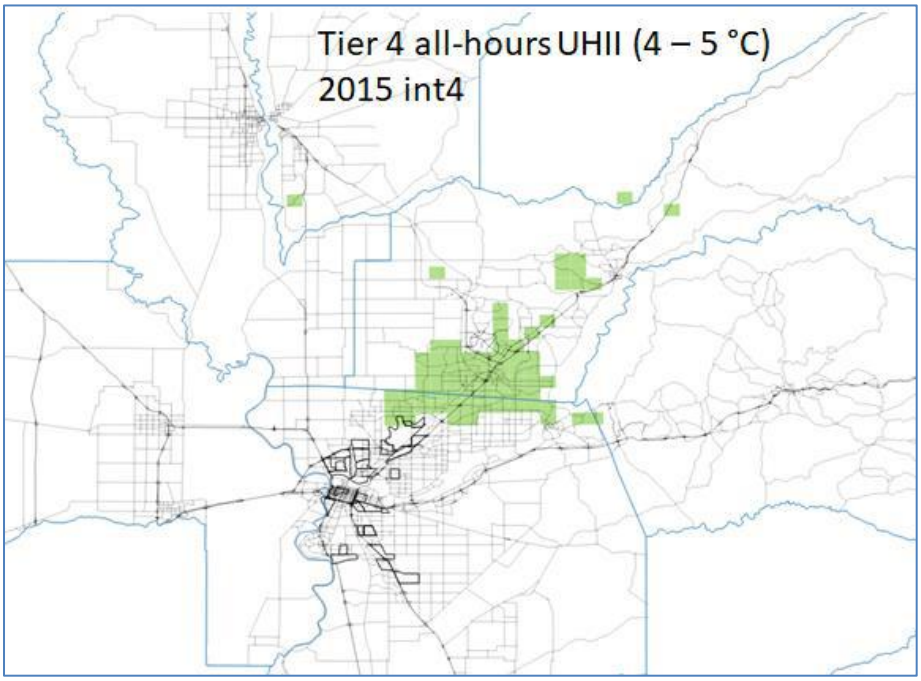

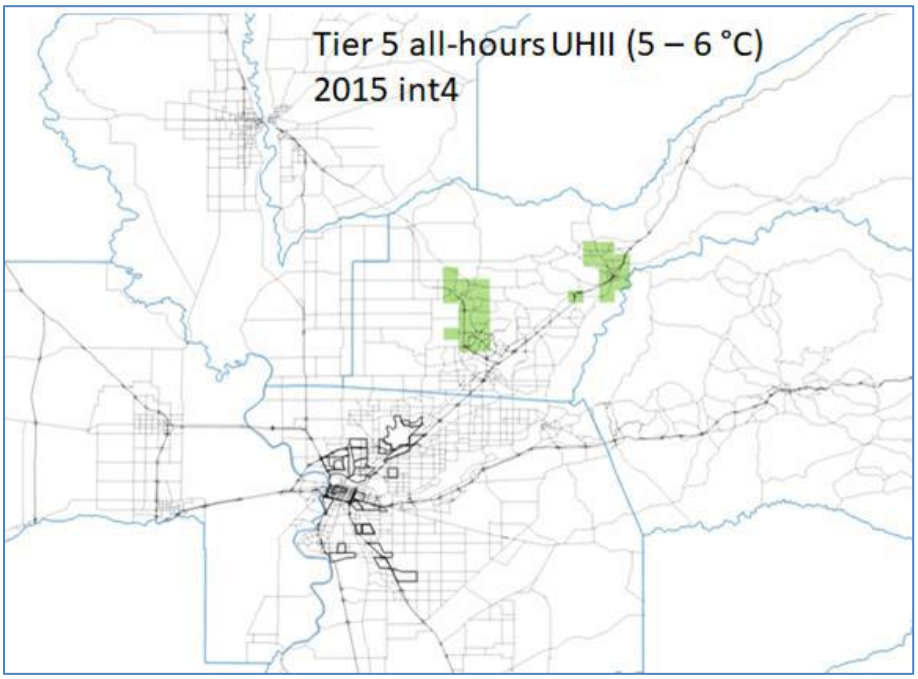

Figure EX-3a, continued.

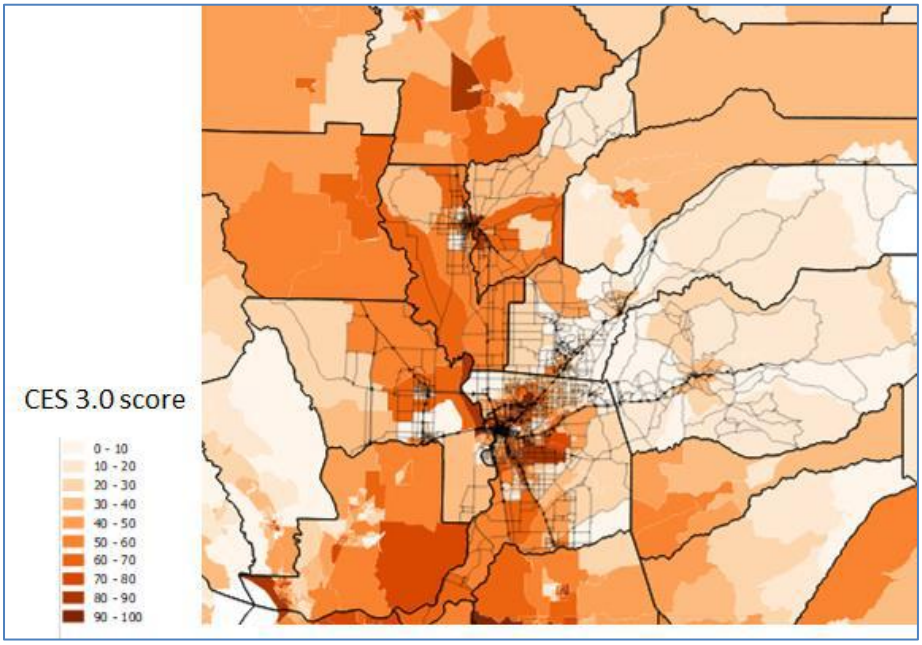

Figure EX-3b: Temperature-weighted UHII score (tiers 1 through 4 are lowest to highest scores). The weighted UHII score, wuSCORE, is discussed in the report.

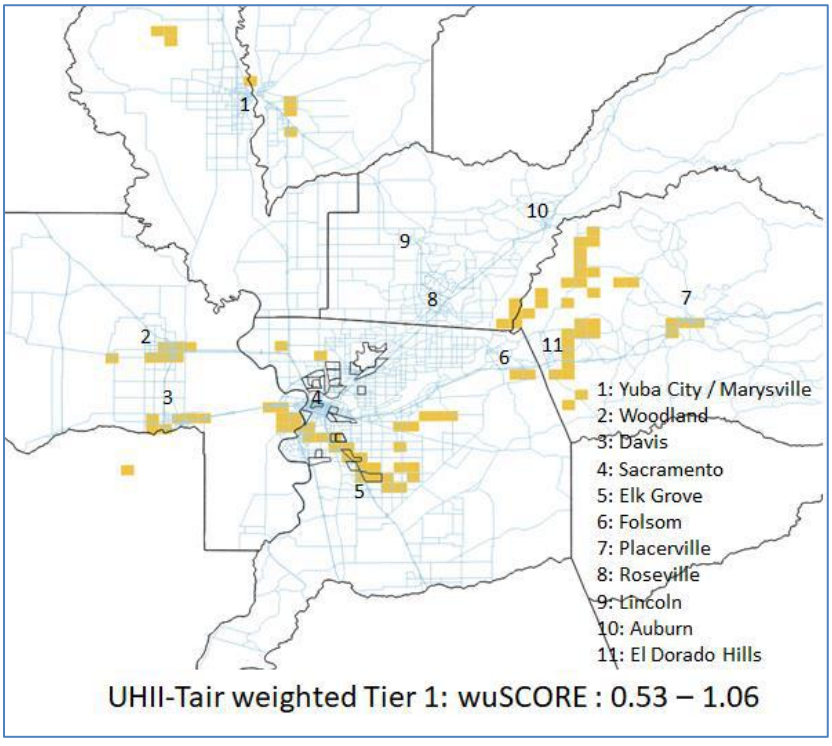

Figure EX-3b, continued.

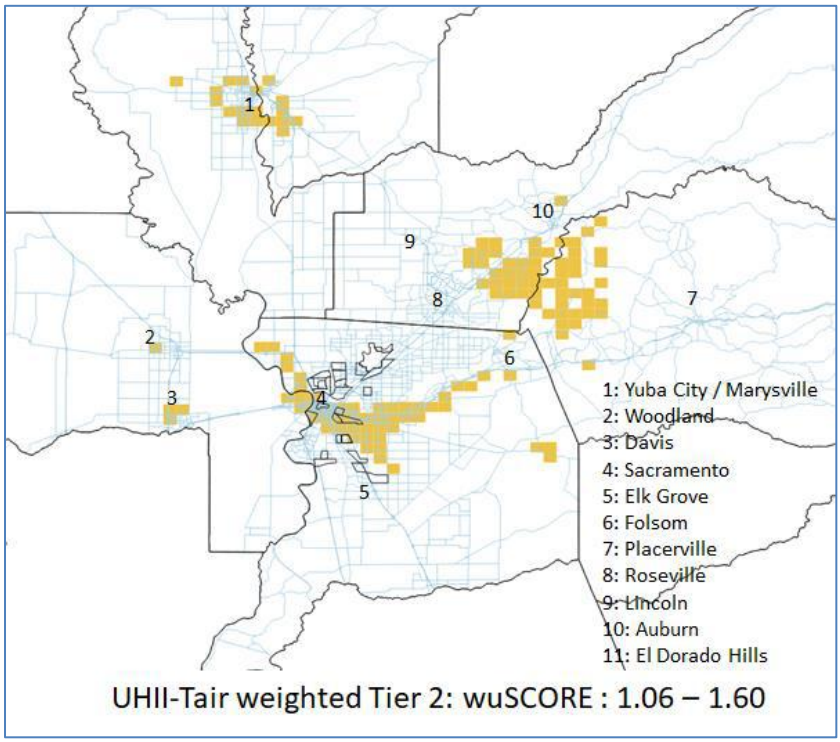

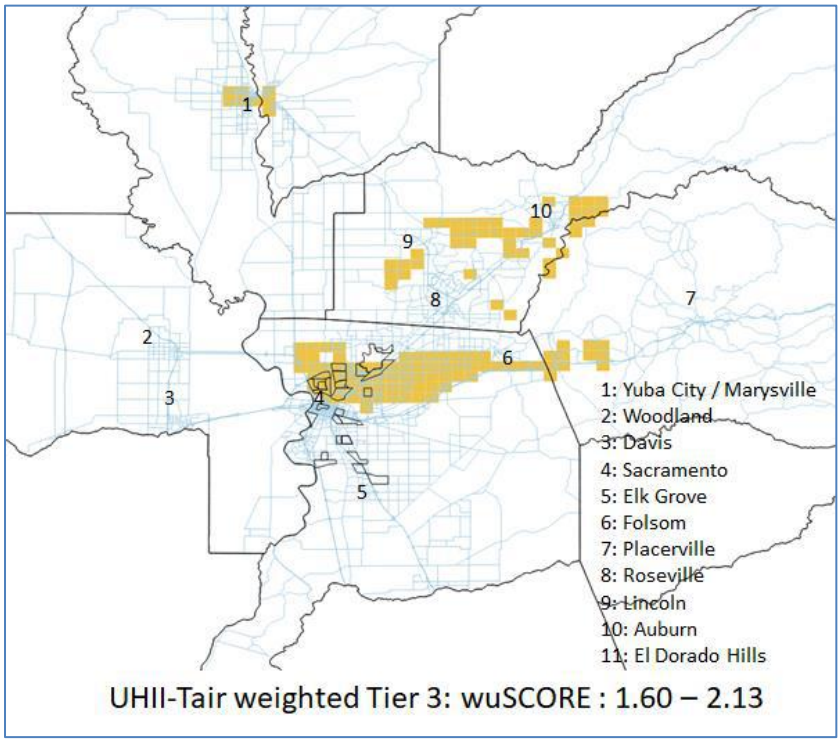

Figure EX-3b, continued.

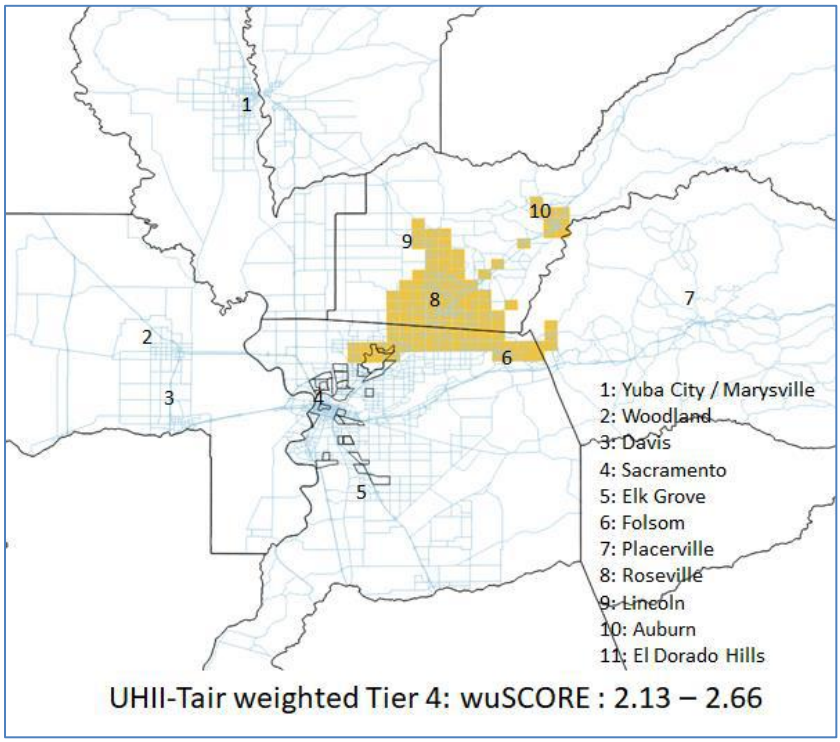

E.4 DEFINING URBAN-HEAT MITIGATION MEASURES AT THE REGIONAL SCALE

At the coarse, regional scale, i.e., the 6-counties Capital region, measures related to cool surfaces and vegetation-canopy cover were defined as follows. These were determined based on results from prior studies indicating the feasibility and reasonability of such measures.

case10: Small increase in albedo -- an increase of 0.15 on impervious surfaces. At this scale (2-km resolution), there is no distinction between roof and pavement albedo changes. Difference between this case and the base case is labeled “del10”.

case20: Larger increase in albedo -- an increase of 0.25 on impervious surfaces. Difference between this case and the base case is labeled “del20”.

case01: A first-level increase in canopy cover (about 2.5 – 3 million trees throughout the 6-counties Capital region, which is about a 12% increase in canopy cover, i.e., an additional 12% of a cell’s area is covered with canopy. Difference between this case and the base case is labeled “del01”.

case02: This is a second-level (extreme) increase in canopy cover (~20% cover or adding 5 million trees throughout the entire 6-counties Capital region), i.e., an additional 20% of a cell’s area is covered with canopy. This is not a realistic or practical

scenario at this time, and thus not used in the combined scenario (case31, below) or in some of the analysis in this report. This scenario is included only as a test for potential upper-bound effects, per suggestions from local tree organizations. Difference between this case and the base case is labeled "del02".

case31: A realistic-high scenario of combined albedo and canopy-cover increases. The increase in impervious albedo is slightly larger (0.35 increase) than in case20 and the increase in canopy cover corresponds to that of case01. Difference between this case and the base case is labeled "del31".

E.5 QUANTIFYING THE EFFECTS OF HEAT-MITIGATION MEASURES AT THE REGIONAL SCALE

E.5.1 Instantaneous and averaged effects of mitigation measures in current climate and land use

A random sample from snapshots of instantaneous effects of mitigation measures is provided in Figure EX-4. The purpose of presenting instantaneous effects is to help formulate a general impression as to spatial characteristics of changes in the temperature field that can be expected to result from implementing urban-cooling measures in the 6-counties Capital region. Thus, this is a general sketch of the geographical extent, locations, and levels of changes in temperature that could be anticipated in the region at coarse scale (2-km resolution).

In Figure EX-4, the instantaneous temperature impacts of five mitigation measures (defined in Section E.4, above) are presented for the random hour at 1300 PDT, July 28, 2015. These temperature perturbations result from case01, case02, case10, case20, and case31, respectively (A – E).

For this sample hour, the temperature reductions reach up to 0.7, 1.4, 1.5, 2.4, and 3.9 °C, respectively, for the measures and scenarios listed above and are larger for the cases involving cool surfaces than those with only vegetation-cover increase (during the daytime). The spatial pattern of cooling follows the urban boundaries and the magnitude of cooling increases with built-up density. We note here that the mitigation measures can also inadvertently cause some warming outside of the modified areas, generally downwind of the urban land use. However, the warming is small compared to the cooling effect both in magnitude (maximum of 0.3 °C) and in the geographical extent affected by the temperature changes, as seen in Figure EX-4.

Furthermore, different measures produce different spatial patterns of cooling. For example, vegetation canopy measures (case01 and case02) produce an effect that is somewhat spatially

uniform throughout the modified urban areas (figures A and B), whereas the albedo measures (case10 and case20, figures C and D) produce more distinguishable features or spatially differentiated patterns in the temperature field. For example, areas along the American River and surroundings (the lighter-colored curved path seen in figures C and D, in the middle of the Sacramento region) do not get as much cooling in the albedo scenarios because of the relatively smaller built-up fraction in those areas (i.e., less roofs and paved surfaces available for albedo modifications).

Lastly, the area affected by cooling increases from the lower scenarios to the higher ones, e.g., compare case31 (figure E) to any other of the graphs. This is caused not only by the larger local temperature reductions but also by the increased transport of cooler air downwind from the modified urban areas (this is discussed in detail in the technical report following this summary).

To provide a different perspective, Figure EX-5 shows the all-hours average impacts from mitigation measures for a period of interest (June – September, 2013 -2016). The areas of Davis, Sacramento, Woodland, and Yuba City see larger cooling effects and also the larger inter-quartile ranges of temperature change. Excluding case02 (extreme increases in canopy cover) it can be seen that albedo (case20) and canopy (case01) measures have generally comparable effects and that the combination scenario (case31) is the most effective in cooling the urban areas. The all-hours metric is skewed towards the vegetation-canopy effects (rather than albedo) because of the nighttime cooling effects of vegetation (a time at which the albedo modifications have small or no effects). Thus, the order (i.e., efficacy) of cooling measures is different during daytime hours or at times of peak temperature than at night. In the Project Technical Report, following this Executive Summary, information is provided in detail for other time periods, scenarios, combinations, and locations.

Figure EX-4 (A – E)**:** Instantaneous differences in air temperature (°C) at a random hour and date for five different mitigation scenarios.

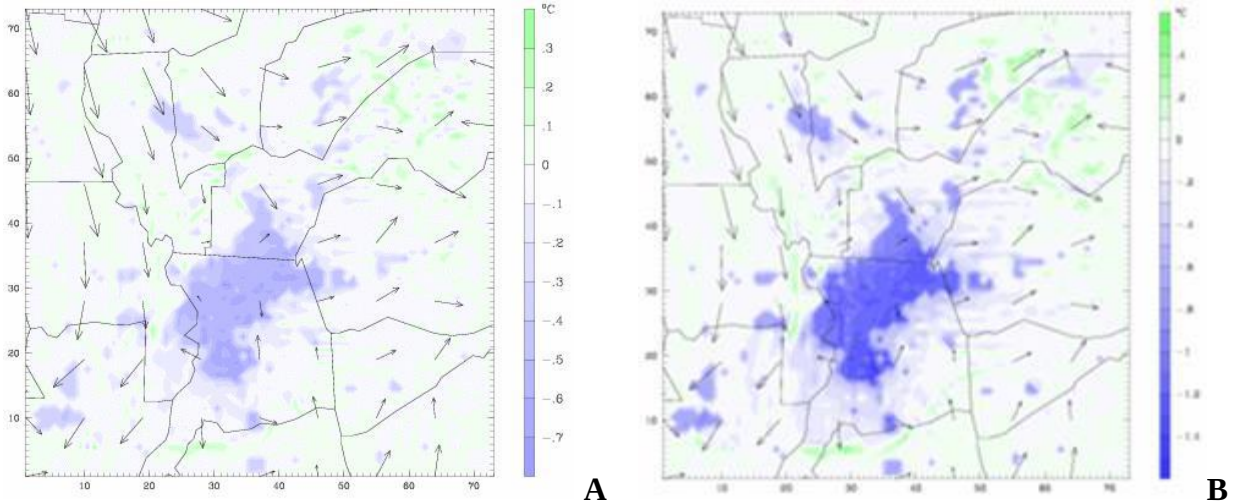

A **B**

Left: del01: 1300 PDT, July 28, 2015, horizontal wind vector (base) at 2 m AGL, Maximum change at this hour: -0.7 °C. Right: same but for del02, maximum change at this hour: -1.4 °C.

Figure EX-4, continued.

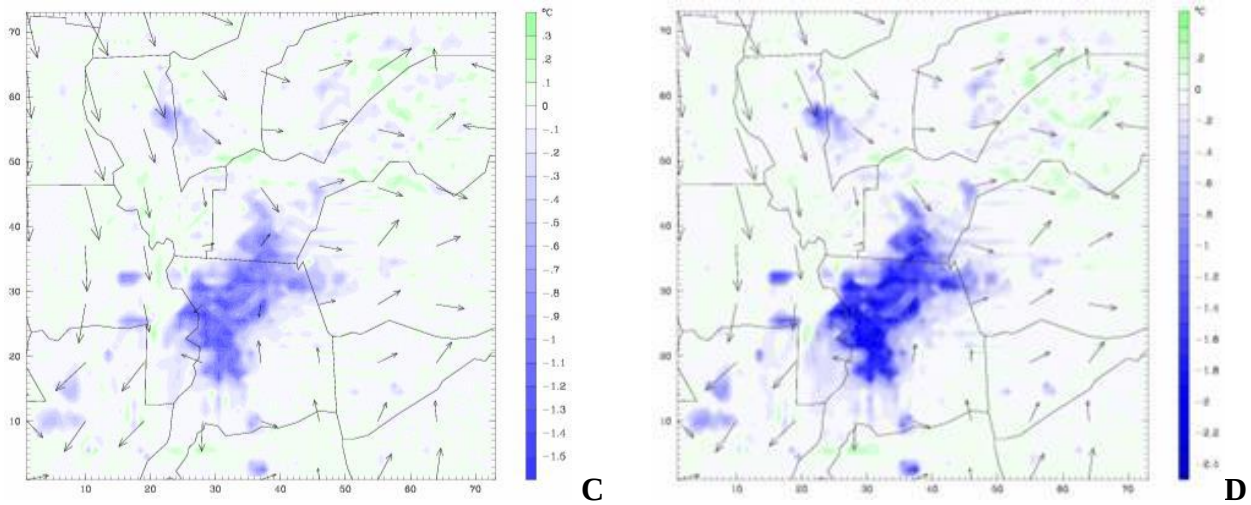

C **D**

Left: del10: 1300 PDT, July 28, 2015, horizontal wind vector (base) at 2 m AGL, Maximum change at this hour: -1.5 °C. Right: same but for del20, maximum change at this hour: -2.4 °C.

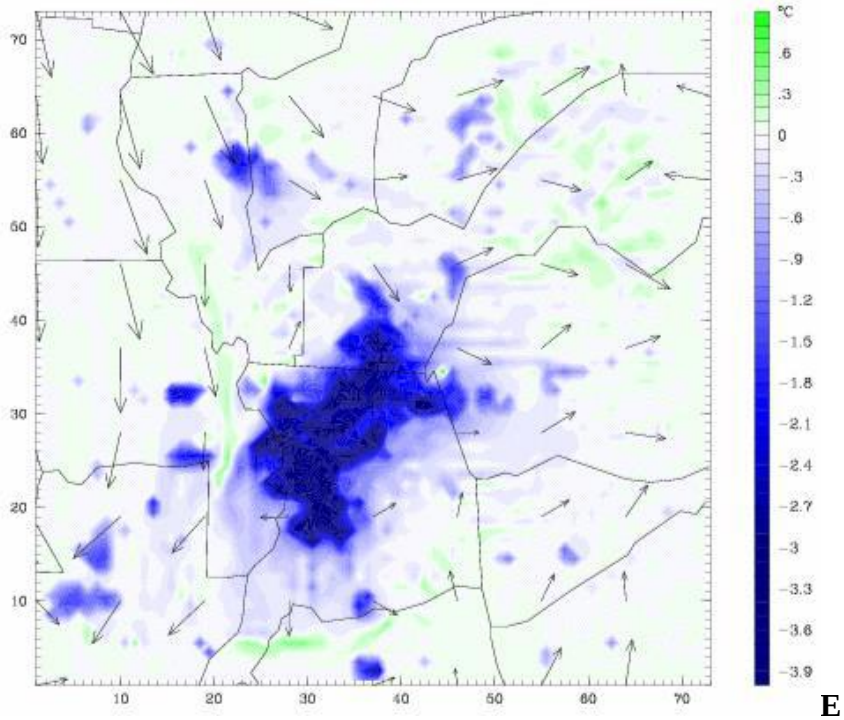

E

del31: 1300 PDT, July 28, 2015, horizontal wind vector (base) at 2 m AGL, Maximum change at this hour: -3.9 °C.

Figure EX-5: Summary of all-hour average temperature changes from five mitigation scenarios. Median, quartiles, and maxima/minima are shown with box-and-whisker plots.

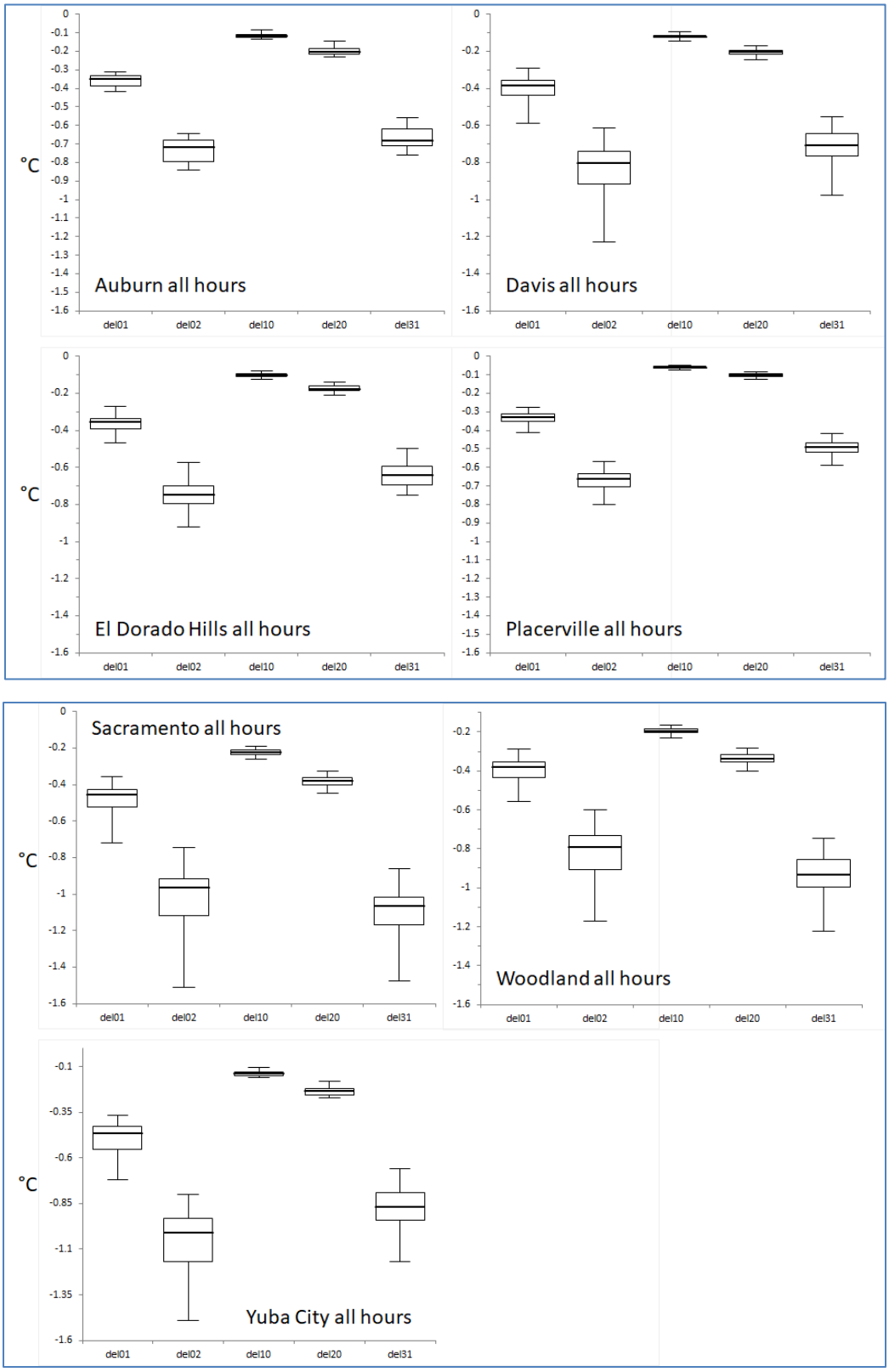

E.5.2 Quantifying the impacts of heat-mitigation measures on outdoor thermal conditions and heat exposure in current climate

Because of their significant cooling potentials, UHI-mitigation measures can affect various public-health heat indicators – for example, they can help decrease or offset exceedances in the National Weather Service Heat Index (NWS HI) above critical warning thresholds and reduce the number of heat-wave or excessive heat-event days. Table EST-1 provides an example from the analysis for the hour at 1700 PDT in terms of average potentials for reductions in the NWS HI levels resulting from case31 (defined in Section E.4). In the table, cumulative metrics (i.e., % change in degree-hours above specified warning thresholds) are provided. For each selected probing point (P0001 through P0032; see Glossary) throughout the 6-counties Capital region, the table gives the percent reduction in degree-hours (DH) above the NWS HI thresholds 106 °F (Danger), 91 °F (Extreme caution), and 80 °F (Caution). Of note – in this report, the NWS HI is the only instance where °F is used; the report in its entirety uses SI units and °C.

Results in Table EST-1 indicate that the combination measure (case31) can reduce the NWS HI exceedances above 106 °F (Danger) by between 50% and 100% (except for one location) and the exceedances above 91 °F (Extreme Caution) by between 18% and 36%.

Table EST-1: Reductions in exceedances (DH) above three NWS HI levels at 1700 PDT (averages over all intervals) in current climate for selected probing locations (P####) defined in the report. All numbers in the table are percentages.

	HI threshold	Probing location						
		P0001	P0004	P0008	P0011	P0013	P0014	P0018
% reduction in DH above thresholds	Caution (%)	-5.8	-5.0	-5.2	-9.4	-4.9	-6.1	-4.7
	Extreme caution (%)	-31.9	-28.6	-30.5	-28.0	-33.5	-36.2	-27.0
	Danger (%)	-66.2	-49.7	-100.0	N/A	-79.8	-83.2	-85.5

	HI threshold	Probing location					
		P0020	P0022	P0026	P0028	P0029	P0032
% reduction in DH above thresholds	Caution (%)	-4.8	-4.8	-4.2	-4.8	-2.6	-3.5
	Extreme caution (%)	-31.9	-23.3	-22.3	-18.7	-22.1	-29.5
	Danger (%)	-100.0	N/A	-79.7	-1.1	-58.7	-75.6

In terms of locally mitigating the effects of excessive heat events or heat waves (see Glossary), Table EST-2 provides a summary of the mitigation potential of case31. The table shows the number of days with NWS HI of 105 – 110 ºF at each selected probing location and for three heat-wave events identified in this study (listed in the table). The reduction in the number of heat-wave days at each location (as a result of implementing case31) is also shown.

Table EST-2: Number of consecutive days with NWS HI 105 – 110 ºF during three time periods.

		Number of days with NWS HI 105 – 110 ºF					
Probing location	Heat wave?	6/30 – 7/4, 2013		6/30 – 6/31, 2016		7/28 – 7/30, 2016	
		base	case31	base	case31	base	case31
P0001 AB617 (Sac)	yes	5	1	0	0	2	0
P0004 AB617 (Sac)	yes	3	1	0	0	2	0
P0008 AB617 (Sac)		1	0	0	0	0	0
P0011 AB617 (Sac)		1	0	0	0	0	0
P0013 Citrus Heights	yes	5	1	1	0	1	0
P0014 Roseville	yes	5	2	1	0	2	0
P0018 Lincoln	yes	4	3	1	0	2	0
P0020 El Dorado Hills		1	0	0	0	0	0
P0022 Placerville		0	0	0	0	0	0
P0026 Woodland	yes	3	0	0	0	0	0
P0028 Davis	yes	4	0	0	0	0	0
P0029 Marysville	yes	4	4	2	0	3	2
P0032 Yuba City	yes	4	4	2	0	3	1

As seen in Table EST-2, all areas can locally offset the heat-wave effects, except for one period in each of the Yuba City and Marysville locations. During the 6/30 – 7/3, 2013 heat wave, case31 reduces the number of heat-event days from 5 or 4 to 1 or 0 in most locations, except for Marysville and Yuba City. During the 6/30 – 6/31, 2016 heat event, case31 reduces the number of days to zero in all locations. The same occurs during the interval 7/29 – 7/30, 2016, i.e., heat-wave days are reduced to zero, except for Marysville and Yuba City where they are reduced from 3 to 2 and from 3 to 1 days, respectively.

Considerations to minimize or prevent any potential inadvertent health impacts from thermal or air-quality changes resulting from UHI-mitigation measures are discussed in the report.

E.5.3 Ranking the effectiveness of heat-mitigation measures at the regional scale under current climate and land use

Figure EX-6a is a high-level summary of the regional-scale UHI-mitigation potentials of the five measures defined in Section E.4 in current climate and land use / land cover conditions. Information in this chart can be used to rank the measures for implementation in each area. Thus, for example, once an area's weighted UHII score is identified (from Section E.3, Figure EX-3b) the chart in Figure EX-6a can be used to obtain an initial assessment of the efficacy of measures per a given location, i.e., as defined at the top of the chart. Thus, the combined information is shown in Figure EX-6b, which is essentially a combination of Figure EX-3b and Figure EX-6a. However, this does not mean that a city or local jurisdiction is obligated to adopt such rankings for implementation purposes. As will be seen later in Section E.8 (and Table EST-4) the effectiveness

of measures in attaining the UHII is further provided as an additional layer of information for jurisdictions to develop their own UHI-mitigation priorities or "mix and match" several measures.

As explained in the technical report, case02 is an extreme scenario of vegetation-cover increase and should be disregarded for practical purposes. However, it is included here as a test for upper bounds (largest cooling effects) per suggestions from local tree organizations.

Of note, Figure EX-6a does not provide the spread (e.g., inter-quartile ranges) of the cooling effects from a particular measure nor how close various measures are to each other (or how far apart they are in terms of their cooling effects). The chart simply shows the ranking of measures even if differences between one measure and another are very small or almost tied in some instances (these details are discussed in the report). Cases that are tied are indicated in Figure EX-6a with a repeated number and color code. It is important to note that these rankings are based on air-temperature changes averaged over 2-km and that they can differ at the finer scales (500 m) where the magnitudes of the temperature reductions also get larger when averaged at finer resolutions.

In Figure EX-6a (and EX-6b), the various time bands may be of interest in different applications. For example, the 0600 PDT and allHRS bands could be of interest from a heat-wave perspective, the 1400-2000 PDT band may be of interest to utilities, the 1500-PDT band could be used in relation to peak cooling demand analysis, and the band at 1300 PDT may be of relevance to assessments of measures around solar noon.

The modeling of future climates, as discussed in the report, shows that except for a number of instances, the ranking (and ordering) of measures shown in Figure EX-6a remains largely unchanged into the future. That is, the ranking of measures in terms of their effectiveness in current climates and LULC is the same to mitigate urban heat under conditions of future climate and urbanization. While the ranking (order) can be relatively similar, the magnitudes of the cooling effects can differ.

Table EST-3 provides the numerical values of the cooling associated with these rankings (values are averaged over all grid cells in each region and for the given time period) with case02 excluded, as explained above. The chart below the table is simply a graphical representation of the values listed. Table EST-3 and the chart exclude case02 to provide a fairer comparison among measures. At the finer scales (i.e., specific projects and 500-m resolution), the cooling effects are significantly larger than the 2-km averaged effects reported in Table EST-3.

Thus, it can be noted from Figure EX-6a and Table EST-3 that albedo scenarios (e.g., cool roofs and cool pavements) are the top choice for reducing daytime urban air temperature. But because the vegetation canopy cover can cool the air both during the day and at night, its impacts are dominant in the 24-hour average metrics and early-morning averages. It can also be seen that case31 generally produces the largest cooling regardless of time of day, whereas the ranking of the other measures does vary from one part of the day to another. For instance, and aside from case31, case01 produces the largest cooling at night whereas case20 the largest cooling during the daytime. Lastly, some of the urban areas seem to consistently experience larger cooling effects, e.g.,

Sacramento, among others in the Capital region especially in case31. This is mainly a result of the larger areas available for implementing UHI-mitigation measures

Figure EX-6a: Summary of urban-heat mitigation potential: ranking of measures case01 through case31 by cooling effectiveness in current climate (1 to 5, or darker to lighter = largest to smallest cooling)**. Note that case02 should be excluded in some analysis. Also note that these are impacts on temperature, not UHII.

		Auburn	Davis	El Dorado Hills	Placerville	Sacramento	Woodland	Yuba City
0600 PDT	case01	3	3	3	3	3	3	3
	case02	1	1	1	1	1	1	1
	case10	5	5	5	5	5	5	5
	case20	4	4	4	4	4	4	4
	case31	2	2	2	2	2	2	2
1300 PDT	case01	4	5	4	3	5	5	4
	case02	2	2	2	2	3	3	2
	case10	5	4	5	4	4	4	5
	case20	3	3	3	3	2	2	3
	case31	1	1	1	1	1	1	1
1400 - 2000 PDT	case01	4	4	4	3	5	4	4
	case02	2	2	2	2	2	2	2
	case10	5	5	5	5	4	3	5
	case20	3	3	3	4	3	2	3
	case31	1	1	1	1	1	1	1
1500 PDT	case01	4	5	4	4	5	5	4
	case02	2	2	2	2	3	3	2
	case10	4	4	4	5	4	4	4
	case20	3	3	3	3	2	2	3
	case31	1	1	1	1	1	1	1
allHRS	case01	3	3	3	3	3	3	3
	case02	1	1	1	1	2	2	1
	case10	5	5	5	5	5	5	5
	case20	4	4	4	4	4	4	4
	case31	2	2	2	2	1	1	2

** Scenarios were defined earlier in Section E.4. As a recap, case01: realistic-high increases in canopy cover; case02: extreme increases in canopy cover; case10: small increases in albedo; case20: larger increases in albedo; case31: combined albedo and canopy-cover scenario.

Figure EX-6b: Combining the temperature-weighted UHII score with the area-specific ranking of measures efficacies. See the technical report for a full discussion of this approach. The ribbons in this figure are slices from the chart in Figure EX-6a, above.

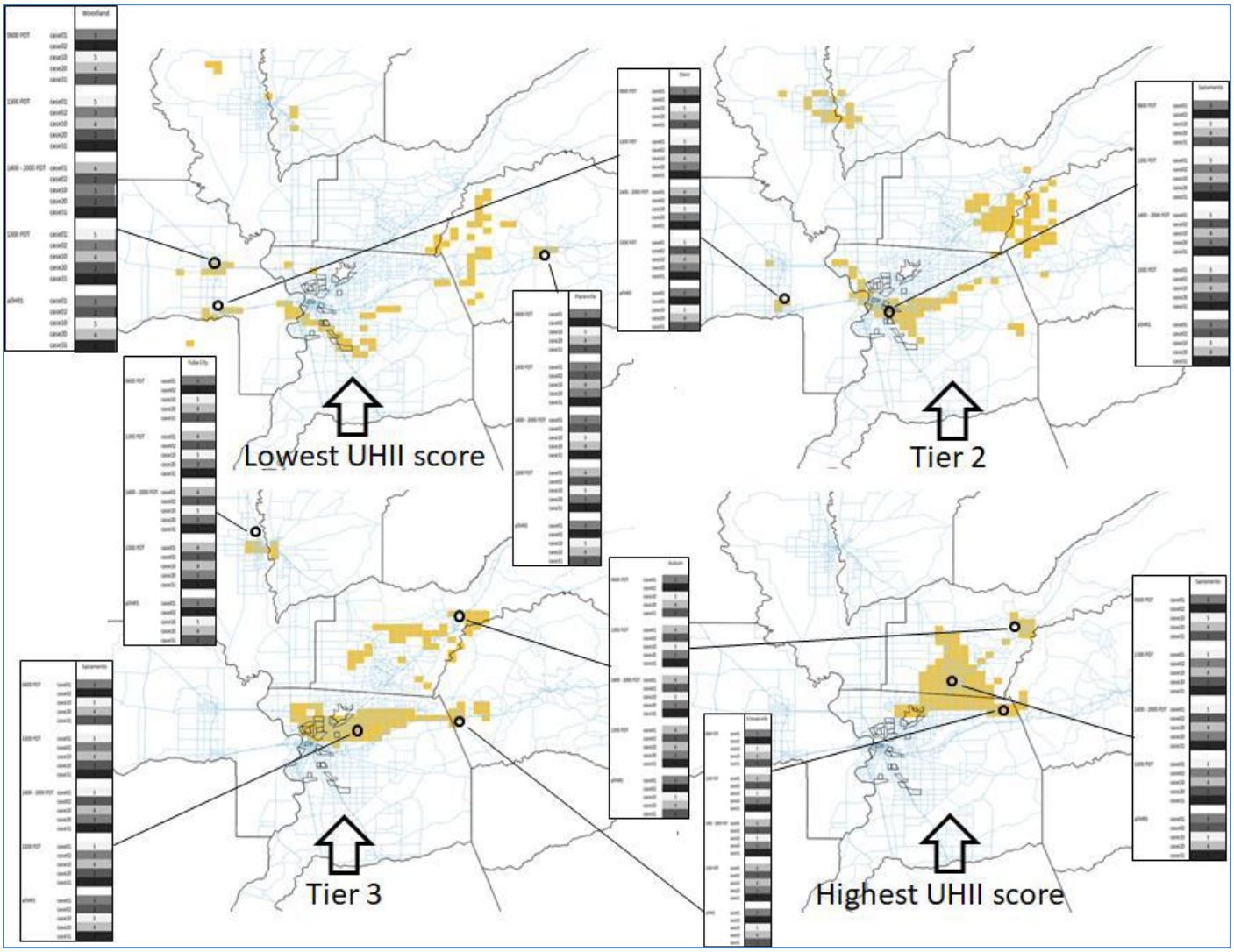

Table EST-3: Numerical values (°C) corresponding to the rankings in Figure EX-6. In this table, case02 has been excluded.

		Auburn	Davis	El Dorado Hills	Placerville	Sacramento	Woodland	Yuba City
0600 PDT	case01	-0.40	-0.60	-0.50	-0.50	-0.70	-0.60	-0.75
	case10	-0.08	-0.15	-0.09	-0.09	-0.10	-0.10	-0.10
	case20	-0.10	-0.20	-0.10	-0.10	-0.20	-0.20	-0.20
	case31	-0.50	-0.90	-0.60	-0.55	-1.00	-0.90	-1.00
1300 PDT	case01	-0.20	-0.18	-0.22	-0.12	-0.25	-0.18	-0.22
	case10	-0.20	-0.20	-0.20	-0.08	-0.40	-0.30	-0.20
	case20	-0.30	-0.30	-0.30	-0.12	-0.65	-0.50	-0.33
	case31	-0.60	-0.60	-0.70	-0.32	-1.30	-0.95	-0.70
1400 - 2000 PDT	case01	-0.22	-0.19	-0.22	-0.18	-0.23	-0.16	-0.20
	case10	-0.20	-0.15	-0.15	-0.10	-0.25	-0.22	-0.15
	case20	-0.32	-0.25	-0.30	-0.15	-0.47	-0.35	-0.25
	case31	-0.72	-0.55	-0.70	-0.40	-1.00	-0.76	-0.60
1500 PDT	case01	-0.18	-0.14	-0.21	-0.14	-0.20	-0.13	-0.17
	case10	-0.18	-0.15	-0.21	-0.10	-0.33	-0.25	-0.18
	case20	-0.30	-0.27	-0.36	-0.16	-0.55	-0.45	-0.30
	case31	-0.64	-0.52	-0.80	-0.37	-1.10	-0.80	-0.60
allHRS	case01	-0.35	-0.40	-0.35	-0.32	-0.45	-0.38	-0.47
	case10	-0.12	-0.17	-0.10	-0.05	-0.20	-0.20	-0.15
	case20	-0.20	-0.20	-0.18	-0.10	-0.37	-0.33	-0.22
	case31	-0.65	-0.70	-0.60	-0.50	-1.06	-0.92	-0.85

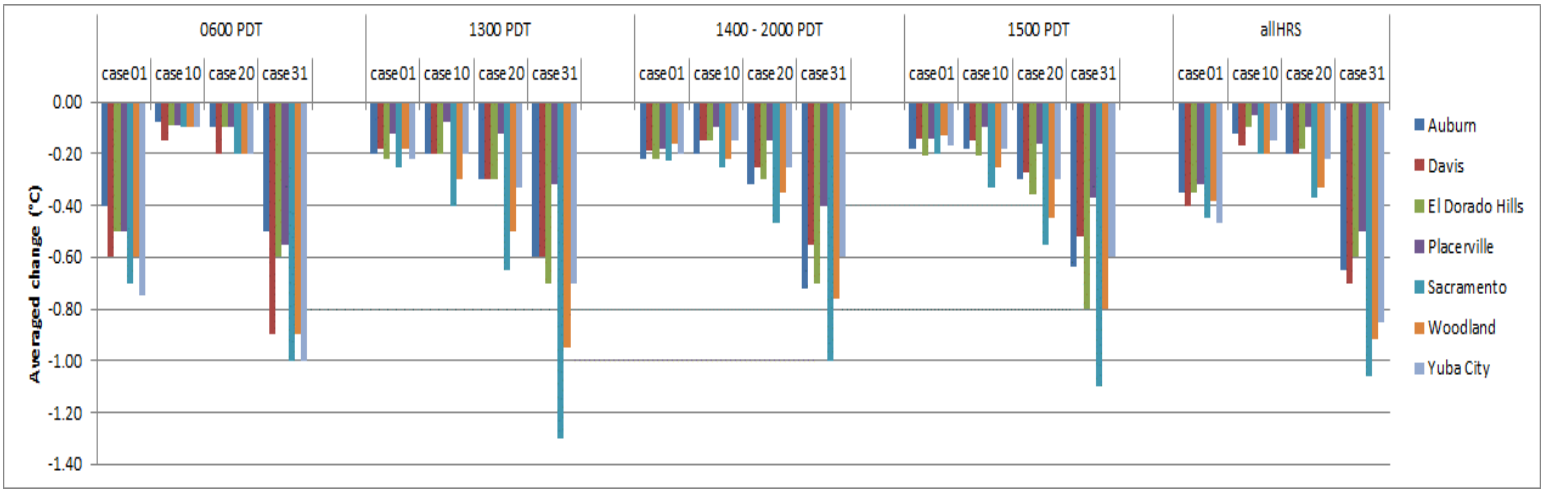

E.6 DEFINING HEAT-MITIGATION MEASURES AT THE COMMUNITY SCALE OR PROJECT LEVEL

In addition to the regional (2-km averaged) assessments discussed above, this study also evaluated the localized, site-specific effects of UHI-mitigation measures in areas of interest and at specific MTP (Metropolitan Transportation Plan) roadway project locations. The following reasonable and realistic scenarios were modeled at the community scale (500-m resolution) for current climate and LULC conditions depending on domain and/or specific requests received from the project participants, cities, SMAQMD / LGC, and the project Technical Advisory Committee (TAC). All of these scenarios are discussed in detail in the Project Technical Report and are briefly summarized below. The various measures have different impacts and effectiveness that vary from one location or project to another. The efficacy and rankings of these measures in each area are summarized later in Section E.8.

- Albedo scenarios:
    - For MTP projects, the roadway albedo is increased from a mean of 0.12 (average for current conditions) to 0.35. This is a cap to minimize glare issues.
    - For AB617 communities and other urban areas of interest, such as downtown or specific projects, the roof albedo is increased from a current mean of 0.17 to 0.5 and the roadway albedo from a mean of 0.12 to 0.30. These are caps to minimize potential glare or radiative concerns at pedestrian level.
- Heat-emission scenarios:
    - A vehicle-electrification scenario is applied in designated areas or in transportation corridors of interest. Time- and location-dependent heat emissions from mobile sources are reduced by up to 25% (per CEC and SMAQMD studies that propose an electric-vehicle ownership level of 25%). This scenario also involves quantifying the impacts of electrification per SMAQMD's ZEV Readiness Plan.
- Vegetation-canopy scenarios:
    - Increases in canopy cover are applied in areas of interest defined by the SMAQMD, LGC, and project TAC, including AB617 communities, downtown areas, and other disadvantaged communities (DAC). As an estimate, about 300 large trees are added to a neighborhood of ~ 0.25 km^2, which is equivalent to a cover increase of 8% of a model grid-cell area.
- Cool-wall scenarios:
    - In addition to other cool-surface measures, the albedo of walls is increased in this scenario from an existing average of 0.15 to a maximum of 0.40.
- Solar PV scenarios:
    - Solar PV panels are added to roof- or ground-based surfaces, e.g., parking lots, with different coverages, conversion efficiencies, background albedo, and other parametric considerations, as discussed in the Project Technical Report. In this analysis, the focus is on ground-based solar PV.

- Combination scenarios:
    - These are scenarios combining cool surfaces, vegetation cover, and tailpipe heat emission reductions.

E.7 IDENTIFYING PROJECT AREAS AT THE COMMUNITY SCALE

Unlike the UHII priority areas and rankings that were defined at the regional scale (2-km level) based solely on climate criteria (as shown, for example, in Figure EX-3a,b), the 500-m level priority areas were additionally defined per local project requirements. This was based on areas or projects proposed by the TAC, cities, and SMAQMD / LGC, as well as MTP roadway projects some of which were identified by WSP. In these areas and project sites, the above-defined measures (Section E.6) were applied. Of note, the background grid of dark dots in Figures EX-7 through EX-12 is of no relevance to the discussion in this section (and these mean different things in different contexts) but are discussed in detail in the technical report. Further, the domain labels used in this discussion, i.e., D05 through D10, are also defined in the report (and in Appendix A-2). Note that the following figures are not to the same scale.

Domain D05 (Yuba City / Marysville)

Figure EX-7 depicts the MTP project locations and areas of interest in domain D05. The yellow outline is downtown Marysville, an area designated of interest per project TAC, the orange lines are roadway and bridge projects identified by the City of Yuba City, and the red lines are MTP project locations. The major highways of relevance to electrification scenarios are highlighted with bold black lines.

Figure EX-7: Locations of roadway projects and areas of interest in the Yuba City / Marysville domain.

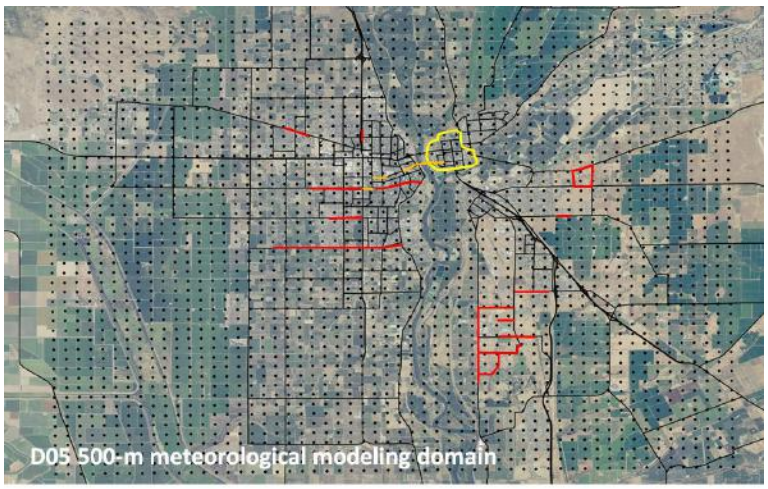

Domain D06 (Woodland)

Figure EX-8 depicts the roadway project and areas of interest in and near the City of Woodland. The yellow line highlights an area of interest (per TAC) in the northwestern part where future urbanization is expected to intensify. The red lines depict the MTP roadway projects and the highways of interest to electrification scenarios are highlighted with bold black lines.

Figure EX-8: Locations of roadway projects and areas of interest in the Woodland area.

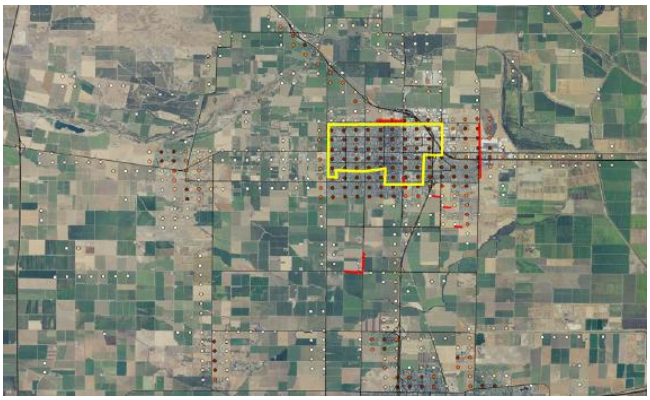

Domain D07 (Sacramento)

The yellow areas in Figure EX-9 are AB617 communities defined by SMAQMD that also are of interest to the project TAC and the cities in this area. The red lines are MTP projects identified by WSP and the major highways of interest in electrification scenarios are highlighted with bold black lines.

Figure EX-9: Locations of roadway projects and areas of interest in the Sacramento area.

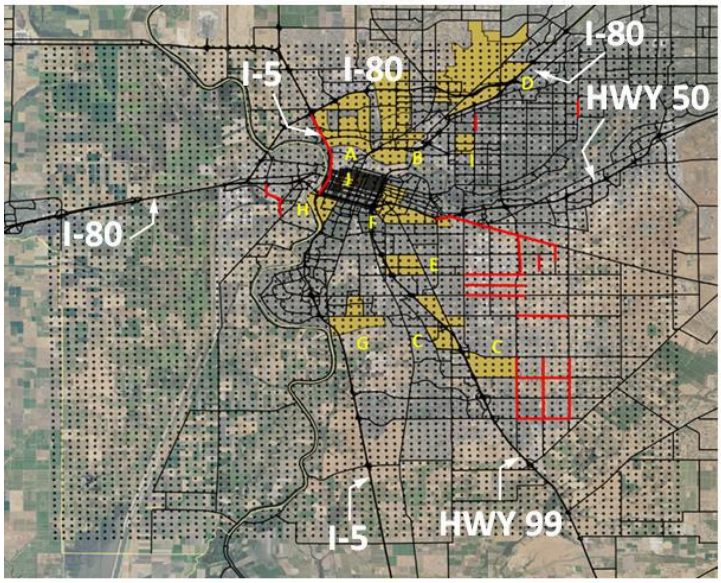

Domain D08 (Sacramento – Roseville – Granite Bay)

In the Sacramento – Roseville – Granite Bay region (Figure EX-10) the yellow area is AB617 community "D" defined by SMAQMD. The red lines are MTP roadway projects and the major highways of relevance to electrification are highlighted with white lines.

Figure Ex-10: Locations of projects and areas of interest in Sacramento – Roseville – Granite Bay area.

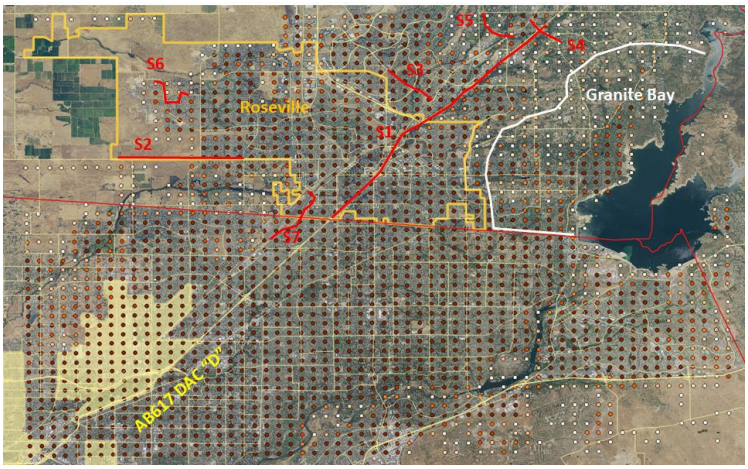

Domain D09 (Folsom – El Dorado Hills)

Figure EX-11 shows the roadway projects and areas of interest in the Folsom – El Dorado Hills region, including the MTP projects (red lines) and the urban areas in both cities. The highways of interest in electrification scenarios are highlighted in white.

Figure EX-11: Locations of roadway projects and areas of interest in the Folsom – El Dorado Hills area.

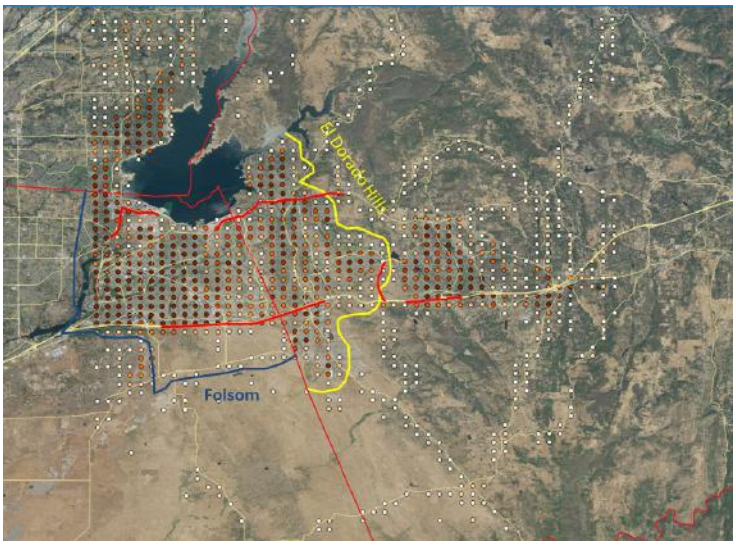

Domain D10 (Placerville – Diamond Springs)

The roadway project locations in the Placerville – Diamond Springs region are highlighted in red in Figure EX-12. The yellow lines delineate the urban areas of interest and the highways of relevance to electrification scenarios are also identified.

Figure EX-12: Locations of roadway projects and areas of interest in Placerville – Diamond Springs area.

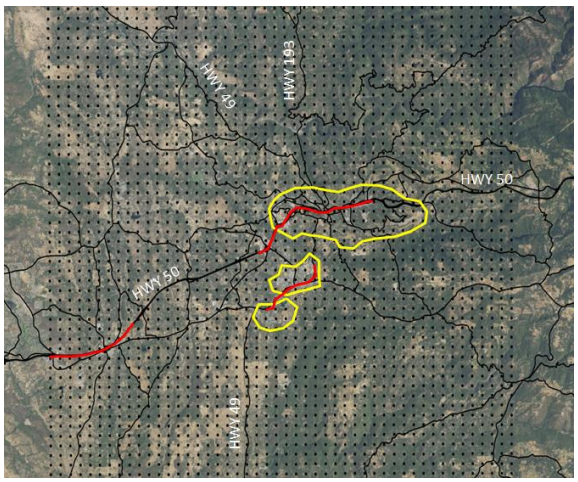

E.8 ATTAINMENT OF THE UHII AT COMMUNITY AND PROJECT SCALES IN CURRENT CLIMATE AND LAND USE

One way to evaluate and inter-compare the mitigation efficacies of various project- or area-specific measures is to quantify their potential to offset the local UHII, i.e., its value at the specific location where the measures are being implemented and evaluated. Thus, the effects of mitigation measures at community level (500-m scale) were compared to the local all-hours UHII computed for current climate conditions and urbanization levels, such as shown earlier in the example in Figure EX-1a. The UHII offset via each UHI-mitigation measure was evaluated for two situations: (1) a scenario where only the community implements the measure and no other nearby communities take any action, and (2) a scenario where both the community and its upwind neighbors implement the measures. In this second situation, the community will benefit from cooler air transported from upwind areas in addition to the local cooling resulting from implementation of its own UHI-mitigation strategies. This is akin to "doubling" the local cooling effects.

The evaluations are summarized in Table EST-4 for each measure in standalone fashion. The total effects of combinations of measures are non-linear (i.e., cannot be computed as simple sums) and are smaller than the sum of the individual components. Still, the information in Table EST-4 can provide Caltrans and urban planners with rough magnitudes of the cooling effects that can be anticipated if measures were combined.

Table EST-4: Potential of local projects in mitigating the all-hours UHII in current climate and land use.

Project area	All-hours Tair UHII (°C)**		Localized/no advection UHII attainment local mitigation only	Localized+advection UHII attainment local mitigation+advection
D05	2.41			
Yuba City / Marysville		Cool roofs / pavements	-58%	-82%
Downtown YC and M		Cool pavements	-46%	-70%
		Electric vehicles	-7%	-31%
		Vegetation cover	-71%	-95%
D06	2.14			
Woodland		Cool roofs / pavements	-60%	-93%
DAC census tracts		Cool pavements	-69%	-101%
		Electric vehicles	-7%	-39%
		Vegetation cover	-51%	-84%
D07	4.48			
Sac / SE Sac		Cool roofs / pavements	-29%	-63%
AB617 A, B, D		Cool pavements	-31%	-65%
		Electric vehicles	-6%	-39%
		Vegetation cover	-33%	-67%
D07	2.33			
Sac / SE Sac		Cool roofs / pavements	-56%	-93%
AB617 C, E, G		Cool pavements	-60%	-97%
		Electric vehicles	-11%	-48%
		Vegetation cover	-63%	-101%

Project area	All-hours Tair UHII (°C)**		Localized/no advection UHII attainment local mitigation only	Localized+advection UHII attainment local mitigation+advection
D08	5.07			
Granite Bay		Cool roofs / pavements	-28%	-48%
		Cool pavements	-34%	-54%
		Electric vehicles	-6%	-27%
		Vegetation cover	-21%	-41%
D08	5.83			
Roseville		Cool roofs / pavements	-24%	-52%
		Cool pavements	-30%	-57%
		Electric vehicles	-5%	-33%
		Vegetation cover	-18%	-46%
D09	4.91			
El Dorado Hills		Cool roofs / pavements	-30%	-47%
		Cool pavements	-34%	-51%
		Electric vehicles	-4%	-20%
		Vegetation cover	-23%	-39%
D09	4.86			
Folsom		Cool roofs / pavements	-31%	-52%
		Cool pavements	-35%	-56%
		Electric vehicles	-4%	-25%
		Vegetation cover	-23%	-44%
		Doubled cover increase	-40%	-61%
D10	1.36			
Placerville / Diamond Springs / El Dorado City		Cool roofs / pavements	-88%	-113%
		Cool pavements	-118%	-143%
		Electric vehicles	-6%	-31%
		Vegetation cover	-96%	-121%

**Averaged over three periods: 2015_int1 (lower range), 2016_int5 (mid-range), and 2013_int3 (upper range).

As shown in Table EST-4, some measures, even in standalone fashion, can completely offset the local UHII. Furthermore, when neighboring communities also implement UHI-mitigation strategies, the local benefits increase significantly -- but of course vary from one measure and location to another. It is to be re-emphasized that these are localized effects, i.e., temperature changes at or near the surface of the modified roadways or air temperature within the urban canyons of the selected communities. Thus, in table EST-4, the effects of cool pavements alone can sometimes be larger than the effects of combined cool pavements and cool roofs because the levels of increase in pavement albedo for the main highways and freeways in the region are larger than for the local roadways in the selected communities (see definitions in Section E.6). In addition, there is a shading effect in the canyons that can reduce the effectiveness of cool pavements in those communities compared to the wide-open freeways where there is minimal shading and a large modifiable area for implementing cool pavements.

E.9 ADDITIONAL COMMUNITY-LEVEL MEASURES

This section presents some additional community-level measures that were not included in the analysis above (in Table EST-4) and that were requested by SMAQMD, LGC, the project TAC, or the cities in the Capital region.

E.9.1 Electrification per SMAQMD ZEV Readiness Plan

Fine-scale modeling was carried out to evaluate the potential temperature impacts from heat-emission reductions following the SMAQMD's ZEV Readiness Plan. Figure EX-13 shows the locations of proposed charging facilities in the region (per SMAQMD) superimposed on the UHII tiles of the Capital region. The type of information shown in the figure can provide SMAQMD with general priorities for implementing the charging stations assuming the UHII is sole criterion.

In this modeling assessment, a zone was defined by a 10-km radius of influence around each station. A Cressman weighting scheme was then applied within each influence zone to decrease electrification levels from 25% at the station locations to zero at the perimeter of each influence zone. This was then used in quantifying the atmospheric impacts from ZEV ownership.

In Table EST-5, sample results are presented from this analysis of the air temperature (*Tair*) and surface temperature (*Tsfc*) impacts of implementing the SMAQMD's ZEV Readiness Plan. While reported separately in this table, *Tair* and *Tsfc* should actually be averaged to get a better representation of the temperature effects from reduced tail-pipe heat emissions via electrification. The "average max cooling" column in the table is the average of the largest daily surface cooling over all days in the given period. The "1700 PDT" averages in the table are averages of all 1700 PDT hours and the "all hours" column entries are averages over every hour in the given period. The modeling and analysis were applied to the Sacramento region (domains D07 and D08 defined in the report) for the time periods identified in Table EST-5.

Figure EX-13: Charging/H2 stations vs. UHII composite tiles in July 16-31, 2015.

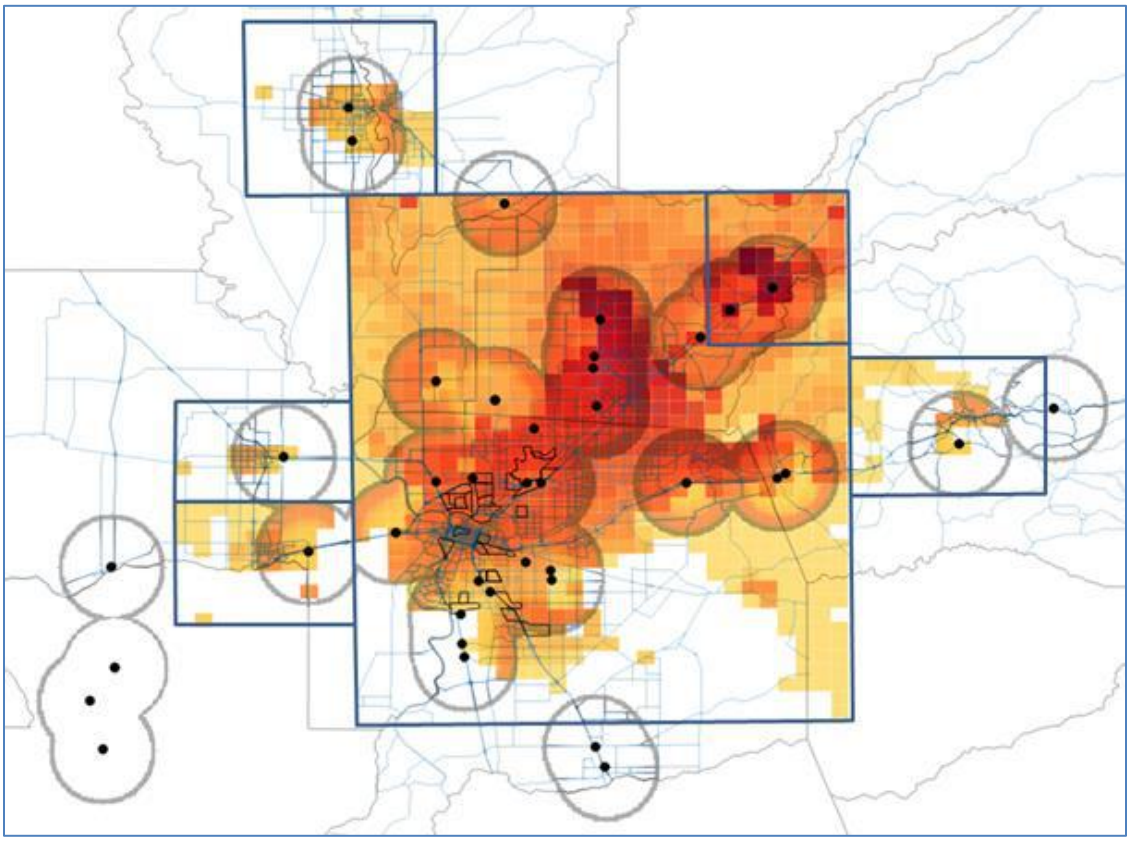

Table EST-5: SMAQMD ZEV Readiness Plan impact on temperature (changes in °C)

Domain and interval	1700 PDT			all hours		
	averages		average max. cooling (Tsfc)	averages		average max. cooling (Tsfc)
	Tair	Tsfc		Tair	Tsfc	
D07						
Jul 1-15, 2013	-0.32	-0.55	-2.97	-0.17	-0.28	-0.87
Jun 1-15, 2015	-0.20	-0.37	-2.81	-0.16	-0.27	-0.84
Aug 1-15, 2016	-0.24	-0.41	-3.34	-0.16	-0.27	-0.86
D08						
Jul 1-15, 2013	-0.27	-0.44	-1.58	-0.18	-0.29	-0.73
Jun 1-15, 2015	-0.25	-0.42	-2.17	-0.17	-0.27	-0.74
Aug 1-15, 2016	-0.26	-0.45	-1.79	-0.18	-0.30	-0.74

E.9.2 Installation of solar PV

Per interest from the City of Folsom and the SMAQMD, the potential impacts of solar PV arrays on near-surface temperature, that is, temperature near the ground, were evaluated and compared to the effects of tree canopies on parking lots. Various parameters were considered in evaluating the standalone effects of ground-based (e.g., parking lots) and roof-based solar PV. The Project Technical Report discusses this measure in additional detail along with the various parameters considered in the analysis.

As there can be a number of possible combinations of such parameters as well as their evolution over time and under future climates and urban surface properties, Table EST-6 lists a subset of the scenarios that were modeled and discussed here. Table EST-7 presents a summary of results for the near-surface temperature impacts from solar PV deployment in the Folsom area.

Table EST-6: Scenarios of solar PV implementation (ε is conversion efficiency; c is cover).

	Surface = roof (#0)			Surface = paved / parking lot (0#)		
Scenario	roof albedo	ε	c	paved albedo	ε	c
casePV10	f(LULC) ~ 0.17 – 0.20	0.15	40%	-	-	-
casePV20	f(LULC) ~ 0.17 – 0.20	0.30	40%	-	-	-
casePV30	0.50	0.30	60%	-	-	-
casePV01	-	-	-	f(LULC) ~ 0.10 – 0.12	0.15	60%
casePV02	-	-	-	f(LULC) ~ 0.10 – 0.12	0.30	60%
casePV03	-	-	-	0.30	0.30	80%
casePV22	f(LULC) ~0.17 – 0.20	0.30	40%	f(LULC) ~ 0.10 – 0.12	0.30	60%

Table EST-7: Changes in near-surface temperatures (°C) within the urban canopy layer resulting from various solar PV scenarios in the Folsom area. Note that scenarios PV03 and PV30 also include significant increases in background albedo, not only installation of solar PV.

	PV scenario							
	PV01	PV02	PV03	PV10	PV20	PV30	PV22	PV30vsAA
1500 PDT average								
Near-surface temperature	-1.17	-2.44	-4.04	-0.03	-0.08	-0.20	-2.49	+0.18
All hours average								
Near-surface temperature	-0.52	-1.18	-1.89	-0.01	-0.03	-0.09	-1.19	+0.08

As expected, the analysis indicates that urban canopy temperatures near the ground are affected more by ground-based PV panels – e.g., those installed over parking lots – than those installed at roof level. This is because (1) the effects from roof modifications occur at generally higher elevations above street level (or urban canyon) and as such, have smaller impacts on temperature near the ground, (2) because the albedo of roofs and the effective albedo of the solar panels are more comparable and both higher than albedo of pavements at ground level, and (3) the effects of shading the ground on near-surface temperatures, e.g. parking lots, is larger than shading at roof level (which sometimes is non-existent). However, near the top of the canopy layer and above roof level, both roof-based and ground-based solar PV have significant and similar effects on air temperature.

With respect to current typical albedo of roofs and pavements, the solar PV scenarios PV01 and PV02 (ground-based PV) produce average all-hours near-surface temperature reductions (localized cooling) of 0.52 and 1.18 °C, respectively. This can reach a maximum of 1.17 and 2.44 °C, respectively, during peak hours. As discussed in the report, other studies found larger cooling at night than during the day from roof-based panels, but in this analysis, the effect of albedo and shading at ground level were evaluated (for the reasons explained above) and found to be dominant and larger during daytime.

The larger cooling in case PV02 relative to that in case PV01 is entirely caused by increased PV conversion efficiency (ε) from 0.15 to 0.30, and represents the range of possible cooling effects from today's PV technology in today's typical albedo ranges in urban areas. The reductions in near-surface temperature as a result of roof-based solar PV installations (cases PV10 and PV20) are smaller, roughly up to 0.1 ºC, for the reasons listed above. Nevertheless, these numbers show that the electric benefits from solar PV installations at roof level can be attained without incurring negative atmospheric effects, i.e., increasing air temperature at street level. As discussed in the report, the temperature effects reported here are generally comparable to those from other studies.

In a scenario where both roof- and ground-based solar PV are implemented, e.g., case PV22, the cooling is slightly larger than in case PV02, but by a small amount. In this scenario, reductions in 1500-PDT and all-hours temperatures of 2.49 and 1.19 °C, respectively, are predicted.

In cases PV03 and PV30, the background albedo (of roofs and pavements) is also increased significantly in addition to installing solar PV – hence the resulting large cooling effects are attributable mostly to the increases in background albedo. These scenarios represent future conditions where roof albedo, pavement albedo, PV cover, and conversion efficiency all have increased. Finally, case PV30vsAA demonstrates the potential negative effects of solar PV if implemented widely in the future when cool roofs and cool pavements also would have been deployed at a larger scale. In this case, the installation of solar PV can have the potential to increase near-surface temperature by an average of 0.08 °C (all-hours) and 0.18 °C at the time of the peak (1500 PDT) relative to if only cool roofs and pavements were installed, although still cooler than in the base scenario.

E.9.3 Smart growth measures

Per SMAQMD's interest, this study evaluated a scenario of smart urban growth whereby 15% less urbanization occurs by 2050 relative to a business-as-usual scenario (BAU). Figure EX-14 depicts the BAU and smart-growth cases as represented on the 2-km grid of the model. The green areas are current urban and the pink areas are new urban by 2050. The current urban LULC was defined based on NLCD 2011-2016 datasets and the BAU scenario based on USGS LUCAS projections, as discussed in detail in the technical report.

While there are several ways the impacts of smart growth could be quantified, including averaging over an entire region or over different sub-domains, here the impacts were evaluated mainly at those locations where urbanization was prevented (Figure EX-14). Clearly, this criterion would result in greater cooling relative to averaging over larger areas, i.e., including currently-urbanized regions.

Figure EX-14: BAU (left) and smart-growth (right) urbanization by 2050 on the model 2-km grid

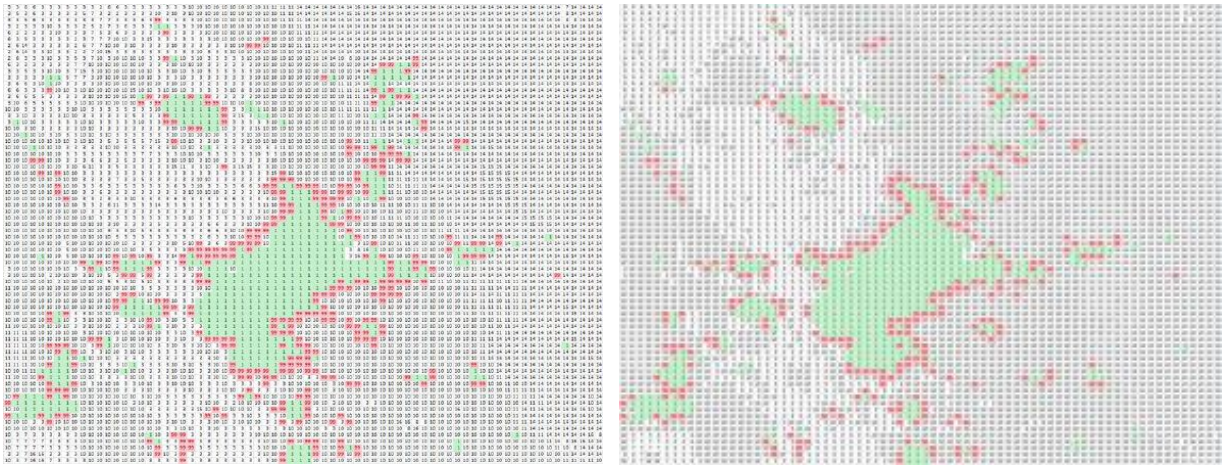

The model results indicate that while there are variations by area and time interval, the overall average avoided warming at 0600 PDT is about 2 °C in those areas where urbanization was prevented or minimized. On the other hand, if averaged over each subdomain, the effects of smart growth are smaller, e.g., an avoided warming of between 0.05 and 0.15 °C region-wide. At 1300 PDT, the avoided warming ranges from an average of 0.05 °C in Davis to up to an average of 0.4 °C in Auburn. If averaged over each subdomain, the effects of smart growth are an avoided warming of between 0.05 and 0.1 °C region-wide.

For the hours between 1400 and 2000 PDT, and similar to 1300 PDT, there are more variations in avoided warming across the regions than is the case at 0600 PDT. At 1400 – 2000 PDT, the avoided warming ranges from an average of 0.6 °C in Davis to up to an average of 1.2 °C in Auburn. Again,

if averaged over each subdomain, the effects of smart growth are smaller, e.g., an avoided warming of between 0.05 and 0.15 °C region-wide

At 1500 PDT, the avoided warming ranges from an average of 0.20 °C in Davis to up to an average of 0.6 °C in Auburn and Yuba City and, if averaged over each subdomain, the effects of smart growth are an avoided warming of between 0.08 and 0.15 °C area-wide. Finally, for all-hour averages, the smart growth scenario shows that except for Auburn and El Dorado Hills, there is less variation across the regions and relatively similar avoided warming of between 1.2 and 1.6 °C.

One observation that can be made from this analysis is that the impacts of smart growth measures are larger (i.e., larger avoided warming) during the nighttime than during the day. This is a direct result of urbanization affecting nighttime temperatures more than those during the daytime, i.e., the classical definition of the urban heat island effect.

E.9.4 Combinations of measures

As discussed above, several mitigation measures were evaluated at the community scale (500-m resolution) in standalone mode. Combinations of measures were not presented as there would be a large number of arbitrary possibilities. However, per interest from the City of Elk Grove, an example of a combination scenario was evaluated, as presented in Figure EX-15.

This assessment was conducted based on fine-scale modeling of the combined measures in D07, a domain containing the City of Elk Grove (see Figure EX-9, above). The results indicate that the combination of measures provides significantly larger cooling benefits than each measure in standalone mode but, with two small exceptions, the total cooling (of combination of measures) is smaller than the sum of the individual components (cooling from each standalone measure). In this domain, and for the modeled periods, the total effect of the combination scenario (green bars in the chart) is about 5 – 15% smaller than the simple sum of the individual cooling effects.

Figure EX-15 summarizes these findings and also shows the significant cooling benefits for the roadway surfaces ("Roadway temperature") during daytime hours, as well as for the 24 hours average. The other columns in this figure are as follows: "UCL temperature" is the air temperature within the urban canopy layer (canyon) and "surface temperature" is the average temperature of various surfaces making up the ground cover. The red bars in Figure EX-15 represent the effects of vegetation canopy alone; the blue bars represent the effects of cool surfaces alone; and the green bars represent their combined effects plus the effects of heat-emission reductions from electrification.

Figure EX-15: Temperature effects of combination of measures in D07. Vertical axis is change in temperature in degrees C.

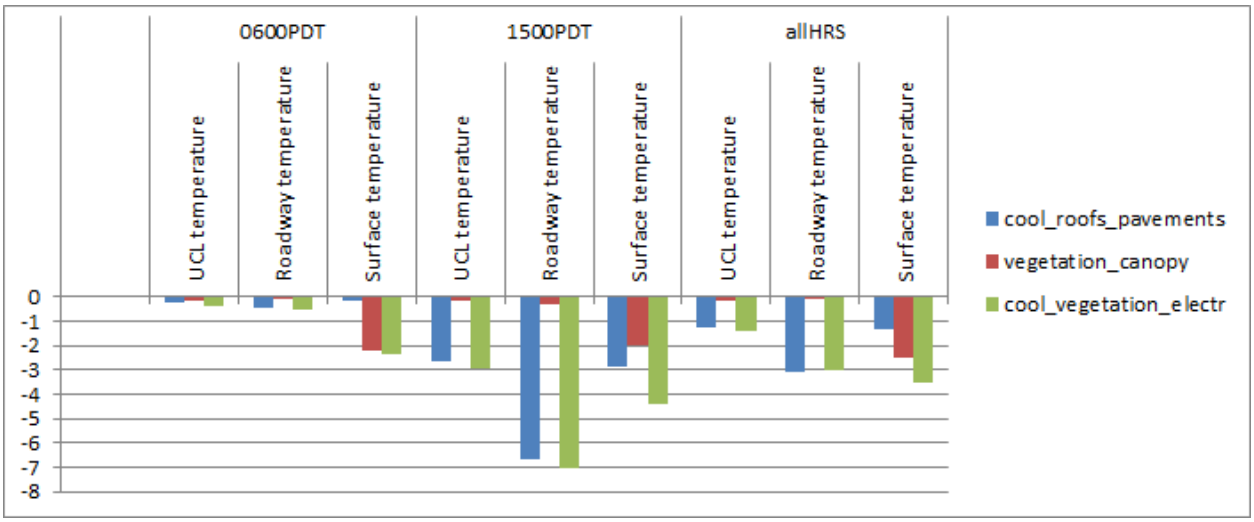

E.9.5 Cool walls

The potential impacts of cool walls were quantified for a scenario where wall albedo was increased from a current average of 0.15 to a maximum value (capped at) 0.40. Figure EX-16 shows the cooling effects as averaged over time intervals (periods) of interest, representing various summer conditions in the City of Elk Grove. As expected, the wall albedo effects are largest during the daytime reaching up to a maximum average localized cooling of 1.4 ºC.

Figure EX-16: Averaged temperature effects of cool walls.

E.10 CHARACTERIZING THE IMPACTS OF CHANGES IN CLIMATE AND URBANIZATION ON THE FUTURE UHII

The changes in local meteorology corresponding to conditions of future climate were evaluated by applying the Altostratus-modified urban WRF in dynamically downscaling the 2050 RCP 4.5 and RCP 8.5 CCSM4 climate-model fields and using them along with future urbanization and land-use change projections (per USGS LUCAS).

The characteristics of the future UHII are dictated mainly by two effects: (1) in areas currently urbanized, the main impacts on the temperature field and the UHII are those from local climate-change effects, whereas (2) in areas that will be urbanizing between now and 2050, the impacts on air temperature will result from both changes in land use (urbanization) and changes in climate. In general, the UHII in 2050 RCP 8.5 is larger than in RCP 4.5, as one would like to expect – however, there are deviations from this tendency, as seen in Table EST-8 and Figure EX-17, in the areas of Yuba City / Marysville and Woodland (first two sets of bars in the figure).

What the results suggest for these two areas may seem counter-intuitive at first, i.e., that the UHII can be slightly smaller (in this example time period) in RCP 8.5 than in RCP 4.5. The reason is that the non-urban areas surrounding Yuba City / Marysville and Woodland warm up faster (on the long run) than the urban areas in these two regions. This might be the result of lower vegetation cover in the non-urban areas than in the urban ones in these two regions (discussed in the report). Since these non-urban areas warm up slightly faster than the urban ones in this case, the UHII, by definition, becomes smaller – despite the fact that the absolute urban temperatures are higher in RCP 8.5 than in RCP 4.5. In all other parts and areas of the study domain, the RCP 8.5 UHII is larger than the RCP 4.5 UHII, as seen in Table EST-8 and Figure EX-17.

Table EST-8. All-hours UHII and changes (temperature equivalent in °C).

Domain	Area	All-hours UHII (temperature equivalent °C)		
		2013-2016	2050 RCP 4.5	2050 RCP 8.5
D05	Yuba City / Marysville	2.41	2.96	2.64
D06	Woodland	2.14	2.80	2.57
D07	Sacramento AB617 A, B, D	4.48	5.00	5.13
D07	Sacramento AB617 C, E, G	2.33	2.67	2.99
D08	Granite Bay	5.07	5.55	5.72
D08	Roseville	5.83	6.42	6.63
D09	El Dorado Hills	4.91	5.02	5.22
D09	Folsom	4.86	5.46	5.62
D10	Placerville	1.36	1.59	1.60

Figure EX-17: Changes (increases) in the UHII from current climate and LULC to 2050.

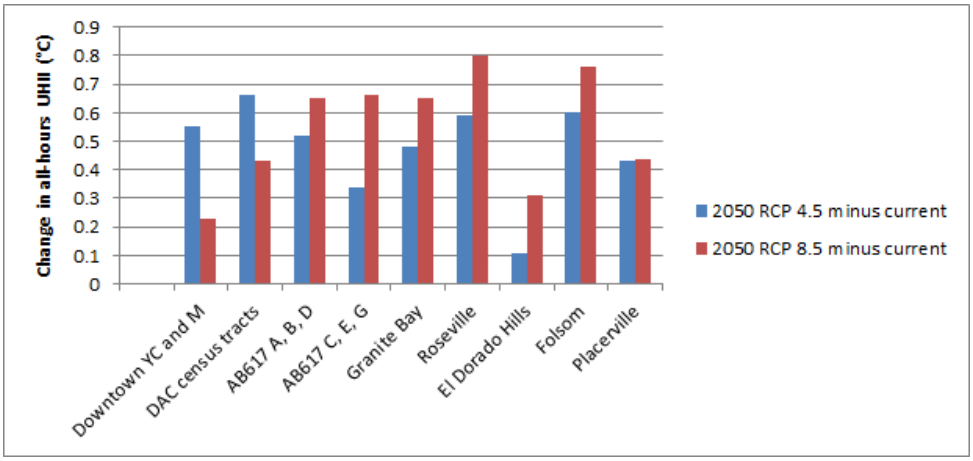

E.11 QUANTIFYING THE LOCAL OFFSETS TO THE UHII IN FUTURE CLIMATES AND URBANIZATION

The effects of local, community-scale heat-mitigation measures (i.e., at the 500-m level) were re-evaluated as in Section E.8, but this time in the context of future climate and land use. The goal was to assess the effectiveness of local mitigation measures in offsetting the future-climate UHII, e.g., as characterized in Table EST-8. In Tables EST-9 and EST-10, the future-climate all-hours UHII in 2050 is presented for each of the areas identified earlier and for RCP 4.5 and RCP 8.5, respectively, along with the effects of mitigation measures in a standalone mode of implementation (if combined, the effects can be larger, as discussed earlier, but are not linear).

The model results show that the effectiveness of the mitigation measures in 2050 is similar to their effectiveness in the current climate. In other words, the UHII attainment levels for various measures are of the same magnitudes in 2050 (RCP 4.5 and RCP 8.5) as in current climate – compare the last two columns in Tables EST-9 and EST-10 with the last two columns in Table EST-4. This is because the increased extent of urbanization, while contributing to additional local warming, also means an increase in technical potential (i.e., area available) for the deployment of mitigation measures, thus keeping the UHII offset levels similar to those in current climates or slightly larger in some cases.

As was the case for current conditions, shown earlier in Table EST-4, some measures in future climates (Tables EST-9 and EST-10), even in standalone fashion, can completely offset the local future-climate UHII. And, as before, when neighboring communities also implement UHI mitigation measures, the local benefits increase significantly. It is reiterated here that these are localized effects, i.e., temperature changes at or near the surface of the modified roadways or air temperature within the urban canyons of the selected communities, which can explain the different effectiveness of cool pavements alone versus combinations of cool roofs and pavements, as discussed in Section E.8, above.

Table EST-9: Potential of local projects in mitigating the all-hours UHII in future climate (2050 RCP 4.5) and urban land use.

Project area	All-hours Tair UHII (°C)**		Localized/no advection UHII attainment local mitigation only	Localized+advection UHII attainment local mitigation+advection
D05	2.96			
Yuba City / Marysville		Cool roofs / pavements	-47%	-73%
Downtown YC and M		Cool pavements	-37%	-63%
		Electric vehicles	-6%	-31%
		Vegetation cover	-57%	-83%
D06	2.80			
Woodland		Cool roofs / pavements	-46%	-80%
DAC census tracts		Cool pavements	-53%	-87%
		Electric vehicles	-5%	-39%
		Vegetation cover	-39%	-73%
D07	5.00			
Sac / SE Sac		Cool roofs / pavements	-26%	-62%
AB617 A, B, D		Cool pavements	-28%	-64%
		Electric vehicles	-5%	-41%
		Vegetation cover	-30%	-66%
D07	2.67			
Sac / SE Sac		Cool roofs / pavements	-49%	-87%
AB617 C, E, G		Cool pavements	-52%	-90%
		Electric vehicles	-9%	-47%
		Vegetation cover	-55%	-93%

Project area	All-hours Tair UHII (°C)**		Localized/no advection UHII attainment local mitigation only	Localized+advection UHII attainment local mitigation+advection
D08	5.55			
Granite Bay		Cool roofs / pavements	-25%	-50%
		Cool pavements	-31%	-56%
		Electric vehicles	-6%	-30%
		Vegetation cover	-19%	-44%
D08	6.42			
Roseville		Cool roofs / pavements	-22%	-54%
		Cool pavements	-27%	-59%
		Electric vehicles	-5%	-37%
		Vegetation cover	-16%	-48%
D09	5.02			
El Dorado Hills		Cool roofs / pavements	-30%	-50%
		Cool pavements	-34%	-54%
		Electric vehicles	-4%	-24%
		Vegetation cover	-22%	-43%
D09	5.46			
Folsom		Cool roofs / pavements	-27%	-53%
		Cool pavements	-31%	-57%
		Electric vehicles	-4%	-29%
		Vegetation cover	-20%	-46%
D10	1.59			
Placerville /		Cool roofs / pavements	-75%	-99%
Diamond Springs /		Cool pavements	-101%	-125%
El Dorado City		Electric vehicles	-5%	-29%
		Vegetation cover	-82%	-106%

Table EST-10: Potential of local projects in mitigating the all-hours UHII in future climate (2050 RCP 8.5) and urban land use.

Project area	All-hours Tair UHII (°C)**		Localized/no advection UHII attainment local mitigation only	Localized+advection UHII attainment local mitigation+advection
D05	2.64			
Yuba City / Marysville		Cool roofs / pavements	-53%	-79%
Downtown YC and M		Cool pavements	-42%	-67%
		Electric vehicles	-6%	-32%
		Vegetation cover	-64%	-90%
D06	2.57			
Woodland		Cool roofs / pavements	-50%	-83%
DAC census tracts		Cool pavements	-57%	-91%
		Electric vehicles	-6%	-39%
		Vegetation cover	-42%	-76%
D07	5.13			
Sac / SE Sac		Cool roofs / pavements	-25%	-61%
AB617 A, B, D		Cool pavements	-27%	-63%
		Electric vehicles	-5%	-40%
		Vegetation cover	-29%	-64%
D07	2.99			
Sac / SE Sac		Cool roofs / pavements	-43%	-83%
AB617 C, E, G		Cool pavements	-47%	-86%
		Electric vehicles	-8%	-47%
		Vegetation cover	-49%	-88%

Project area	All-hours Tair UHII (°C)**		Localized/no advection UHII attainment local mitigation only	Localized+advection UHII attainment local mitigation+advection
D08	5.72			
Granite Bay		Cool roofs / pavements	-25%	-48%
		Cool pavements	-30%	-54%
		Electric vehicles	-5%	-29%
		Vegetation cover	-18%	-42%
D08	6.63			
Roseville		Cool roofs / pavements	-21%	-53%
		Cool pavements	-26%	-57%
		Electric vehicles	-5%	-36%
		Vegetation cover	-16%	-47%
D09	5.22			
El Dorado Hills		Cool roofs / pavements	-29%	-47%
		Cool pavements	-32%	-51%
		Electric vehicles	-4%	-22%
		Vegetation cover	-21%	-40%
D09	5.62			
Folsom		Cool roofs / pavements	-27%	-51%
		Cool pavements	-30%	-55%
		Electric vehicles	-3%	-28%
		Vegetation cover	-20%	-44%
D10	1.6			
Placerville / Diamond Springs / El Dorado City		Cool roofs / pavements	-75%	-100%
		Cool pavements	-100%	-125%
		Electric vehicles	-5%	-30%
		Vegetation cover	-81%	-106%

E.12 SUMMARY RANKING OF HEAT-MITIGATION MEASURES IN FUTURE CLIMATES AND LAND USE

The following chart in Figure EX-18 summarizes the rankings of measures discussed above for 2050 RCP 4.5 and RCP 8.5 and provides a comparison to the rankings under the current climate and land use / urbanization levels that were summarized in Figure EX-6. The chart is color-coded so that black is most effective and near-white is least effective. Again, the caveat regarding case02 should be reiterated (an extreme measure) and that it should be excluded from this comparison to a certain extent.

From Figure EX-18, the following can be observed in terms of ranking the cooling potential of various measures:

1. For the 0600-PDT UHII:
    a. The rankings of mitigation measures (order) are similar and consistent across all regions.
    b. Within each region, the rankings are similar across current and future climates.
2. For the 1300-PDT UHII:
    a. The rankings are different across the regions.
    b. In Davis and Sacramento, the rankings are different in future climate than they are in current climate (but are similar in RCP 4.5 and 8.5).
3. For the 1400 – 2000 PDT UHII:
    a. The rankings are different across the regions.
    b. In Woodland, the rankings are different in future climate than they are in current climate (but are similar in RCP 4.5 and 8.5).
4. For the 1500 PDT UHII:
    a. The rankings are different across the regions.
    b. In Auburn, Davis, El Dorado Hills, and Yuba City, the rankings are different in future climate than they are in current climate (but are similar in RCP 4.5 and 8.5).
5. For the all-hours UHII:
    a. The rankings are different across the regions.
    b. Within each region, the rankings are similar across current and future climates.

This type of information may be useful to planners if they need to specifically target certain times of day, e.g., peak temperatures, or are interested in mitigating all-hour UHII averages for a particular region.

Figure EX-18: Summary of urban-heat mitigation potential: ranking of measures case01 through case31 by cooling effectiveness (darker to lighter = largest to smallest cooling) in future climate (2050). Note that case02 should be excluded in some analysis. Also note that this is impacts on air temperature, not UHII.

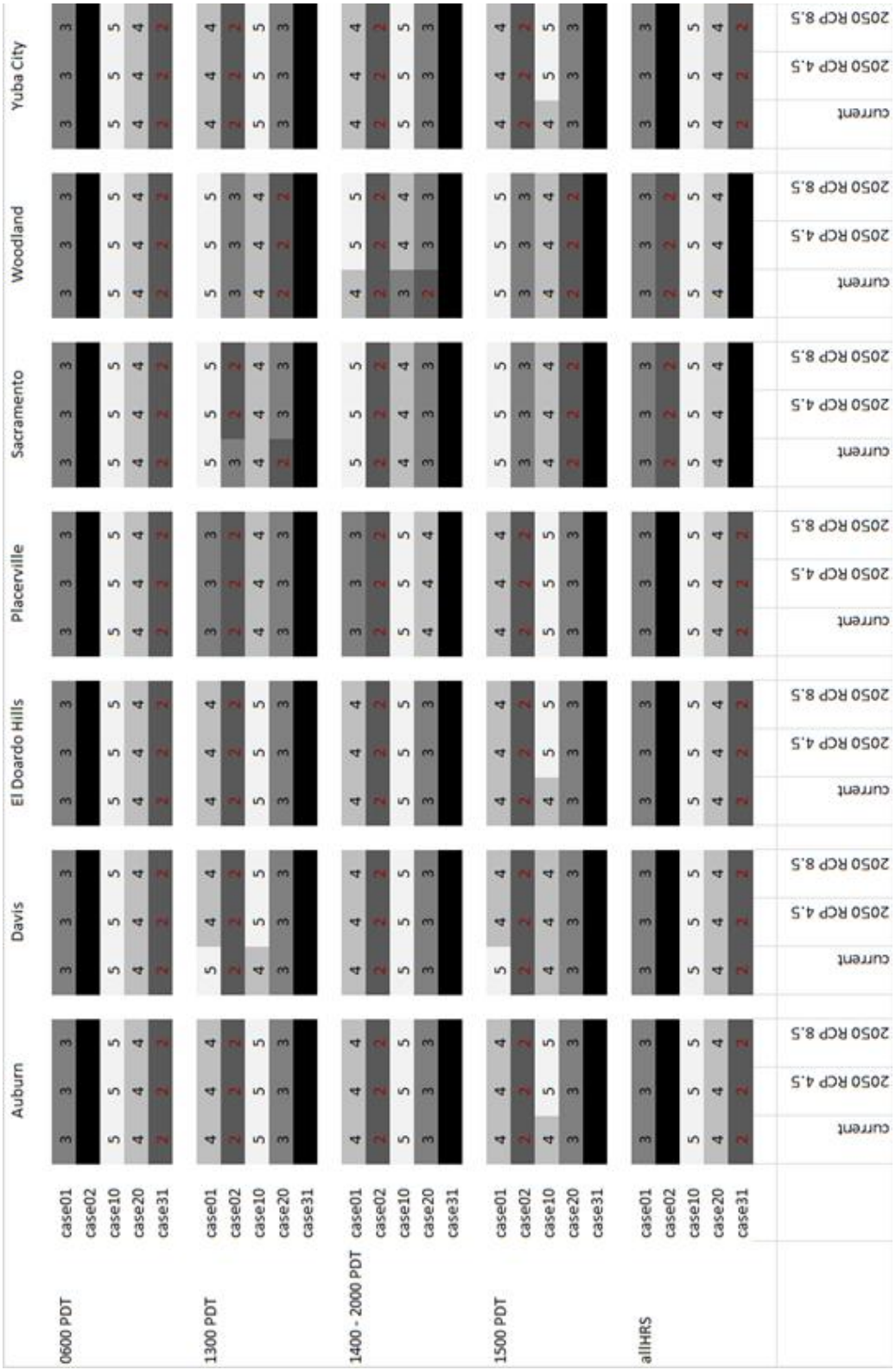

E.13 CONCLUSION AND QUALITATIVE TAKEAWAYS

In concluding this Executive Summary, a few qualitative talking points, or takeaways, from the foregoing discussion are provided, in no particular order:

1. Significant urban-heat pollution exists throughout the 6-counties Capital region. The UHI and the UHII are larger in urban areas that are (1) more densely built up, (2) cover a larger geographical area, (3) located at the downwind end of an urban zone (trajectory-wise), (4) located at higher elevations, and (5) surrounded by non-urban areas that cool down significantly faster at night.
2. While temperatures in the region generally increase from current climate to future (e.g., to 2050 RCP 4.5 and then to 2050 RCP 8.5), the corresponding UHII also increases in this direction except for two urban areas where the UHII can be smaller in RCP 8.5 than in RCP 4.5 (although still larger than in current climate). This is a result of accelerated warming in the surrounding non-urban areas.
3. It is possible and highly feasible to mitigate the current UHI and offset the UHII (in some cases completely) using materials and practices that are reasonable and readily used throughout the 6-counties Capital region. The proposed UHI mitigation measures are reasonable – meaning they do not require some hypothetical or extreme implementation levels, only what is already available and used in the existing market and current practices.
4. Mitigation measures can offset the local UHII in standalone fashion, in some cases completely. Various combinations of measures can further attain or further offset the UHII, although the total effects of combinations of measures are not linear (not simple sums) and generally smaller than the sums of the individual cooling effects of various components.
5. The measures can have significant beneficial effects in terms of public heat health as indicated by their ability to lower the warning levels in the National Weather Service Heat Index (NWS HI). This was assessed by modeling various UHI-mitigation scenarios in this study, in both current and future climates.
6. The cooling measures can significantly reduce or completely erase the number of heat-wave days during several excessive-heat event periods identified in the study.
7. The mitigation measures are as effective under conditions of future climate and land use as they are under current conditions.
8. Different mitigation measures affect urban heat and temperature differently during different times of the day. Hence it is possible to target certain specific time intervals, e.g., peaks, night, day, or all hours (per a community or city's needs) by choosing a specific mitigation measure or combinations of measures.

9. If, in addition to a community's heat-mitigation actions, neighboring communities also implement UHI-mitigation measures, the local cooling effects could double (although there is a range of effects depending on location, time, specific measures, etc.).
10. Some measures that are not conventionally associated with urban cooling (or urban heat island mitigation), such as (1) vehicle electrification, (2) solar PV installations, and (3) smart urban growth, all appear to have significant urban-cooling effects.
11. The cooling effects are beneficial across various urban areas in the Capital region, including AB617 and disadvantaged communities, which can help improve thermal comfort, reduce emissions of air pollutants, and improve air quality.
12. In this modeling study, ranking of mitigation efficacy was done for each region, each measure, and each time interval (e.g., specific hours, a range of hours, or 24 hours, etc.) for current and future climates and land use. Some areas or time intervals have a consistent ranking of measures, others vary by location, and others vary in future climate relative to current conditions.
13. Information generated in this modeling study can be used by Caltrans, SMAQMD, LGC, the cities and communities in the Capital region to prioritize projects and implementation of various measures or in the allocation of resources per urban-heat criteria under current climate conditions as well as for future climate and land use.

1. INTRODUCTION

Hot weather can cause a myriad of unwanted effects including heat-health impacts, increased cooling energy demand, higher emissions of air pollutants, and worsening air quality (Taha 2015a; Alfaro et al. 2004, 2006; Founda and Santamouris 2017; Gershunov et al. 2009; Li and Bou-Zeid 2013). Thus, urban areas in the warmer parts of the world have implemented or begun to implement various measures to combat heat, whether urban or not. In the context of heat-mitigation measures, it is useful to distinguish between the terms "urban heat" and "urban heat island" (UHI) or "urban heat island index" (UHII) and clarify some of the concepts involved.

To re-state the obvious, the goal of this and similar studies is to design and implement measures that reduce urban heat, not urban heat islands per se. In other words, the goal is to cool down the ambient air in any hot urban area, regardless of how much hotter or cooler it may be compared to some other urban areas or some non-urban reference points (the latter being the definition of the urban heat island). Thus, if so, what is the purpose of characterizing urban heat islands (or the UHII)? The simple answer is that the UHI and UHII are just quantitative indicators or yardsticks that tell us how much cooling we can reasonably expect to achieve at a certain urban location. In other words, the UHI (or UHII) simply is an indicator as to how much cooling is needed to bring the temperature of a certain urban location down to that of a nearby non-urban area (Taha 2013a, 2017). Of course, the actual cooling that is achievable at a certain location could be smaller or larger than the UHI or UHII, as will be discussed later in this report.

Furthermore, there is a subtle difference between the UHI and the UHII, as used in this study, that can be defined as follows:

UHI: Urban heat island, is an instantaneous temperature difference between an urban location and a non-urban reference point (e.g., an instantaneous measurement). Thus, the units of UHI are ^{o}C.

UHII Urban heat island index, is a cumulative (total) temperature difference between an urban location and a non-urban reference point calculated over a determined time interval, e.g., several hours or several days, etc. The units of UHII are degree-hours, e.g., ^{o}C · hr, or degree-days, and so on.

An important point to emphasize here is that urban heat indicators quantified in this study (including UHI and UHII, for example) are air-temperature-based, not derived from skin-surface temperature (such as shown in many studies of "urban hot spots" that are basically satellite / thermal remote-sensing imageries) also referred to as "surface-temperature urban heat island", or SUHI. Hence, the spatial patterns of urban heat analyzed in this study and presented in this report differ from those seen in satellite imagery most of which simply shows hot roofs and roadways surrounded by cooler vegetation or pervious surfaces. This is discussed in some more detail later in Section 3.4.

Having established this basic understanding of urban heat and the purpose of computing the UHI (or UHII), we can now proceed with discussing the characterization of the UHI and UHII in the Capital region.

In 2015, the California Environmental Protection Agency (Cal/EPA) developed a first-of-its-kind Urban Heat Island Index (UHII) for the state of California (Taha and Freed 2015). In that effort, four levels of the UHII were defined (Taha 2017), as shown in Figure 1-1. However, only the Level-1 UHII was developed and modeled in that undertaking (additional information can be found at https://calepa.ca.gov/wp-content/uploads/sites/6/2016/10/UrbanHeat-Report-Report.pdf).

Essentially, the various levels were defined such that the progression of the UHII, as an indicator or metric, goes from characterizing the problem (Level-1) to characterizing the mitigation (Level-4).

Figure 1-1: UHII levels (source: Taha 2017).

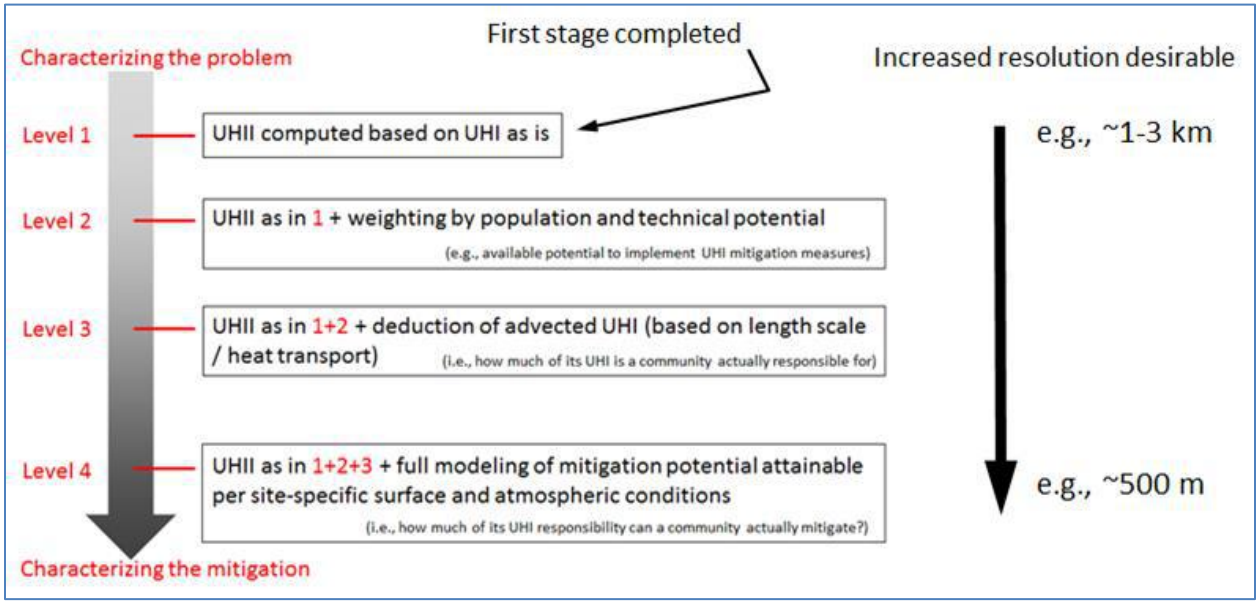

In consultation with the Cal/EPA and the stakeholders in that study, the Level-1 UHII was defined in its simplest form as in equation (1-1):

$$UHII = \sum_{h=1}^{H(JJA)} \left[T_{u(k),h} - min\left(T_{u(k),h}, T_{nu\,(k),h} \right) \right] \qquad (1\text{-}1)$$

where the *UHII* (C·hr) is computed over several time periods, e.g., June, July, and August (JJA) over several years, T_u is urban air temperature at a specific location *k*, T_{nu} is non-urban, upwind, reference temperature corresponding to (i.e., paired with) urban location *k*, and *h* is the time index,

e.g., hour. The non-urban temperature (T_{nu}) corresponding to each urban point *k* is time-varying and depending on wind approach direction, that is, the direction from which the wind is approaching the urban location *k*.

The same definition of the UHII was used in this study, except that it was applied to longer and different time periods in years 2013 through 2016. In the simplest terms, per Equation 1-1, the UHII is the temperature difference between an urban location *k* at hour *h* and its corresponding upwind non-urban reference point (at the same hour), but only when the urban temperature is larger than the non-urban reference temperature.

In the present study, several aspects of the UHII beyond Level-1 were directly or indirectly addressed and discussed in the report. To evaluate UHII Levels 2 – 3, i.e., heat generation and transport, the following factors were considered:

- Heat that is generated at the transportation system (corridors, roadways, facilities, infrastructure, stations, rail, airports, maintenance yards, etc.) and transported to other areas -- quantified by accounting for surface physical properties of roadways and infrastructure, as well as heat emissions from motor vehicles;
- Urban heat advected to the transportation system -- quantified by evaluating the effects of surface physical characteristics in urban areas, morphological / geometrical properties, and heat emissions; and
- Urban heat generation and transport throughout the region -- a result of large-scale climate effects and forcings.

When mitigating or reversing urban-heat effects, which entails the development of a Level-4 assessment of the changes in UHII, the following factors were considered:

- Direct effects, e.g., impacts on structural integrity / lifespan of pavement and on transportation infrastructure as indicated by changes in surface temperature and other related variables;
- Indirect effects, e.g., impacts on air temperature in urban corridors and the advection of cooler air into the surrounding urban areas (which has implications on thermal conditions, emissions, and air quality);
- Thermal and environmental comfort of the transportation system's users, as quantified by changes in air temperature near the ground and in the urban canopy layer; and
- Emissions impacts, e.g., lower pavement temperatures and shading of parking lots and structures (with solar PV or vegetation canopy) thus reducing evaporative / fugitive hydrocarbon emissions, as quantified by changes in surface and air temperatures in areas affected by mitigation measures.

Urban-heat mitigation measures can benefit both the transportation system and the communities which they serve. Urban cooling, i.e., reductions in surface and air temperatures, can benefit the transportation sector in some or all of the following ways, depending on scale and proximity to areas where the mitigation measures are implemented:

- Reducing the impacts of heat stress on roadways (in current climate, heat events, and future climate), which has benefits in terms of slowing the aging of bitumen, the stiffness of asphalt, deformation and rutting, i.e., past certain surface temperature thresholds, as well as reducing tensile stresses, cracking, and impacts on expansion joints;
- Reducing surface traffic restrictions as urban cooling can bring down air temperature below the thresholds that dictate roadways closures (e.g., asphalt temperature threshold for roadways to remain open to traffic), as well as potential reductions in wildfires in nearby areas;
- Minimizing impacts on operations at stations, parking lots, facilities and the impacts on users of the transportation system, by reducing heat and radiation (comfort, energy), reducing impacts on vehicles air conditioners, tires, overheating, evaporative emissions, reducing heat effects on railways (buckling or failure), and reducing impacts on aircraft operations, e.g., required runway length for takeoffs and landings; and
- City-wide impacts on transportation infrastructure.

The urban-cooling measures can also benefit the communities by improving summer thermal comfort, reducing heat stress, reducing cooling energy demand, air-pollutant emissions, and improving public air-quality and heat health.

Considering all of the above factors, the SMAQMD, with interest from communities in the area, as well as SMUD, LGC, the cities, and local organizations, participated in this SB-1/Caltrans-funded effort to build upon the Cal/EPA Level-1 UHII and address the needs and impacts of the transportation sector. Thus, the overarching objectives of this project were to:

- Characterize and quantify urban heat in current and future climates in the 6-counties Capital region (including the counties of Sacramento, El Dorado, Placer, Yuba, Sutter, and Yolo);
- Identify urban areas and transportation-system zones that are subject to higher temperatures under conditions of current and future climate and land use (urbanization); and
- Evaluate and quantify the effectiveness of urban-cooling measures and rank their potentials in mitigating heat (in current and future climates).

Various cooling measures have been investigated in the past via either modeling or observations (or some combinations thereof), e.g., Taha (2007, 2015a,b), Akbari et al. (1999), Georgescu et al. (2014), Gilbert et al. (2017), and Levinson et al. (2007), among many other U.S. and international

studies, too numerous to list here. In this study, the following measures were evaluated and modeled:

- For area-wide transportation and non-transportation urban cooling, that is, to achieve regional effects benefiting urban areas as a whole in the 6-counties Capital region, the measures considered in this study and evaluated at the coarse (2-km) scale included:
  - Cool roofs and cool pavements;
  - Vegetation canopy cover;
  - Combinations of measures; and
  - Smart growth (for future climate), i.e., infill or greenfield developments.

- For localized effects at community scale, transportation corridors, specific roadway projects, and specific neighborhoods, i.e., to achieve localized benefits regardless of whether any actions are taken by other communities at the regional scale, the following measures were considered (these were modeled at 500-m resolution):
  - Cool roofs;
  - Cool pavements;
  - Vegetation canopy cover;
  - Vehicle electrification;
  - Solar PV; and
  - Cool walls.

Green roofs were not considered in this study in response to recommendations from the project TAC because of their high initial and maintenance costs, as well as effectiveness issues.

It is important to note that the urban-heat mitigation measures and mitigation levels proposed and modeled in this study, and whose effects are presented in this report, are reasonable, i.e., can already be found in the study region and are not some hypothetical or extreme measures as is sometimes assumed in this type of studies. Thus:

1. The reasonability of the measures means that the scenarios studied in this project are based on reasonable increases in albedo, vegetation cover, vehicles electrification, etc. This means that we are simply encouraging people to use more of the measures and products that are already available and easily implemented locally, not some extreme levels or hypothetical mitigation measures that are impractical. In other words, this is simply encouraging a wider use of materials and methods that already exist in the current market and in current construction and building practices.
2. Keeping the modification levels reasonable also means minimizing any potential negative effects on the atmosphere, e.g., air quality impacts, that could result from decreased mixing (venting), increased UV albedo, increased biogenic emissions, or increasing visual

environmental concerns such as glare (these factors will be discussed in Section 5.6). Thus, the mitigation levels assumed in this study were also meant to be kept below "city-specific" thresholds in each area, if identifiable, as discussed in Taha (2005, 2007).

2. LAND USE AND LAND COVER ANALYSIS

2.1 OBJECTIVES OF LULC ANALYSIS

The main purposes of land-use and land-cover (LULC) analysis in this project were to (1) define study domains and modeling grids for the project area with focus on the 6-counties Capital region, (2) acquire most recent LULC datasets as needed, (3) reformat and recast the data into direct and derived parameters for input to the land-surface and atmospheric models used in this study, (4) characterize LULC change and urbanization over time, e.g., through 2050 or beyond, and (5) develop technical potentials for deployment of mitigation measures in various parts of the region.

This task entailed assembling and analyzing LULC data for current conditions (by merging various sources of information, as discussed in Section 2.3, below) and future growth scenarios. The task also involved characterization of urban morphology / geometry, transportation system, roadways, infrastructure, and deriving the surface physical properties of relevance to urban heat, e.g., albedo, canopy cover, roughness length, soil moisture, shade factor, various plan-, top-, and frontal-area densities for calculations of various building and vegetation-canopy parameters, and anthropogenic heat emissions, using a bottom-up approach discussed in the following sections. Another product from the LULC analysis is technical potential for the development of mitigation scenarios and identification of implementation levels

2.2 SELECTION OF MODELING DOMAINS

This study used a version of the WRF modeling system that is continuously modified, updated, and customized at Altostratus Inc., as described elsewhere (e.g., Taha 2017, 2008a-c; Taha et al. 2018). An analysis and modeling domain structure was configured for this study (Figure 2-1) based on a nested-grid system of 54, 18, 6, 2, and 0.5 km resolutions. The 2-km grid is used to model and analyze the impacts of heat mitigation measures at the regional scale in the Capital region, i.e., the effects that will result from region-wide implementation of certain strategies. The 500-m grids, on the other hand, are used to evaluate localized mitigation measures at the project or community scales (independently of actions taken collectively at the regional scale) and to evaluate in more detail their localized impacts. The 500-m grids (Figure 2-2) were configured based on LULC analysis and feedback received from the SMAQMD and LGC. The grids also contain all areas of interest, current and future, that were identified by the project TAC. For each of these 2-km and 500-m modeling grids, LULC was thoroughly characterized and data were generated for input to the land-surface and atmospheric models, as discussed below.

Figure 2-1: Ten-domain atmospheric-model grids configuration (D01-D10). Domain D04, shown again in yellow in Figure 2-2, below, encompasses the Capital region.

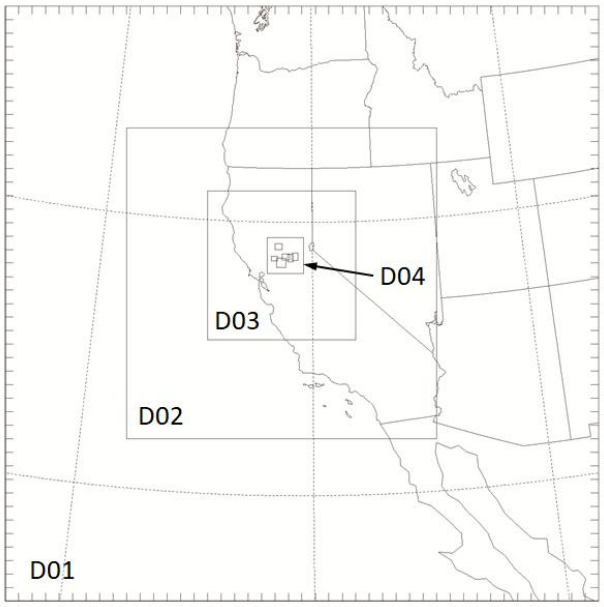

Figure 2-2: 2-km domain (yellow rectangle, D04), for the Capital region, and 500-m grids (white rectangles, D05-D10) for detailed simulations of localized heat-mitigation measures. Also shown in the figure are areas deemed of interest by the project TAC and participating cities and organizations (blue, red, and grey overlays and blue markers). The latitude/longitude coordinates of the 2-km domain corners are also shown.

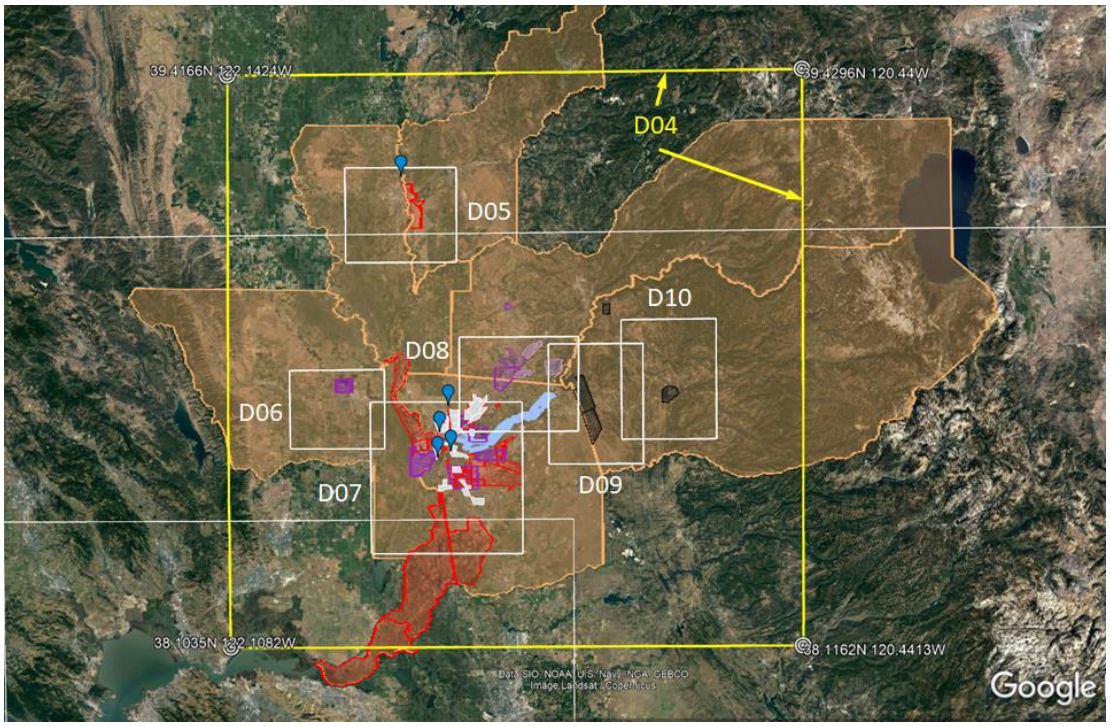

Figure 2-3 shows the actual positions of the model grid points (also known as mass points or cell centers) in the study region. The white dots represent the 2-km domain (D04) grid points and the smaller dots are those of the 500-m domains (D05 – D10). They are difficult to distinguish in Figure 2-3 because of their close spacing – thus Figure 2-4 is provided as an example to show the detail of how the 500-m grids mesh with the 2-km grid, in this case how D07 (red dots) meshes with D04 (white dots). Viewing these figures at a magnification of ~300% allows for a better distinction of various features and grid points.

Each point in these 2-km and 500-m domains was characterized in terms of LULC and surface physical properties based on a detailed bottom-up approach developed at Altostratus Inc. (Taha 2017, 2013a,b). At the finer scales, this approach is more accurate and area-specific than the common urban surface characterizations used in atmospheric modeling such as NUDAPT / WUDAPT (Ching et al. 2009) or similar other approaches used with the WRF modeling system. Depending on available information, some characterizations are reverted to default, others are extremely grid-specific, that is, based on data available from cities, counties, or other GIS data sources, as well as from in-situ observations. The detailed bottom-up surface characterization approach used in this study is discussed in the following sections.

Throughout this report, and aside from the coarse domains D01 – D03 (Figure 2-1), the finer-scale domains are identified and referred to as follows:

D04: This is a 2-km grid encompassing all six counties in the Capital region (yellow rectangle in Figure 2-2 and white dots in Figure 2-3)
D05: 500-m grid for the Yuba City / Marysville area (in Yuba and Sutter counties)
D06: 500-m grid encompassing Woodland (in Yolo County)
D07: 500-m grid for various areas in Sacramento (in Sacramento County)
D08: 500-m grid for the Roseville and Granite Bay areas (in Sacramento and Placer counties)
D09: 500-m grid encompassing Folsom, El Dorado Hills, and surrounds (in Sacramento and El Dorado counties)
D10: 500-m grid for the Placerville area (in El Dorado County).

As mentioned above, the fine-scale domains were selected per recommendations received from the project TAC, SMAQMD, and LGC (see markups in Figure 2-2). In addition, SMAQMD (2018) identified ten AB617 communities (DACs) in the Sacramento area, as shown in Figure 2-5. Thus, domains D07 and D08 were also designed to encompass these communities.

Figure 2-3: Locations of atmospheric-model mass points in the study region. D04 is 2-km in resolution and all other domains (D05 – D10) are at 500-m resolution.

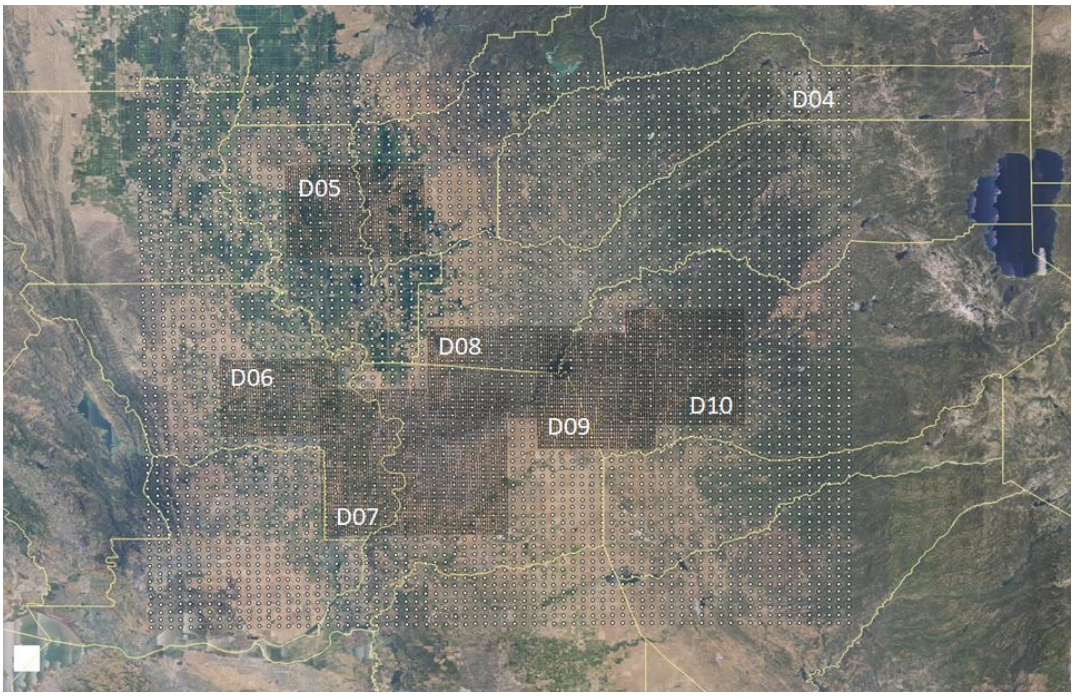

Figure 2-4: Example showing details of meshing between a 500-m grid (D07, small red points) and a 2-km grid (D04, white circles).

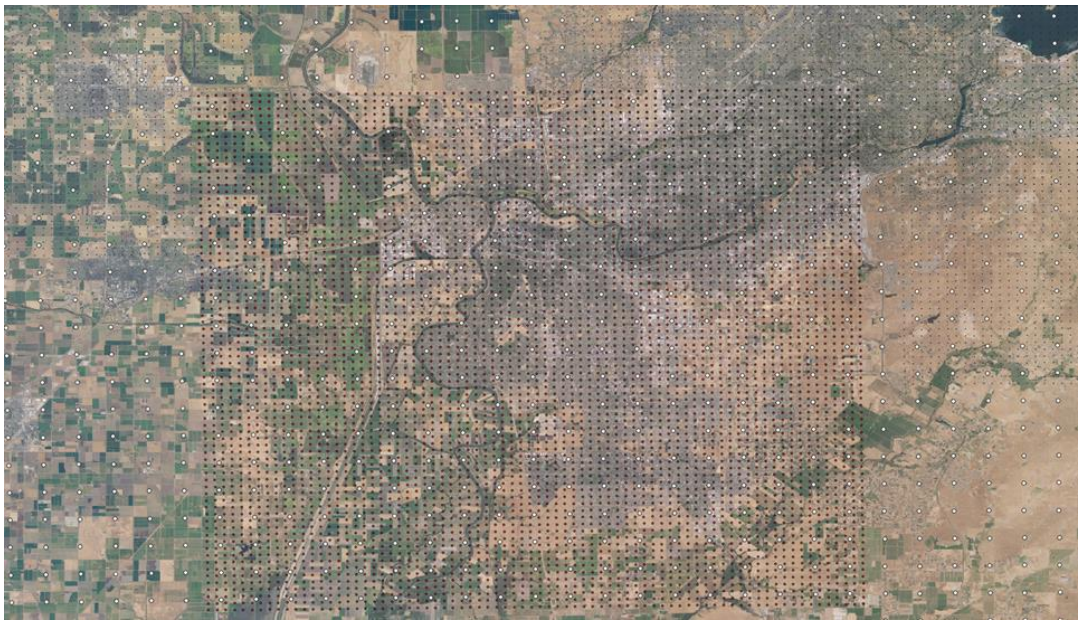

Figure 2-5: AB617 disadvantaged communities A – J, per SMAQMD (2018).

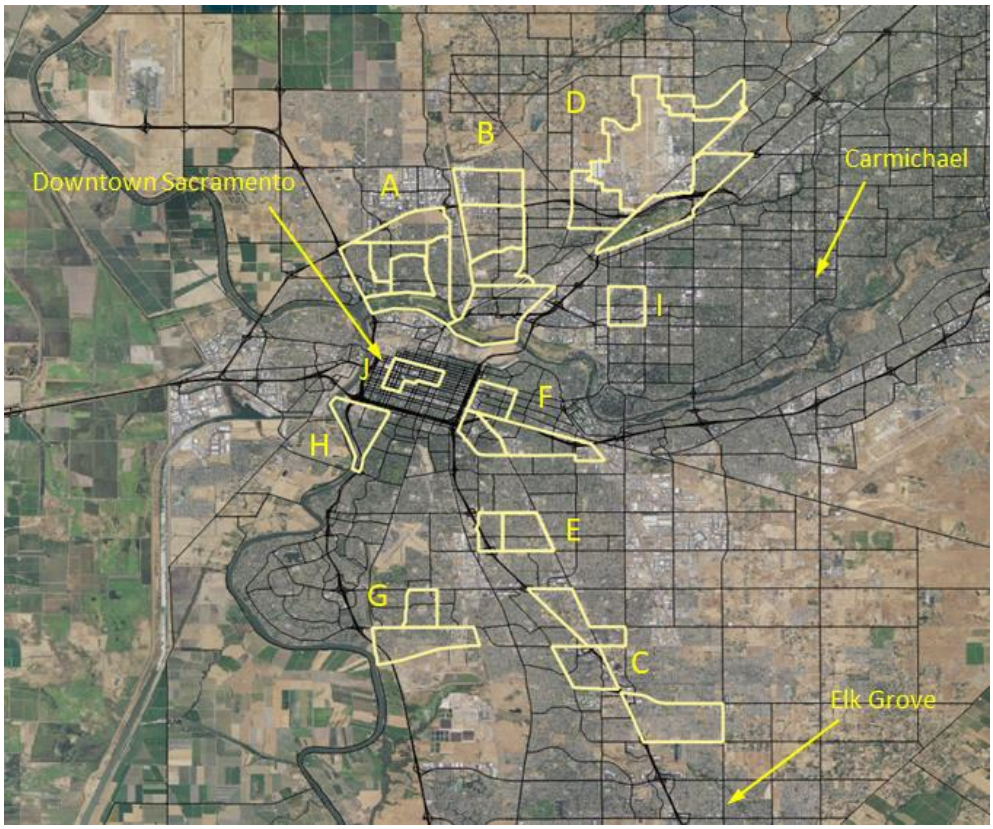

2.3 LULC AND SURFACE-PROPERTIES DATASETS

To develop a detailed, bottom-up surface physical characterization input to the meteorological model, several LULC data types were used in this project. These included:

- 30-m National Land Cover Data (NLCD 2011 / 2016) for current LULC (MRLC 2011);
- 30-m NLCD 2011 / 2016 impervious cover, for current conditions (MRLC 2011);
- 30-m USGS Anderson Level-II and Level-IV LULC, for current conditions (Anderson et al. 2001);
- USGS LUCAS datasets for future-year LULC projections through year 2100 (Sleeter et al. 2017a,b);
- 1-m to 30-m USGS Anderson Level-IV LULC, from SACOG for current conditions (data.sacog.gov);
- Google Earth Pro urban morphological and land-cover data for specific area characterizations of urban morphology (google.com);

- 1-m aerial photography-based roof albedo characterizations (Lawrence Berkeley National Laboratory) for current conditions, https://heatisland.lbl.gov/projects/projects-california-roof-albedo (Ban-Weiss et al. 2015);
- 1-m area-specific urban morphological and geometrical data (National Urban Datasets and Portal Tool N/WUDAPT) for current conditions (Burian et al. 2003; Ching et al.2009);
- 1-m Earth Define / CAL FIRE urban tree canopy cover datasets (www.earthdefine.com);
- 1-m Quick Bird UFORE urban tree canopy dataset (UC Davis / USFS) for urban areas in the Sacramento region, current conditions (Simpson and McPherson 2007);
- MRLC canopy cover (30-m resolution) for current conditions (MRLC 2011); and
- MODIS albedo for current conditions (MRLC 2011).

In addition to the above, area-specific datasets were also used as suitable from the following sources:

- CALTRANS GIS: www.dot.ca.gov/hq/tsip/gis/datalibrary;
- SACOG regional GIS clearinghouse: https://www.sacog.org/regional-gis-clearninghouse;
- CalEnviroScreen 3.0: https://oehha.ca.gov/calenviroscreen (OEHHA 2013);
- Sacramento County: http://generalmap.gis.saccounty.net/JSViewer/county_portal.html#;
- Sacramento County general plan: http://www.per.saccounty.net/PlansandProjectsIn-Progress/Pages/GeneralPlan.aspx;
- City of Sacramento: http://data.cityofsacramento.org/datasets/general-plan;
- Sacramento County GIS: http://data-sacramentocounty.opendata.arcgis.com/;
- El Dorado County GIS: http://gem.edcgov.us/ugotnetextracts/;
- Sacramento County Building footprints: //data-sacramentocounty.opendata.arcgis.com/; and
- Sacramento County parcels information: //data-sacramentocounty.opendata.arcgis.com/.

The LULC datasets were analyzed and model parameters were calculated based on characterizations from the above-listed data sources. These datasets were used to develop grid cell-by-cell surface characterizations, as discussed in the following sections. Furthermore, crosswalks among different datasets were also established as needed to bridge the gaps in data coverage and provide parameters required as input to the atmospheric models. The crosswalks will be discussed later in this report.

2.3.1 Calculations of urban tree canopy cover based on Earth Define / CAL FIRE data

Calculations specific to this dataset were performed in this study to derive tree-canopy cover in those areas defined as urban (per Earth Define, www.earthdefine.com) in the domains of interest. Figure 2-6 (A) shows the data extent in this study domain and depicts the 1-m resolution canopy cover toggle (tree/no tree) in urban areas of the 6-counties region.

The data obtained from CAL FIRE / Earth Define were recast, vectorized, and modified (and used in combination with other data sources) to derive the model-input parameters related to vegetation cover that are needed in this study, including cover, leaf-area index, height, and geometrical properties of the canopy. The calculations were carried out at the 2-km level (D04) and then repeated at the 500-m resolution for domains D05 – D10. After vectorizing and aggregating, the data was re-gridded into the model's map projection for the specific domains to derive additional vegetation-related parameters such as albedo, roughness length, soil moisture, and shade factor (Taha 20-8a-c, 2017).

Examples from these calculations are shown in Figure 2-6 (B – h), where the caption below each figure identifies the corresponding domain. This canopy cover information is merged with the tree-cover data derived from NLCD 2011 / 2016 as well as from specific Sacramento-area datasets (discussed further below) to develop full-domain tree canopy characterizations.

Figure 2-6: (A) 1-m resolution urban tree canopy cover toggle (tree / no tree) based on Earth Define / CAL FIRE datasets for the study region and an example detail; (B – H) computed gridded tree cover in domains D04 – D10 (only in grid cells defined as "urban").

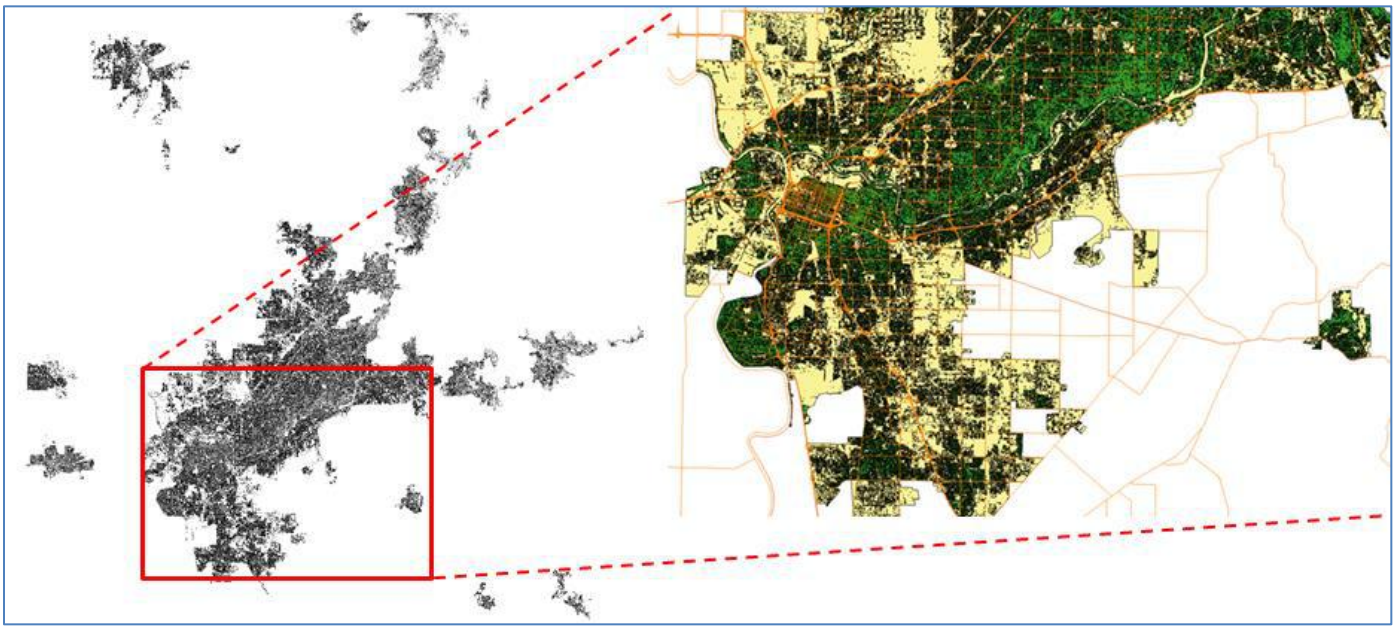

2-6.A

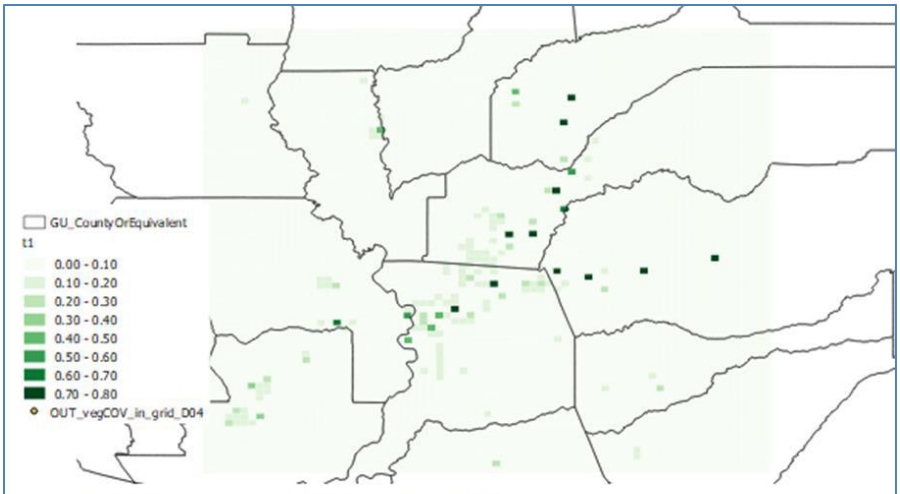

CALFIRE tree cover in D04 (2 km domain). Cover is only in urban land use.

2-6.B

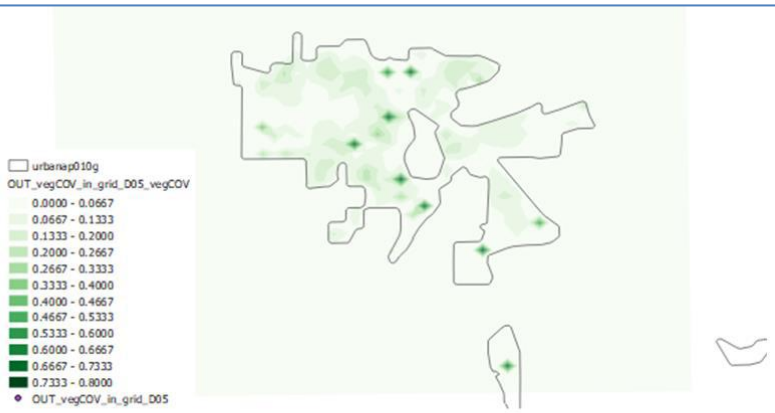

CALFIRE tree cover in D05 (500 m domain). Cover is only in urban land use. Black lines are approximate urban boundaries.

2-6.C

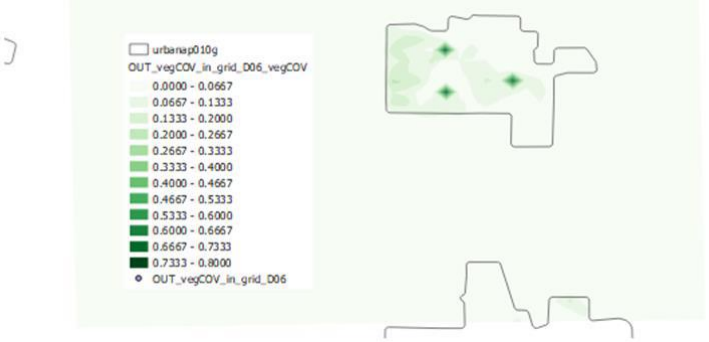

CALFIRE tree cover in D06 (500 m domain). Cover is only in urban land use. Black lines are approximate urban boundaries.

2-6.D

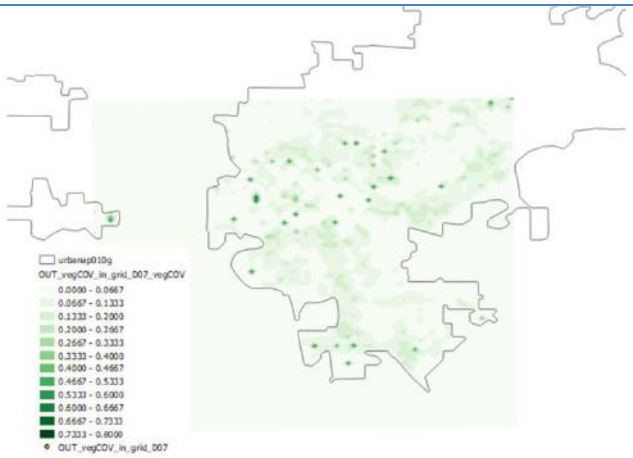

CALFIRE tree cover in D07 (500 m domain). Cover is only in urban land use. Black lines are approximate urban boundaries.

2-6.E

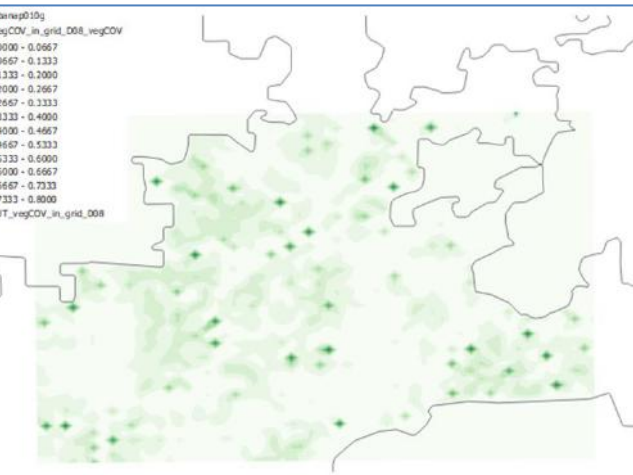

CALFIRE tree cover in D08 (500 m domain). Cover is only in urban land use. Black lines are approximate urban boundaries.

2-6.F

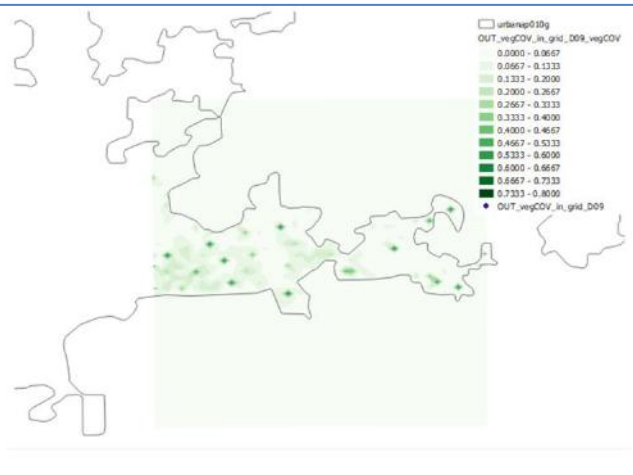

CALFIRE tree cover in D09 (500 m domain). Cover is only in urban land use. Black lines are approximate urban boundaries.

2-6.G

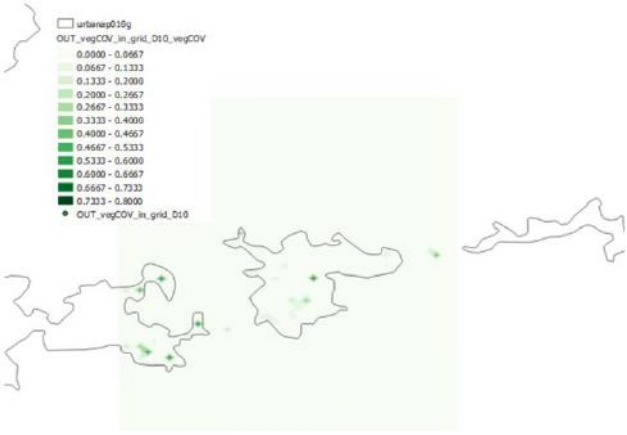

CALFIRE tree cover in D10 (500 m domain). Cover is only in urban land use. Black lines are approximate urban boundaries.

2-6.H

The maps in Figure 2-6 (B – H) show some discontinuity in coverage, areas of unusually large cover, or blank areas because of the distributions of urban cells in the domains (i.e., the CAL FIRE data exist only in urban cells). In other words, those blank areas in the figure actually contain vegetation cover in various amounts, e.g., crops, forests, open spaces, etc., but they don't appear in these figures because they are not in cells classified as urban. Areas with unusual cover were handled separately or excluded from the analysis as outliers.

Considering only those cells with vegetation cover greater than 0.01, i.e., urban cells as defined here, the median and range of vegetation cover are shown in Figure 2-7 and summarized in Table 2-1 (for the 500-m domains). Medians and quartiles are shown as boxes superimposed upon the scatter plots in each graph.

Thus, according to this dataset, the bulk of the canopy cover in urban areas of the Capital region rarely exceeds 0.26. The highest values are found in domains D07 and D08 representing central Sacramento and immediate surroundings. These may be in fact why central Sacramento and areas near downtown are generally cooler than other parts of the greater Sacramento region (as will be discussed in Section 3.4). This is also the reason why certain scenarios of canopy-cover increase in urban areas (larger than case01, see Section 5.5), are deemed to be hypothetical and unfeasible at this time.

Table 2-1: Median and range of canopy cover in urban cells of 500-m domains D05 through D10 (based on CAL FIRE / Earth Define datasets). The range in this table is not specified as difference between maximum and minimum values but, rather, the range of the bulk of the canopy cover values in the specified domains, as seen in Figure 2-7.

Domain (500-m grid)	Median of canopy cover	Range of canopy-cover bulk
D05	0.068	0.01 – 0.20
D06	0.055	0.01 – 0.15
D07	0.059	0.01 – 0.24
D08	0.059	0.01 – 0.26
D09	0.045	0.01 – 0.22
D10	0.027	0.01 – 0.14

Figure 2-7: Distribution of canopy cover in 500-m domains D05 – D10 (only in grid cells defined as urban) computed based on Earth Define / CAL FIRE data. Superimposed boxes show median and quartiles.

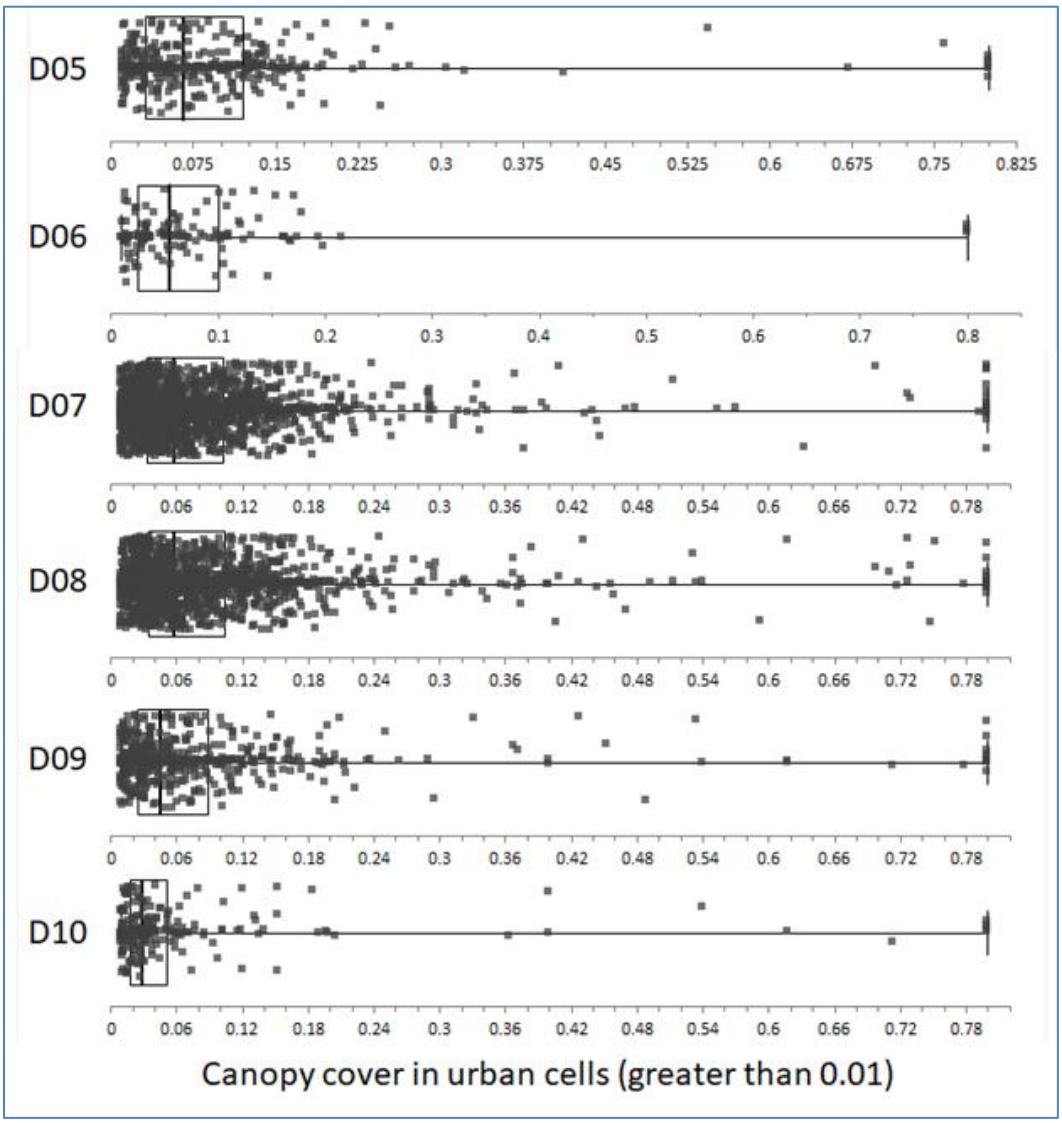

2.3.2 Calculation of canopy cover based on NLCD 2011 / 2016

To enhance the tree-cover characterizations beyond the Earth Define / CAL FIRE datasets (discussed above) and to bridge the data gap with canopy-cover information in non-urban areas, additional calculations were carried out using 30-m resolution NLCD 2011 / 2016 data (MRLC 2011) for the 500-m domains. The canopy-cover dataset in NLCD 2011 / 2016, developed by the U.S. Forest Service (USFS), covers both urban and nonurban areas.

Thus, the NLCD data were processed to remap and re-grid the information per the domain configurations used in this study. Examples from these calculations are shown in Figure 2-8 (A – H), where the computed cover is for the 2-km grid (D04) and for 500-m grids D05 - D10 (the caption below each figure identifies the domain). The results are also summarized in Figure 2-9.

Figure 2-8 (A – H): Gridded canopy cover computed from 30-m NLCD 2011, USFS datasets.

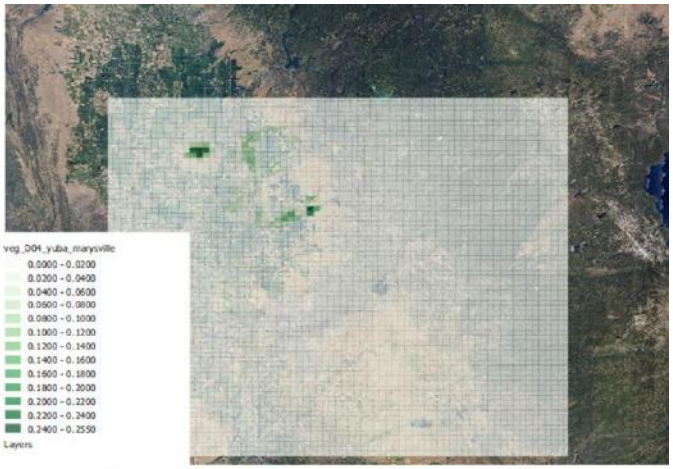

NLCD 2011-based calculations of canopy cover in D04 Yuba City / Marysville **2-8.A**

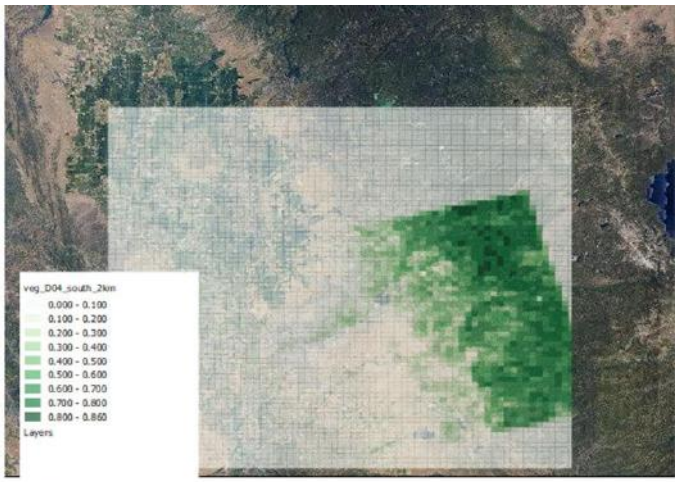

NLCD 2011-based calculations of canopy cover in D04 south 2km **2-8.B**

NLCD 2011-based calculations of canopy cover in D05 500 m domain **2-8.C**

NLCD 2011-based calculations of canopy cover in D06 500 m domain **2-8.D**

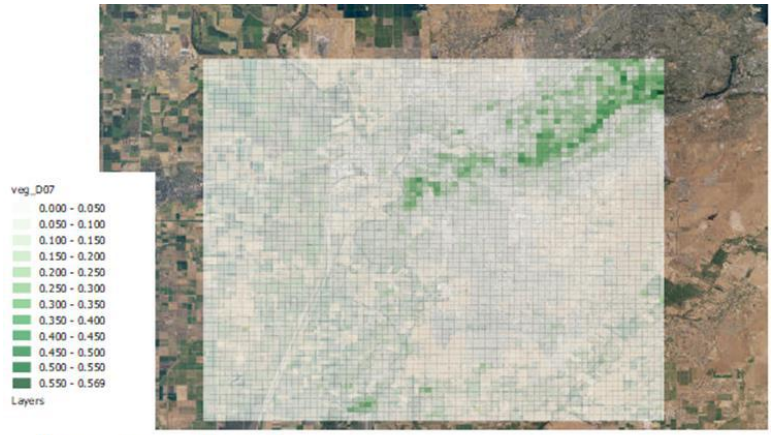

NLCD 2011-based calculations of canopy cover in D07 500 m domain **2-8.E**

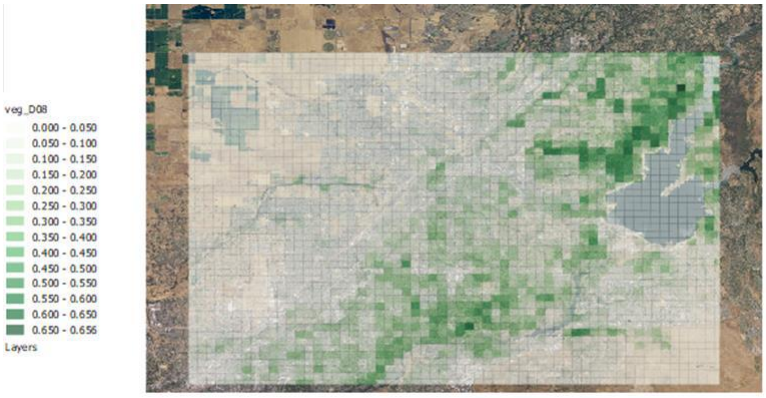

NLCD 2011-based calculations of canopy cover in D08 500 m domain **2-8.F**

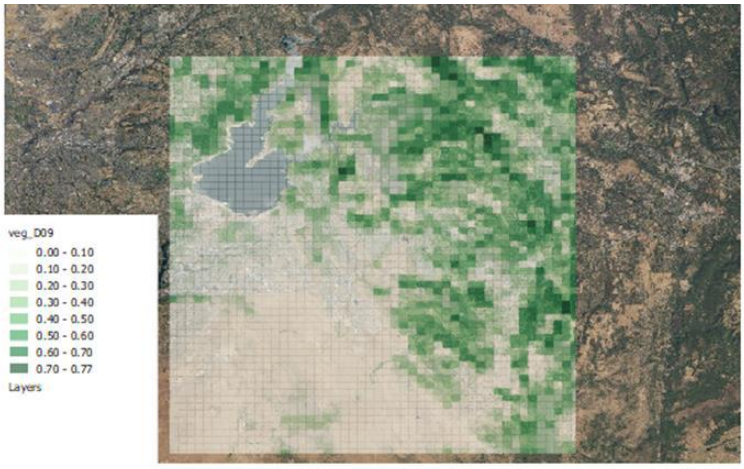

NLCD 2011-based calculations of canopy cover in D09 500 m domain **2-8.G**

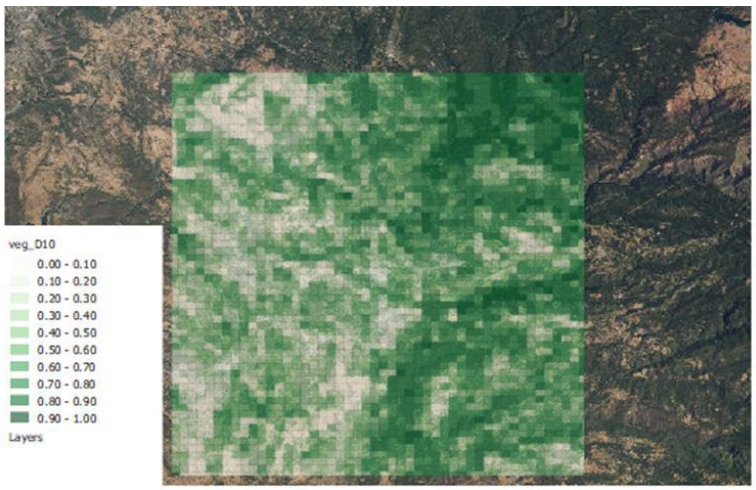

NLCD 2011-based calculations of canopy cover in D10 500 m domain **2-8.H**

Figure 2-9: Distribution of computed canopy cover in 500-m domains D05 – D10 (in urban and non-urban cells) based on NLCD 2011 / USFS data. Superimposed boxes show medians and quartiles.

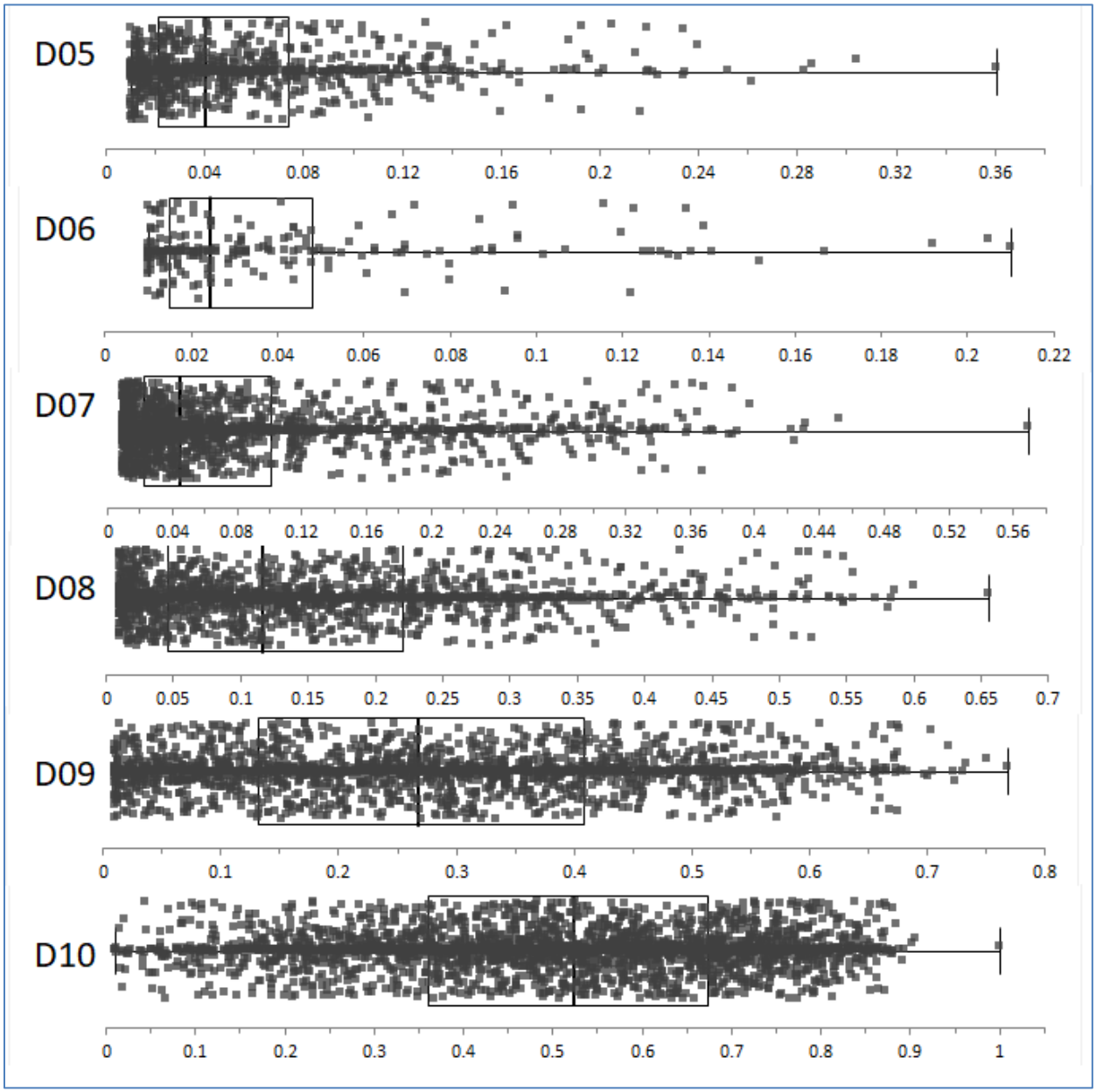

Canopy cover in urban and non-urban cells (greater than 0.01)

Compared to the urban-only canopy cover (from the CAL FIRE dataset, see Section 2.3.1), the inclusion of non-urban canopy cover in the analysis (Figure 2-9 and Table 2-2) shows that non-urban areas have larger canopy cover than their corresponding urban areas, in general, although a smaller canopy is seen in some cases, e.g., in the Yuba City / Marysville and the Woodland regions where non-urban canopy cover is smaller than the urban one (compare Tables 2-2 and 2-1).

This could be one reason why the non-urban areas in these two domains (D05 and D06) warm up faster than their corresponding urban areas, in future climate, producing a smaller UHII in 2050 RCP 8.5 than in 2050 RCP 4.5, as discussed in Section 6.6.

Combining the information from both sources discussed above serves as basis for the cell-by-cell characterization of canopy cover, i.e., following the bottom-up approach that directly characterizes cover without using LULC information as proxy (Taha 2008a-c; Taha 2017). As will be seen later, in some cases, additional information on tree cover, e.g., for a specific street or project site, can also be gleaned from Google Earth Pro.

Table 2-2: Medians and ranges of canopy cover in urban and non-urban cells in 500-m domains D05 through D10 based on NLCD 2011 / 2016 (USFS datasets). The range, in this table, is not specified as difference between maximum and minimum values but, rather, the range of the bulk of the canopy cover values in the specified domains, as seen in Figure 2-9.

Domain (500-m grid)	Median of canopy cover	Range of canopy-cover bulk
D05	0.040	0.01 – 0.160
D06	0.025	0.01 – 0.070
D07	0.045	0.01 – 0.360
D08	0.120	0.01 – 0.525
D09	0.260	0.01 – 0.650
D10	0.525	0.01 – 0.900

2.3.3 Calculations of impervious cover

Impervious cover in the NLCD 2011 / 2016 dataset (MRLC 2011) consists of roofs and ground-based paved surfaces at a resolution of 30 m. This is an important parameter to characterize in this study as it can provide an assessment of technical potential for the deployment of high-albedo materials on roadways and buildings. It can also provide a basis for computing dynamics- and physics-related parameters input to the models indirectly, e.g., roughness length or drag coefficients, soil moisture, anthropogenic heat emissions (tailpipe exhaust), and heat capacity. Gridded impervious fraction was computed for each domain as shown in the following examples (Figure 2-10), as identified by the captions below each figure.

The impervious cover information is also merged with the vegetation cover data to develop cell-by-cell characterizations of mitigation potential, particularly in the areas designated of interest by the project TAC.

Figure 2-10 (A – F): Gridded impervious cover computed based on NLCD 2011 datasets.

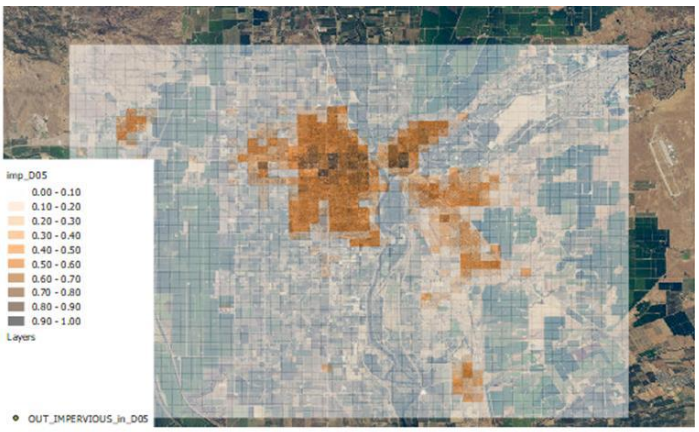

NLCD2011-based calculation of impervious cover: D05 500-m

2-10.A

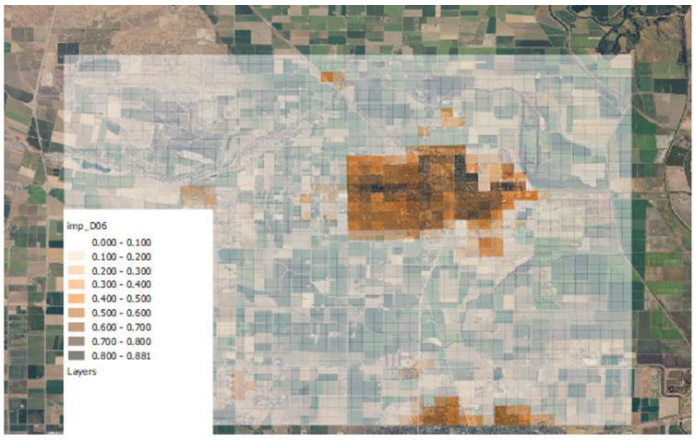

NLCD2011-based calculation of impervious cover: D06 500-m

2-10.B

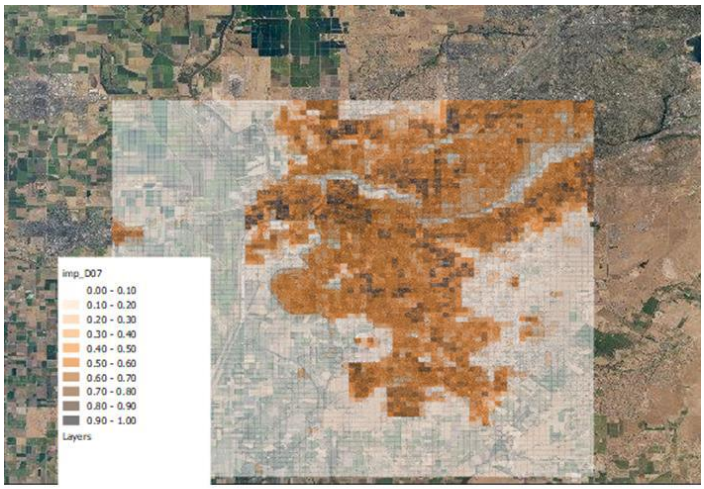

NLCD2011-based calculation of impervious cover: D07 500-m

2-10.C

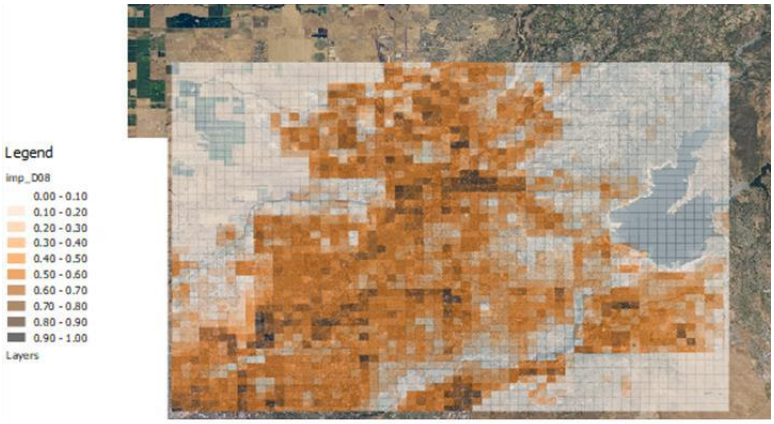

NLCD2011-based calculation of impervious cover: D08 500-m **2-10.D**

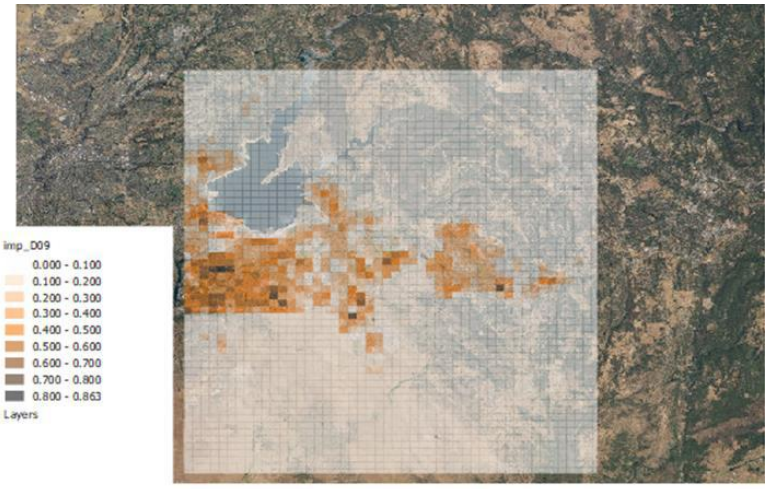

NLCD2011-based calculation of impervious cover: D09 500-m **2-10.E**

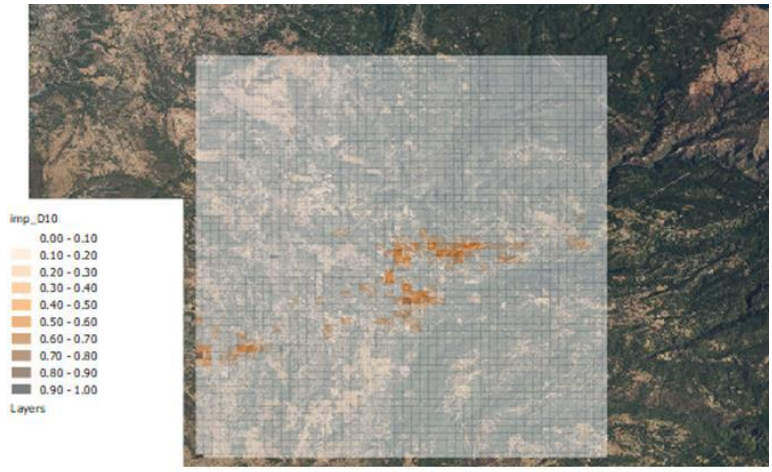

NLCD2011-based calculation of impervious cover: D10 500-m **2-10.F**

To characterize the distribution of impervious cover in the 500-m domains, values greater than 1% in each cell were examined. This analysis is visualized in Figure 2-11 and Table 2-3. It can be seen that except for domains D07 and D08 (the main urban Sacramento area), all other urban areas in the 6-counties Capital region have impervious cover below 28% (medians and inter-quartile ranges are indicated with superimposed boxes). In domains D07 and D08, the bulk of impervious cover is generally up to about 50%. Also, as a general estimate, roughly half of impervious cover is made up of roofs and the other half of pavements and roadways (Akbari et al. 1999; Rose et al. 2003). Cleary at any specific location it may be different but as an average over the domains, this is a sufficiently accurate characterization.

Figure 2-11: Distribution of impervious cover in 500-m domains D05 – D10 (in urban and non-urban cells) computed based on NLCD 2011 / 2016 data. Superimposed boxes show medians and quartiles.

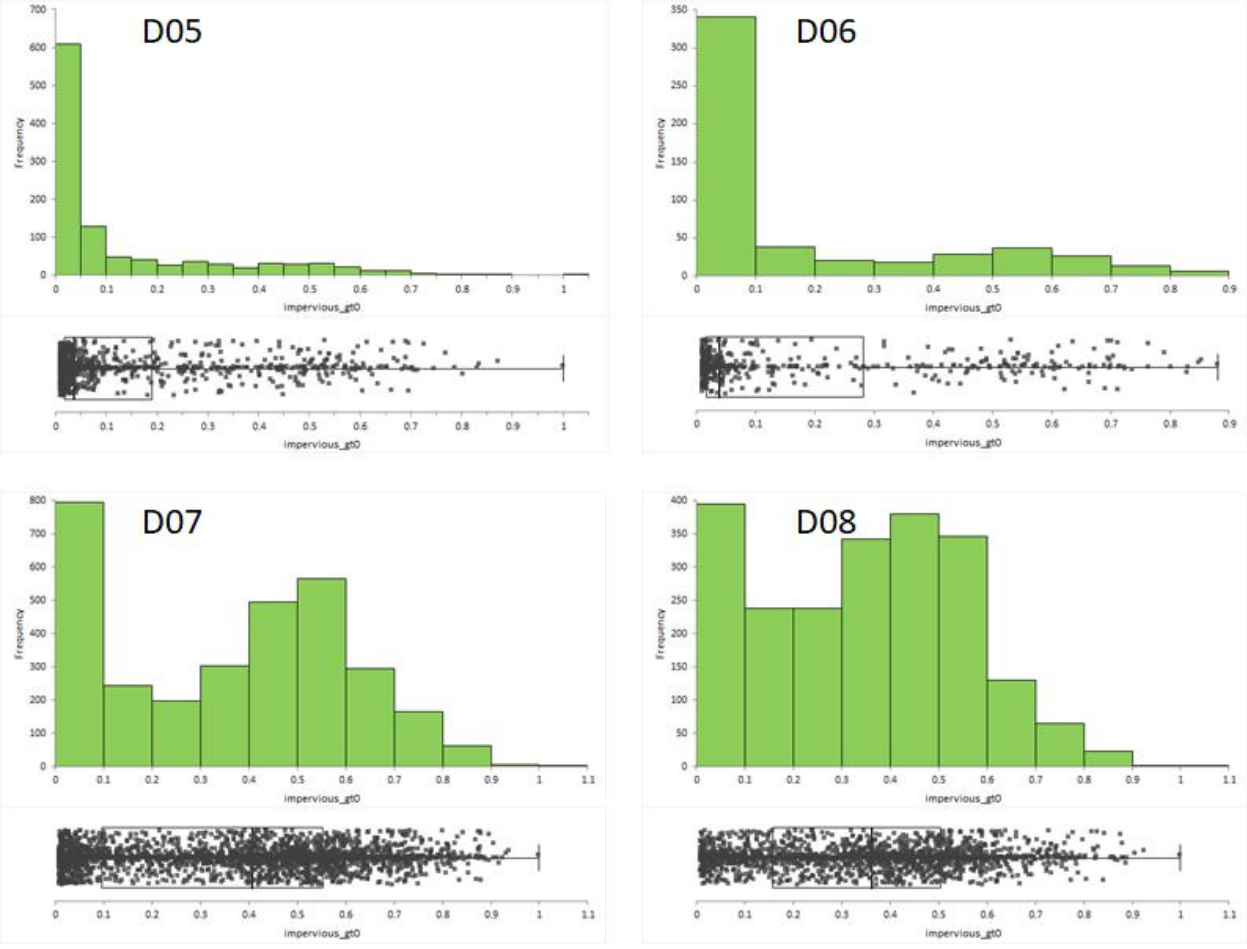

Figure 2-11, continued.

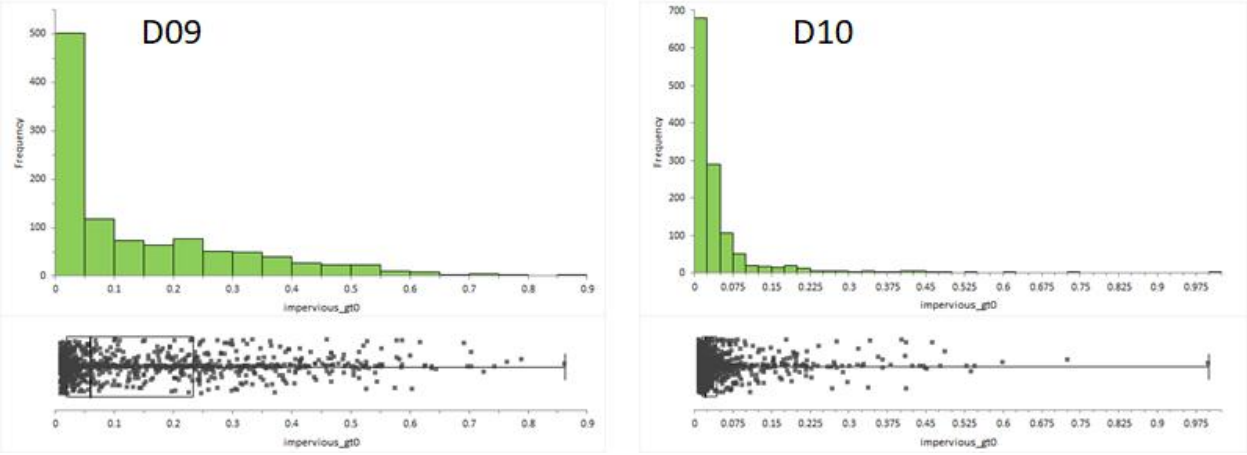

Table 2-3: Median, bulk ranges, and maxima of impervious cover in urban and non-urban cells in 500-m domains D05 through D10 based on NLCD 2011 datasets. The range in this table is not specified as difference between maximum and minimum values but, rather, the range of the bulk of the canopy cover values in the specified domains, as seen in Figure 2-11.

Domain (500-m grid)	Median of impervious cover	Range of impervious-cover bulk	Bulk maximum
D05	0.037	0.01 – 0.19	0.7
D06	0.040	0.01 – 0.28	0.8
D07	0.400	0.01 – 0.55	0.9
D08	0.360	0.01 – 0.51	0.8
D09	0.060	0.01 – 0.23	0.5
D10	0.020	0.01 – 0.04	0.2

Figure 2-12 shows the main transportation routes and their densities in the 6-counties Capital region. It is clear that the density of roadways is proportional to the impervious cover computed above. The transportation routes are a major component of LULC characterization and input to the atmospheric / land-surface models and have a significant impact on surface and air temperatures. In many of the figures in the following sections, these major routes stand out with different values of thermo-physical properties relative to those of the background.

We will also see later when discussing modeling results that urban heat is proportional to impervious fraction as is heat emission from mobile sources. Conversely, the cooling from increased albedo (e.g., cool roofs and pavements) also is proportional to impervious cover.

Figure 2-12: Main transportation routes in the study domain (data source: SACOG).

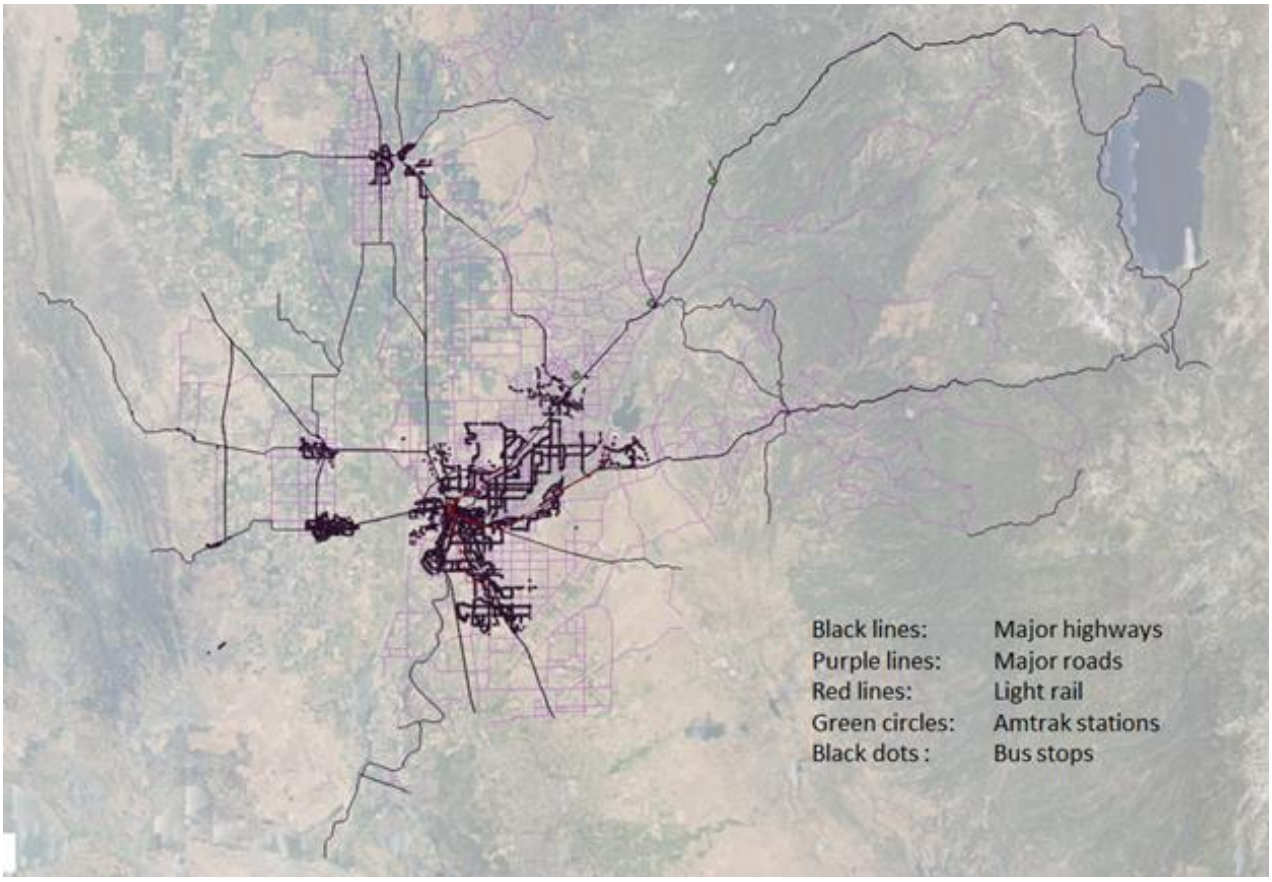

2.3.4 Calculations of thermo-physical parameters

Various thermo-physical parameters, depending on modeling scheme or parameterizations, are required to characterize the surface in the atmospheric models. In the 2-km domain, where the Altostratus AREAMOD approach was applied (Taha 2005, 2007, 2017), most of the needed parameters are standard, meaning similar to those used in standard WRF model, except that their derivation, pre-processing, and ingestion in the various model components are done differently from the standard WRF. In the AREAMOD approach, site-specific bottom-up characterization of model grid cells is carried out individually using any and all information that is available for each cell. At the 500-m level, on the other hand, additional parameters are needed beyond these standard variables, as discussed elsewhere in this report (i.e., in developing input to the urban WRF and the Altostratus-modified version of the urban canopy model, per Taha 2008a-c, 2017, 2019).

In this section, the calculations of some of the standard parameters are presented. Since these multi-parameter calculations are repeated for each of domains D04 to D10, figures resulting from this exercise will occupy considerable space. Thus, only the calculations for D04 (2 km) and D07 (500

m) are shown here as examples. Maps of variables and parameters for the other domains are included in Appendix A-1. Of these parameters, the most relevant to heat mitigation measures at the regional, 2-km level, are (1) urban fraction, (2) surface albedo, (3) vegetation cover / soil moisture, (4) roughness length, and (5) shade factor. These are relevant because the mitigation measures of interest usually involve perturbing one or more of these properties.

In this study, the parameters were computed based on different sources of information and spatial resolutions (listed above in Section 2.3) then scaled up to 500 m or 2 km depending on the domain. The actual process of deriving these parameters is quite lengthy and is discussed in Taha (2008a-c). Examples from this analysis are shown in Figure 2-13. Figures A – E are for domain D04 and Figures F – J are for domain D07 (as indicated above, other domains are presented in Appendix A-1). In the 500-m domains, these properties are further weighted by the non-urban fraction in each grid cell and the urban-fraction properties are based on site-specific information.

Figure 2-13 (A – J): Examples of computed gridded parameters for domains D04 and D07

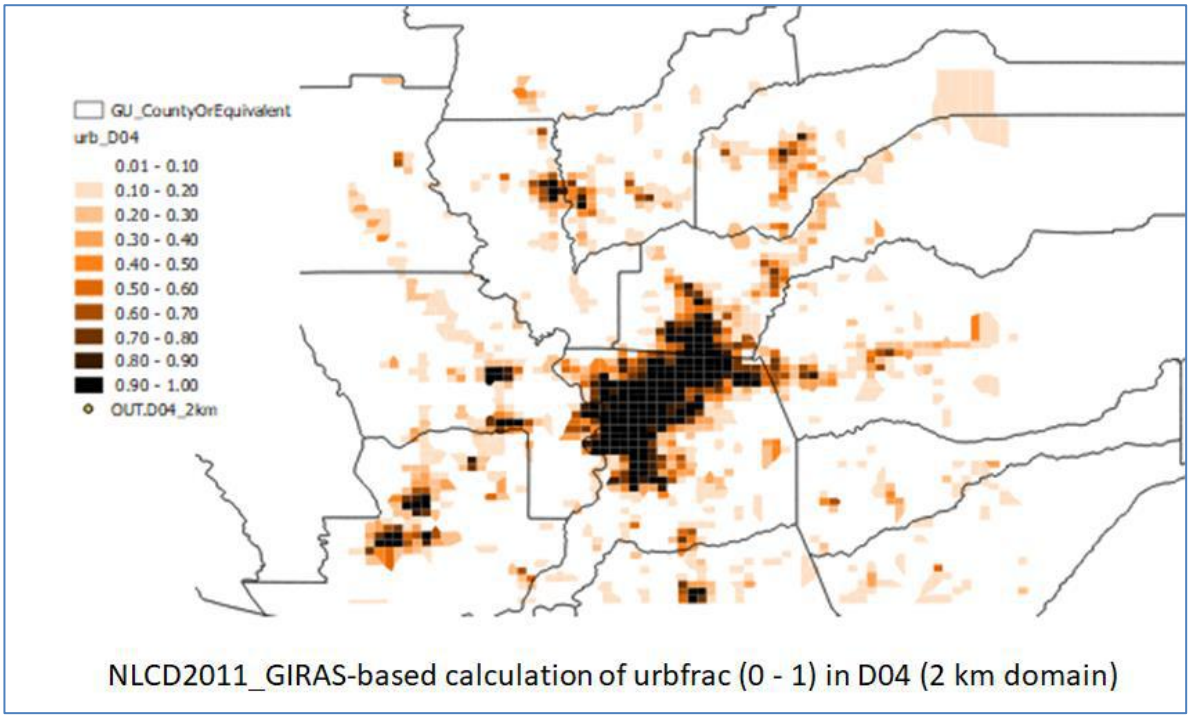

A

Figure 2-13, continued.

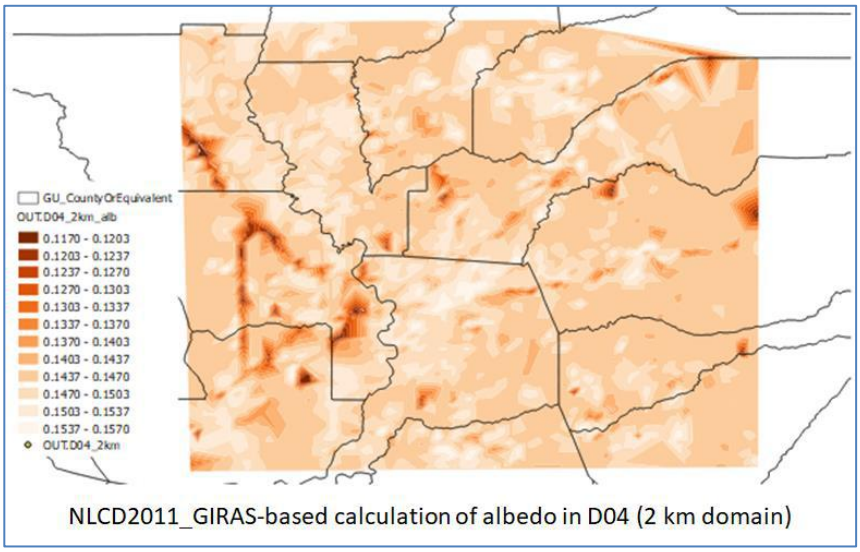

NLCD2011_GIRAS-based calculation of albedo in D04 (2 km domain)

B

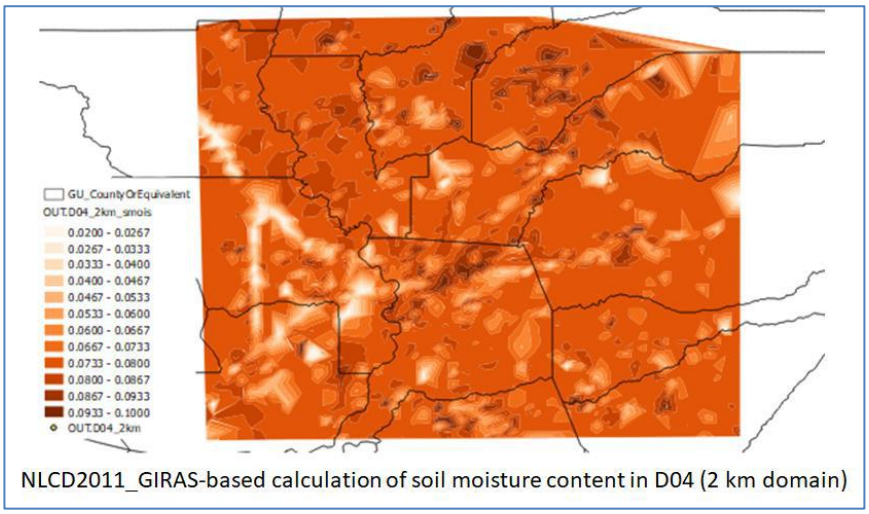

NLCD2011_GIRAS-based calculation of soil moisture content in D04 (2 km domain)

C

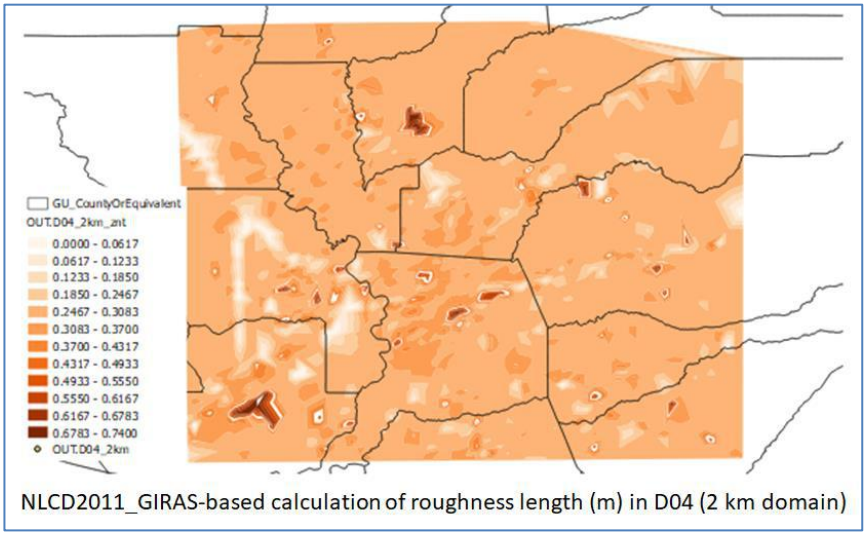

NLCD2011_GIRAS-based calculation of roughness length (m) in D04 (2 km domain)

D

Figure 2-13, continued.

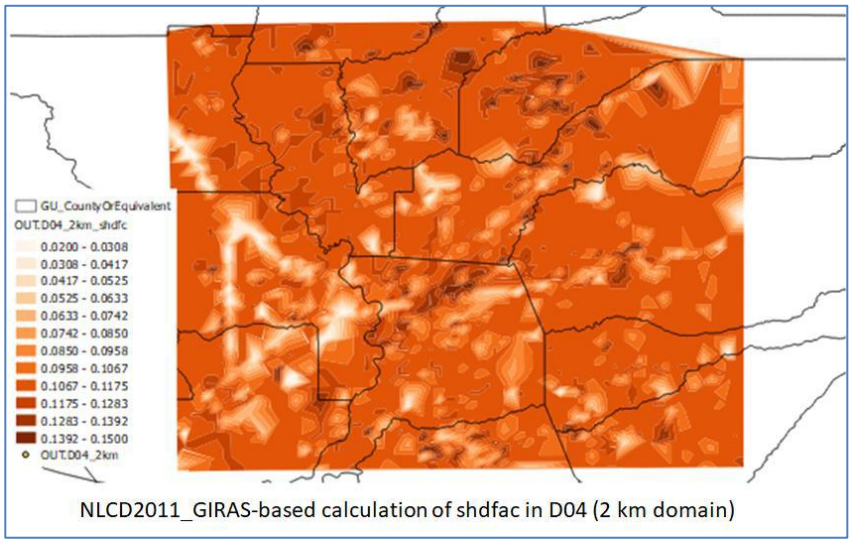

NLCD2011_GIRAS-based calculation of shdfac in D04 (2 km domain)

E

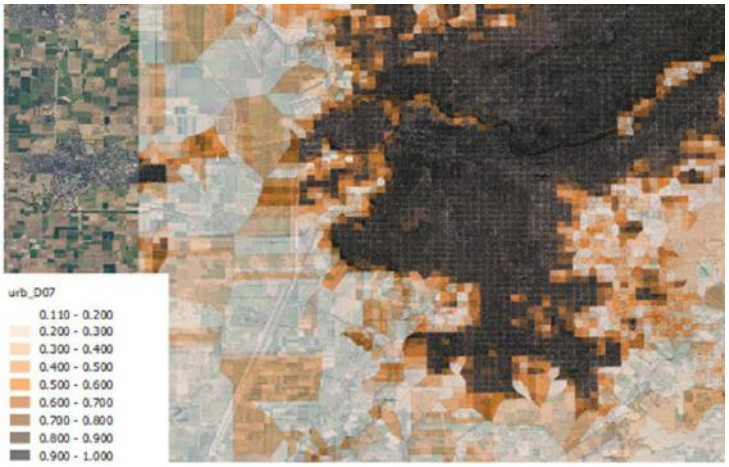

NLCD2011_GIRAS-based calculation of urbfrac (0 - 1) in D07 (500 m domain)

F

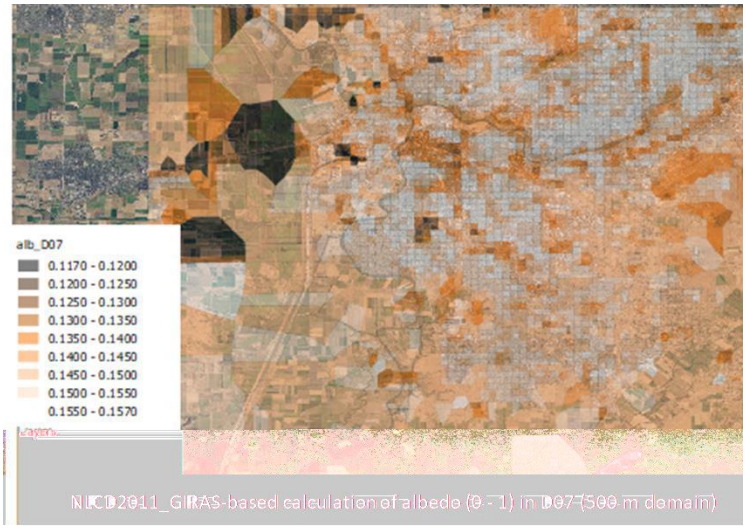

NLCD2011_GIRAS-based calculation of albedo (0 - 1) in D07 (500 m domain)

G

Figure 2-13, continued.

NLCD2011_GIRAS-based calculation of soil moisture content in D07 (500 m domain) **H**

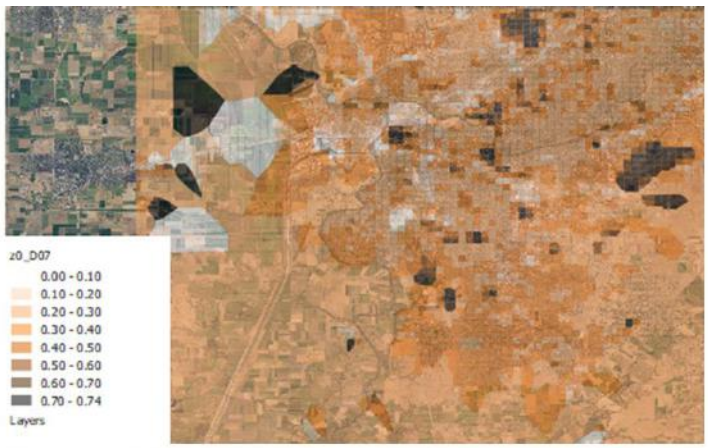

NLCD2011_GIRAS-based calculation of roughness length (m) in D07 (500 m domain) **I**

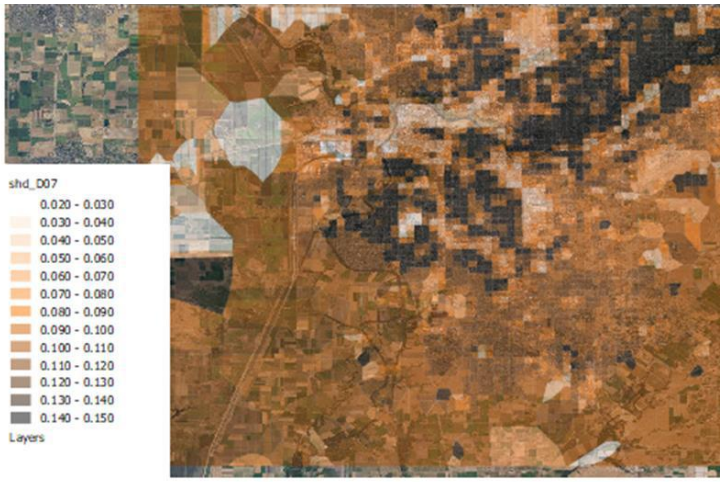

NLCD2011_GIRAS-based calculation of shdfac in D07 (500 m domain) **J**

2.4 DEVELOPMENT OF CROSSWALKS AND URBAN GEOMETRY PARAMETERS

Because the geographical extent (coverage) varies from one data type to another, and some datasets have large gaps or are sparse in coverage, a crosswalk among different datasets becomes necessary at some point to develop continuous physical characterizations of the surface. One particular such instance occurs in the derivation of urban geometry parameters (e.g., heights, frontal-, plan-, and top-area densities, sky view factor, and drag and roughness length parameters) from building footprint information. It is often the case that building footprint datasets are more limited in coverage than more general LULC data (see for example Figure 2-14) -- in such cases a crosswalk between building morphometric characteristics and LULC classes is necessary to extend the areal coverage of data with building information. It is acknowledged here that derivation of such parameters from crosswalks relies on certain assumptions being made and thus can lead to biases or inaccuracies. However, short of any other feasible approach to characterize large areas with gaps in data, this probably is the most optimal methodology.

As seen in Figure 2-14, for example, the publicly-available building footprint information for Sacramento County covers only a part of the region. Thus, a correlation with LULC is developed, in this case, for gridded building plan (λ_p) and frontal (λ_f) area densities to compute the roughness length parameter (z0) per MacDonald et al. (1998) and Grimmond and Oke (1999), as well as other variables.

Figure 2-14: Spatial coverage of available building-footprint datasets for Sacramento County.

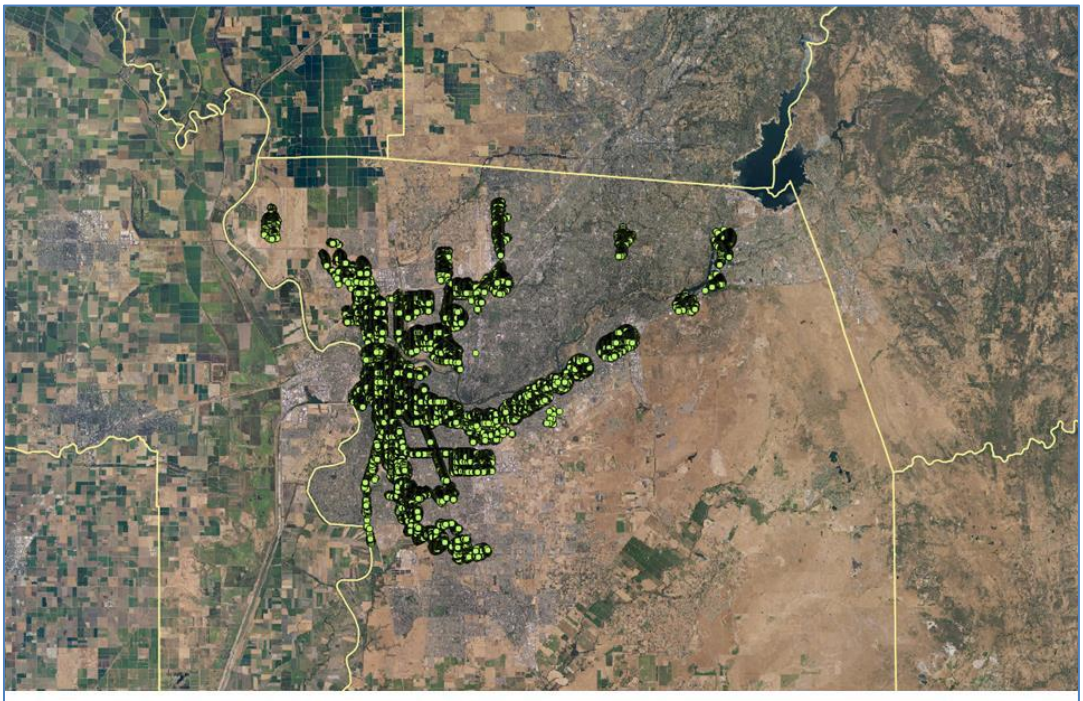

Figures 2-15 and 2-16 (A – D) show samples from this analysis. Figure 2-15 is an example from building footprint and geometry characterizations for the downtown Sacramento area. This figure is a blow-up from Figure 2-14, centered over downtown Sacramento, showing building outlines and footprints that are used in developing the gridded 3-dimensional properties input to the urban atmospheric model (Taha 2008a-c, 2017, 2018). Building heights, spacings, street orientations, street widths, and floor-plan areas are used in combination with other information to derive urban canyon properties and various geometrical parameters input to the meteorological model.

In each pair of graphs in Figure 2-16, the top two show the distributions of λp (vertical axis) for various LULC classes (on horizontal axis). In the bottom graphs of each figure, the distribution of parameter λf is plotted on the vertical axis and the LULC classes on the horizontal. This analysis is done for a large number of LULC classes (thus a small sample is shown in Figure 2-16) and used to develop crosswalks. In Table 2-4, the LULC classes are identified and the corresponding computed parameter values are listed.

For the 500-m domains, as simulated with the Altostratus-updated urban model (modUCM, Taha 2017, 2018), additional geometrical parameters are needed beyond those for the standard WRF, including detailed 3-dimensional morphological characterizations, as discussed in the following sections. Parameters derived from building footprint datasets include building plan-, top-, and frontal-area densities, sky-view factor, building heights, canyon orientation and geometry, street width, roughness length, and technical potential for deployment of project-specific UHI mitigation measures in each community.

Figure 2-15: Building footprints: example detail from downtown Sacramento. Data source: County and City of Sacramento.

Figure 2-16 (A – D): Development of crosswalks between LULC and building footprint characteristics in Sacramento County: a sample from the analysis and derivation of λp and λf parameters (top and bottom graphs in each figure, respectively).

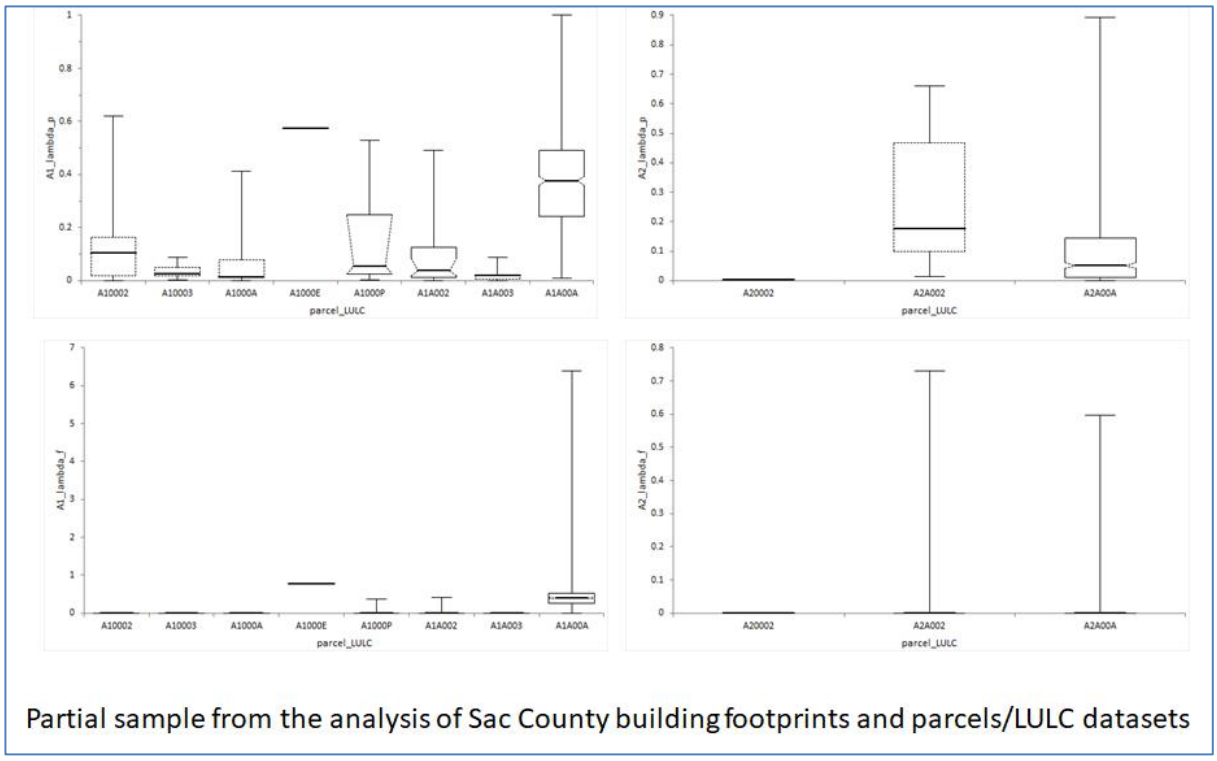

A

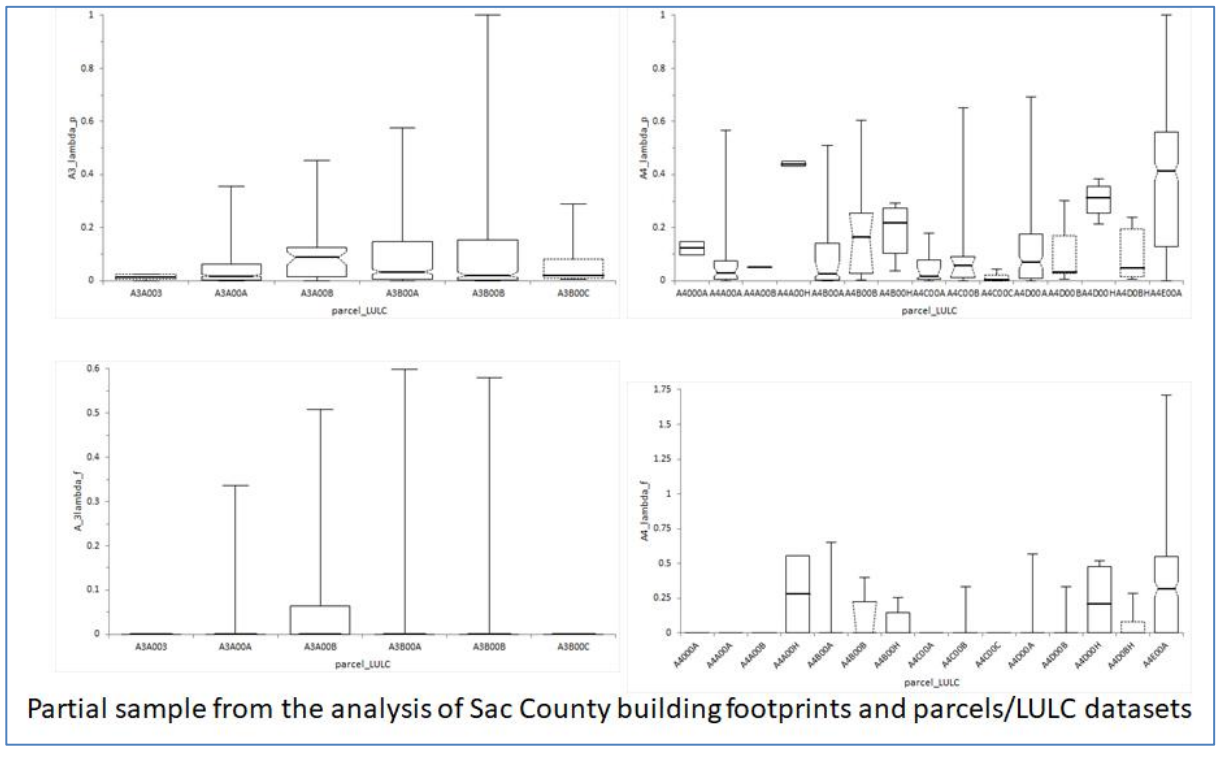

B

Figure 2-16, continued.

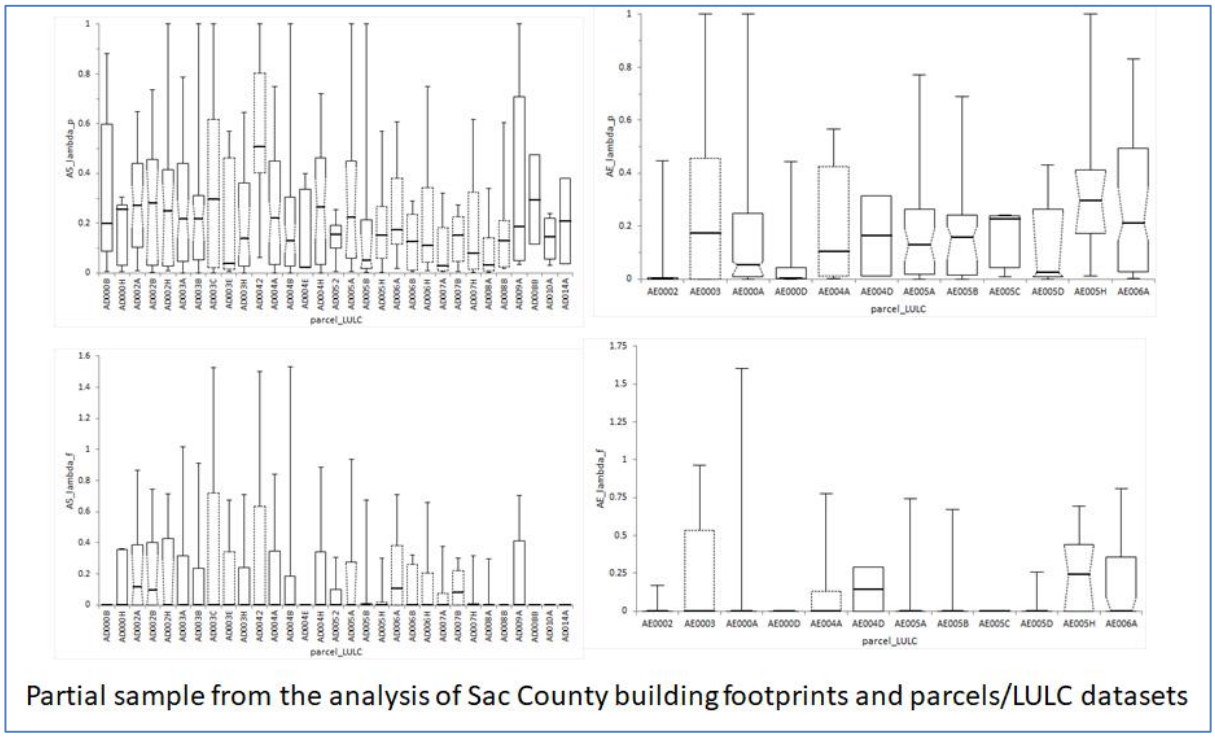

Partial sample from the analysis of Sac County building footprints and parcels/LULC datasets

C

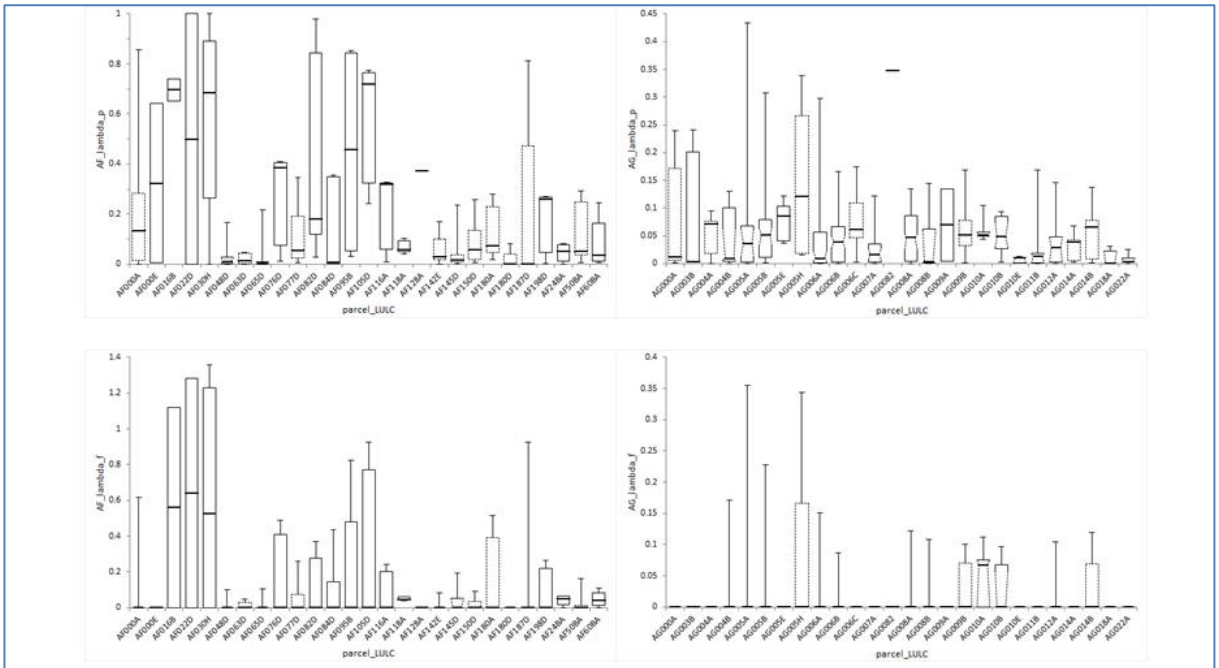

Partial sample from the analysis of Sac County building footprints and parcels/LULC datasets

D

Table 2-4: LULC classes in calculation of building geometrical parameters for Sacramento County.

			λp	λf		Zd/Zh	Z0/Zh	Zh	Z0
A1	single family residential		0.342	0.441		0.605	0.044	9.0	0.40
A2	two family residential		0.097	0.283		0.218	0.111	10.0	1.11
A3	three family residential		0.077	0.244		0.176	0.107	12.0	1.28
A4	four family residential		0.237	0.470		0.463	0.087	12.0	1.04
A5			0.229	0.438		0.451	0.085		
AE	low-rise apartments		0.161	0.362		0.340	0.101	16.0	1.62
AF	high-rise apartments		0.142	0.265		0.305	0.082	42.0	3.45
AG	residential court		0.046	0.094		0.110	0.038	0.5	0.02
AH	mobile home park		0.001	0.000		0.003	0.000	3.5	0.05
AJ	hotel		0.081	0.482		0.186	0.188	24.0	4.52
AK	boarding house		0.292	0.576		0.541	0.077	12.5	0.96
AL	rooming house		0.149	0.331		0.318	0.099	12.5	1.24
AN	motel		0.061	0.222		0.141	0.105	8.0	0.84
AQ	residential common area		0.062	0.156		0.145	0.069	0.5	0.03
AR	bed and breakfast		0.187	0.408		0.384	0.099	9.0	0.89
AT	mobile home		0.066	0.003		0.154	0.000	3.0	0.05

			λp	λf		Zd/Zh	Z0/Zh	Zh	Z0
B0	retail / commercial		0.011	0.004		0.028	0.000	5.0	0.10
BA	small retail		0.179	0.430		0.371	0.108	4.0	0.43
BB	store-office combo		0.199	0.451		0.405	0.101	16.0	1.62
BC	restaurant		0.131	0.448		0.286	0.141	6.0	0.85
BD	large retail		0.056	0.138		0.132	0.062	12.0	0.74
BE	shopping center		0.048	0.388		0.114	0.185	6.0	1.11
BF	vehicle-oriented		0.118	0.240		0.259	0.084	5.0	0.42
BG			0.002	0.001		0.006	0.000		
BI			0.026	0.004		0.062	0.000		
BQ			0.054	0.005		0.127	0.000		
CA	office (general)		0.194	0.318		0.397	0.074	14.0	1.04
CB	office / large, single tenant		0.097	1.143		0.217	0.297	12.0	3.56
CC	bank		0.106	0.261		0.236	0.098	8.0	0.78
CD	savings and loan		0.072	0.112		0.167	0.041	8.0	0.33
CE	broadcasting / radio / TV		0.081	0.241		0.184	0.103	20.0	2.06
CF	post office		0.045	0.069		0.107	0.022	7.0	0.16
CG	medical / dental		0.127	0.253		0.276	0.085	15.0	1.27
CH	veterinarian		0.035	0.183		0.083	0.098	6.0	0.59
CJ	office / residential conversion		0.207	0.378		0.417	0.083	12.0	0.99
CQ	office / common area		0.032	0.004		0.077	0.000	3.0	0.05

Table 2-4, continued.

			λp	λf		Zd/Zh	Z0/Zh	Zh	Z0
DA	acute care hospital		0.016	0.049		0.038	0.014	25.5	0.35
DB	skilled nursing facility		0.073	0.248		0.168	0.110	11.0	1.21
DC	health / residential care facility		0.110	0.318		0.245	0.116	5.0	0.58
DD	retirement home		0.134	0.675		0.291	0.188	12.5	2.36
DE	day nursery		0.112	0.297		0.249	0.108	4.0	0.43
DF	mortuary / cemetery		0.054	0.316		0.126	0.153	0.5	0.08
EE	church		0.084	0.216		0.191	0.090	25.0	2.25
EF	church / private school		0.050	0.131		0.117	0.059	15.5	0.92
EK	church / private social service agency		0.057	0.249		0.135	0.120	4.5	0.54
FA	golf course		0.006	0.001		0.015	0.000	0.2	0.02
FB			0.331	0.008		0.591	0.000		
FC			0.263	0.006		0.501	0.000		
FE	marina		0.006	0.004		0.014	0.000	0.2	0.00
FF	theater		0.120	0.363		0.263	0.125	36.0	4.51
FG	private club		0.125	0.272		0.273	0.093	4.0	0.37
FH	sports court / field / stadium		0.024	0.045		0.058	0.011	25.0	0.28
G0	industrial		0.013	0.004		0.031	0.000		
GA	light industrial		0.086	0.326		0.195	0.135	10.0	1.35
GB	heavy industrial		0.029	0.008		0.071	0.000	15.0	
GC	industrial warehouse		0.124	0.288		0.272	0.098	15.0	1.47
GD	industrial / building materials		0.054	0.179		0.127	0.086	10.0	0.86
GE	industrial / aerospace		0.019	0.006		0.047	0.000	25.0	
GF	industrial / truck or transit terminal		0.032	0.194		0.078	0.105	8.0	0.84
GG	industrial / food processing		0.085	0.239		0.194	0.100	8.0	0.80
GI	industrial		0.002	0.001		0.004	0.000	5.0	
GJ	industrial		0.012	0.002		0.030	0.000	5.0	
GK	industrial		0.021	0.006		0.052	0.000	5.0	
GL	industrial / mini storage		0.044	0.089		0.104	0.035	3.0	0.11
GM	industrial / multi tenant		0.094	0.005		0.213	0.000	9.0	
GQ			0.052	0.002		0.123	0.000		

			λp	λf		Zd/Zh	Z0/Zh	Zh	Z0
IA	vacant / residential		0.086	0.528		0.197	0.197	2.0	0.39
IB	vacant / commercial / retail		0.116	0.380		0.255	0.133	2.0	0.27
IC	vacant / office		0.159	0.426		0.336	0.118	2.0	0.24
ID	vacant / care / health		0.011	0.008		0.026	0.000	2.0	0.00
IF	vacant / recreational		0.051	0.169		0.121	0.081	2.0	0.16
IG	vacant / industrial		0.041	0.190		0.097	0.099	2.0	0.20
IH	vacant / agricultural		0.010	0.004		0.025	0.000	2.0	0.00
MA			0.116	3.606		0.255	0.426		
MB			0.006	0.001		0.016	0.000		
MD			0.011	0.008		0.028	0.000		
ML			0.010	0.008		0.024	0.000		
MP			0.040	0.273		0.095	0.143		
MR			0.103	0.277		0.230	0.106		
MS			0.130	3.913		0.284	0.414		
MU			0.053	0.288		0.125	0.141		
MW			0.069	0.006		0.160	0.000		
WA	public/utilities federal		0.027	0.598		0.065	0.274	35.0	9.60
WB	public/utilities state		0.029	0.109		0.070	0.052	25.5	1.34
WC	public/utilities county		0.029	0.316		0.070	0.171	20.0	3.43
WD	public/utilities city		0.060	0.183		0.141	0.085	25.5	2.17
WF	public/utilities public school		0.011	0.096		0.027	0.048	15.0	0.73
WG	public/utilities special district		0.034	0.009		0.081	0.000	8.0	0.00
WH	public/utilities SBE property		0.026	0.260		0.064	0.146	8.0	1.17

3. OBSERVATIONAL WEATHER DATA

3.1 OBJECTIVES OF OBSERVATIONAL METEOROLOGICAL ANALYSIS

The main objectives of observational meteorological analysis were to (1) acquire weather data from a dense network of mesonet monitors in the 6-counties Capital region, (2) quality-check and recast the data, (3) use the observational data in initial characterization of microclimates and the temperature field in the region, (4) recast the data for use in 4-dimensional assimilation in the meteorological model (FDDA), and (5) prepare the observations for use in thorough statistical model performance evaluation (as discussed in Section 4).

Thus, data were acquired from various sources, as discussed next, and summer months (May through September) of years 2013 – 2016 were analyzed. The purpose was also to identify intra-urban variability in meteorological fields based on observations.

3.2 OBSERVATIONAL METEOROLOGICAL DATA

Several datasets were identified, evaluated for use in this study, and acquired as suitable. Datasets were examined at multiple spatial resolutions and geographical coverages including both point and gridded data (analysis). The following observational meteorological data were considered. Overlap exists, sometimes completely, among these datasets and, in such cases, only a subset was used in this study.

- MADIS (Meteorological Assimilation Data Input System; madis-data.ncep.noaa.gov): An extensive and comprehensive repository of hourly weather datasets maintained by the National Centers for Environmental Prediction (NOAA / NCEP). It consists of and synthesizes data from various providers and, as such, was used as the main source of observational data in this study.
- URBANET / National mesonet: An urban-monitors hourly dataset by the National Centers for Environmental Prediction that can be partially or fully accessed via MADIS (depending on a user's access privileges).
- National Weather Service / NOAA Cooperative Observer Program (COOP): A dataset of annual averages and daily maximum and minimum temperatures and precipitation (nws.noaa.gov/om/coop/).
- Daymet (daymet.ornl.gov and urs.earthdata.nasa.gov): Gridded datasets at 1-km resolution of parameters including daily maximum and minimum air temperature, humidity, and precipitation. The data is prepared and maintained by the Oak Ridge National Laboratory (ORNL).
- WeatherBug (weatherbug.com): A commercial dataset consisting overwhelmingly of citizen weather observing program (CWOP) monitors. While both coverage and the spatial resolution

of the monitoring network are relatively high, data quality is difficult to ascertain and/or check via post-processing.

- Weather Underground (wunderground.com): A commercial dataset covering swathes of urban areas at relatively higher coverages and resolutions in some parts but, as with the WeatherBug datasets, the quality is not consistently checked and most monitors are privately owned, i.e., CWOP – thus not always subject to WMO-standard siting criteria, maintenance, and/or calibration.
- NOAA MesoWest (wrh.noaa.gov/mesowest): Map-based surface meteorology (point observations). Areas covered in California include the San Francisco Bay Area, Sacramento, San Diego, Los Angeles region, and the Fresno – Bakersfield areas. MesoWest also provides historical data (climate and daily weather information) as well as specific weather-station data.
- PRISM Climate Group (prism.oregonstate.edu) and PRISM UCAR (climatedataguide.ucar.edu): Gridded (analysis) historical meteorology datasets including daily temperature maxima, minima, and precipitation.
- NCAR dataset 472.0: Hourly historical point weather observations at airports or near airways. The dataset is developed and maintained by NCAR and made available for use as input to atmospheric models. This dataset also is useful in model performance evaluation.
- MesoWest mesonet (mesowest.utah.edu/): Mesonet data covering most of California and other western states. This dataset is also included in the MADIS system.
- NOAA daily datasets: National gridded datasets of daily temperature maxima and minima, and other daily variables, e.g., precipitation, based mainly on the NOAA COOP observations. Available for several decades to present with a spatial resolution of 6 km (data.ncdc.noaa.gov).
- California Irrigation Management Information System (CIMIS): A dataset developed mainly for agricultural applications with limited observations in urban areas.
- Network-specific California datasets: Data from various California agencies including the Air Resources Board and Air Quality Management Districts. e.g., SMAQMD, FRAQMD, YSAQMD, EDCAQMD, and PCAPCD.
- California Climate Data Archive, CALCLIM (calclim.dri.edu): A climate monitoring and data access website for the state of California, sponsored by the California Energy Commission as a joint effort with the Scripps Institute of Oceanography and the Western Regional Climate Center (WRCC). CALCLIM lists many of the same networks found in MADIS and other data sources listed above. Other useful climate datasets at WRCC can be accessed from wrcc.dri.edu/coop-inventory/ and wrcc.dri.edu/climate-maps.

The monitor locations (~400 stations) in the study domain, i.e., the 6-counties Capital region and surrounding areas, are shown in Figure 3-1 along with a listing of the main data providers. Figure 3-2 shows the locations of mesonet and metar monitors that are closest to AB617 communities in Sacramento County, as defined by the Sacramento Metropolitan Air Quality District (SMAQMD 2018).

Figure 3-1: Weather monitor locations in the study domain and MADIS data providers.

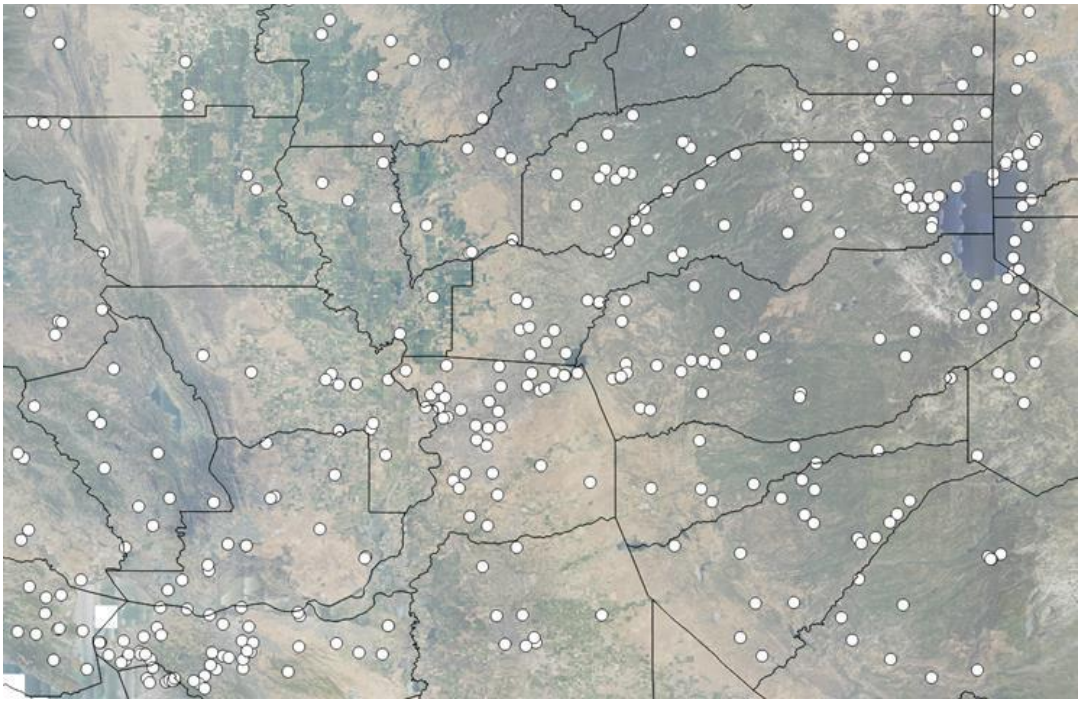

AWOS (Automated weather observing system)
APRSWXNET (Automatic position reporting system)
RAWS (Remote automated weather stations)
HADS (Hydro-meteorological automated data system)
CA-HYDRO (California hydro-meteorological networks)
MesoWest (Automated environmental monitoring)
AirNow (U.S. EPA monitoring networks)
ASOS (Automated surface observing systems (airways))

Data acquired from each of these monitors include (among an extensive number of variables) the following parameters: (1) air temperature, (2) dew point, (3) relative humidity, (4) wind speed, (5) wind direction, (6) wind gusts, (7) solar radiation, (8) atmospheric pressure, (9) precipitation, (10) geopotential height, (11) virtual temperature (12) visibility, (13) cloud base, and (14) soil moisture / temperature. In addition to use in analysis of observed meteorology, the acquired datasets were recast for use in model performance evaluation as will be discussed in Section 4. The data were also reformatted for input to meteorological model, i.e., in 4-dimensional data assimilation (FDDA) as needed.

The data were quality-checked to ensure suitability. MADIS allows for various levels of data screening based on: (1) static, station-specific verifications and (2) spatial analysis of observations at the target monitor relative to nearest-neighbor stations (analysis) which, in this case, generally includes some 4-6 stations surrounding the target (buddy check).

Figure 3-2: Locations of mesonet and metar monitors closest to AB617 communities in Sacramento County.

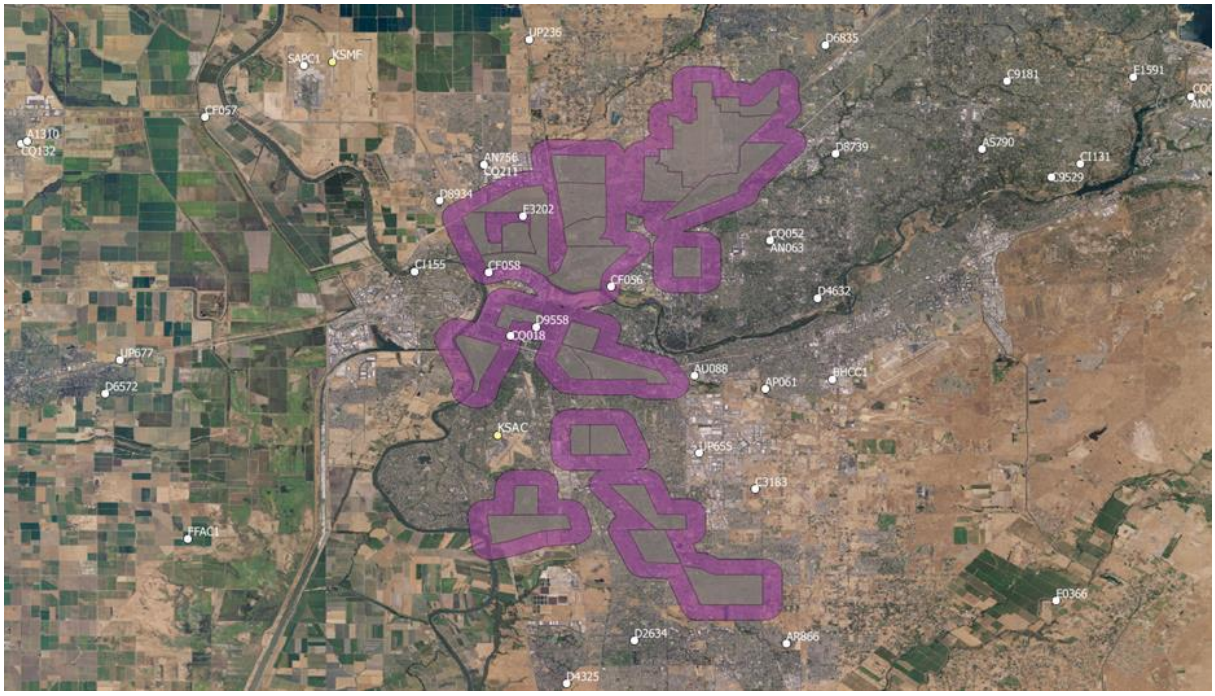

Figure 3-2 shows the following stations and proximities to AB617 communities or zones in the Sacramento area:

- Station E3202 is in area “A”;
- Station CF056 is close to area “B”;
- Stations UP655 and C3183 are close to areas “C” and “E”;
- Station AU088 is close to area “F”;
- Station KSAC is close to area “H”;
- Stations CQ052 and AN063 are close to area “I”; and
- Stations D9558 and CQ018 are in area “J”.

These station locations will be referenced when evaluating the potential impacts of and benefits from various UHI-mitigation measures in subsequent discussions in this report.

3.3 CHARACTERIZATION OF THE OBSERVATIONAL TEMPERATURE FIELD

The analysis of observed meteorology was carried out with focus on the temperature field in the 6-counties Capital region. To keep the discussion relatively compact in this section, the temperature field is presented as cumulative metrics, such as degree-hours, and localized tendencies, i.e., warming and cooling at each station location. Since the data is quite extensive, only a few snapshot examples are presented here.

In Figure 3-3, the graphs captioned "YYYYMM_dhpd" show examples from the cumulative analysis of temperature. In each figure, YYYYMM denotes the year and month and "dhpd" indicates degree-hours per day ($^oC \cdot hr\ day^{-1}$) as averaged for the given month. Thus, for example, "201306_dhpd" indicates an all-hours averaged temperature computed as DH day^{-1} for the month of June in 2013 (this is a non-threshold DH day^{-1} metric). In these figures, the progression of color codes from light to dark indicates lower to higher temperatures or DH day^{-1}. The dhpd metric is computed at each mesonet station, for all hours, and averaged for the given month and year.

Similarly, the figures labeled "YYYYMM_1400PDT" and YYYYMM_0200PDT" show examples from the analysis of the temperature field near the time of the daily maximum and near the time of minimal nighttime activity, respectively. In each figure, "1400PDT" or "0200PDT" indicates that the figures show the average of all 1400 or 0200 PDT hours in the given month and year.

Although the daily maximum temperature can occur anytime between 1200 and 1800 PDT depending on weather conditions, here, 1400 PDT is selected as an indicator to daily peaks. Thus, in Figure 3-3, the average of all 1400 PDT hours is shown for each mesonet station for the given month and year (YYYYMM_1400PDT). Similarly, the daily minimum typically occurs just before sunrise but here 0200 PDT (YYYYMM_0200PDT) is examined since this is a time with lower nighttime activity. Of note, this is a characterization at coarse scales and is meant to provide a general picture of the temperature field in the 6-counties Capital region. The study focuses on much finer resolutions in the modeling and analysis tasks discussed later in this report.

Overall, there are significant variations from month to month and year to year, as well as between the DHPD, 1400 PDT, and 0200 PDT metrics. However, some general semi-persistent patterns in the temperature field can be observed. In Sacramento County, the eastern and northern parts are generally warmer than the central-western parts in DHPD and the 1400-PDT time frame. At 0200 PDT, on the other hand, the western and north-western parts of Sacramento County are generally warmer, i.e., areas closer to downtown and more urbanized parts of Sacramento are relatively warmer at night, which is a typical nighttime UHI situation. The boundary between Sacramento and Placer counties, i.e., North Highlands and areas to its northeast, such as Rocklin and Roseville, is significantly warmer than the rest of the county in most conditions (across months and years). The area immediately near downtown Sacramento is generally either average compared to or cooler than the rest of the county during the day (1400 PDT) but can be slightly warmer at night (0200 PDT). The northwestern part of Sacramento County also is generally warmer than the central or southern parts.

In El Dorado County, topography causes the western parts to be warmer than the others. However, the temperature contrast between the western and eastern parts of this county are larger during the day than at night. Within the western parts, the DHPD indicator and the temperature field during the day (1400 PDT) show that the areas of Placerville and El Dorado Hills are consistently warmer than their surroundings in that part of the county. Furthermore, Placerville can be warmer than El

Dorado Hills, even though it is located further east and surrounded by denser forests. In Placer County, as with El Dorado, topography causes the western parts to be warmer than the eastern higher-elevation areas. Within the western part, there are some variations in the temperature field as well. For example, the area near Lincoln is consistently warmer than other parts in western Placer County. The temperature field also suggests that Granite Bay is warmer than its surroundings and that Roseville is also warmer at times.

In Yuba County, an area (monitor) about 5 km south of Marysville (in Olivehurst) appears to be consistently warmer than other monitors in that region during the day. At night, it can be warmer during some periods and cooler during others. It is interesting to note that the atmospheric model also produces an isolated large UHII just to the south of that monitor location (it can be seen in most figures in Section 5).

In Sutter County, the monitor at Yuba City shows that it is consistently warmer than areas to the south. Compared to a monitor in Sutter (city), the data suggests that Yuba City is sometimes similar to and at other times cooler than Sutter. However, the small number of monitors in Yuba and Sutter counties may render these assessments biased. Finally, in Yolo County, the monitor at Woodland indicates that it is consistently warmer than or similar to Davis. However, both of Davis and Woodland are generally cooler than areas in the western parts of Yolo County.

All of these observations suggest significant urban-generated heat in the region. As will be discussed in the modeling sections, further below, the observations also support the modeling results and the model characterization of the temperature field in the Capital region.

Figure 3-3: Observational temperature field as DH day^{-1} (ºC · hr day^{-1}), 1400 PDT, or 0200 PDT averages (ºC) for the 6-counties Capital region. Figures are labeled YYYYMM_*.

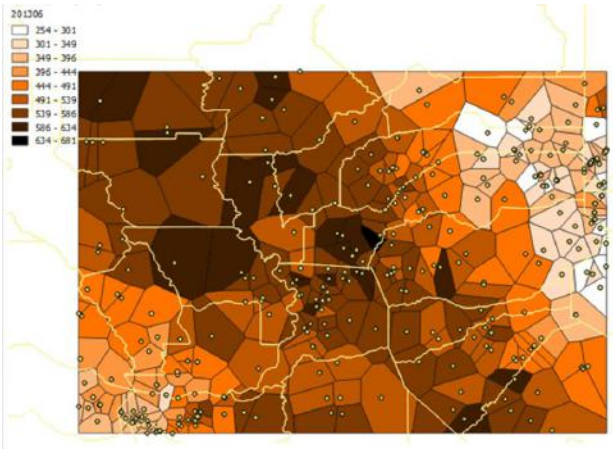

201306_dhpd

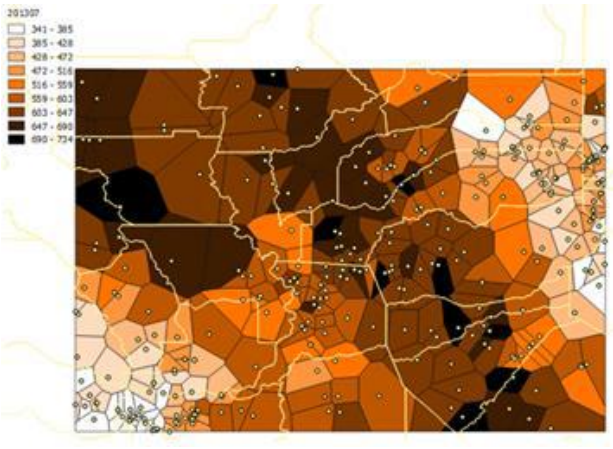

201307_dhpd

Figure 3-3. continued.

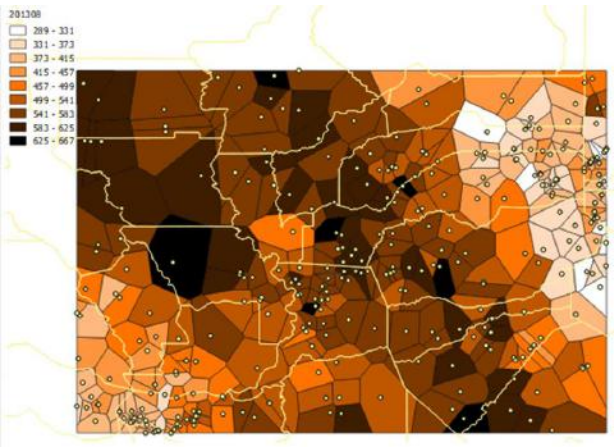

201308_dhpd

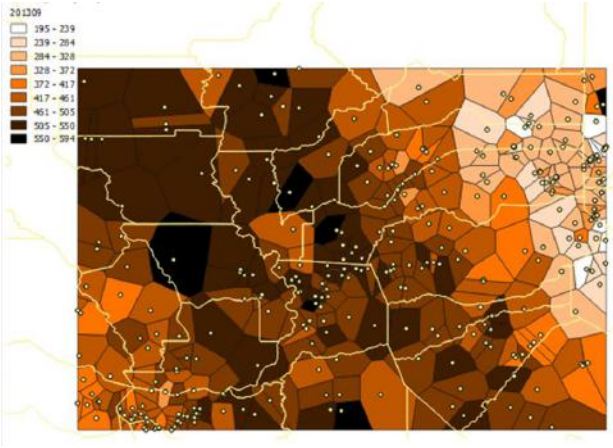

201309_dhpd

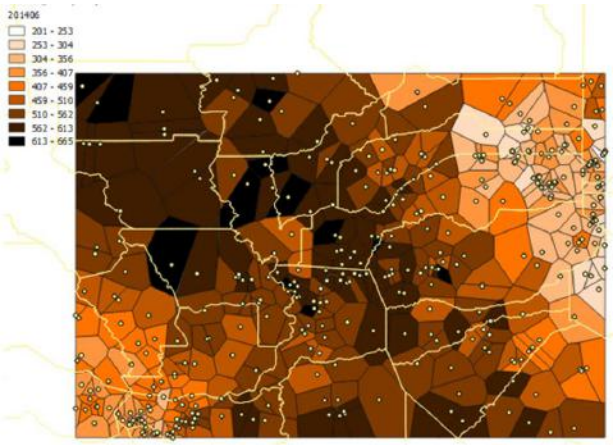

201406_dhpd

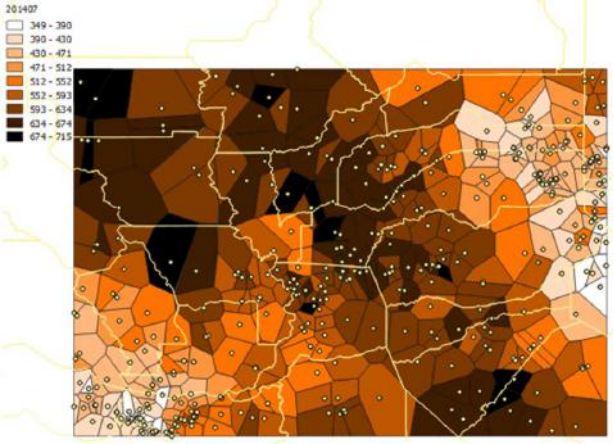

201407_dhpd

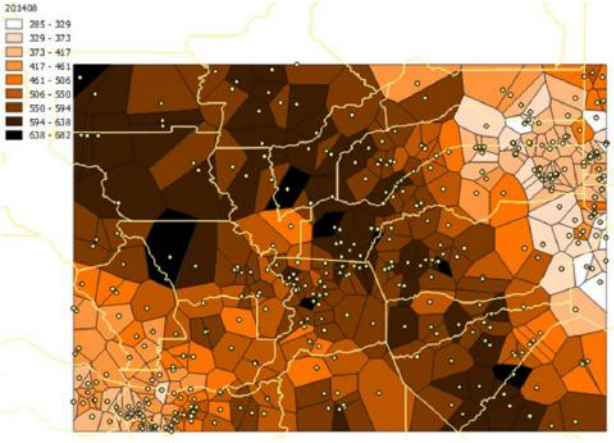

201408_dhpd

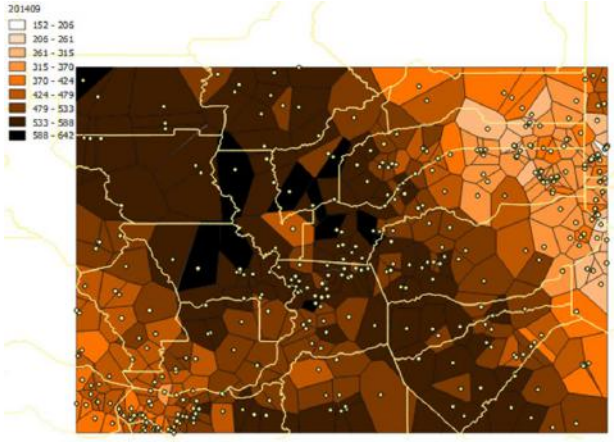

201409_dhpd

Figure 3-3. continued.

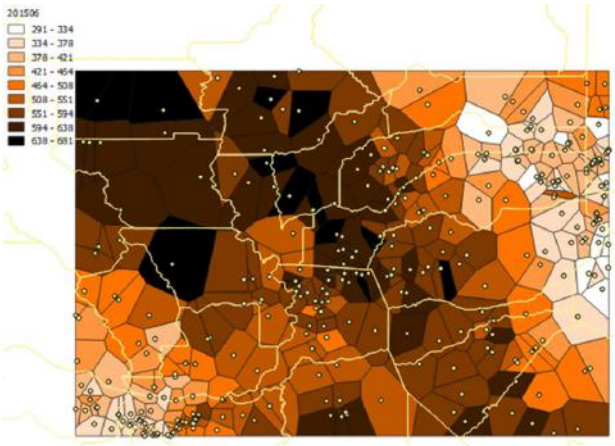

201506_dhpd

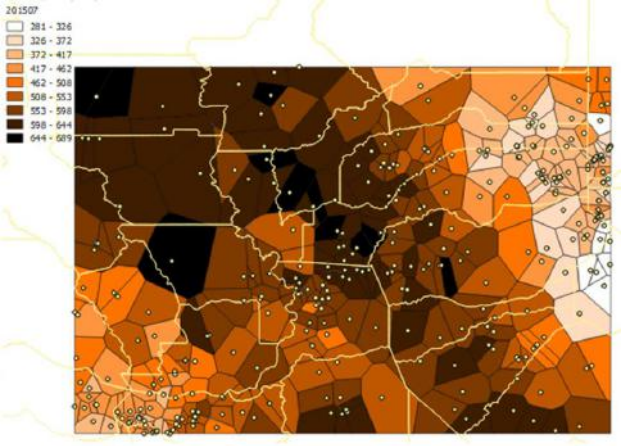

201507_dhpd

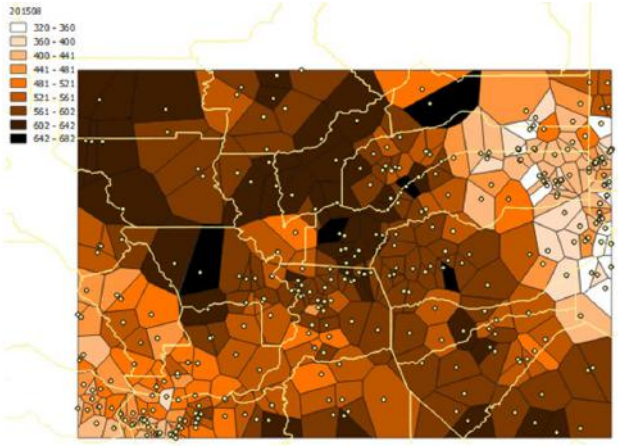

201508_dhpd

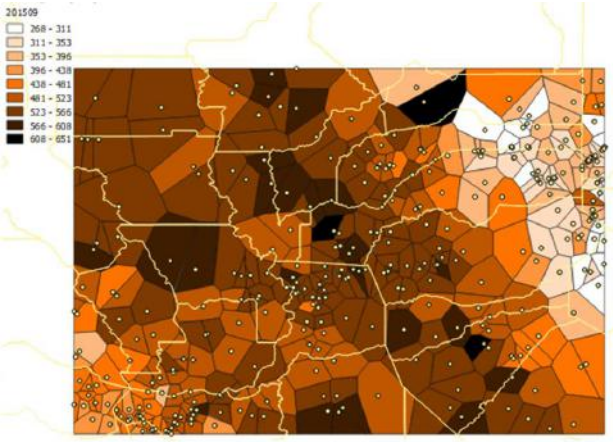

201509_dhpd

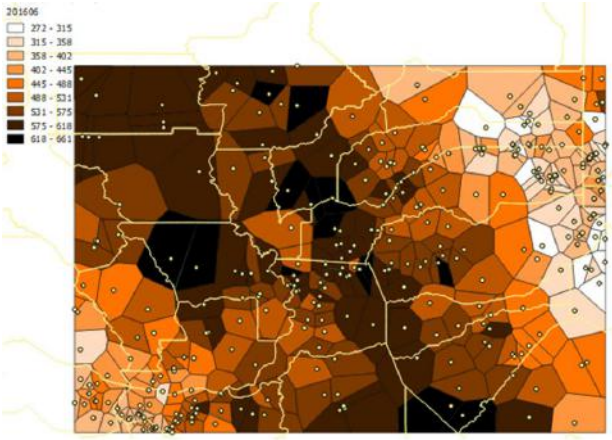

201606_dhpd

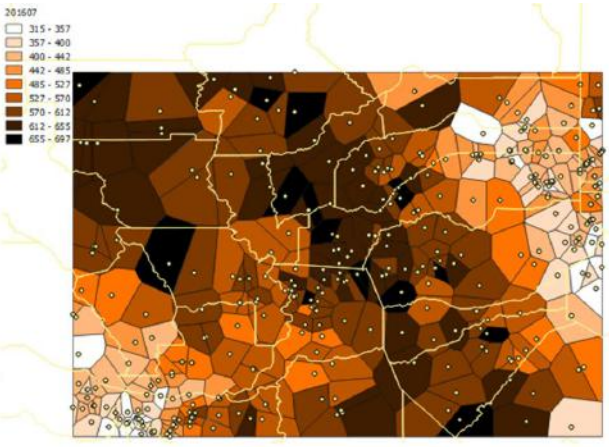

201607_dhpd

Figure 3-3. continued.

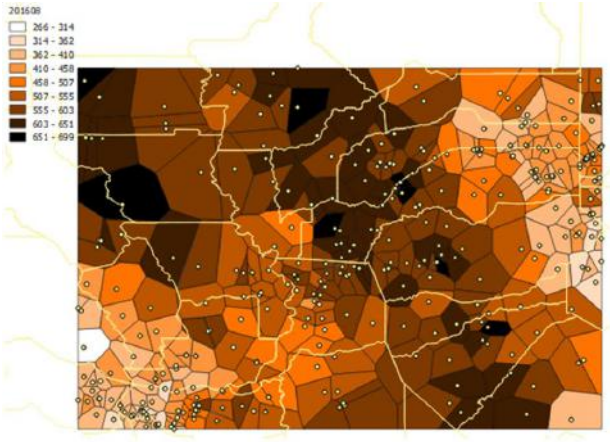

201608_dhpd

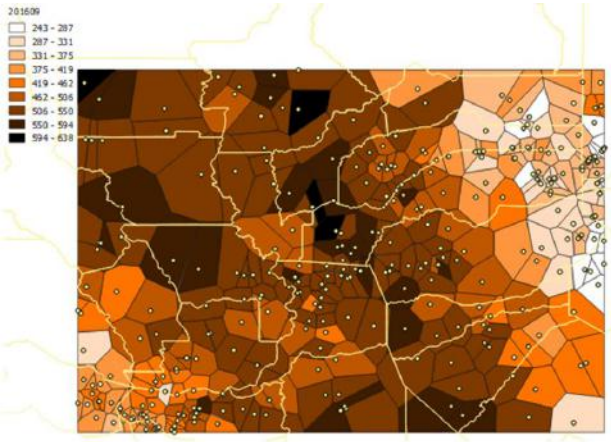

201609_dhpd

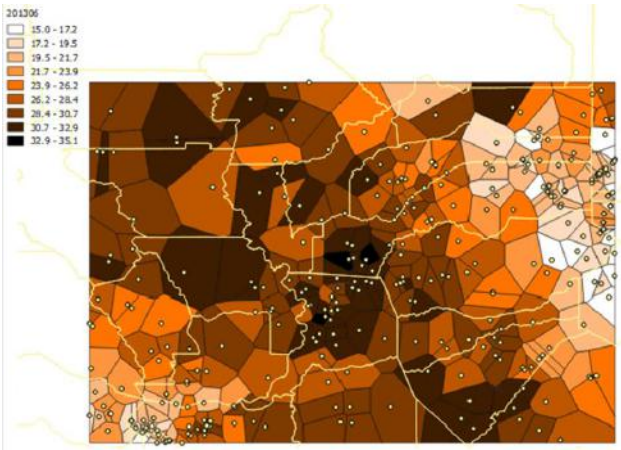

201306_1400PDT

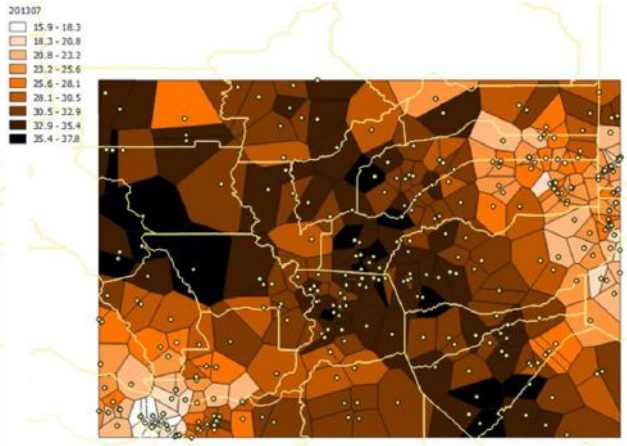

201307_1400PDT

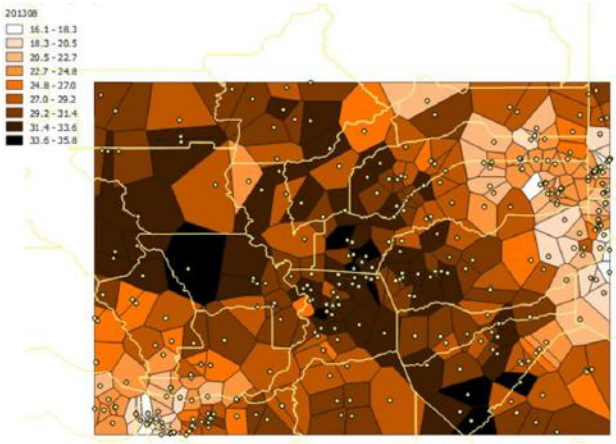

201308_1400PDT

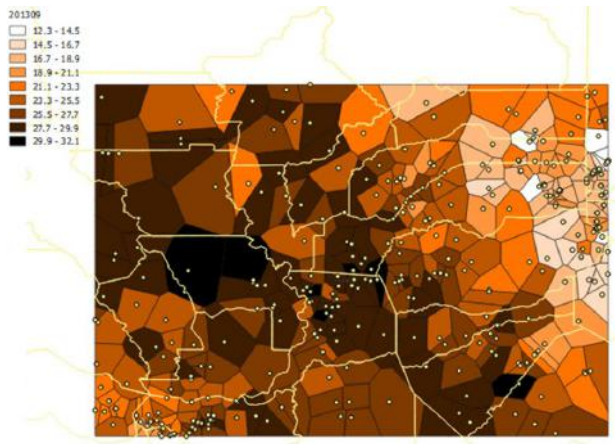

201309_1400PDT

Figure 3-3. continued.

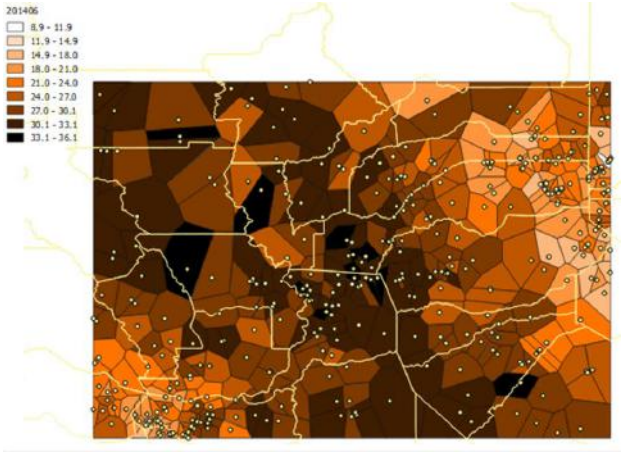

201406_1400PDT

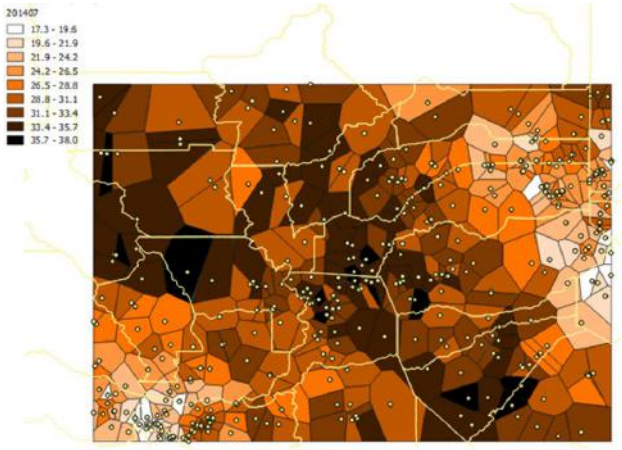

201407_1400PDT

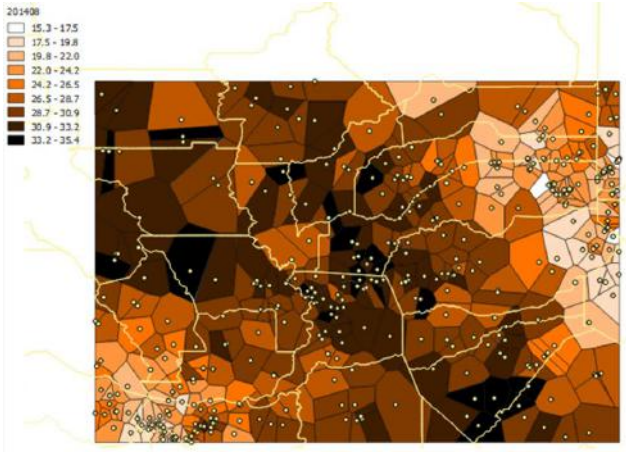

201408_1400PDT

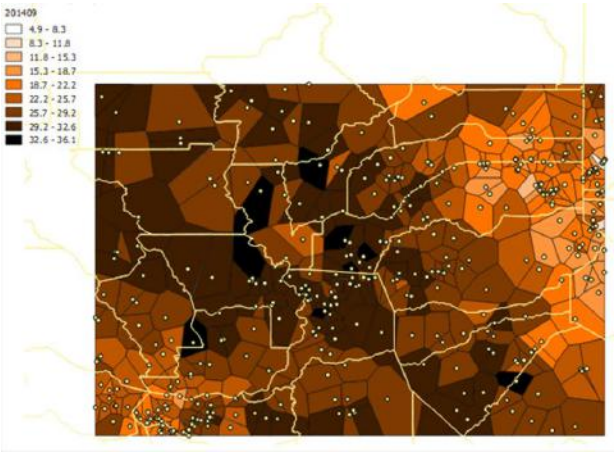

201409_1400PDT

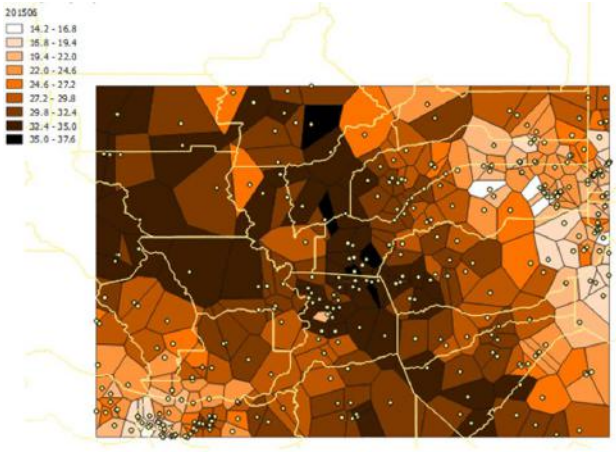

201506_1400PDT

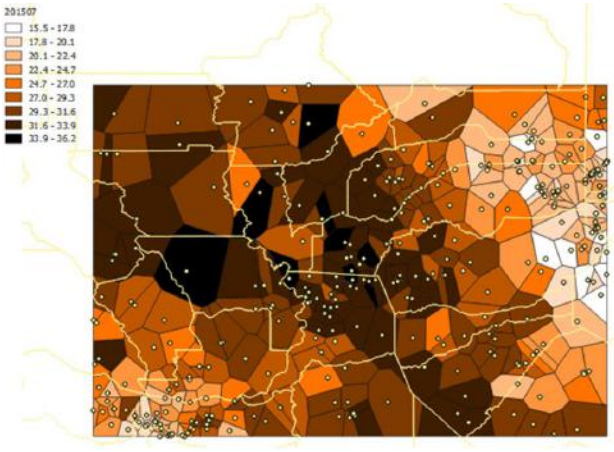

201507_1400PDT

Figure 3-3. continued.

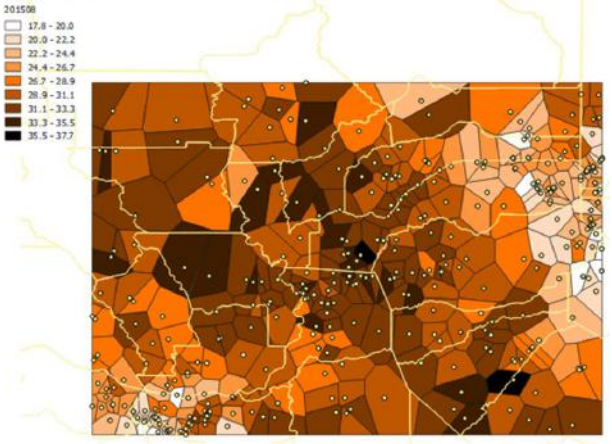

201508_1400PDT

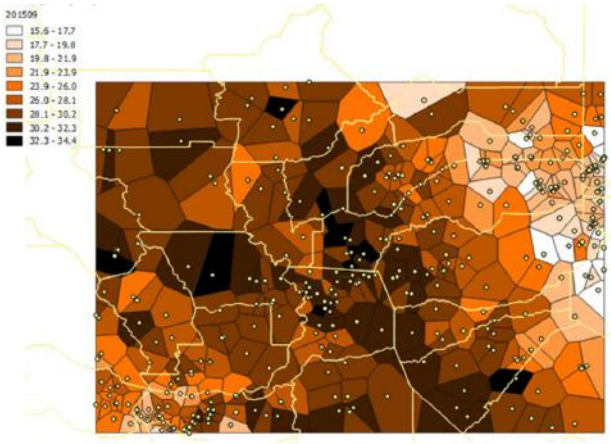

201509_1400PDT

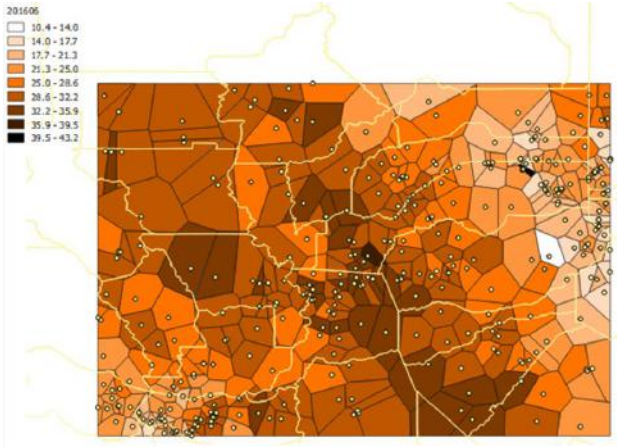

201606_1400PDT

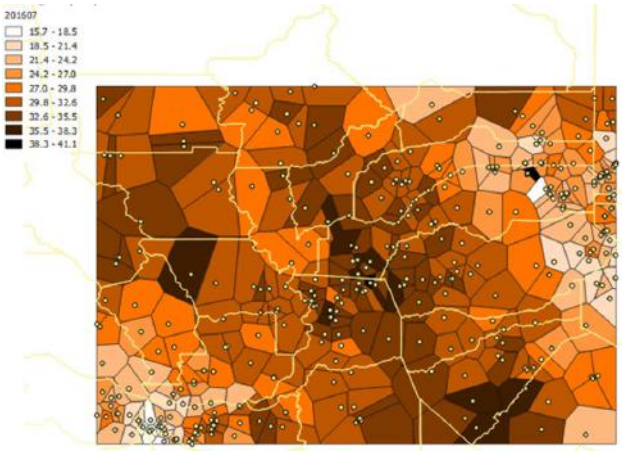

201607_1400PDT

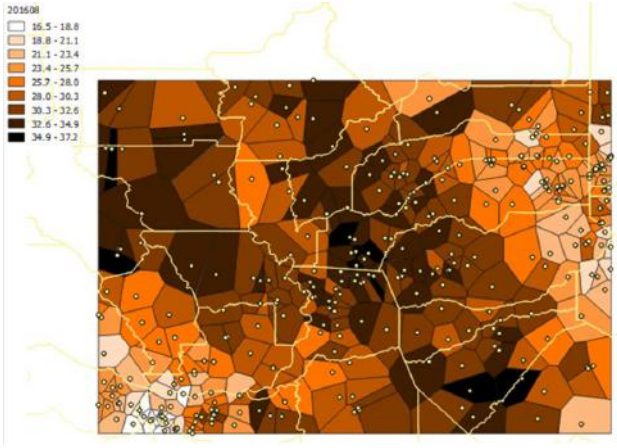

201608_1400PDT

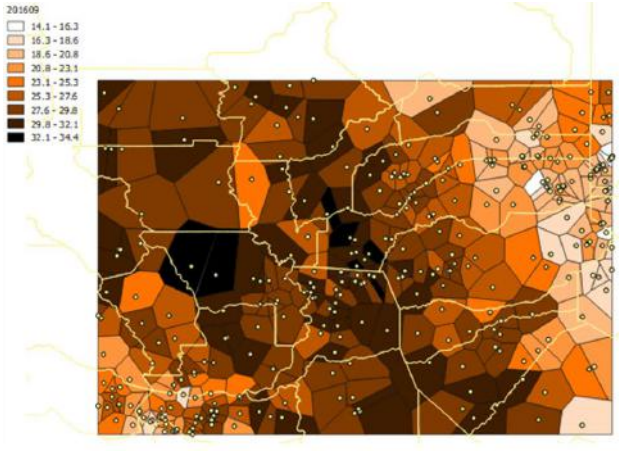

201609_1400PDT

Figure 3-3. continued.

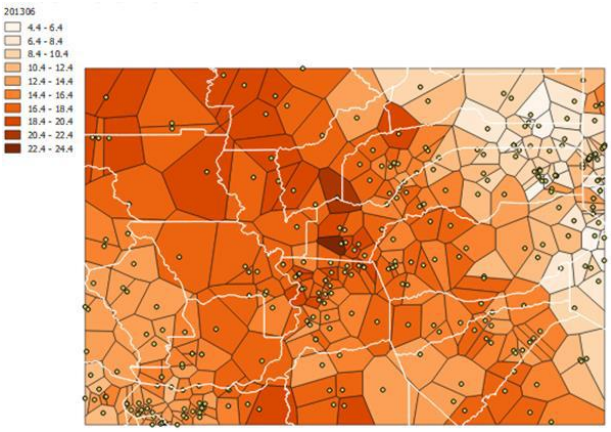

201306_0200PDT

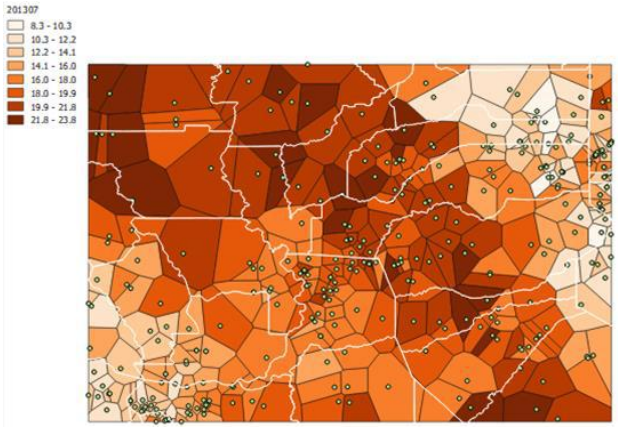

201307_0200PDT

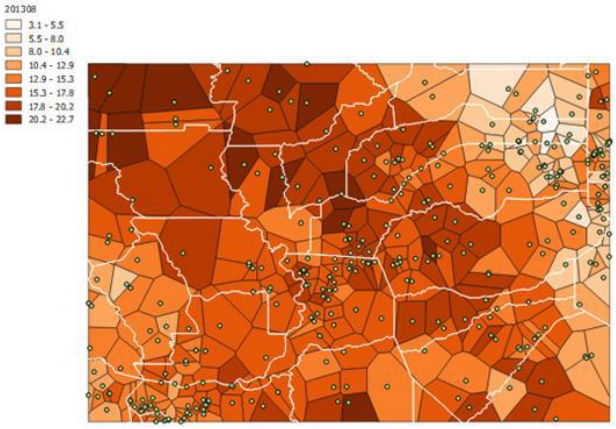

201308_0200PDT

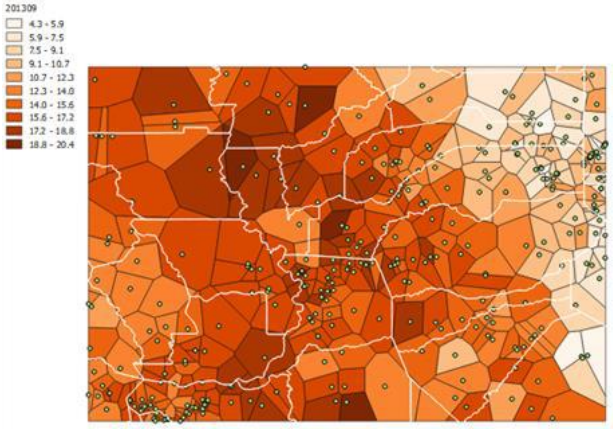

201309_0200PDT

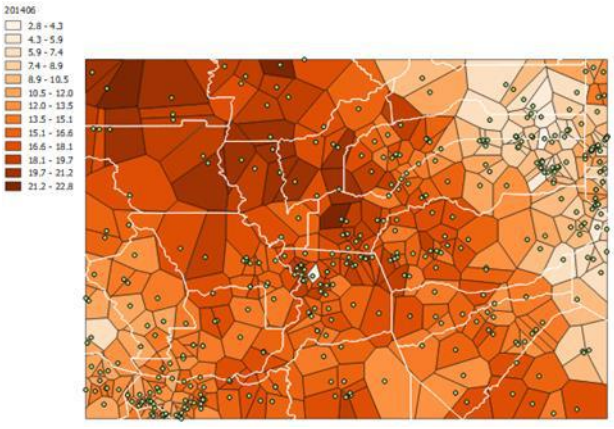

201406_0200PDT

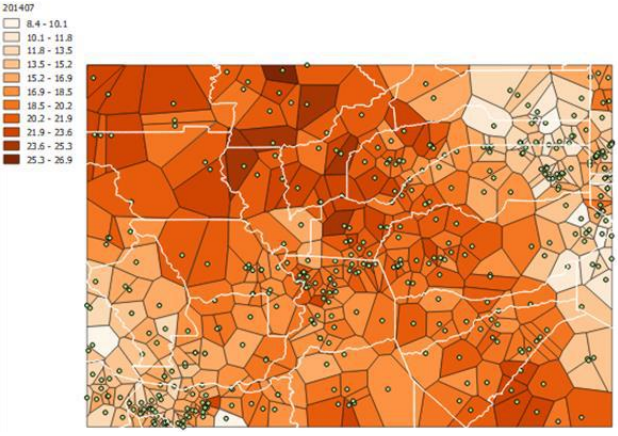

201407_0200PDT

Figure 3-3. continued.

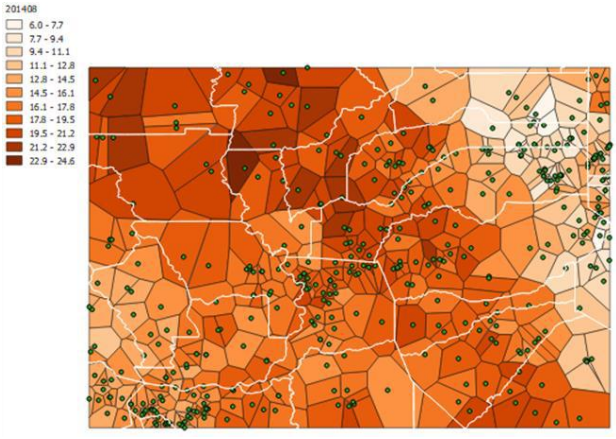

201408_0200PDT

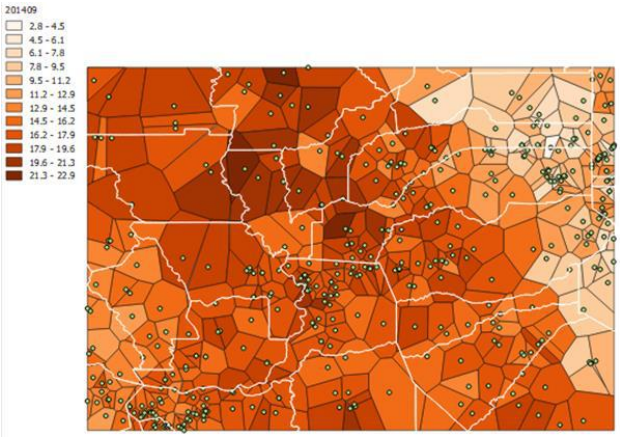

201409_0200PDT

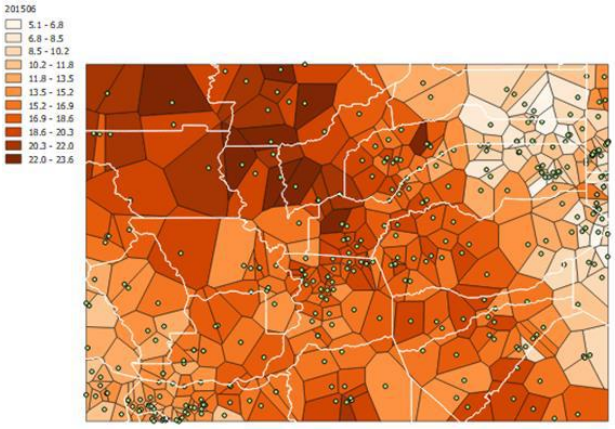

201506_0200PDT

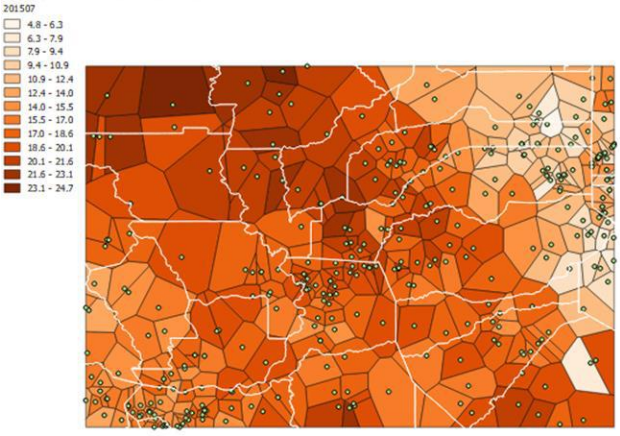

201507_0200PDT

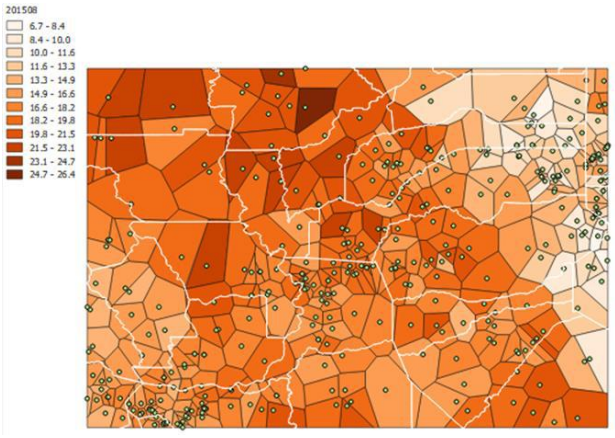

201508_0200PDT

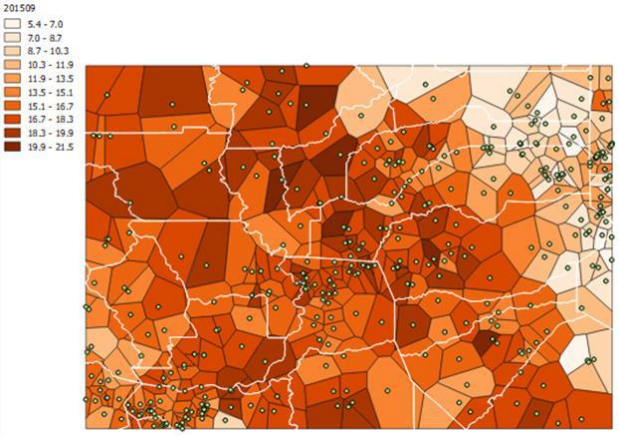

201509_0200PDT

Figure 3-3. continued.

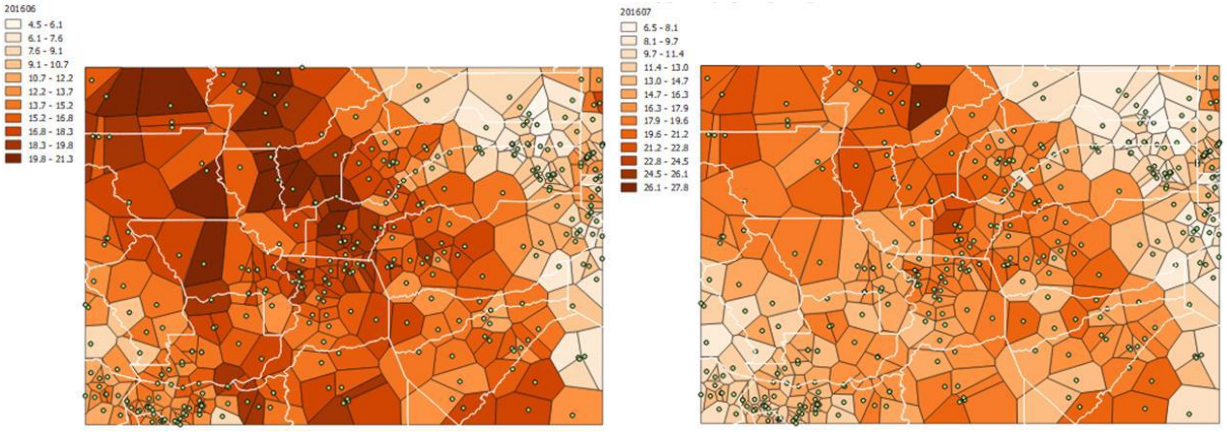

201606_0200PDT 201607_0200PDT

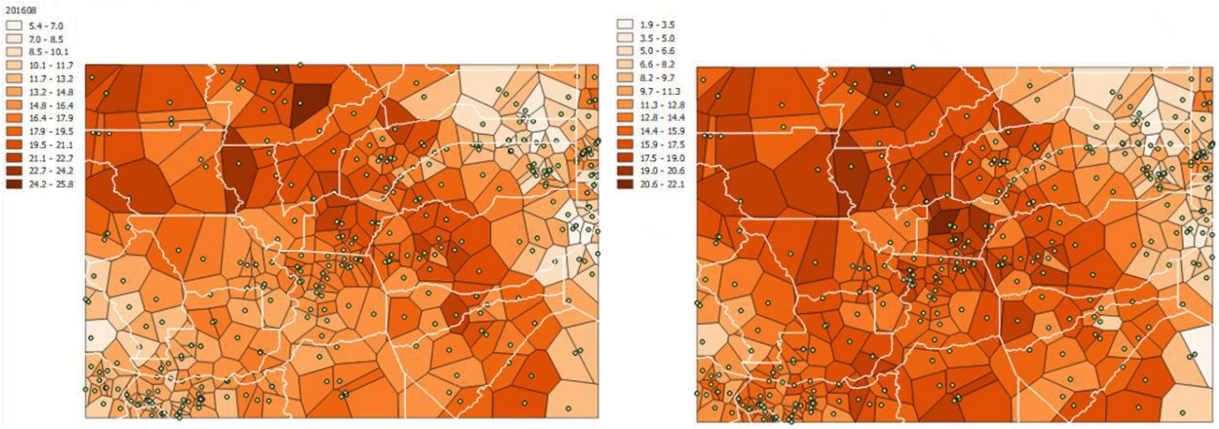

201608_0200PDT 201609_0200PDT

3.4 URBAN HEAT IN RELATION TO URBAN CORE AREAS

As discussed earlier in this report, the urban heat indicators, including the UHI and the UHII, characterized and quantified in this study are air-temperature-based, not derived from skin surface temperature such as shown in some urban "hot-spot" assessments from satellite / remote-sensing data or imagery, sometimes referred to as "surface temperature urban heat island", or SUHI. Thus, the spatial patterns of urban heat presented in this report can differ significantly from those seen in satellite imagery. For example, heat plumes and air-temperature peaks can be displaced downwind from urban cores. Furthermore, the SUHI is irrelevant to characterizing air-pollutant emissions rates, air quality (chemistry), and transport of heat from one area to another.

It has become almost an unshakable impression or thinking that downtown areas are the epicenters of heat islands. In reality, this is not always the case and the confusion may be a result of

misinformation from said "hot-spot" surface temperature characterizations. In effect, however, hot roofs in downtown or in high-rise areas can be high enough above ground that their influence on street-level air temperature is small to nil. In addition, the streets and urban canyons are well shaded by the tall buildings and likely receive no more than an hour or two of direct sunlight every day (depending on orientation), and sometimes none. The tall walls are exposed to sunlight, one or two directions at a time, but can dissipate heat rather efficiently because of the lower temperatures, stronger winds, and mixing at higher elevations away from the ground. By the same token, increased turbulence of air flowing over the rough downtown area increases mixing of temperature and accelerates cooling. Thus, an area such as downtown Sacramento can be warm but not necessarily the warmest all the times. Furthermore, in the specific case of Sacramento, the downtown area is heavily treed (see again Figure 2-7, domain D07) which helps keep it cooler than its surrounds. The observational meteorological data from the Sacramento area, e.g., Figures 3-3 and 3-4, support this argument.

Taha (2017) shows that this also is the case in the Los Angeles urban climate archipelago. However, he also demonstrates that smaller, low-rise downtown areas, such as in Fresno or Bakersfield, do indeed get warmer than their surrounds. In the Sacramento area the warmest parts stretch from AB617 communities A, B, and D east to Folsom and El Dorado Hills and northeast to Rocklin, Roseville, and Lincoln. In the discussion of model results, later in this report, the same will be seen – that the hotter parts of the Sacramento area are displaced to the east and northeast and that the downtown area is relatively cooler than some of the surrounds. This was also observed in the Level-1 Cal/EPA UHII (Taha 2017; Taha and Freed 2015).

Figure 3-4: Observational mesonet all-hour average air temperature contours. Left: 201306; Range: 306 – 646 ºC·hr day^{-1}. Right: 201307; Range: 389 – 701 ºC·hr day^{-1}

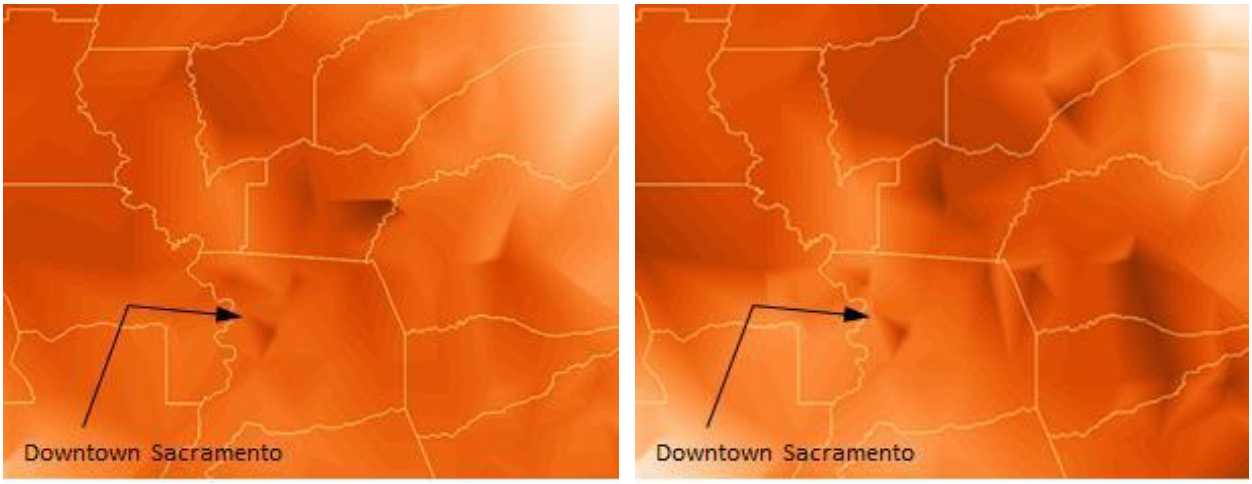

3.5 OBSERVATIONAL INTRA-URBAN TEMPERATURE RANGE

To provide an "at a glance" characterization of the temperature field across the study domain shown in Figures 3-3 and 3-4, above, the observed air temperature across the region is plotted, in Figure 3-5, as a cumulative distribution function (solid line, CDF) along with a 95% confidence band (dashed lines). While this exercise can be done for any time period or time of day, various averages, and so on, here we examine the CDF of monthly averages of the 1400-PDT observed air temperature. The labels on each graph of Figure 3-5 are YYYYMM. Thus, the figure provides a quick visual comparison of the temperature field across various years and months.

It can be seen that regardless of the actual intra-urban temperature range, the CDF signature is relatively similar throughout all periods except in some cases such as June and September 2014, and June and July 2016 that show a slightly steeper CDF. This indicates that the spatial characteristics of the temperature field, and hence the UHI and UHII, are relatively similar, in general, across the various summer weather conditions (but, of course, the absolute temperature differs from month to month and year to year). This implies that the design (spatial pattern of deployment) of mitigation measures will be equally valid and effective throughout different summer months and seasons.

The analysis also shows that relative to a specified threshold, e.g., 35 °C (which will be used later in evaluating impacts per electric utilities criteria) the observational data for the years and periods examined here indicate that 9% of the weather stations in this domain exceed the threshold in July 2013, 2% in June 2014, 5% in July 2014, 1% in both August and September 2014, 2% in both June and July 2015, 1% in August 2015, 1% in June 2016, 6% in July 2016, and 2% in August 2016. Considering that these are month-long averages of 1400 PDT temperatures, these exceedances are quite significant and indicative of a serious overheating problem in the region. Furthermore, the observational analysis shows that the warmest period (of the intervals studied in this effort) is July 2013, followed by July 2016 and July 2014. All of these indicators are taken into consideration when selecting modeling periods at the fine scales (500 m) as will be discussed later in this report.

Figure 3-5: Cumulative distribution function (CDF) and 95% confidence band for month-averaged observational air temperature at 1400 PDT.

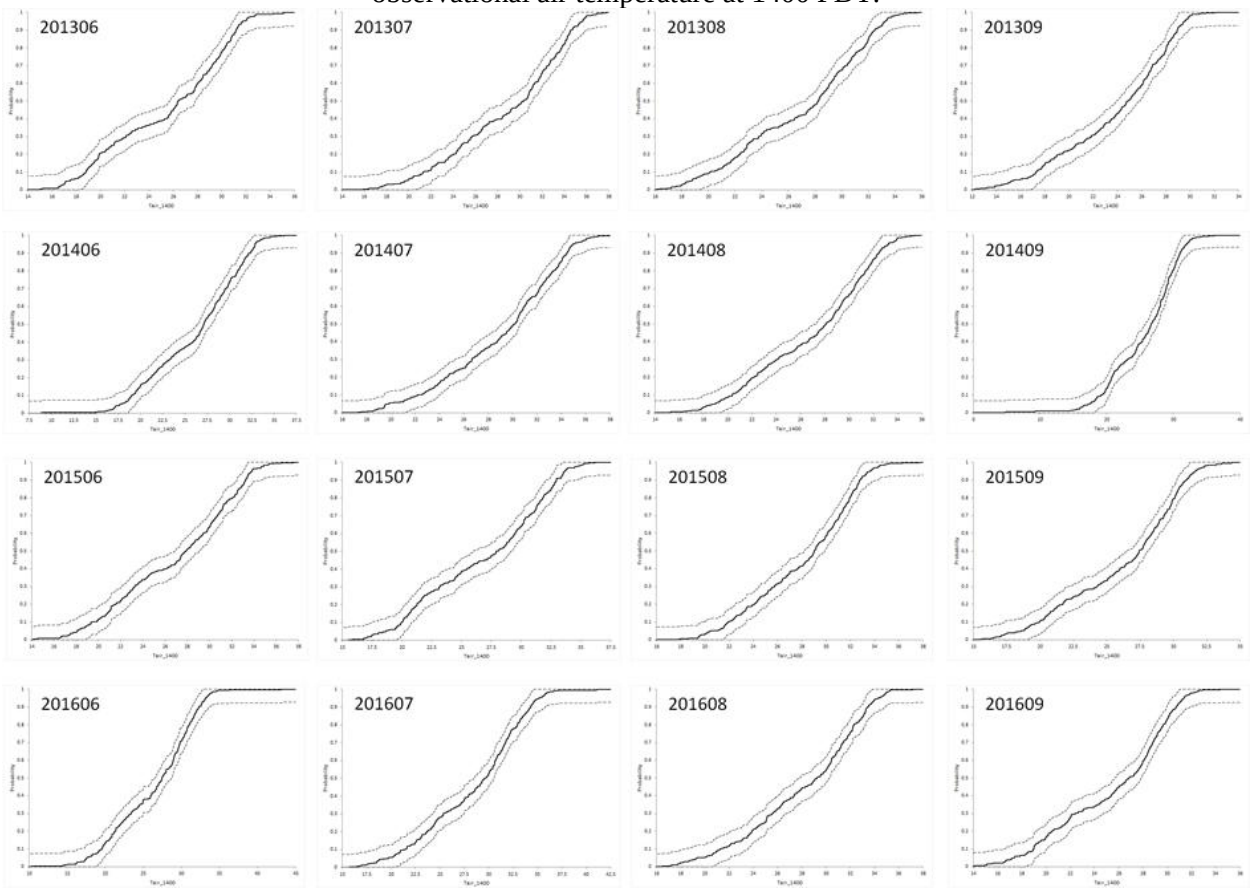

3.6 ANALYSIS OF OBSERVED LOCAL TENDENCIES

As discussed in Section 3.5, the general signature of the temperature field is relatively similar across the summer months and years examined in this study. However, there were also some month-to-month variations (as can be expected) producing different signatures in Figure 3-5. In this section, the spatial aspects of these variations in profiles are examined, i.e., identifying the geographical areas affected by those departures from the "typical" profiles in Figure 3-5.

To crudely characterize (based on observational data) the intra-seasonal magnitudes of warming or cooling in different parts of the domain as the background weather changes, local tendencies were computed at each mesonet station location relative to its own conditions during the month of June, as reference. Thus, for example, Figure 3-6 (A – F) shows the averaged changes in 1400 PDT temperatures (at each station relative to its own location) for July, August, and September in years 2013 and 2016, relative to June of 2013 or 2016, respectively.

To reiterate, what is shown in Figure 3-6 is not an absolute temperature field that can be compared across the domain (i.e., the figures cannot be used to evaluate which area is warmer or cooler than another) – each figure is a mosaic that only shows how much each area (weather station location) warms up or cools down relative to its own conditions in June (here, the month of June is used as reference, but any other reference would be equally useful). Thus, graphs A – C are for July, August, and September of 2013 (relative to June 2013) and graphs D – F are for July, August, and September of 2016 (relative to June 2016). They all show the averaged tendencies at 1400 PDT at each station for each given month. The caption below each figure provides the actual range of temperature change in each month and year. The following is a brief discussion.

July 2013 minus June 2013 (Figure 3-6 A): In July, the entire Sacramento County area warms up relative to June, but the eastern and southeastern parts warm up relatively more than the rest of the county. There is also larger warming in the North Highlands area and northeast of it into Placer County. A monitor south of Sacramento also registers higher-than-average warming. In El Dorado County, most areas warm up but the central parts of the county warm up more, including Placerville and surrounding areas. In El Dorado Hills, the warming is relatively smaller than at Placerville. In Placer County, the eastern parts warm up more than the western parts that are closer to Sacramento County. Areas near Lincoln and Roseville, while still warming up, do not heat up as much as the eastern parts of the county. In Yuba County, the eastern parts warm up more than the areas near Marysville. Yuba City, in Sutter County, warms up more than Sutter (City) and more than Marysville. Finally, in Yolo County, there is moderate warming, and it is larger in Woodlands than in Davis.

August 2013 minus June 2013 (Figure 3-6 B): The eastern and southeastern parts of Sacramento County warm up more than the rest of the county. Areas along the boundary between Sacramento and Placer counties also warm up more than its surroundings. There is a cooling signal in the southern part of the domain, relative to June. In El Dorado County, most areas warm up, but the central parts warm up more, including Placerville and surrounding areas. In El Dorado Hills, the warming is negligible relative to June. In Placer County, the eastern parts warm up more than the western parts. However, southern parts of the county, i.e., at the boundary with Sacramento County, including areas near Roseville warm up as well. The areas near Lincoln have negligible change relative to June. In Yuba and Sutter counties, the areas to the north and south of Yuba City and Marysville warm up, but at these two locations, there is relatively small change compared to June. In Yolo County, there is moderate warming, and, again, it is larger in Woodlands than in Davis.

September 2013 minus June 2013 (Figure 3-6 C): In September, the region is cooler than in June except for a few monitor locations around the San Francisco Bay Area. In general, all areas appear to cool down uniformly relative to June, except for some sporadic monitors where there is larger cooling than at others.

In general, the eastern parts of the 6-counties region cool down more (relative to June) than central or western areas.

July 2016 minus June 2016 (Figure 3-6 D): The entire area of Sacramento County warms up relative to June but, in this case, the largest warming is found in the western parts (rather than eastern), south of Sacramento, and in southern areas of the county. There is also large warming in the Roseville area. In El Dorado County, all monitor locations, except for two, appear to warm up uniformly. The area around Placerville still warms up slightly more than areas near El Dorado Hills. In Placer County, all monitors appear to warm up uniformly, except for larger warming in the Roseville area. In Lincoln, the warming also is larger than in its surroundings. In Yuba and Sutter counties, the warming is uniform across all monitor locations except for one cooling and one larger heating. Yuba City and Marysville warm up in similar amounts. Finally, in Yolo County, Woodlands warms up more than it surroundings and more than Davis.

August 2016 minus June 2016 (Figure 3-6 E): The spatial pattern of warming in the 6-counties region is similar to that in July-minus-June (Figure D) albeit at slightly different absolute temperatures.

September 2016 minus June 2016 (Figure 3-6 F): As with 2013 September-minus-June, there is relatively uniform cooling across monitors in this domain. There are, of course, some monitor locations that cool down more than others and some warm up slightly, but are outside of the urban areas of interest in this discussion.

Thus, to summarize the foregoing discussion, the meteorological observations indicate that while absolute air temperature changes significantly from month to month and between urban and non-urban areas, there are small intra-urban variations across the months. In other words, urban areas warm up or cool down in a relatively similar fashion. Independently from this, some of the largest departures (whether warming or cooling) are also found along the foothills and higher elevations in the eastern half of the domain as well as in some non-urban areas in the Yuba City and Woodland regions.

Thus, conversely, it can be argued that the impacts of the UHI-mitigation measures (in urban areas), spatially, should remain relatively similar across the different summer months and years. This will be discussed in more detail later in this report, when comparing the rankings of various measures across different geographical areas and in the different current and future climates.

Figure 3-6: Local monthly tendencies in temperature.

2013 July minus June difference (°C) in averaged 1400 PDT temperature. Actual range is -2.64 to +6.99 °C. Based on observations from mesonet stations.

A

2013 August minus June difference (°C) in averaged 1400 PDT temperature. Actual range is -2.71 to +5.38 °C. Based on observations from mesonet stations.

B

2013 September minus June difference (°C) in averaged 1400 PDT temperature. Actual range is -9.06 to +5.07 °C. Based on observations from mesonet stations.

C

Figure 3-6, continued.

2016 July minus June difference (°C) in averaged 1400 PDT temperature. Actual range is -3.91 to +11.63 °C. Based on observations from mesonet stations.

D

2016 August minus June difference (°C) in averaged 1400 PDT temperature. Actual range is -10.4 to +12.78 °C. Based on observations from mesonet stations.

E

2016 September minus June difference (°C) in averaged 1400 PDT temperature. Actual range is -7.69 to +10.65 °C. Based on observations from mesonet stations.

F

4. BASE ATMOSPHERIC MODELING

4.1 OBJECTIVES OF BASE MODELING

In this study, atmospheric modeling was conducted with the WRF system (Skamarock et al. 2008) and an Altostratus Inc.-modified and updated version of its urban canopy model (Taha 2017; Martilli et al. 2002; Chen et al. 2010). This advanced version, applied at the 500-m level, will be referred to as "modUCM" in the rest of this report to distinguish it from the standard versions of the WRF model. This is in addition to the coarse-scale Altostratus AREAMOD approach, applied at the 2-km level, which was introduced earlier in Section 2.3.4.

The Altostratus modifications include improvements to the urban-canopy layer and land-surface parametrizations, as well as modifications to the single and multi-layer models (UCM and BEP/BEP-BEM) of WRF (Martilli et el. 2002; Salamanca and Martilli 2009). The modifications also involve innovative trigger mechanisms that call the urbanized modules at specified locations in the model domains (Taha 2018). Furthermore, Altostratus also uses different data preparation, surface characterization, and parameter-ingestion schemes (in the AREAMOD approach) than the standard WRF pre-processing system, resulting in more cell-specific characterizations in the LULC bottom-up approach discussed earlier in this report.

Thus, a base modeling task was performed at the beginning of this project to test any further model updates and evaluate model performance. The following was carried out:

- Configure, modify, and customize the atmospheric model's urban modules and parameterizations for study-domain specifics, such as available data and domain characteristics;
- Develop cell-specific surface-characterization input using the bottom-up approach discussed earlier along with available current-conditions urban morphology and geometry datasets;
- Develop current-climate meteorological input (initial, boundary, and surface conditions) based on observational weather data (MADIS) and reanalysis (NNRP; Kistler et al. 2001);
- Perform current-climate simulations, for the years 2013 – 2016, focusing on summer seasons (May – September, MJJAS);
- Define point-forecast locations, regional means, or other metrics for developing the reference-state meteorology;
- Carry out statistical model performance evaluation based on modeling-community-recommended benchmarks; and
- Diagnose model results to quantify the urban-heat effects of interest, per various metrics and thresholds defined later in Section 5.9.

Another objective of the base modeling was to evaluate length scales (fetch effects) of surface perturbations, e.g., albedo increase, to assess the Level-3 UHII implications in this region. This will be discussed in Section 5.8.

4.2 URBAN REPRESENTATIONS IN THE ATMOSPHERIC MODEL

Sub-grid or sub-filter scale parameterizations that are used to "urbanize" a meteorological model are as follows, per DuPont et al. (2005), Martilli et al. (2002), and Taha (2008a-c). Note that some or all of these parameterizations are used and implemented per model configuration and specific application.

$$\frac{\partial\, \rho u_i}{\partial t} = F_{g(ui)} + F_{ui}^{j} + \sum_{j} D_{ui}^{j} \qquad (4\text{-}1)$$

$$\frac{\partial\, \rho\theta}{\partial t} = F_{g(\theta)} + H_j + Q_f \qquad (4\text{-}2)$$

$$\frac{\partial\, \rho q}{\partial t} = F_{g(q)} + S_j \qquad (4\text{-}3)$$

$$\frac{\partial E}{\partial t} = \frac{\partial\, u_i E}{\partial x_i} + \left\{ k_m \left[\left(\frac{\partial u}{\partial z} \right)^2 + \left(\frac{\partial v}{\partial z} \right)^2 \right] S_{air} + F_E^{bui} \right\} + \left\{ \frac{g}{\theta_v} \langle w\theta_v \rangle + H_E \right\} - \frac{1}{\rho} \frac{\partial\, (\rho \langle wE \rangle)}{\partial z} - \varepsilon + \sum_{j} w_E^{j} - \sum_{j} D_E^{j} \qquad (4\text{-}4)$$

Equations 4-1 – 4-4 are for momentum, heat, mass (water vapor), and turbulent kinetic energy (TKE), respectively.

In equations (4-1) – (4-3), the terms *Fg* are the general forcing terms (i.e., original model dynamics and physics) and the additional terms represent the urban parameterizations, i.e., subgrid-scale terms to account for the effects of urban land use and morphology. The two additional terms in equation (4-1) are (a) friction forces by the horizontal surface of buildings, roofs, and vegetation canopies, and (b) drag forces resulting from the vertical surfaces of buildings, obstacles, and vegetation canopies. The additional two terms in equation (4-2) are (a) sensible heat fluxes from buildings/roofs, pavements/streets, and vegetation, and (b) sensible heat flux from anthropogenic sources, e.g., motor vehicles and building cooling towers. The additional term in equation (4-3) is evapotranspiration from vegetation surfaces and evaporation from roofs and pavements. In equation (4-4), there are four additional terms (terms *F, H, W, and D*) that represent (a) shear

production of TKE by horizontal buildings and vegetation canopy surfaces, (b) buoyancy production of TKE by heat flux from building and vegetation and from anthropogenic heating (e.g., motor vehicles), (c) wake production by buildings and vegetation canopies, and (4) accelerated dissipation (cascade / sink), respectively.

For a detailed discussion of these terms and model urbanization, the reader is referred to DuPont et al. (2005), Martilli et al. (2002), and Taha (2008a-c).

4.3 INITIAL REGIONAL 2-km SIMULATIONS

One of the first objectives in this study was to enhance the representation of urban areas in the atmospheric model so as to improve performance and increase area-specificity of the simulations and results. This was done via (1) improving input to the model, i.e., more site- and area-specific surface characterizations, and (2) updating model parameterizations and calculations as presented above.

As discussed in Section 2, the LULC input to the model was improved via use of a bottom-up approach in characterizing the surface. An immediate result of this improvement can be seen in the more responsive temperature field to a better representation of the urban areas in the modeled domains. As an example, Figure 4-1 (left) shows the difference in the simulated temperature field at a random hour (1600 PDT on May 30th, 2013) between a run using the standard WRF model and a run using the Altostratus Inc. AREAMOD approach.

As can be seen in the figure, the standard WRF misses the urban areas highlighted in blue and underpredicts urban air temperature by up to 3.5 ºC in those areas. In other words, the standard WRF model does not "see" these urban areas shown in blue but they are captured in the AREAMOD approach (per more recent LULC input and more accurate bottom-up characterization of surface). This is a significant difference, especially since this study is about modifications to urban areas with UHI-mitigation measures. Thus, the correct capture of urban extent is necessary.

Compare the left graph in Figure 4-1 with the right one showing the updated urban LULC from the analysis in Section 2. The central, "hollow" areas in many urban zones in the left figure, especially in the Sacramento metropolitan area, is what actually exists in the standard WRF and the blue areas are the additional representations in the AREAMOD approach (Taha 2017). As we will see later, this has a very significant effect on the modeled meteorology, UHII, and the impacts of further urban expansion in future climates (e.g., 2050).

It is likely that urban modelers will not use the standard WRF as is "out of the box" and will improve urban representation in some fashion – still, the purpose here is to show the AREAMOD approach's effectiveness in improving the WRF simulations. Furthermore, Altostratus Inc. also continually improves and customizes the fine-scale models, such as UCM of Kusaka and Chen (Chen et al 2010; Kusaka et al. 2001) by extensively expanding their ability for site-specific modeling, resulting in the "modUCM" version introduced above (Taha 2017, 2018). Figure 4-2

shows a comparison between the temperature fields produced by the standard UCM and the modUCM. It can be seen that modUCM captures features that the standard UCM is unable to, including, for example, the main roadways in the area (some of which were purposefully made cooler in this example for the Sacramento 500-m domain, D07), which is relevant to the transportation aspect of this study.

Figure 4-1. Left: Temperature difference between standard and Altostratus-modified WRF. Right: urban land use per most recent datasets.

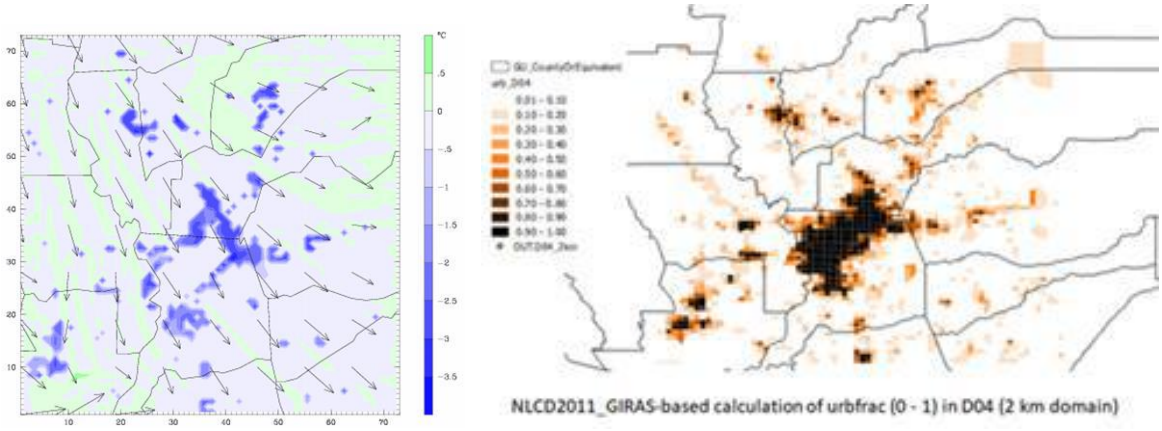

Figure 4-2. Temperature difference between standard and Altostratus-modified urban canopy model simulations of the Sacramento area.

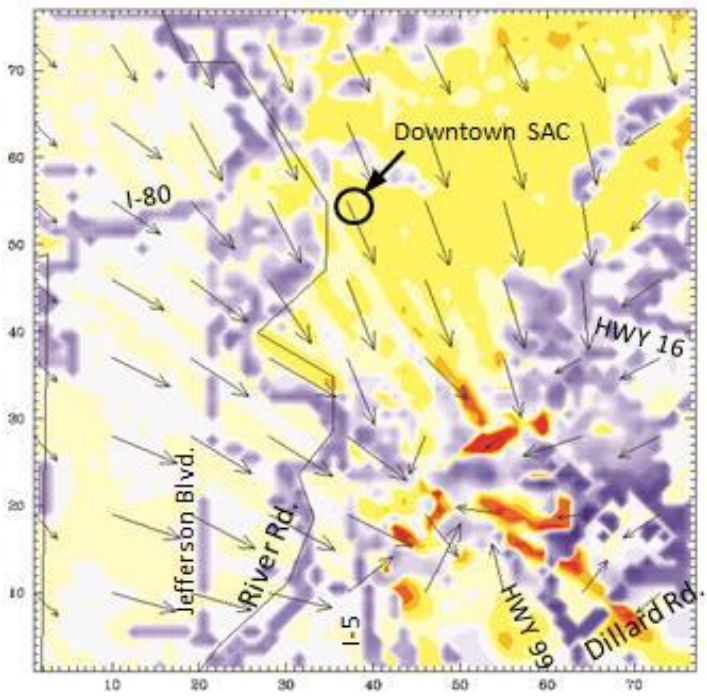

4.4 COARSE GRIDS SIMULATIONS (D01 – D03)

As discussed earlier in Section 2.2 (and shown in Figure 2-1), the atmospheric model was run on a multi-domain configuration that included 10 different grids at horizontal resolutions of 54 km (one domain), 18 km (one domain), 6 km (one domain), 2 km (one domain), and 500-m (six domains). Random samples from the 6-km domain (D03) simulations are shown in Figure 4-3.

The first three domains (D01 – D03) were run using the standard WRF model and pre-processors (Sakamarock et al. 2008), with some of the more relevant options being Kain-Fritsch for microphysics, TKE boundary-layer scheme MYJ, WSM 3 class, and the NOAH land-surface model (other details are explained elsewhere). In the 2-km domain (D04), Altostratus Inc.'s AREAMOD approach, configurations, and pre-processing were applied (Taha 2015b, 2017, 2018). In the 500-m domains (D05 – D10) Altostratus Inc.'s modUCM model in combination with AREAMOD were used as part of the urbanized WRF system.

The atmospheric model was run with 27 or 55 vertical level as needed per models and parameterizations being applied in each domain. Domains D01 – D04 were run with two-way feedback, whereas the 500-m grids (D05 – D10) were run via one-way nesting (Taha 2017, 2018).

In this report, results from domains D01, D02, and D03 are not presented. However, the results were evaluated against surface and upper-air observational meteorological data to ensure that the model captured the synoptic features during selected time intervals and that it produced the corresponding spatial patterns of temperature and wind flow throughout the region. Note that the quantitative model performance evaluation via thorough statistical analysis was done at the 2-km level (D04) as presented later in Section 4.5.3). In this report, only the results from the 2-km resolution domain (D04) and the 500-m resolution domains D05 through D10 are presented.

Figure 4-3: Sample model results (at random hours) from the 6-km resolution domain D03 for a summer and winter set of simulations. 2-m air temperature and 10-m winds at 1700 PDT, August 13, 2016 (left) and at 1600 PST, January 31, 2016 (right).

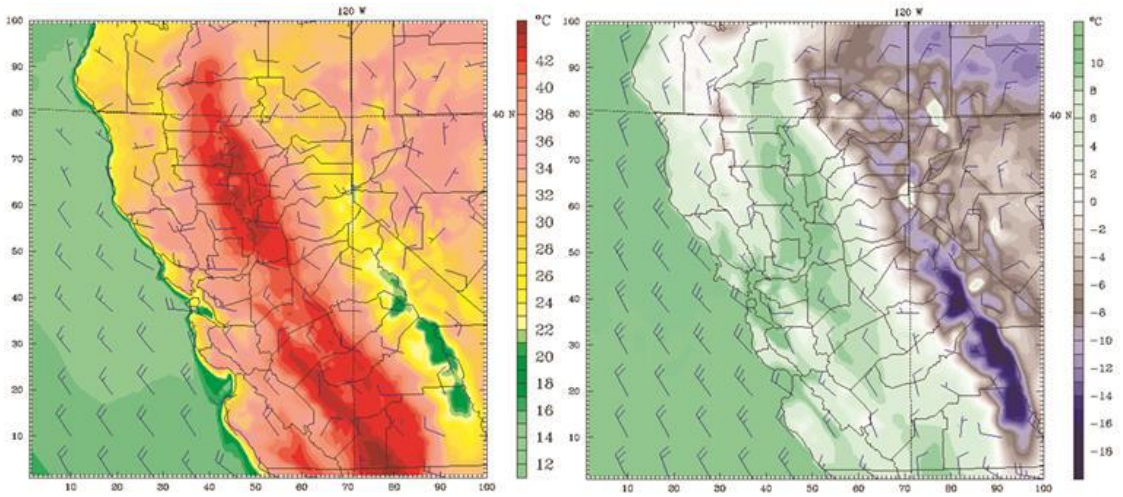

4.5 RESULTS FROM BASE MODELING OF THE 2-km DOMAIN (D04)

As discussed earlier in the analysis of observational weather data in Section 3, the mesonet network in this domain is relatively dense – yet there still are significant gaps in coverage over urban areas that need to be evaluated in this effort. To do so, a number of "probing" points or locations were added in this study to the network of mesonet monitors in order to increase the number of locations where model output can be evaluated in urban areas. Figure 4-4 shows the locations of the mesonet stations (white circles) and the additional probing locations (blue circles). Both sets of points are used in model output analysis but, obviously, only the locations with observations (mesonet – white circles) are used in model performance evaluation, as will be discussed in Section 4.5.3. The probing points were added to several locations in urban areas deemed of interest by the project TAC, SMAQMD, and LGC.

Figure 4-4 also shows a random sample from the model temperature field highlighting the higher temperatures in and around urban areas and the locations of mesonet stations and probing points relative to urban heat plumes in this region. In this example, the field is for all-hours average air temperature at 2 m above ground level for June 15 – 30, 2016 at a resolution of 2 km. In this example, the range of average temperature (from light color to dark) is 13.7 – 28.6 °C and each color level (interval) is 0.5 °C.

Figure 4-4: Locations of mesonet weather stations (white circles) and additional probing point locations (blue circles) in relation to urban heat plumes in the 6-counties Capital region.

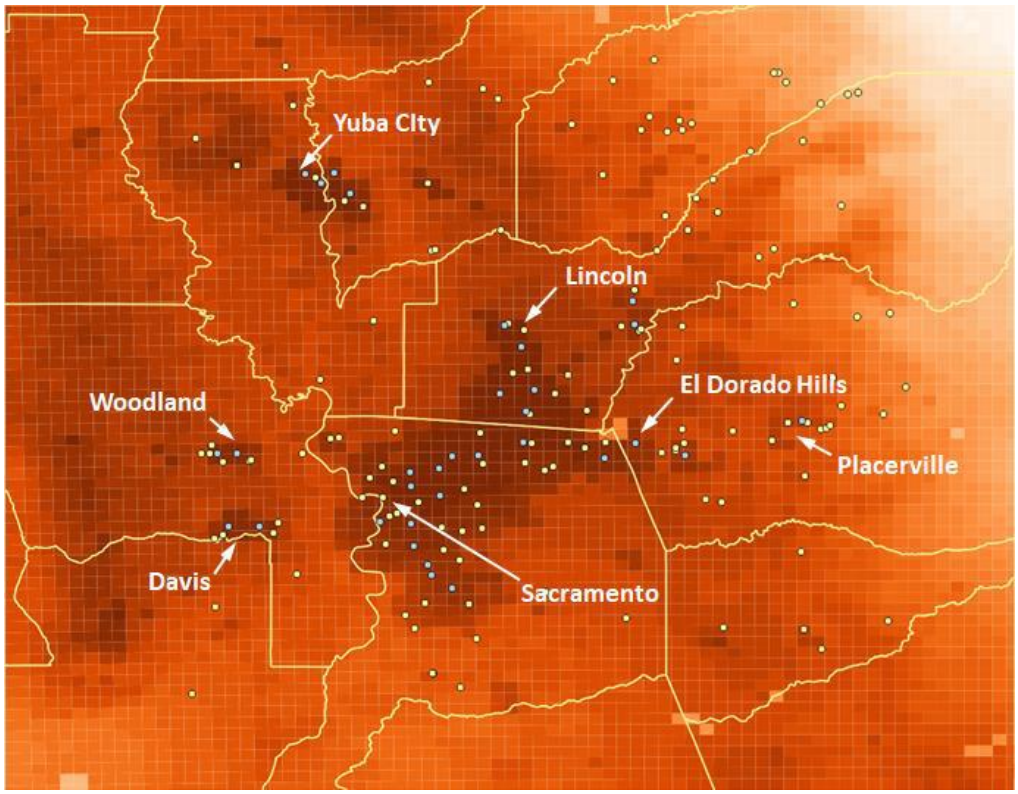

4.5.1 Sample daytime results at 2 km

Figure 4-5 provides a sample of results for the 2-km domain simulated with 55 vertical levels using the Altostratus Inc. AREAMOD approach. Random daytime hours from the simulations of June 2013 are presented. The first figure simply shows the locations of various cities of interest in this study. The subsequent figures provide model temperature fields at 2 m AGL (above ground level) along with the horizontal wind vector (at the lowest atmospheric level) for sample time stamps identified below each figure A – F between 1500 and 1900 PDT. The purpose of Figure 4-5 is to highlight the daytime UHI characteristics and the displacement of heat plumes with wind direction.

It can be seen that urban heat plumes are pushed to the south and southeast by the northwesterly wind (A), to the east by westerly wind (B), and to the east and southeast by westerly and northwesterly wind (C). In figures D, E, and F, the heat plumes are pushed to the north and northeast by the mostly southwesterly wind.

While the general spatial pattern of temperature over the urban areas in this region is relatively similar across different random time stamps, there are significant intra-urban variations in the temperature field from one time interval to another. Thus, whereas the UHI is easily identifiable in all time stamps in the areas of Yuba City / Marysville, Woodland, Davis, and Placerville, the UHI pattern in the central area (the greater Sacramento region) varies from one period to another. For example, in figures A, B, and C the UHI extends throughout the large urban area, whereas in figures D, E, and F, the hottest parts are seen north of the Sacramento-Placer counties boundary line, i.e., in the areas of Rocklin, Roseville, and Lincoln. It can also be seen that the higher temperatures are transported significant distances downwind from urban areas to non-urban, rural, and agricultural land use. The length scale for urban heat transport will be discussed in Section 5.8.

Figure 4-5: Model 2-m temperature field during daytime hours in the 2-km domain.

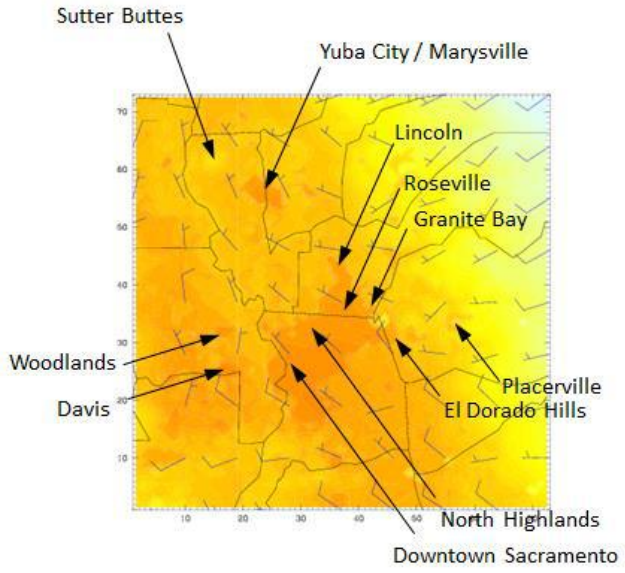

Figure 4-5, continued.

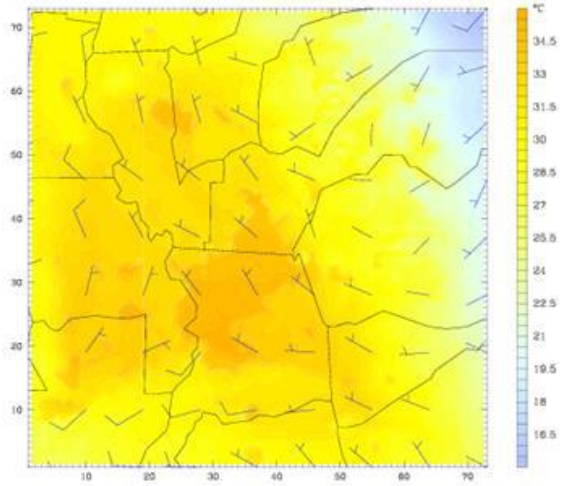

A: 1900 PDT, June 1st, 2013

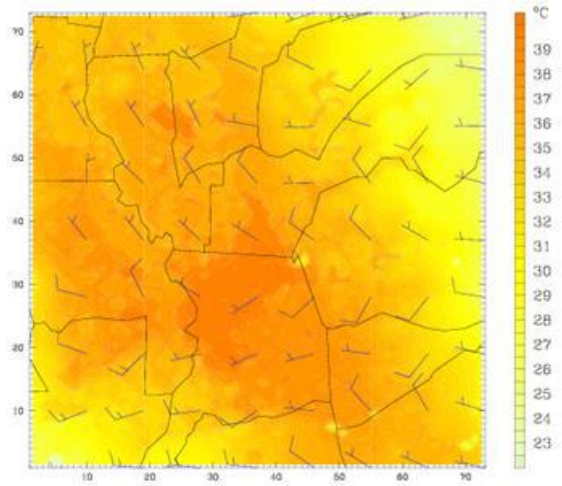

B: 1500 PDT, June 3rd, 2013

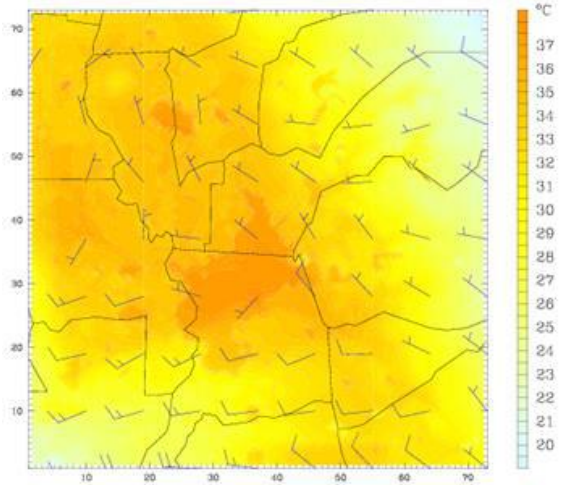

C: 1800 PDT, June 3rd, 2013

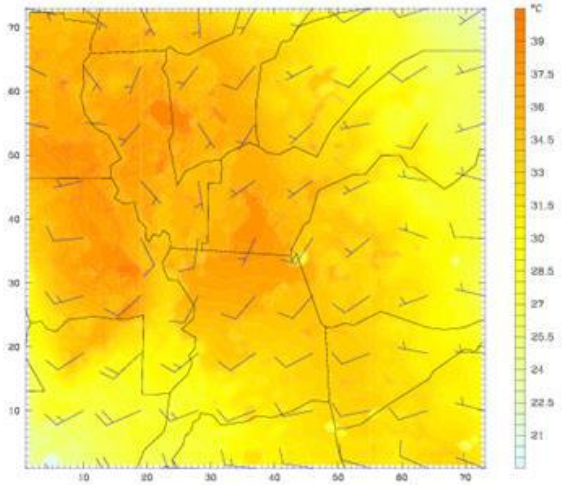

D: 1500 PDT, June 4th, 2013

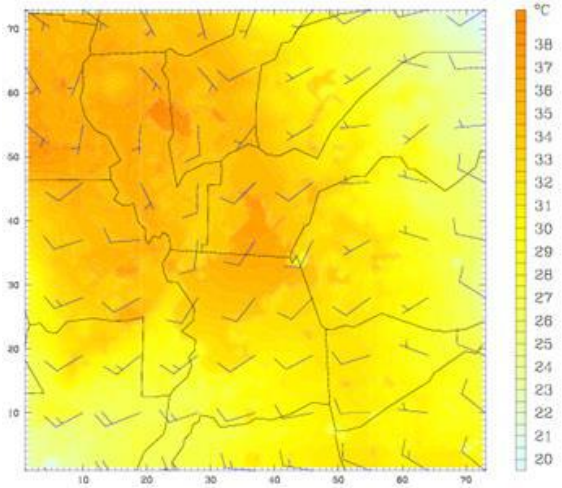

E: 1700 PDT, June 4th, 2013

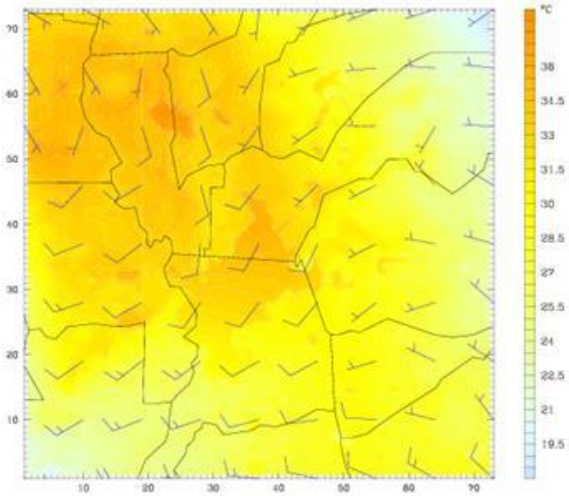

F: 1800 PDT, June 4th, 2013

4.5.2 Sample early morning results

Figure 4-6 is a sample snapshot from the model temperature field at 0700 PDT on two different days, provided here as examples. The figure shows that various areas are warmer than their surroundings, but for different reasons. The central parts of the domain are warmer because they are urban (the outlines of urban areas are clearly identifiable and the UHI is well-defined) whereas the eastern one-third of the domain is warmer because of the higher elevations (nighttime inversion). This is also the reason that the Sutter hills (in the northwestern part of the domain) are warner as are the mountain ranges at the western edge of the domain. These higher elevations are cooler, as expected, during daytime (see Figure 4-5).

Figure 4-6: Model 2-m temperature field during early morning hours in the 2-km domain.

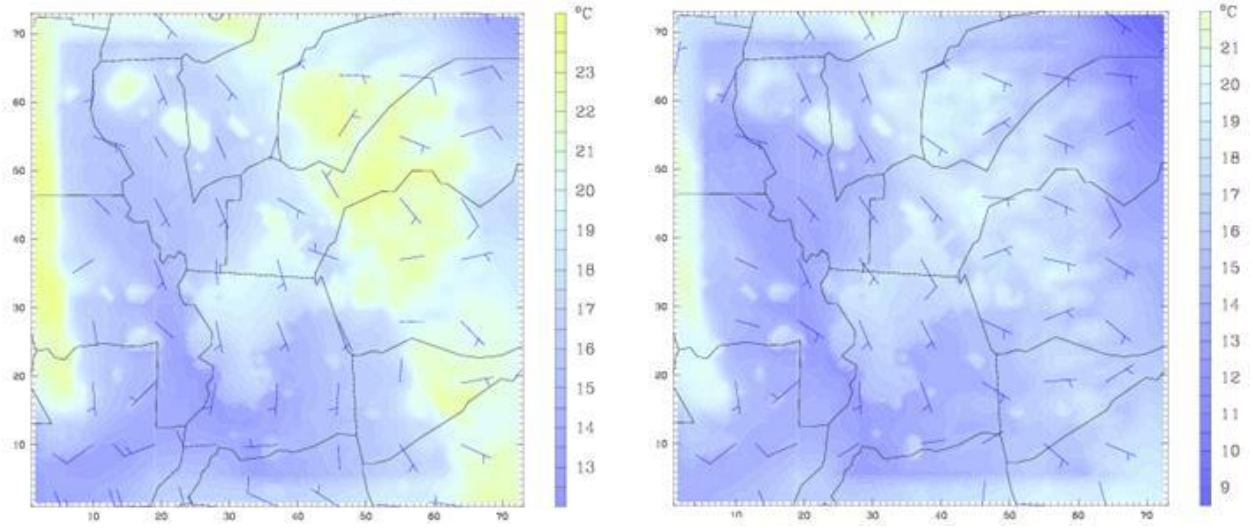

0700 PDT, June 4th, 2013

0700 PDT, June 15th, 2013

4.5.3 Model performance evaluation

Model performance evaluation (MPE) is typically carried out in most modeling projects and, thus, has been historically discussed in a large number of studies, e.g., Tesche et al. (2001). The science and operational basis for MPE will not be repeated here, nor the metrics or benchmarks – only a brief summary of findings is discussed in this section.

In this study, MPE was carried out at the 2-km level for each year and interval at hourly time scales (each interval is 2-weeks long, after removing spin-up days). Variables that were evaluated at each weather station location (Figure 4-4) were (1) air temperature (°C), (2) relative humidity (%), (3) wind speed (m s^{-1}), and (4) wind direction (°).

For 2-m AGL air temperature, two parameters were evaluated: (1) 4-D air temperature (denoted below as "Tair_2m" or "Tair2m") which is interpolated between surface and air temperature at the first ½ eta level of the model and (2) a relatively more "diagnostic" air temperature (denoted as "T2"), computed based on surface temperature and heat-transfer coefficient. Both Tair_2m and T2 were used in this study, depending on MPE results that are area-specific as well as the mitigation measure in question. Some measures require evaluation with T2, others require Tair2m, and, yet, some require use of surface temperature.

MPE statistics that were calculated include mean bias, mean absolute error, root mean squared error, and index of agreement for temperature, humidity, wind speed, and wind direction. Each of the statistics was computed at every station and all hours of model and observations (hours when observations were available at a weather station).

Table 4-1 is a condensed summary of MPE statistics for the 2-km grid. In the table, mean bias (MB), mean error (mean absolute error) (MAE), and RMSE statistics are provided for each of the variables listed above. RMSE is a more stringent indicator than MAE as it is much more sensitive to outliers because of its squared term and, thus, MAE may be a better indicator of performance. In Figure 4-7, the metrics and their ranges are shown with box-and-whiskers plots. The center horizontal line is the median, first to third quartiles shown as a box, and minima and maxima as whiskers with caps. The 95% confidence interval for the median is shown as a notch on the box.

The metrics values for each variable were found to be reasonable and comparable to results from many other studies of California that had good model performance. Of interest to this study is air temperature, where this MPE suggests that Tair_2m is a slightly better indicator than T2 (2.5 °C MAE median versus 2.75 °C) but that both can be used equally well in this application. These values are comparable to recommended benchmarks of 2 - 3 °C as seen in a large number of studies for California.

In terms of relative humidity (RH), in Figure B, there are no specific community-recommended benchmarks, rather, there are some benchmarks for water vapor mixing ratio. However, the RH metrics shown in this figure are reasonable (a median MAE of about 10%) considering the range of RH encountered in the large and varied study domain.

Wind speed statistics (Figure C) show a median MAE of 2 m s^{-1} which is reasonable per community-recommended benchmarks of 2 m s^{-1}. Finally, wind-direction statistics (Figure D) indicate a median MAE of less than 90°. This is considered reasonable as it generally represents the correct flow direction. The recommended benchmarks are between 30° and 60° and in this modeling effort, the median MAE is 55°, which is considered reasonable especially in light of the varied land cover and topography in the region.

Table 4-1: Condensed summary of MPE for D04.

interval	RH_MB	RH_MAE	RH_RMSE	T2_MB	T2_MAE	T2_RMSE	Tair2m_MB	Tair2m_MAE	Tair2m_RMSE	wdr_MB	wdr_MAE	wdr_RMSE	wsp_MB	wsp_MAE	wsp_RMSE
2013_int1	-8.58	11.53	14.19	2.29	2.88	3.52	1.49	2.77	3.38	30.20	70.35	98.66	1.79	2.05	2.40
2013_int2	-10.06	12.15	15.42	1.97	2.53	3.10	0.58	2.13	2.64	25.15	67.36	93.37	1.78	2.05	2.36
2013_int3	-5.84	9.54	12.18	2.46	2.89	3.60	1.40	2.53	3.22	5.69	56.69	76.80	1.75	1.98	2.26
2013_int4	-4.84	9.39	12.02	2.07	2.81	3.37	0.89	2.40	3.01	2.45	47.30	62.82	1.86	2.06	2.30
2013_int5	-8.26	11.26	13.97	2.49	2.89	3.47	1.00	2.22	2.76	0.32	49.64	65.50	1.76	1.97	2.26
2013_int6	-12.34	13.57	16.31	2.02	2.71	3.30	0.76	2.37	2.96	-1.16	53.83	71.88	1.74	2.00	2.30
2013_int7	-13.40	14.65	18.29	1.94	2.81	3.59	0.62	2.38	2.98	-1.69	58.40	82.08	1.56	1.81	2.06
2014_int1	-9.65	11.96	15.41	2.42	2.78	3.31	1.92	2.79	3.45	27.61	72.71	100.24	1.77	2.11	2.47
2014_int2	-5.06	8.88	11.22	1.92	2.62	3.11	0.75	2.25	2.76	20.28	63.22	88.51	1.69	2.05	2.40
2014_int3	-6.58	9.09	11.49	2.44	2.90	3.62	1.78	2.68	3.50	10.68	55.67	75.33	1.91	2.14	2.44
2014_int4	-5.98	9.59	12.27	1.59	2.62	3.27	0.25	2.09	2.62	5.62	52.57	72.46	1.92	2.10	2.39
2014_int5	-8.44	12.12	15.53	2.26	3.04	3.95	0.97	2.55	3.25	-7.38	54.56	73.28	1.74	1.98	2.25
2014_int6	-8.55	10.36	12.81	2.05	2.64	3.23	0.73	2.04	2.52	2.01	53.31	72.49	1.49	1.78	2.03
2014_int7	-14.21	15.44	18.70	2.32	2.84	3.38	1.64	2.64	3.17	2.75	69.29	91.65	1.36	1.66	1.93
2015_int1	-8.15	11.97	15.90	2.13	2.79	3.62	1.11	2.51	3.21	11.13	63.20	86.43	1.67	2.02	2.34
2015_int2	-4.92	8.61	11.03	2.18	2.69	3.20	1.21	2.53	3.17	6.37	54.08	73.39	1.78	2.01	2.28
2015_int3	-3.20	9.08	11.74	1.25	2.49	3.08	-0.04	2.27	2.83	1.17	44.28	58.37	1.89	2.12	2.41
2015_int4	-6.18	10.95	13.76	2.44	2.78	3.38	1.81	2.66	3.40	13.27	61.23	84.22	1.84	2.12	2.41
2015_int5	-5.28	9.36	11.85	2.08	2.67	3.32	0.75	2.22	2.77	-0.80	47.16	65.91	1.69	1.95	2.21
2015_int6	-7.60	10.29	13.00	1.89	2.56	3.25	0.68	2.20	2.86	1.84	54.92	76.61	1.41	1.71	1.96
2015_int7	-7.34	10.96	13.68	2.07	2.76	3.42	1.20	2.63	3.27	4.72	66.40	95.50	1.38	1.79	2.11
2015_int1	-5.94	10.67	13.54	1.86	2.62	3.20	0.98	2.50	3.11	14.51	61.54	86.59	1.55	1.98	2.30
2015_int2	-11.01	12.86	16.13	1.83	2.56	3.17	1.35	2.72	3.45	20.31	73.59	99.71	1.48	1.83	2.14
2015_int3	-7.17	9.64	11.65	2.47	2.83	3.34	1.58	2.54	3.12	9.72	53.02	73.88	1.78	2.06	2.34
2015_int4	-9.57	10.97	13.23	2.54	2.85	3.36	1.80	2.55	3.10	6.12	51.73	71.01	1.74	2.00	2.29
2015_int5	-8.54	11.24	13.74	2.51	2.84	3.32	1.52	2.38	2.92	5.51	53.76	72.06	1.62	1.87	2.16
2015_int6	-11.48	13.62	16.98	2.52	3.02	3.61	1.55	2.60	3.18	-1.67	46.79	61.87	1.58	1.82	2.06
2015_int7	-10.87	13.51	16.36	2.39	2.84	3.39	1.26	2.31	2.84	3.97	62.90	86.65	1.56	1.87	2.14

Figure 4-7. MPE metrics for 2-km domain (D04)

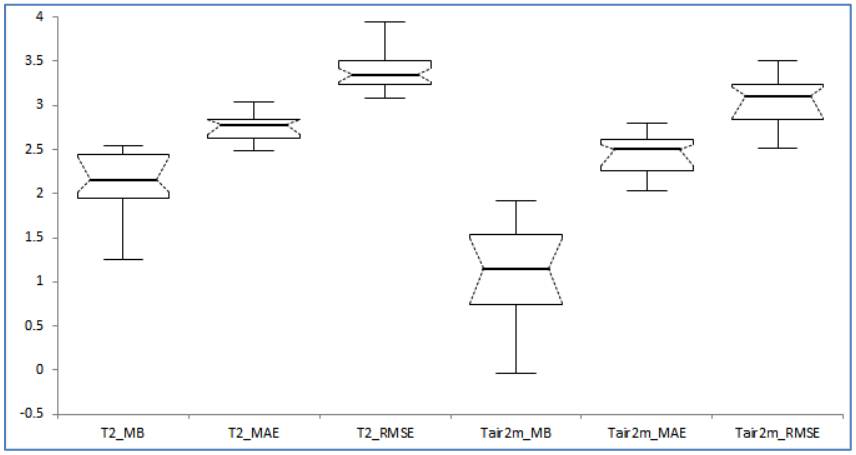

A: Air temperature statistics (int1-int7, 2013-2016); vertical axis is °C.

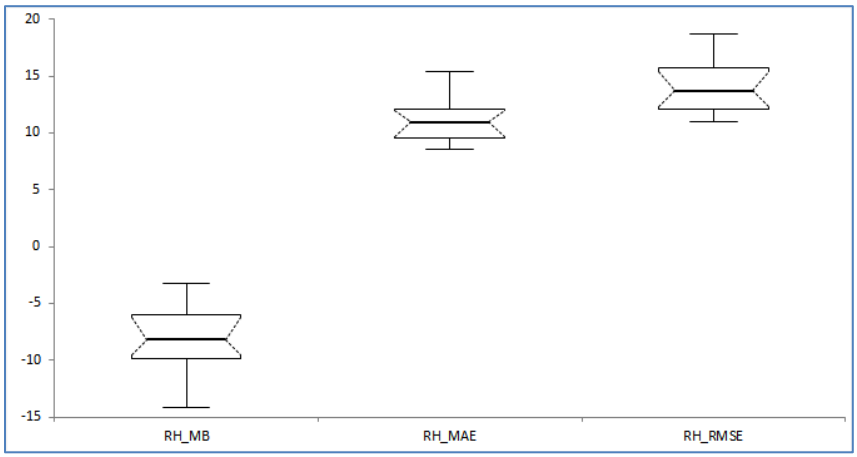

B: RH statistics (int1-int7, 2013-2016); vertical axis is %.

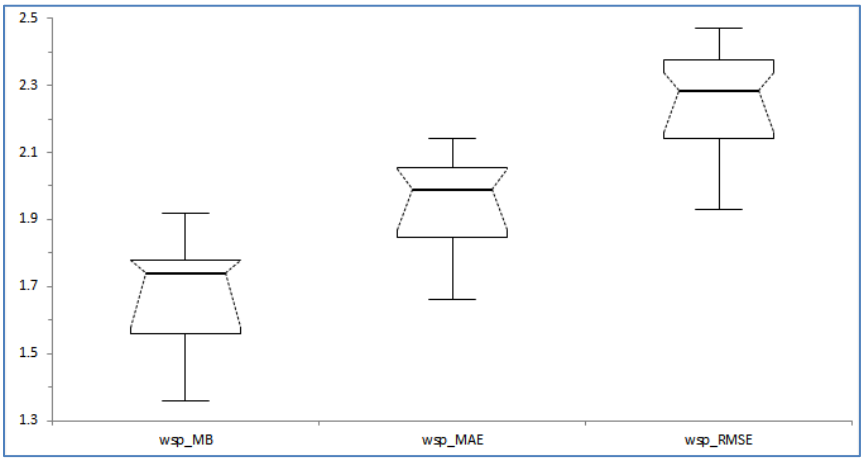

C: Wind speed statistics (int1-int7, 2013-2016); vertical axis is m s^{-1}.

Figure 4-7, continued.

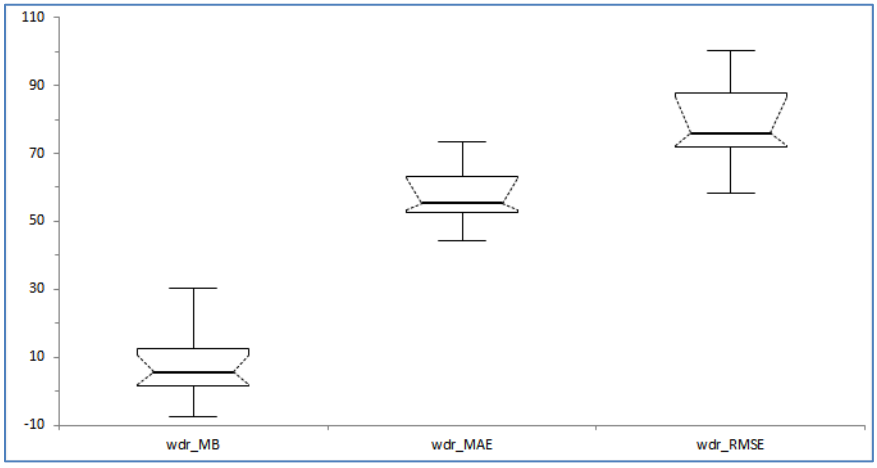

D: Wind direction statistics (int1-int7, 2013-2016); vertical axis is °.

5. EFFECTS OF MITIGATION MEASURES IN CURRENT CLIMATE AND LAND USE

5.1 OBJECTIVES OF MODELING MITIGATION MEASURES IN CURRENT CONDITIONS

Following the establishment of base meteorology and carrying out model performance evaluation as discussed in Section 4, the main objectives of the next steps were to:

- Customize area- and cell-specific characterizations and model input:
  - Present -day meteorological input, initial and boundary conditions
  - Present-day land-use/land-cover
  - Current-conditions urban morphology and surface thermo-physical properties
  - Technical potential for deployment of mitigation measures;
- Perform additional present-day base-case meteorological simulations to characterize current climate conditions, metrics, and UHII as well as develop a more detailed basis against which the mitigation measures are compared;
- Perform present-day simulations of mitigation measures, combinations of measures, and characterize various levels of the UHII;
- Develop metrics and thresholds and apply them in quantification of benefits, e.g., in terms of urban-heat reduction; and
- Develop derivatives and metrics for translation of meteorological model results into planning guidelines for the transportation system and the communities that were selected in the study region.

In this section, results from two modeling components are presented: (1) modeling and analysis at 2-km resolution for the domain encompassing the 6-counties Capital region to evaluate mitigation measures region-wide and (2) modeling and analysis at the 500-m scale to evaluate the potential benefits of localized and project-specific mitigation measures at the community or neighborhood scales.

It is to be noted here that Section 5 (this section) addresses only current conditions of climate and LULC. Future climates and LULC, their effects, and mitigation, are discussed in Section 6.

In this section and in the rest of this report, time intervals 1 – 7 are defined as follows:

Interval 1: June 1 – 15; Interval 2: June 16 – 30; Interval 3: July 1 – 15; Interval 4: July 16 – 31; Interval 5: August 1 – 15; Interval 6: August 16 – 31; and Interval 7: September 1 – 15. The time

periods are also abbreviated as YYYY_int#, for example: 2013_int6, meaning August 16 – 31, 2013.

5.2 MODELING CURRENT CONDITIONS: 2-m TEMPERATURE FIELD

As the model output is very large, this and the following sections focus on and provide some samples from the 2-m AGL temperature field as a subset from the simulation results. In Appendixes B-1 and B-2, averages over intervals 2, 4, and 6 (June 16-30, July 16-31, August 16-31) of each year (2013 – 2018) are presented for all hours and for 1500 PDT. For other times of day, or other intervals, the data is included in the model output but not discussed in this section, nor plotted in the figures.

As discussed in Section 4, modeling of the 2-km regional domain (and the output discussed in this section) was carried out with Altostratus Inc's AREAMOD approach. And while there are many ways, variables, and derivatives that could be presented, here the 2-m AGL temperature field is shown for a few example snapshots as an introduction. Later in this report, various metrics and threshold analyses at the 2-km scale will be presented.

The range of current-climate, modeled 2-m air-temperature across the 6-counties Capital region is summarized in Table 5-1 for intervals 2, 4, and 6. In general, those time intervals with the highest all-hour average temperatures also are the intervals with the highest daily maximum temperatures, e.g., at 1500 PDT. The model temperature ranges and absolute values discussed here compare well with the results from analysis of observational data (from mesonet networks) discussed in Section 3.

Table 5-1: Model temperature range (°C) across the 6-counties region during various time intervals.

	Model temperature range across the 6-counties domain	
	All-hours average (°C)	1500-PDT average (°C)
2013, June 16 - 30	11.52 – 26.18	14.59 – 32.23
2013, July 16 - 31	16.98 – 29.12	18.59 – 36.99
2013, August 16 - 31	15.28 – 28.50	18.43 – 36.29
2014, June 16 - 30	11.91 – 26.70	15.68 – 33.66
2014, July 16 - 31	17.78 – 28.51	19.41 – 36.91
2014, August 16 - 31	14.75 – 27.70	18.07 – 35.64
2015, June 16 - 30	16.91 – 30.20	20.01 – 37.41
2015, July 16 - 31	14.89 – 30.03	17.71 – 37.41
2015, August 16 - 31	16.77 – 28.86	19.77 – 36.46
2016, June 16 - 30	13.71 – 28.55	17.71 – 35.60
2016, July 16 - 31	17.30 – 31.02	20.84 – 39.17
2016, August 16 - 31	17.52 – 28.79	19.06 – 37.57

A random example from the model temperature field is presented in Figures 5-1 – 5-4 as (1) all-hour averages and (2) 1500 PDT averages for selected periods. Figures 5-1 and 5-2 show a sample from the all-hours model temperature field in the 6-counties region, e.g., the all-hour average field for the periods 2013_int2 and 2013_int4, respectively. These periods exhibit two different but common spatial patterns of the temperature field that are seen in many other periods and time intervals as well.

Thus, whereas the absolute temperature range differs between these two periods, the more remarkable difference is in the spatial pattern of urban heat, i.e., temperature field in and around urban areas in the Capital region. The differences arise because of the different dominant wind directions – for example, in Figure 5-1, the dominant wind is mainly northwesterly, northerly, and northeasterly whereas in Figure 5-2, the dominant wind is mostly westerly and southwesterly. It can be seen in the latter case that the temperature contrast in Sacramento County, as well as in the areas of Woodland and Davis, is diminished relative to surrounding areas (compared to Figure 5-1). In this case, most of the higher temperatures are found in areas from Rocklin and Roseville to Lincoln, in Placerville, and Yuba City / Marysville. The relatively consistent higher urban heat in the Rocklin-Roseville area (relative to different wind directions) is one reason why the UHI Index (Taha 2017) for this area is pushed northeast of the central Sacramento area, including downtown Sacramento. This was also seen in the UHI Index developed for the Cal/EPA (Taha and Freed 2015).

To examine this aspect further, Figures 5-3 and 5-4 show the 1500-PDT average temperature field corresponding to the same two periods examined in Figures 5-1 and 5-2. Although now the intra-urban temperature contrast is less obvious at 1500 PDT (relative to all-hours field discussed above), a similar observation can be made with respect to Sacramento County, Davis, and Woodland in that their temperatures are less differentiated from their surroundings, e.g., Figure 5-4 (westerly and southwesterly wind) relative to Figure 5-3 (northwesterly, northerly, and northeasterly wind).

As described in Section 3, the white circles in the figures represent locations of mesonet monitors in the region and the blue circles are the locations of additional probing points used in the analysis of the temperature (and other) fields.

Figure 5-1: All hours, non-threshold, average 2-m AGL air temperature (°C); 2-km domain; Year 2013, interval 2; 30 temperature levels, Δ ≈ 0.5 °C; Actual range: 11.5 – 26.2 °C

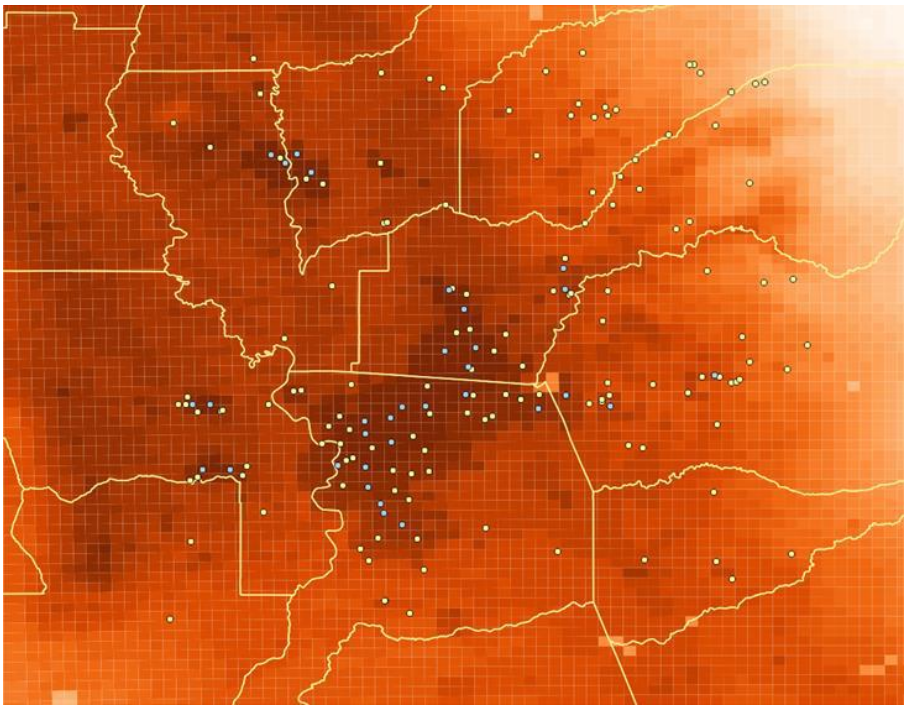

Figure 5-2: All hours, non-threshold, average 2-m AGL air temperature (°C); 2-km domain; Year 2013, interval 4; 25 temperature levels, Δ ≈ 0.5 °C; Actual range: 17.0 – 29.1 °C

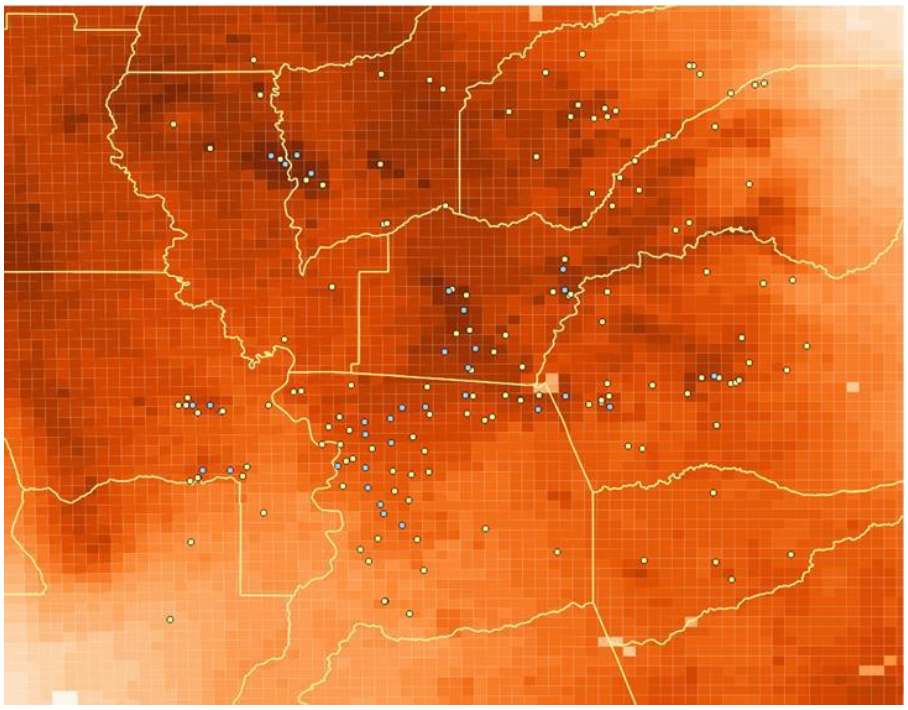

Figure 5-3: 1500 PDT, non-threshold, average 2-m AGL air temperature (°C); 2-km domain; Year 2013, interval 2; 30 temperature levels, Δ ≈ 0.5 °C; Actual range: 14.6 – 32.2 °C

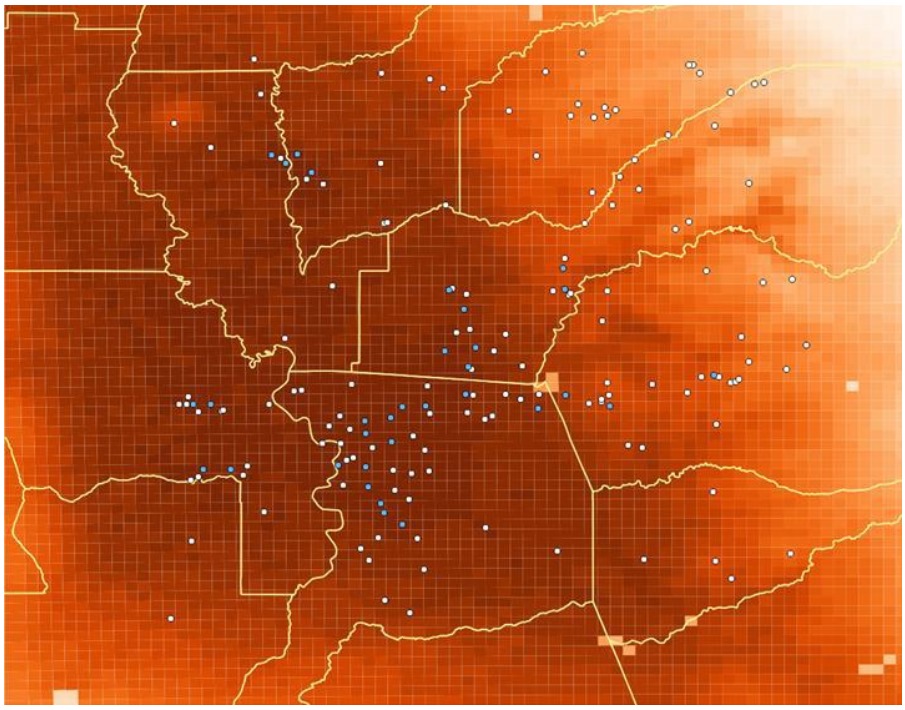

Figure 5-4: 1500 PDT, non-threshold, average 2-m AGL air temperature (°C); 2-km domain; Year 2013, interval 4; 35 temperature levels, Δ ≈ 0.5 °C; Actual range: 18.6 – 37.0 °C

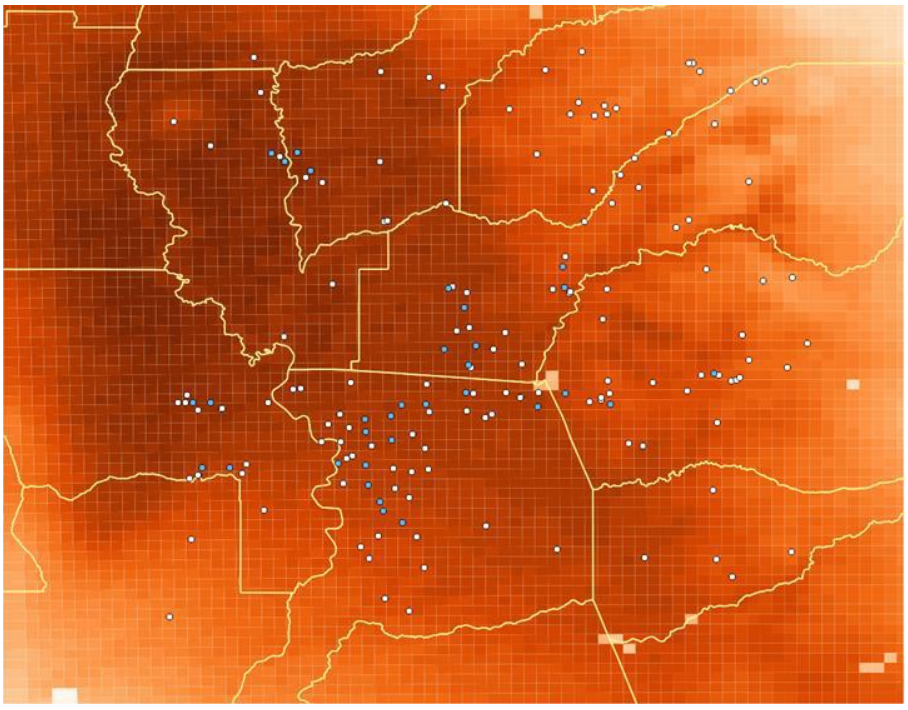

5.3 CHARACTERIZATION OF THE UHI INDEX (UHII) IN CURRENT CLIMATE

The goal of this sub-task was to establish the base-case conditions, as represented by the UHII, resulting from effects of current LULC properties in current climate. This serves both to characterize urban heat and to form a basis against which the benefits (or effects) of mitigation measures can be compared. The model results discussed in this section are for the regional 6-counties Capital region domain, including a separate UHII "tile" for each subregion as shown in Figure 5-5.

Summer months May to September (MJJAS) of years 2013 – 2016 inclusive were modeled. Throughout this report, some results are provided for specific hours or random intervals/times, and other results are presented as averages or cumulatives over the entire modeled periods and/or over various sub-domains.

To increase the accuracy of the simulations, a "leap frog" technique (Taha 2017, 2018; Taha and Freed 2015) was used. This approach minimizes model drift in long simulations and allows the capture of signals in the reanalysis (e.g., NNRP, Kistler et al. 2001) that may no longer be "seen" or refreshed during long simulations. Thus, while this approach increases computational burden by about 15% to 20%, it increases model accuracy over long periods of time. After removal of spin-up days in each interval, the results are presented as "net" 15- or 16-day blocks of time throughout the modeled seasons. In this report, these intervals are labeled int1, int2, int3, and so on, as defined earlier in Section 5.1.

In order to compute the UHII, the 6-counties Capital region was divided into six "tiles" or sub-domains each of which has its corresponding non-urban, upwind temperature reference points (as shown in Figure 5-5). The reason for assigning different, separate reference points for each sub-domain is to cancel out the large-scale, regional climate effects, i.e., the changes in the background temperature across the region. For example, areas to the north of Sacramento (such as Yuba City / Marysville) are generally warmer than south-west Sacramento simply because of changes in the synoptic weather and reduced impacts from the sea breeze (from the San Francisco Bay Area), and this regional heat pattern is unrelated to urban effects. Thus, using separate non-urban reference points for different tiles can address and compensate for these regional climate differences. Furthermore, the UHII at any location (i.e., at each grid cell) within each tile is computed relative to a time-varying, wind-direction-dependent upwind reference point. As it is possible that, at any given time, the wind approach direction is different in various tiles, the UHII is computed per different directions within the region. This approach, while more accurate than standard methodologies of using static reference points, can sometimes produce counter-intuitive spatial patterns of the UHI and UHII.

Figure 5-5: UHII-computation tiles and upwind reference points in the 6-counties Capital region (superimposed on a random-hour temperature field).

The upwind temperature reference points, a subset of which is shown in Figure 5-5, were selected to be outside of the urban heat plumes for each wind direction. This was determined after results from an ensemble of base model runs was examined to characterize the plumes and their variations with time and wind direction. This also took into account the temperature length scales discussed later in Section 5.8.

Counter clock-wise from top in Figure 5-5, the tiles are for the regions of: Yuba City / Marysville, Woodland, Davis, Sacramento, Placerville, and Auburn. At each hourly or sub-hourly interval of the AREAMOD / WRF simulations, the wind approach direction at each grid cell in the tiles is evaluated and the UHII computed per upwind reference point for each tile independently of others.

Based on these reference points and hourly calculations at each grid cell relative to coincident wind direction, the UHII was computed for all years, periods (intervals), and regions. It was calculated for all hours, as well as for specific hours, e.g., early morning, evening, and times of peaks, as well as for a range of hours, e.g., 1400 to 2000 PDT. A graphical example for all-hours UHII is shown in Figure 5-6 where, additionally, several AB617 communities defined by the Sacramento Metropolitan AQMD are highlighted (SMAQMD 2018).

Figure 5-6: Composite of UHII tiles, July 16-31, 2015 all-hours averaged UHI Index for six tiles in the Capital region (A – H are selected AB617 communities).

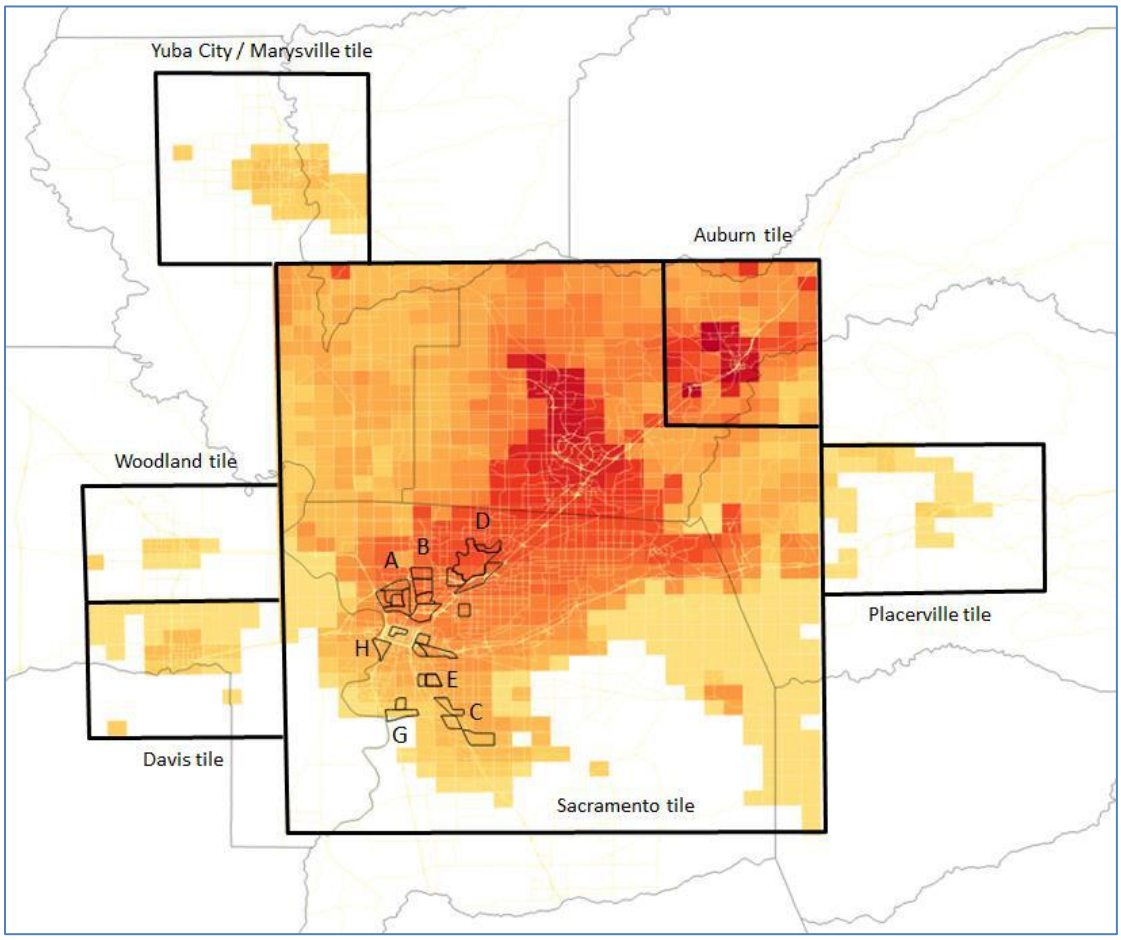

In this example (Figure 5-6), the UHII is computed for the period July 16 – 31, 2015 for which, the all-hours averaged temperature equivalent (i.e., DH hr^{-1}) is as follows (for selected AB617 communities):

A: 3.3 °C; B: 3.6 °C; C: 2.1 °C; D: 3.9 °C; E: 2.1 °C; G: 1.5 °C; and H: 2.7 °C. Other UHII temperature equivalents shown in this figure are Davis: 2.1 °C; Woodland: 1.5 °C; Yuba City: 2.2 °C; Placerville: 1.8 °C; Auburn: 4.5 °C; and Roseville-Lincoln: 4.7 °C. Recall, again, that each tile is independent of the others, even though they are merged and plotted together on the same map shown in the figure.

In areas such as Auburn and Lincoln, the UHII can be elevated at times because of day/night variations in temperature of the natural surroundings, higher elevations (Auburn), or heat transport from upwind urban areas (Lincoln). The latter effect can be explained as follows. As the Taylor series expansion or the total derivative of temperature (*T*) tells us (equation 5-1), the change in air

temperature at any location on Earth (e.g., a point in an urban area) is the sum of (1) temperature change resulting from local heat generation or physical processes and (2) change resulting from transport of heat from upwind sources, e.g., upwind urban areas. The local heat generation could be from anthropogenic origins such as motor vehicles, buildings, etc., or resulting from heat fluxes caused by certain surface physical properties of roofs, pavements, roadways, and so on.

$$\frac{dT}{dt} = \frac{\partial T}{\partial t} + u \cdot \nabla T \qquad (5\text{-}1)$$

The LHS of Equation 5-1 is total derivative for temperature, the first term on RHS is local temperature change, e.g., a result of local sources / sinks of temperature or heat generation, and the last term is advection of temperature from upwind areas, e.g., upwind urban land use or from some other sources of heat.

Thus, if the local heat-generation term were held constant at any given time interval, the change in local temperature becomes proportional to heat transported to the area which, in turn, is proportional to the time and distance an air mass travels over an urban area (for example) before arriving at the location of interest. Figure 5-7 shows an example depicting back trajectories arriving at three locations in the greater Sacramento region, computed based on the Altostratus Inc. AREAMOD / WRF approach. While wind direction varies from day to day and hour to hour, in this example a significant percentage of the approach directions is from the southwest, i.e., from the San Francisco Bay Area.

As seen in the figure, air masses typically travel over mostly crop, natural, and agricultural lands before arriving at AB617 community C, but other air masses travel slightly longer over urban areas before arriving at communities A and B. However, air masses arriving at Rocklin travel for almost 4 hours over urban areas before arriving there. Per Equation 5-1, this partly explains why the UHII is larger in communities A and B than in community C and also why it is significantly larger in the Rocklin area than in communities A and B.

As will be shown later in this report, this is also the reason why reducing the UHII (i.e., cooling) with mitigation measures, assuming region-wide deployment, also increases in this direction. That is, the cooling at Rocklin is generally greater than cooling at communities A and B, and greater than cooling at community C, because the air arriving at Rocklin, for example, is already cooler because of brushing over a longer upwind stretch of cooled urban areas.

Figure 5-7: Back trajectories example, July 16 – 31, 2015, arriving at 1400 PDT on 13 different days. The "4" marker is the position of the air mass four hours prior to arrival, i.e., its position at 1000 PDT. Urban areas are highlighted with brown or orange background.

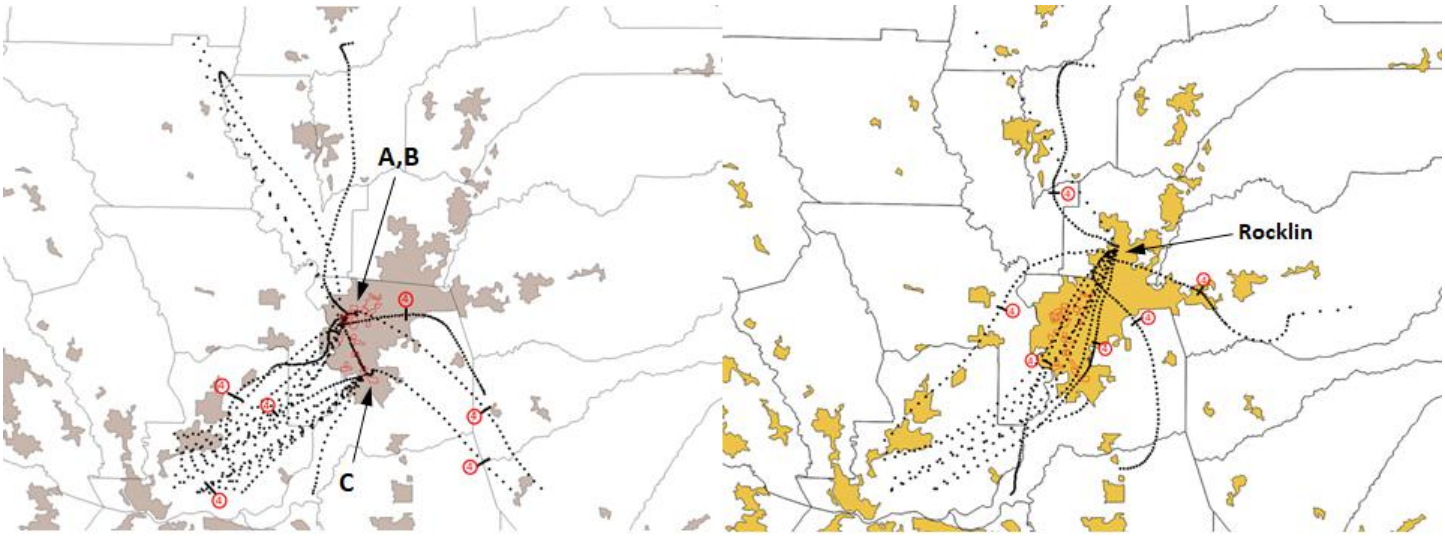

Arriving AB617 communities "A","B" and community "C" at 1400 PDT on 13 different days

Arriving Rocklin area at 1400 PDT on 13 different days

5.4 UHII VERSUS CES 3.0 AND CALTRANS FACILITIES AND ROADWAY PROJECTS

The UHII was computed based on current climate (2013 – 2016) and compared to the CalEnviroScreen (CES 3.0, OEHHA 2013) scores for various areas in the study region (this analysis will be discussed in more detail in Section 5.17). Figure 5-8a provides a qualitative comparison between the two datasets using the UHII for the period July 16 – 31, 2015 as an example. One can see that in the UHII tiles of Yuba City / Marysville, Woodland, Davis, and Placerville, there is a good agreement between the two, that is, the higher the CES score, the higher the UHII. In the larger Sacramento Metro area and in some areas near Auburn, the correlations are mixed because of the significant variability of temperature in the large region. Thus, whereas in the western half of this urban region there is positive correlation between UHII and CES 3.0 score, especially in the AB617 communities (outlined with black lines), in the eastern part, the UHII is high but the CES score is low. Thus, in terms of mitigation, this suggests, at least qualitatively, that the western half is more of a priority for deployment of urban cooling measures.

It is important to re-emphasize that Figures 5-6, 5-8a, and similar others, represent the UHII (in various tiles) and not the absolute temperature as a continuous field. As a result, one might be tempted to conclude, for example, that Auburn is hotter than some parts of Sacramento, say communities A, B, and D (see Figure 5-6). However, this can be misleading -- what the UHII Figures 5-6 and 5-8a show is that the temperature difference between urban and non-urban areas in Auburn is larger than the temperature difference between communities A, B, D, and some non-

urban areas in Sacramento. To clarify this further, Figure 5-8b shows the continuous temperature field (not UHII) for the region, averaged over the period 1400-2000 PDT during the same sample interval (July 16 – 31, 2015). The continuous temperature field shows that Auburn is actually cooler than communities A, B, and D (while its UHII is larger). Some differences are computed as an example (and listed in Figure 5-8b) relative to a single reference point for all areas in this domain, not tiled or wind-direction-dependent as with the UHII (this is done for illustration purposes only) and it can be seen that Auburn is 1.3 °C warmer than the reference point whereas communities A, B, and D are 3.2 to 3.6 °C warmer than that point. In other words, Auburn is about 2.1 °C cooler on average than communities A, B, and D even though its UHII is larger than that of these communities.

Another point that is emphasized throughout this report is that urban heat indicators (e.g., UHI or UHII) addressed in this study are air-temperature-based, not derived from skin surface temperature. Hence, the spatial patterns of urban heat presented in this report (e.g., Figure 5-8a) can differ significantly from those seen in other datasets, e.g., from satellite imagery.

Figure 5-8a: All-hours UHII (2015 int4) versus CES 3.0 scores (percentages). White circles are 0% and dark brown are 100% (highest) CES scores. The UHII ranges from white (0) to dark red (2176 DH/15 days), each step is 155 DH/15 days.

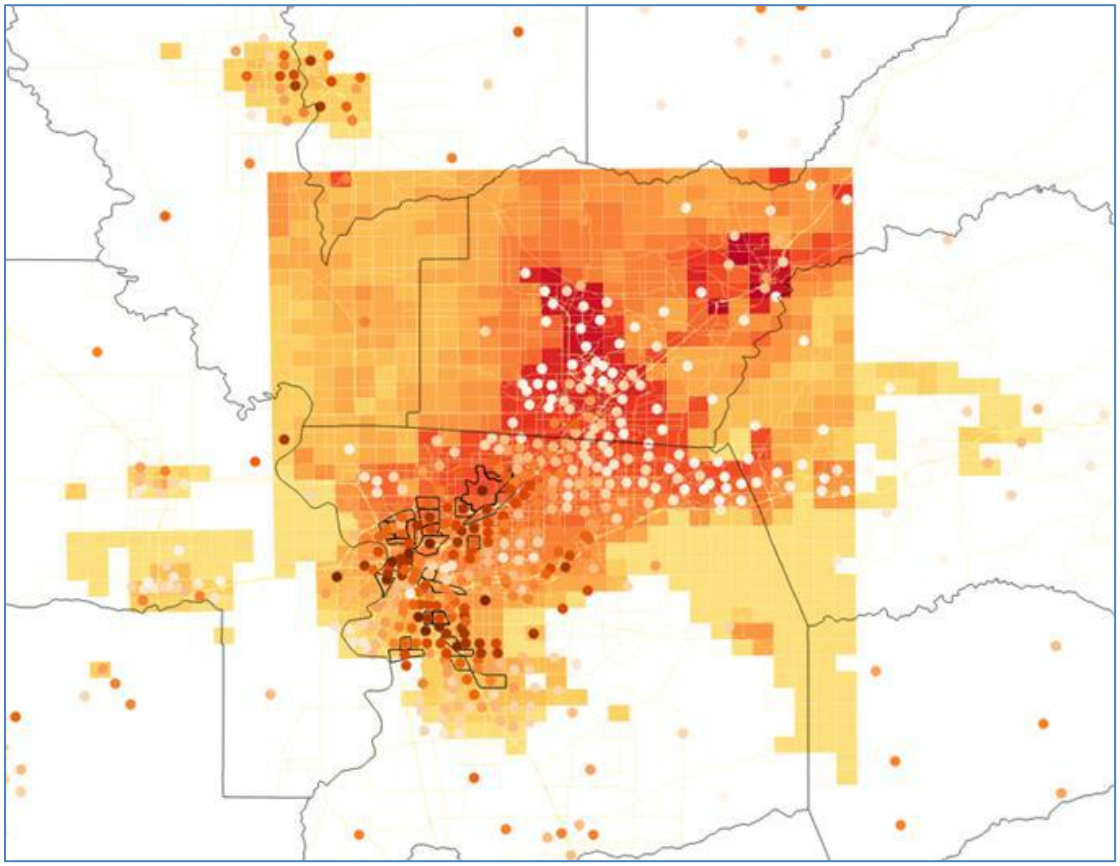

Figure 5-8b: Air-temperature field averaged over hours 1400 – 2000 PDT for July 16 – 31, 2015.

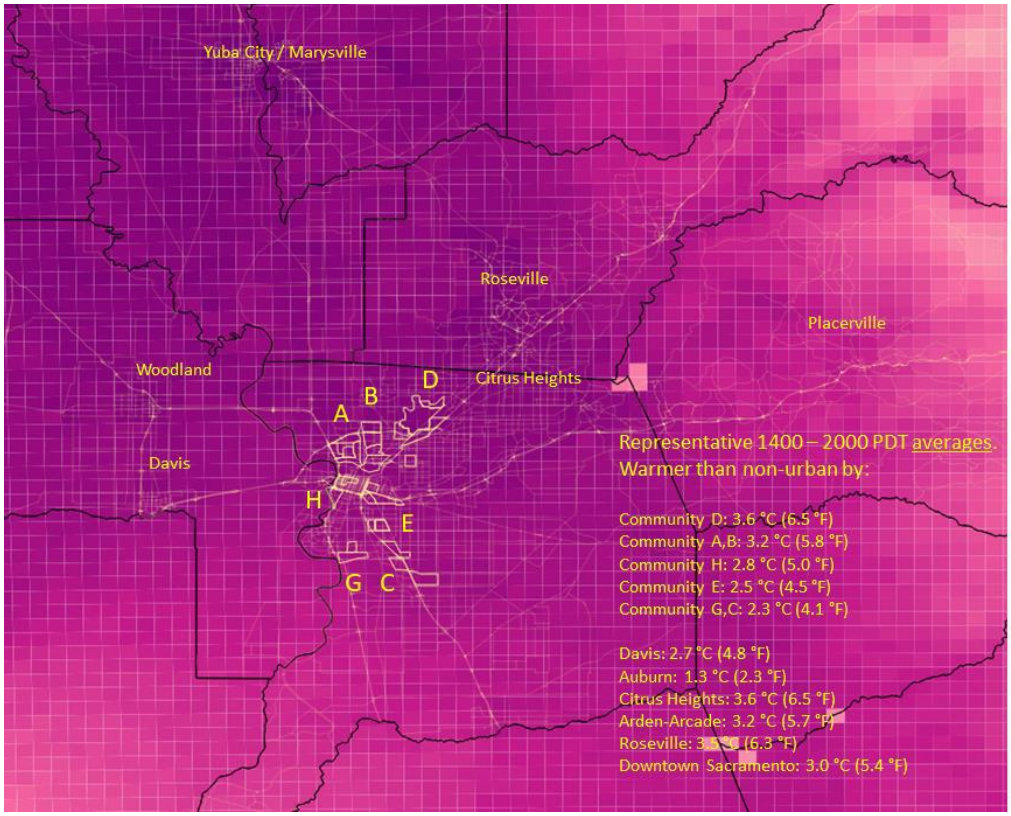

Furthermore, various attributes of urban heat and the UHII may be of interest to Caltrans, cities, local jurisdictions, and communities as they affect various aspects of paving, maintenance of roadways, aging of materials, and the transportation infrastructure in general. The impacts of UHI-mitigation measures on skin surface temperature (that can provide benefits during pavements' initial construction and in long-term maintenance and aging) will be discussed later in this report when presenting results from the fine-scale simulations. Here, in this section, a qualitative assessment of Caltrans's facilities and roadway projects locations in relation to the UHII is provided as an initial prioritization of where urban-cooling measures might need to be introduced first (among other considerations).

Those facilities and roadways that fall within the boundaries of the study domains are superimposed upon the UHII and shown in Figure 5-9. These include locations of airports, Amtrak stations, state highways, and traffic volume within the UHII tiles modeled in this region (tiles were defined above).

This, of course, is only a climate/meteorology basis for geographically prioritizing the mitigation measures, which is one of many considerations. In Figure 5-9, the all-hours UHII for July 16 – 31, 2015, is shown in the background (other years and intervals provide similar information). The UHII range in this example is from 0 to 2176 °C·hr per 15 days and each step change in color is

equivalent to 155 °C·hr per 15 days. Considering the information shown in Figure 5-9, a rough, initial ranking of Caltrans facilities can be formulated based on the UHII, from highest (most severe) to lowest (less severe):

- Airports rankings (highest to lowest UHII):
  - Auburn Municipal (AUN), Lincoln Regional (LHM), Sacramento McClellan (MCC), Rio Linda (L36), Sacramento International (SMF), Sacramento Executive (SAC), Sutter County (O52), Yuba County (MYV), Rancho Murieta (RIU), UC Davis (EDU), Yolo County (DWA), Placerville (PFV), and Woodland (O41);
- Amtrak stations rankings (highest to lowest UHII):
  - Auburn (ARN), Rocklin (RLN), Roseville (RSV), Marysville (MRV), Sacramento (SAC), State Capitol (SCS), Davis (DAV), Placerville (PCV), and Elk Grove (EKG);
- State highways rankings (highest to lowest UHII):
  - 65, 80, 244, 50, and 51; and
- Priorities based on traffic density (represented by the closeness of dots in the figure) versus the UHII and the main routes in the region.

Figure 5-9: UHII versus Caltrans roadways and facilities locations. Data sources for facilities and roadway locations: Caltrans 2019.

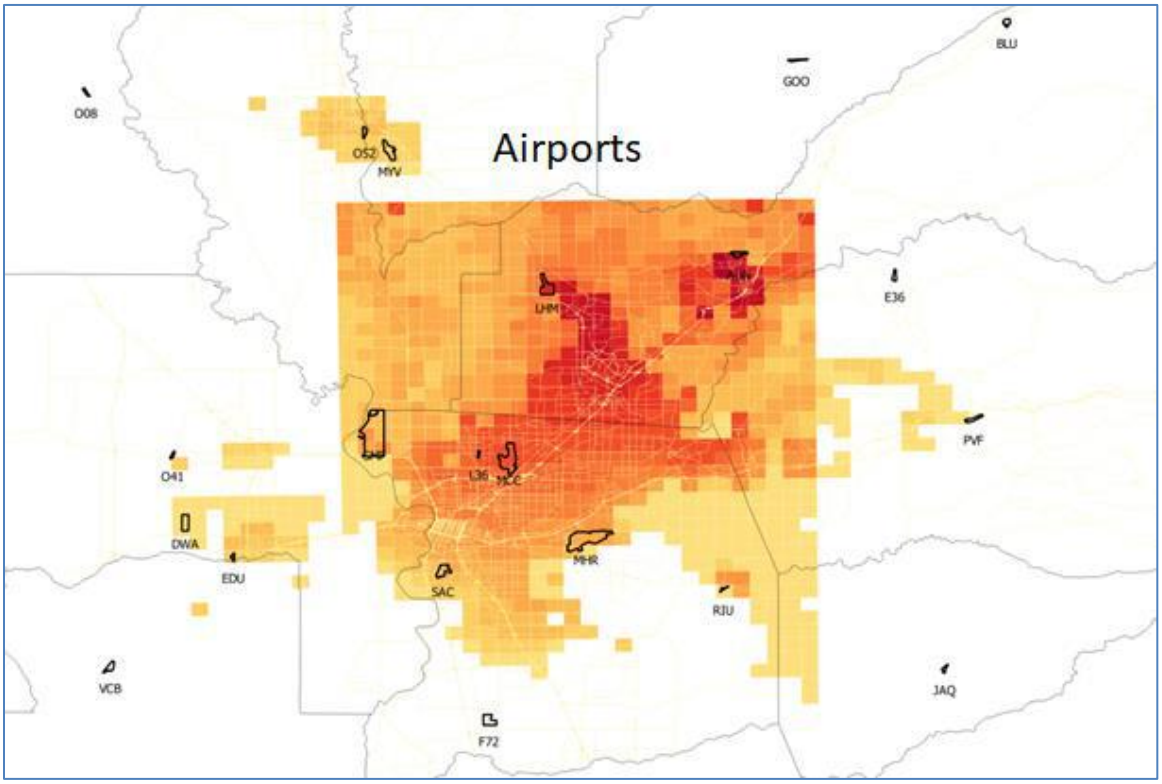

Figure 5-9, continued.

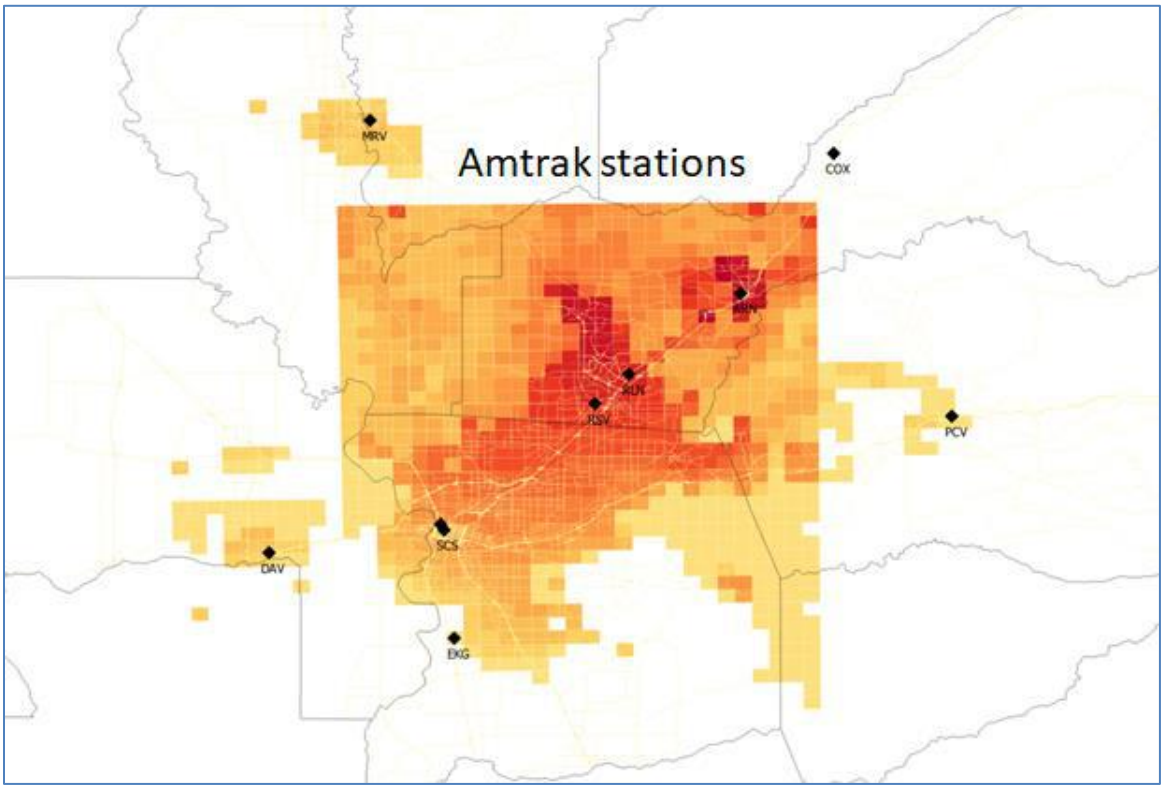

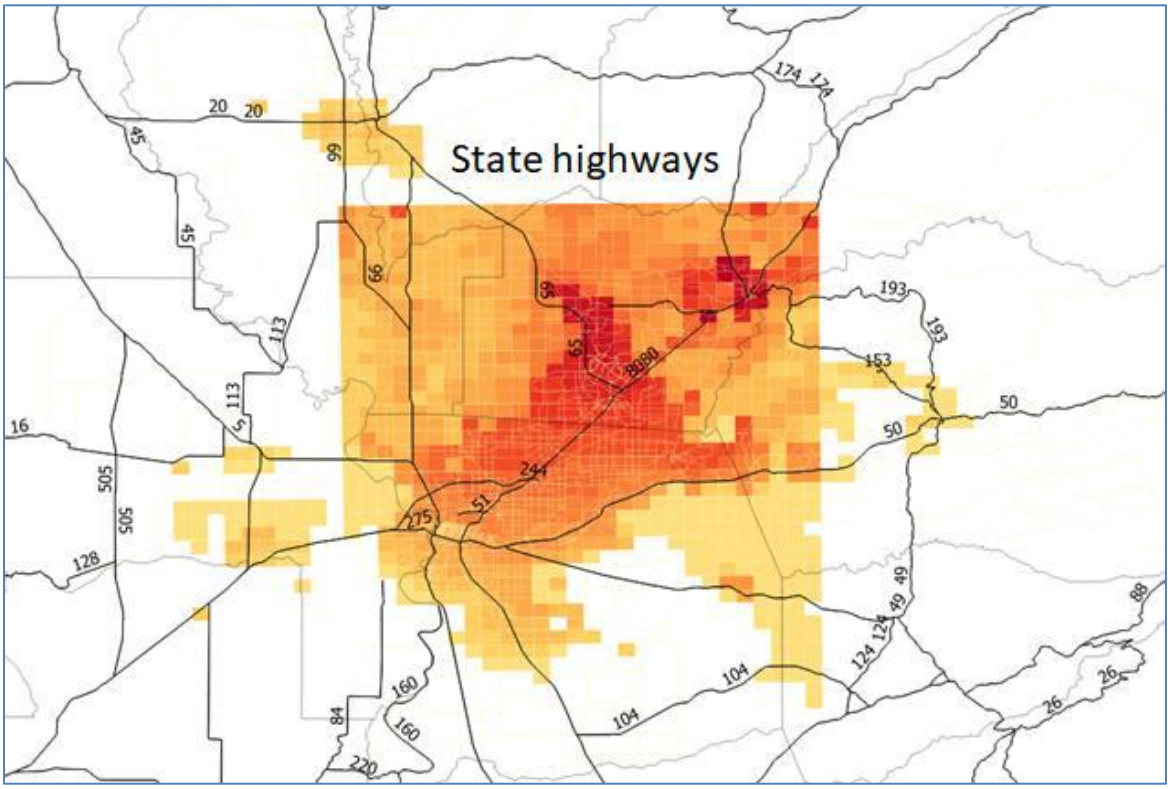

Figure 5-9, continued.

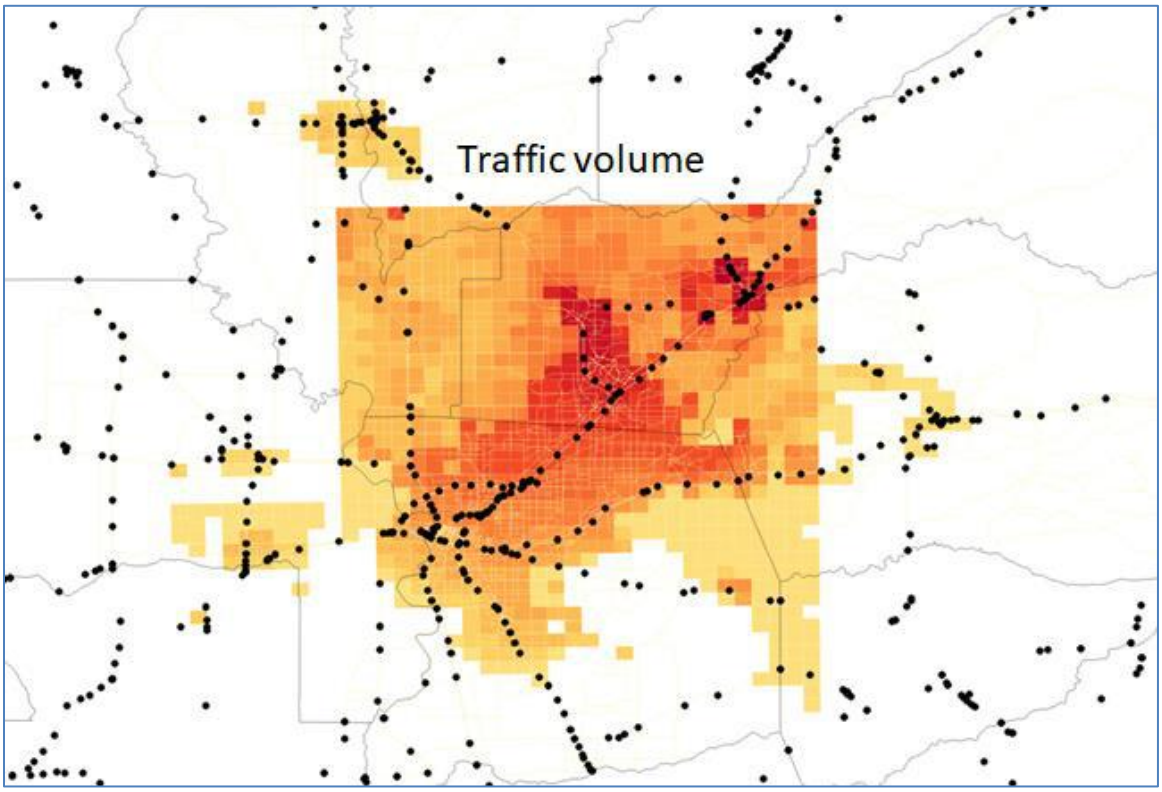

5.5 DEFINITION OF MITIGATION MEASURES AT THE REGIONAL SCALE (2 km)

At the 2 km level, i.e., the Capital-region domain, the mitigation measures modeled in this study included (1) albedo modifications, (2) increases in canopy cover, and (3) a combination of measures. Note that at the community scale, 500-m level, additional measures were modeled as will be discussed later in this report.

Thus, at the regional scale, the following scenarios were defined:

case10: Small increase in albedo -- an increase of 0.15 on impervious surfaces. At this scale (2-km resolution), there is no distinction between roof and pavement albedo changes. Difference between this case and the base case is labeled “del10”.

case20: Larger increase in albedo -- an increase of 0.25 on impervious surfaces. Difference between this case and the base case is labeled “del20”.

case01: A first-level increase in canopy cover, about 2.5 – 3 million trees throughout the entire 6-counties region, which is about a 12% increase in cover, i.e., an additional 12% of a cell’s area. Previous studies, e.g., Simpson and McPherson (2007) and Taha et al. (2011, 2015) estimated that the established urban-forest canopy in

Sacramento is ~14% and that many newer, urbanizing areas have canopy cover that needs to be brought up from ~5% to 14%, hence the 12% increase. To put this increase into context, in a previous study by Altostratus Inc. for the SMAQMD, a control measure of 650,000 replacement trees in the Sacramento Federal Non-Attainment area (SFNA) was assumed (Taha et al. 2011, 2015). Difference between this case and the base case is labeled "del01".

case02: A second (and extreme) level of increase in canopy cover (~20% - 25% cover increase or adding 5 – 6 million trees throughout the entire 6-counties Capital region, i.e., an additional 20% of a cell's area). This is not a realistic scenario nor considered feasible at this time, and thus not used in the combined scenario (case31, below) or some analysis later in this report. However, this scenario is included as a test for potential upper-bound effects per suggestions from local tree organizations. Compared to findings from many other studies, this increase is still smaller than what is typically proposed (canopy increase of 40%) to exert a significant impact on air temperature. Difference between this case and the base case is labeled "del02".

case31: This is a realistic-high case of combined albedo and canopy-cover increases. The increase in albedo is slightly larger (+0.35) than in case20 and the increase in canopy cover corresponds to that of case01. Difference between this case and the base case is labeled "del31".

In addition, and per a request from the City of Sacramento, several intermediate levels of canopy cover were also modeled at the 2-km scale to evaluate the incremental effects of canopy growth (or additional canopy) on air temperature and water usage. Studies by the City of Sacramento and Davey Inc. (Davey 2018), estimate that the canopy cover increases by about 1% per year. Thus, as a crude estimate, the assumptions of going from current cover to ~25% increase would take some 25 years (per literature, a large tree is 65 m^2 in crown area; medium tree 30 m^2; and a small tree 10 m^2).

These additional scenarios mesh with case01 and case02 (defined above) as follows:

- case01A: increase of +3.4% of cell area
- case01B: increase of +7.7% of cell area
- **case01**: increase of +12.0% of cell area
- case02A: increase of +16.3% of cell area
- case02B: increase of +20.6% of cell area
- **case02**: increase of +25.0% of cell area

Thus, the final (maximum) amount of increase in canopy cover (case02) corresponds to +25% which is in line with estimates made by the Sacramento Tree Foundation for a total target canopy

cover of 35% (Torin Dunnavant, SacTree, personal communication). That is, an increase of 25% (of the area) in canopy cover added to an existing cover of between 4% and 15%, will bring the total to 35%. However, as seen above, an increase in cover larger than case01 (+12%) is considered rather too large to be practically implementable at this time and, thus, in some of the analysis in this report, cases larger than case01 (e.g., case02) are not discussed.

The increase in canopy cover in case01 can also be considered a realistic upper bound because it will bring the total canopy cover to about 14% which is the average of the established cover in Sacramento (Simpson and McPherson 2007). In the future, concerted efforts might be followed to reach canopy cover that is similar to cases 02A, 02B and case02.

In terms of albedo increases, e.g., implementation of cool surfaces, the levels assumed here (case10 and case20) are realistic and reasonable – they translate into the surface-specific increases in albedo as summarized in Table 5-2.

Table 5-2: Upper bounds for realistic surface-specific increases in albedo

	Case10 max	Case20 max
Residential roof	+ 0.10	+ 0.25
Commercial roof	+ 0.20	+ 0.30
Roadway	+ 0.15	+ 0.20
Sidewalks/paved	+ 0.10	+ 0.20
Parking lots	+ 0.15	+ 0.25

In Figure 5-10, the translations of surface-specific albedo changes from Table 5-2 to gridded values of albedo increase at the 2-km level are summarized for 495 urban cells in D04 (the 6-counties Capital region domain). As seen in this figure, the albedo changes at 2-km level for case10 are mostly between +0.02 and +0.08, with a small number of cells affected by albedo increases of greater than 0.08. Case20 has a similar distribution except for roughly double the amount of increase in albedo. These are realistic levels of increase and represent materials already found in this region and used in current construction and building practices. Note that the scenarios modeled at finer scales (500-m level) are described later in this report.

Figure 5-10: Translation of surface-specific albedo increase into grid-level increase.

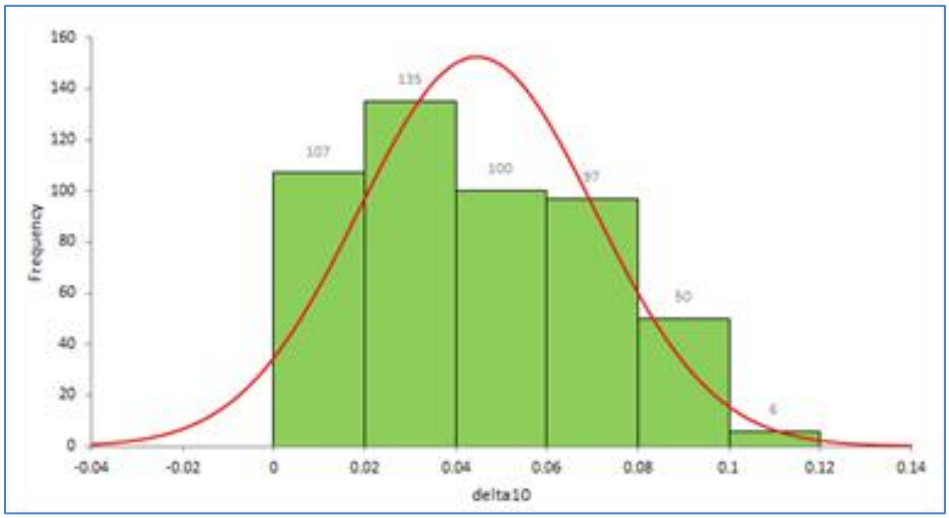

In order to answer some oft-posed questions such as (1) "how many roofs do we need to modify?" or (2) "how many trees do we need to plant?", the following very rough estimates are provided for the 2-km domain (D04). Caveats to keep in mind are the various assumptions made in the following discussion. For the 500-m grids, different project-specific numbers are provided and discussed later in this report.

Domain D04 consists of a total of 5184 cells. Out of these, 3154 cells have an urban fraction greater than zero, but the cells where UHI mitigation measures are actually applied (where urban fraction is greater than 30%) number only 495 cells, in 2015, and 495+360 cells in 2050. Recall that case10, case20, and case31 increase impervious albedo (of roofs and pavements) by +0.15, +0.25, and +0.35, respectively, as discussed above.

The total impervious area in 2015 (based on NLCD 2011 and USGS Level-II data discussed in Section 2) in the 495 urban cells is 630 km^2, which is about 31% of the total area of those 495 cells (and 3% of the entire domain D04). At the 2-km level, it is realistic to assume that, on average, half of the impervious area is pavements and roadways and the other half is roofs -- which is supported by examination of aerial photographs and Google Earth PRO imagery, as well as studies by Akbari et al. (1999) and Rose et al. (2003).

Roofs

Thus 315 km^2 of roof area is available for modification (to varying degrees) in the 6-counties Capital region. Assuming 60% of the total roof area is residential and that a residential (housing unit) roof is 200 m^2 on average, this translates into 945,000 housing units throughout domain D04. A comparison with the number of housing units per census information (census.gov) in Table 5-3 suggests that almost all of the housing units must use cool roofs, if a low level of albedo increase is applied. In other words,

A. to achieve case10, 945,000 roofs (which is nearly all of the residential roofs) in the 6-counties Capital region need to have their albedos increased by a very modest amount of +0.15, or half of the residential roofs will need their albedos increased by +0.30, or one third of residential roofs will need to increase their albedo by +0.45 (all of these scenarios assume that pavements and commercial roof albedos are increased by +0.15). This scenario translates into an albedo increase of +0.046 over the 395 urban cells and +0.0045 over domain D04.

B. To achieve case20, 945,000 roofs in the 6-counties Capital region need to have their albedos increased by +0.25, or half of the residential roofs will need their albedos increased by +0.50 (these two scenarios assume that pavements and commercial roof albedos are increased by +0.25). This scenario translates into an albedo increase of +0.077 over the 395 urban cells and +0.0075 over the regional D04 domain.

C. To achieve case31, 945,000 roofs in the 6-counties Capital region need to have their albedos increased by +0.35, or half of the residential roofs will need their albedos increased by +0.70 (these scenarios assume that pavements and commercial roof albedos are increased by +0.35). This scenario translates into an albedo increase of +0.1 over the 395 urban cells and +0.01 over the D04 domain.

It should be noted that the effects of, say, doubling or tripling the increase in roof albedo while simultaneously halving or reducing the affected roof area to one third is nonlinear. However, the linearity assumption is made here to provide very rough estimates in answering the above question.

Table 5-3: Housing units in the Capital region counties

County	No. of housing units
Sacramento	564,349
El Dorado	89,286
Placer	159,667
Yuba	28,225
Sutter	34,204
Yolo	76,916
TOTAL	952,647

Pavements

In terms of roadways and highways, assuming an overall average road width of 30 m across all types (including curbs, where they exist), then 315 km^2 (from above NLCD-based impervious cover calculations) is equivalent to 10,500 km of roadways available for modification (note:

typical widths of freeways: 60 m, typical widths of streets and avenues in commercial areas: 25 m, and typical widths of roadways in residential areas: 18 m).

Compare with the following:

- Total CA roadways: 631,000 km
- CA public roads: 282,000 km
- SAC DOT roadways: 3,520 km (in Sacramento County only, not including the other 5 counties in the Capital region)

Or, alternatively, the roadways albedo (for case01) could be increased by 0.3 over 5,250 km in the 6-counties Capital region.

Tree cover

As for the needed tree cover, or equivalent number of trees, it can be estimated very crudely as follows (for the 2-km domain):

- case01: +7300 trees per 4 km^2, which equates to about +12% of cell area subject to forestation. This corresponds to up to 3.6 M new trees, depending on size, throughout the 6-counties Capital region.
- case02: + 12000 to +15300 trees per 4 km^2, which is equivalent to +20% to +25% of cell area subject to forestation. This translates into 5 – 7 M new trees, depending on size, throughout the 6-counties Capital region. Again, case02 is considered a relatively extreme scenario in this analysis.

5.6 SELECTING UHI-MITIGATION MEASURES: POSSIBLE IMPACTS ON BVOC EMISSIONS, UV ALBEDO, MIXING, AND THERMAL / VISUAL ENVIRONMENT

As with many environmental control measures, the implementation of urban-cooling strategies can in some cases result in unintended consequences, that is, produce both positive and negative effects (Taha 2013a). The opposing impacts can be seen in meteorology (e.g., cooling and warming), emissions (decrease or increase), and in air quality (e.g., decrease and increase in formation and/or transport of ozone or particulate matter). In this section, factors to consider when designing or selecting UHI-mitigation measures are discussed.

5.6.1 Albedo increase and UV radiation

Taha (2005, 2007) discussed the air-quality effects of changes in UV albedo in detail. Here, some highlights are presented but largely follow that discussion. For the purposes of implementing cool surfaces, the albedo of interest is in the range of 0.28 to 2.8 μm, that is, "solar" albedo. By definition, this includes radiation in the UV, visible, and NIR spectra. Thus, in addition to the main effect of changing visible and NIR albedo, there is the possibility of inadvertently increasing UV

albedo as a result of implementing measures of cool surfaces (Fallmann et al. 2016; Epstein et al. 2017). This may be of concern because the energy in the UV wavelength can influence some of the important photodissociation reactions, e.g., those of NO_2, O_3, and PAN (peroxyacetyl nitrate), that can have potential negative implications, i.e., increasing ozone concentrations. However, in reality, the proposed measures of cool roofs and pavements may have little or no effect on UV albedo as many reflective materials incur no increase in albedo in that wavelength range. In fact, some high-albedo materials actually have lower UV albedo than conventional materials (Berdahl et al. 2002; Berdahl and Bretz 1997, Levinson et al. 2007).

Regardless of whether or not reflective materials actually change UV albedo, the effects of UV radiation changes (e.g., UV-B) on ozone formation are not easy to discern. Increased UV-B in areas with high NOx emissions (e.g., urban and industrial areas) can increase ozone formation (Gery et al. 1988, Thompson 1992, 1991) and the opposite can be true in areas with low NOx emissions, e.g., suburban or rural regions (Liu and Trainer 1988).

The issue of potential UV albedo increase actually involves more than just how much UV radiation is modified; it also involves actinic irradiance and species-specific characteristics such as quantum yield and absorption cross sections (all of which determine the rates of photodissociation for a particular chemical species). But the focus here is on albedo because it is the one parameter that is changing from one surface-modification scenario to another.

Generally, the UV spectrum is defined as UV-A (0.315-0.400 μm), UV-B (0.280-0.315 μm), and UV-C (0.100-0.280 μm). Stratospheric oxygen absorbs UV radiation in the range 0.17-0.24 μm and photodissociates to produce ozone, via:

$$O_2 + h\nu \rightarrow 2\ O\ (^3P) \qquad (5\text{-}2)$$

$$O\ (^3P) + O_2 + M \rightarrow O_3 + M \qquad (5\text{-}3)$$

where M = air = N_2, O_2, etc. This leaves mostly UV-B and UV-A radiation to reach the troposphere because the ozone produced in the above process absorbs UV at and below 0.29 μm. Thus, in the troposphere, wavelengths of relevance to photochemical reactions are 0.30 μm and longer (Seinfeld and Pandis 1998) but still short enough to contain part of the high energy spectrum.

Of the smog-related photochemical reactions in the polluted urban boundary layer, photodissociation pathways of importance to the strategy of increasing albedo are mainly those of NO_2, O_3, and PAN. NO_2 absorbs at wavelengths of 0.45 μm or shorter, but because there is little UV radiation reaching the troposphere at or shorter than 0.29 μm, the theoretical critical UV range of interest for NO_2 is thus between 0.30 and 0.45 μm (Cooper and Alley 1994). Further narrowing this range is the fact that 90% of the NO_2 molecules absorb UV energy below 0.4 μm (Stern et al. 1984) and as a result, the practical range of importance for NO_2 photodissociation is 0.3 to 0.37

μm (Seinfeld 1975). For O_3, the critical UV wavelength range is 0.315 μm or shorter (Harrison 1990) and for PAN, the cutoff is 0.35 μm or shorter (Seinfeld and Pandis 1998). Thus, the inclusive range of 0.3 to 0.37 μm is the overall "envelope" that needs to be considered when modifying surface albedo. This envelope is shown by the area to the left of the vertical red line (and red arrow) in Figure 5-11.

The information shown in Figure 5-11 indicates that it is possible to select reflective materials that do not increase UV albedo, e.g., compare curves B, D, and E that show increase in overall albedo without much changing (if not decreasing) the UV albedo. Furthermore, some high-albedo materials reflect less in the UV range than their low-albedo counterparts, as seen in Figure 5-12. For example, if a cedar shake roof is replaced by either a TiO_2-painted roof or a limestone-based product, the UV albedo actually decreases from about 0.58 to 0.15 while the overall albedo increases from about 0.35 to 0.7.

In Figure 5-11, material A has a very low albedo (~0.05). By moving to material B or C, the overall albedo increases to about 0.25 and 0.60, respectively, whereas the changes in UV albedo are relatively smaller, e.g., from 0.05 to 0.06 or 0.09, respectively. However, materials D and E have much higher solar albedos, e.g., 0.7 and 0.82, respectively, but their UV albedos are similar to (unchanged from) that of material B. In fact, the UV albedo of materials D or E can be lower than that of B. On the other hand, there could be high-albedo materials such as F and G (about 0.7) that also have high UV albedo, e.g., up to about 0.4. Thus, from a photochemistry perspective, careful selection of reflective materials is critical, but it is very possible to select high-albedo materials without altering the UV albedo.

Some earlier studies by Berdahl and Bretz (1997) provided reflectance measurements and albedo values for a variety of materials (some examples shown in Table 5-4). The materials presented in this table are of similar structure, construction, and texture but different albedo. As seen in the table, it is possible to increase solar albedo in the visible and NIR ranges without changing the UV albedo by any significant amount. In some cases, such as the single-ply example, UV albedo actually decreases while visible and NIR albedos increase. For asphalt shingles, there is no change in UV albedo, while overall albedo increases from 0.08 to 0.21.

In summary, it is possible to increase visible and NIR albedo without increasing UV albedo. Thus, it is possible to maximize the expected benefits from lower air temperatures without the inadvertent photochemical effects that might be associated with increases in UV albedo. This is an implicit assumption made in developing albedo scenarios in this modeling study. That is, in the meteorological simulations of modified albedo scenarios, solar albedo is increased whereas UV albedo is assumed unchanged in the photochemical simulations. This is a reasonable and conservative assumption because, as seen above, we could actually decrease UV albedo and incur further air-quality benefits.

Figure 5-11: Spectral reflectance of selected materials based on measurements by Berdahl et al. (2001) and Berdahl and Bretz (1997). The vertical black lines delineate the boundaries of the UV, visible, and NIR ranges, also shown with two-headed arrows at the bottom of the figure. The vertical red line (at left) and arrow show the UV range of practical relevance to photodissociation (in terms of albedo modifications). Other labels are discussed in the text. Figure source: Taha (2004).

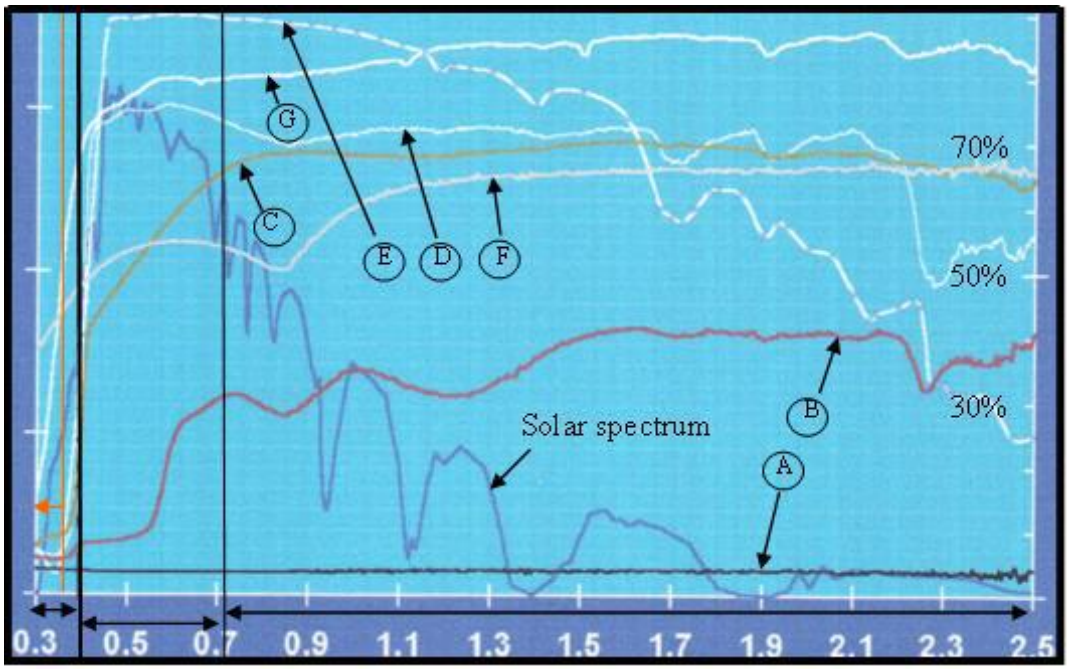

Figure 5-12. Spectral reflectivity characteristics of selected roofing materials. A leaf is also included for comparison. Source: Levinson et al. (2004).

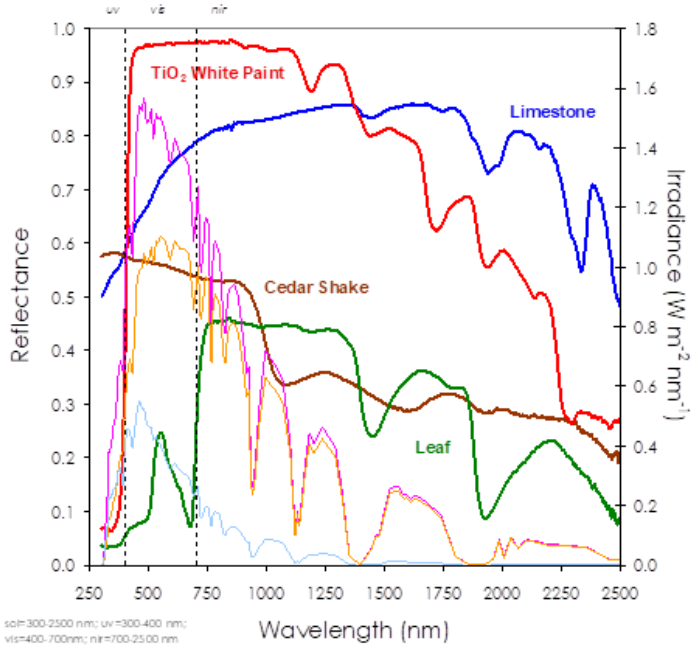

Table 5-4**.** Albedo of selected materials (commercial product names are not given). Based on Berdahl and Bretz (1997).

	Albedo			
	Solar	UV	VIS	NIR
Coatings (in order of increasing solar albedo)				
Product 1	0.74	0.10	0.79	0.76
Product 2	0.83	0.11	0.89	0.85
Product 3	0.85	0.12	0.90	0.87
Single ply membranes (in order of increasing solar albedo)				
Product 1	0.77	0.25	0.80	0.79
Product 2	0.80	0.19	0.87	0.79
Product 3	0.83	0.14	0.91	0.82
Asphalt shingles (in order of increasing solar albedo)				
Product 1	0.08	0.05	0.08	0.09
Product 2	0.08	0.06	0.08	0.09
Product 3	0.12	0.06	0.12	0.12
Product 4	0.20	0.06	0.22	0.19
Product 5	0.21	0.06	0.24	0.21

5.6.2 Vegetation-cover increase and biogenic hydrocarbon emissions

Vegetation cover affects the soil-atmosphere environment via several complex pathways. Stated in the simplest terms, the effects of vegetation canopies can be seen in their impacts on (1) air and surface temperatures, (2) wind speed and turbulent kinetic energy, (3) emissions of biogenic volatile organic compounds (BVOC), (4) dry and wet deposition of air pollutants, and (5) atmospheric humidity.

All of these pathways affect air quality and ozone production via different mechanisms and to varying degrees. Here, we discuss one issue of relevance to photochemical production of ozone, which is the potential increase in BVOC emissions, i.e., those of isoprene and monoterpenes, from increasing urban vegetation cover. In general, the guidance is to use non- or low-emitting vegetation species to avoid negative air-quality consequences. In an earlier modeling study, for example, Taha (1996) showed that for the Los Angeles Basin, tree species emitting at a rate higher than 2 $\mu g\ g^{-1}\ hr^{-1}$ (per dry leaf mass) of isoprene and/or monoterpenes could bring adverse effects on air quality when introduced in large numbers (millions of trees). That study also pointed out that numerous zero-emitting vegetation species exist that could be used in such applications (Benjamin et al. 1996). Thus, when implementing urban forestation strategies, careful selection of tree species is an important factor.

Furthermore, Taha et al. (2015) modeled the effects of converting 650,000 current-mix trees in the Sacramento Federal non-attainment area for ozone (SFNA) into low emitters of BVOC as a voluntary or emerging control measures for maintenance of the 8-hour ozone standard in the area. The results indicated that the daily reductions in ozone from species replacement alone can reach

up to 3 ppb. The 8-hour average peak ozone is reduced by 2%. If canopy cooling effects were also accounted for, the air-quality impacts could be 10 times as large as those of only replacing the tree species (emissions control measure).

In this modeling study, and as discussed in later sections of this report, the additional vegetation introduced in urban areas is assumed to be non-emitting or emitting less than 2 μg g^{-1} hr^{-1} of isoprene and/or monoterpenes (Taha 1997, 2017). In this context, Table 5-5 provides some general information on emissions rates for consideration when implementing urban forestation in the Sacramento region. The air quality ratings in the table are based on the ozone forming potential of each species (Simpson and McPherson 2007). It is also assumed that the planted species do not vary much in albedo from the current species (0.18 – 0.22 albedo).

Table 5-5: BVOC emission rates for species with "excellent", "good", and "fair" air quality ratings, per Simpson and McPherson (2007), US EPA, and Sacramento Tree Foundation (2015).

Tree Common Name	Tree Scientific Name	Isop g tree^{-1} day^{-1}	Terp g tree^{-1} day^{-1}	Air Quality Rating
Bottle tree	Brachychiton populneus	0.0	0.0	Excellent
Cape chestnut	Calodendrum capense	0.0	0.0	Excellent
Chitalpa	Chitalpa x tashkentensis 'Morning Cloud'	0.0	0.0	Excellent
Chitalpa	Chitalpa x tashkentensis 'Pink Dawn'	0.0	0.0	Excellent
Fan-Tex ash	Fraxinus velutina 'Rio Grande'	0.0	0.0	Excellent
Canary Island pine	Pinus canariensis	0.0	0.0	Excellent
Aleppo pine	Pinus halepensis	0.0	0.0	Excellent
Italian stone pine	Pinus pinea	0.0	0.0	Excellent
Fern pine	Podocarpus gracilior	0.0	0.0	Excellent
Evergreen pear	Pyrus kawakamii	0.0	0.0	Excellent
South African sumac	Rhus lancea	0.0	0.0	Excellent
Frontier elm	Ulmus parvifolia 'Frontier'	0.0	0.0	Excellent
Bottle tree	Brachychiton populneus	0.0	0.0	Excellent
Calabrian pine	Pinus brutia	0.0	0.0	Excellent
Afghan pine	Pinus eldarica	0.0	0.0	Excellent
Southern live oak	Quercus virginiana	0.0	0.0	Excellent
Oregon ash	Fraxinus latifolia	0.0	0.0	Excellent
Interior live oak	Quercus wislizenii	0.0	0.0	Excellent
Columnar Red Maple	Acer platanoides 'Crimson Sentry'	0.0	0.0	Excellent
European hackberry	Celtis australis	0.0	0.0	Excellent
Eastern redbud	Cercis canadensis	0.0	0.0	Excellent
Crape myrtle	Lagerstroemia indica	0.0	0.0	Excellent
Flowering pear	Pyrus calleryana	0.0	0.0	Excellent
Capital Pear	Pyrus calleryana 'Capital'	0.0	0.0	Excellent
Chanticleer Pear	Pyrus calleryana 'Chanticleer'	0.0	0.0	Excellent
Blue oak	Quercus douglasii	0.0	0.0	Excellent
Bur oak	Quercus macrocarpa	0.0	0.0	Excellent
Upright English oak	Quercus robur 'Fastigiata'	0.0	0.0	Excellent

Zelkova	Zelkova serrata	0.0	0.0	Excellent
Narrow zelkova	Zelkova serrata 'Musashino	0.0	0.0	Excellent
Princeton elm	Ulmus americana 'Princeton'	0.0	0.0	Excellent
Valley Forge elm	Ulmus americana 'Valley Forge'	0.0	0.0	Excellent
Accolade elm	Ulmus japonica x wilsoniana 'Accolade'	0.0	0.0	Excellent
Washington hawthorn	Crataegus phaenopyrum	0.0	0.0	Excellent
Japanese crabapple	Malus floribunda	0.0	0.0	Excellent
Prairie fire crabapple	Malus hybrid 'Prairifire'	0.0	0.0	Excellent
Robinson crabapple	Malus hybrid 'Robinson'	0.0	0.0	Excellent
Bechtel crabapple	Malus ioenis 'Plena'	0.0	0.0	Excellent
Japanese Flowering Cherry	Prunus serrulata 'Amanogawa'	0.0	0.0	Excellent
Flowering plum	Prunus cerasifera	0.0	0.0	Excellent
Australian willow	Geijera parviflora	0.0	0.0	Excellent
Bronze loquat	Eriobotrya deflexa	0.0	0.0	Excellent
Loquat	Eriobotrya japonica	0.0	0.0	Excellent
Red leaf photinia	Photinia x fraseri	0.0	0.0	Excellent
Sweet bay	Laurus nobilis	0.0	0.1	Excellent
Saratoga sweetbay	Laurus nobilis 'Saratoga'	0.0	0.1	Excellent
Sassafras	Sassafras albidum	0.0	0.1	Excellent
Trident maple	Acer buergerianum	0.0	0.1	Excellent
Paperbark maple	Acer griseum	0.0	0.1	Excellent
Shantung maple	Acer truncatum	0.0	0.1	Excellent
Chinese wingnut	Pterocarya stenoptera	0.0	0.1	Excellent
Cork oak	Quercus suber	0.0	0.1	Excellent
Maidenhair tree	Ginkgo biloba	0.0	0.1	Excellent
Male ginkgo	Ginkgo biloba 'Fairmont'	0.0	0.1	Excellent
Male ginkgo	Ginkgo biloba 'Princeton Sentry'	0.0	0.1	Excellent
Dawn redwood	Metasequoia glyptostroboides	0.0	0.1	Excellent

Tree Common Name	Tree Scientific Name	Isop g tree^{-1} day^{-1}	Terp g tree^{-1} day^{-1}	Air Quality Rating
Desert willow	Chilopsis linearis	0.0	0.3	Good
Chinese fringe tree	Chionanthus retusus	0.1	0.0	Good
Hedge maple	Acer campestre	0.0	0.4	Good
Norwegian Sunset maple	Acer saccharum ssp. nigrum	0.0	0.4	Good
Tartarian maple	Acer tartaricum	0.0	0.4	Good
Norwegian Sunset maple	Acer truncatum 'Norwegian Sunset'	0.0	0.4	Good
Pacific Sunset shantung maple	Acer truncatum 'Pacific Sunset'	0.0	0.4	Good
Deodar cedar	Cedrus deodara	0.0	0.5	Good
Japanese snowbell	Styrax japonicus	0.2	0.1	Good
Japanese lilac tree	Syringa reticulata 'Ivory Silk'	0.2	0.1	Good
Chaste tree	Vitex agnus-castus	0.2	0.1	Good
Red maple	Acer rubrum	0.0	0.5	Good
Bohall Maple	Acer rubrum 'Bohall'	0.0	0.5	Good
Columnar red maple	Acer rubrum x freemani 'Armstrong'	0.0	0.5	Good
California Incense cedar	Calocedrus decurrens	0.0	0.6	Good

California buckeye	Aesculus californica	0.3	0.1	Good
Bailey acacia	Acacia baileyana	0.0	0.8	Good
Southern magnolia	Magnolia grandiflora	0.0	0.9	Good
Saucer magnolia	Magnolia soulangiana	0.0	0.9	Good
Kentucky coffee tree	Gymnocladus dioica	0.3	0.1	Good
Katsura tree	Cercidiphyllum japonicum	0.4	0.1	Good
His majesty amur cork tree	Phellodendron amurense 'His Majesty'	0.4	0.1	Good
Macho amur cork tree	Phellodendron amurense 'Macho'	0.4	0.1	Good
Eye stopper amur cork tree	Phellodendron lavallei 'Longenecker'	0.4	0.1	Good
True Shade locust	Gleditsia tricanthos inerm	0.4	0.1	Good
Japanese pagodatree	Sophora japonica	0.4	0.2	Good
Valley oak	Quercus lobata	0.5	0.0	Good
Pistache	Pistacia chinensis	0.0	1.2	Good
Brisbane box	Lophostemon confertus	0.5	0.1	Good
Briotti red horse chestnut	Aesculus x carnea 'Briotti'	0.5	0.2	Good
Italian alder	Alnus cordata	0.5	0.2	Good
River birch	Betula nigra	0.5	0.2	Good
Japanese white birch	Betula platyphylla japonica	0.5	0.2	Good
Pyramidal European hornbeam	Carpinus betulus 'Fastigiata'	0.5	0.2	Good
Bald Cypress	Taxodium distichum	0.0	1.5	Good
Tulip tree	Liriodendron tulipifera	0.4	0.8	Good
Hardy rubber tree	Eucommia ulmoides	0.7	0.2	Good
Chinese parasol tree	Firmiana simplex	0.7	0.2	Good
Littleleaf linden	Tilia cordata	0.7	0.2	Good
Cajeput tree	Melaleuca quinquenervia	0.8	0.1	Good
Pink trumpet tree	Tabebuia impetiginosa	0.0	2.1	Good
Tristania var. 'Elegant'	Tristania laurina 'Elegant'	0.9	0.1	Good
Mountain silverbell	Halesia monticola	1.0	0.3	Good
Japanese Stewartia	Stewartia pseudocamellia	1.0	0.3	Good

Tree Common Name	Tree Scientific Name	Isop g tree^{-1} day^{-1}	Terp g tree^{-1} day^{-1}	Air Quality Rating
Tupelo	Nyssa sylvatica	1.6	0.5	Fair
American hophornbeam	Ostrya virginiana	1.6	0.5	Fair
Carob tree	Ceratonia siliqua	1.6	0.7	Fair
California buckeye	Aesculus californica	1.8	0.5	Fair
Red oak	Quercus rubra	2.2	0.4	Fair
Sawtooth oak	Quercus acutissima	2.3	0.1	Fair
Shumard oak	Quercus shumardii	2.3	0.1	Fair
Goldenrain tree	Koelreuteria bipinnata	2.4	0.0	Fair
Chinese flame tree	Koelreuteria paniculata	2.4	0.0	Fair
California sycamore	Platanus racemosa	2.7	0.0	Fair
Coast redwood	Sequoia sempervirens	0.0	6.4	Fair
European beech	Fagus sylvatica	2.7	0.1	Fair
Silver linden	Tilia tomentosa	2.5	0.7	Fair
American linden	Tilia americana	2.5	0.7	Fair

Willow oak	Quercus phellos	3.0	0.0	Fair
Southern live oak	Quercus virginiana	3.0	0.1	Fair
Scarlet oak	Quercus coccinea	3.0	0.7	Fair
Holly oak	Quercus ilex	3.7	0.1	Fair
Chestnut leaf oak	Quercus castaneifolia	3.7	0.2	Fair
Bunya-bunya	Araucaria bidwillii	3.7	1.1	Fair
London plane	Platanus X acerifolia	4.7	0.0	Fair
Lombardy poplar	Populus nigra 'Italica'	4.7	0.0	Fair
Black oak	Quercus kelloggii	5.0	0.1	Fair
Coast live oak	Quercus agrifolia	5.2	0.0	Fair
Turkey oak	Quercus cerris	7.7	0.4	Fair

5.6.3 Urban cooling and reduced mixing

Urban cooling can affect both vertical and horizontal mixing, advection, and flow patterns. In coastal areas of California, urban cooling can also weaken the sea-breeze, thus affecting the flushing of air pollutants. Reduced vertical mixing can cause increased ozone concentrations under certain conditions whereas reduced horizontal mixing (venting) can result in higher temperatures downwind of urban cooling and thus potentially higher ozone in these areas (Taha 2007). Reduced vertical mixing and venting can also increase the concentrations of particulate matter (Epstein et al.2017; Fallmann et al. 2016).

Taha (2013a, 2005, 2007) suggested that there exists a city-specific cooling threshold for effects of changes in temperature and mixing, that, if heeded, can maximize the benefits from reduced air temperature without inadvertently impacting air quality. Another aspect of importance, especially beyond the urban scale, i.e., at regional and global scales, is the potential impact of heat-island mitigation on convective cloud enhancement. Some of these negative effects have been evaluated on the global scale by Jacobson and TenHoeve (2011) and at the regional scale by Georgescu et al. (2014). However, these are not critical factors in the coastal and semi-arid climates of California where rain occurs during winter and is not dependent on convective activity.

In this modeling assessment for the Capital region, these competing positive and negative effects of mitigation measures were accounted for in the detailed simulations at 2-km and 500-m scales and, thus, the final results embody these various possible outcomes. While the study did not include an air-quality modeling component similar to Taha (2015b, 2013a,b, 2008a,c), the potential negative impacts on air quality were minimized or averted, hypothetically, by defining optimal levels of urban cooling. Thus, avoiding those negative impacts was addressed indirectly in this study by (1) constraining the increases in albedo and/or canopy cover (as well as other measures) to reasonable amounts (at the 2-km level), i.e., avoiding the extreme hypothetical increases that can result in larger urban cooling, and (2) by evaluating the changes in heat fluxes and temperature at the top of the urban boundary layer and assessing the net effects. If there is roughly similar cooling and warming at the top of this layer, as a result of implementing mitigation measures, then

this may imply that there are close to zero net effects throughout the planetary boundary layer, i.e., relatively unchanged vertical mixing and venting.

5.6.4 Reflective materials, glare, and possible pedestrian concerns

In addition to imposing some constraints on UHI-mitigation levels to avoid any potential negative air-quality impacts, as discussed above, such constraints are also imposed to prevent possible issues related to the visual/thermal environment at street level. In order to minimize or avoid potential problems with glare in the lowest parts of the urban canopy layer, the highest albedo of roadways and pavements is limited to a maximum of 0.30 or 0.35, depending on location (as defined earlier in Section 5.5 for the 2-km scale and later in Section 5.19 for the 500-m scale). These are reasonable and realistic increase levels that should not cause glare issues. For the same reasons, the maximum roof albedo is assumed to be 0.50.

A question arises in some situations with regard to cool pavements and potential negative impacts on pedestrian thermal comfort. The argument is that increasing the albedo of pavements would increase radiation reflected onto subjects in the area. This is discussed with some physical and geometrical insight.

From a physical perspective, i.e., heat transfer between two objects, these effects should be evaluated on a site-by-site basis. When the albedo of pavements is increased, it affects several factors, most notably convective and radiative heat transfer. Increased pavement albedo results in lower skin-surface temperature which, in turn, results in lower air temperature. Increased albedo also means increased reflected visible and NIR radiation onto surrounding objects (the concern in this case is pedestrians) but, also, because the surface is cooler, there is smaller heat gained by subjects because of reduced long-wave radiation. Furthermore, with regard to shortwave radiation, the amount of heat gained depends on a myriad of factors down to the albedo of the clothing worn by subjects, as well as other biophysical characteristics.

Thus, the tradeoffs between cooling effects (from reduced surface and air temperatures and reduced longwave radiation) and heating effects (from increased shortwave radiation) will have to be evaluated on a case by case basis. Several studies, e.g., Gilbert et al. (2017) and Levinson et al. (2017), have examined these effects. However, this assessment is based purely on a heat-transfer exercise that does not take into account any implementation or geometry/location aspects that are likely to be the overriding factors in this context.

Thus, more important than the physical considerations discussed above are the practical considerations, levels and locations of implementation, and geometrical aspects when implementing cool pavements. To begin with, the highest priorities for cool pavements deployment should be assigned to major freeways and highways, as well as main routes and roads through the areas of interest. This includes, for example, I-5, I-80, HWY 50, HWY 99, and so on, where there is practically non-existent pedestrian traffic. However, in reality, even suburban

residential neighborhoods have little pedestrian activity during the day. A benefit of targeting the main freeways and highways is their large areas available for albedo modification which is especially relevant in light of their continuous exposure to solar radiation throughout the daytime.

On the other hand, in areas with significant pedestrian traffic, say, downtown Sacramento as an example, or some commercial areas, cool pavements are not desirable in the first place because the urban geometry (e.g., taller buildings and canyon orientations) limit exposure of roadway surfaces to the sun to only a few hours during the daylight and sometimes not at all (i.e., completely shaded). Hence, it serves no purpose implementing cool pavements in such places as they will have little or no effects on temperature. Thus, in areas with tall buildings and high pedestrian volume, we assume no cool-pavement measures.

Finally, an important factor is the sensible level of increase in pavement albedo, as discussed above. All of the foregoing discussion should be viewed in the context of the actual increases in albedo, e.g., such as assumed in this study. The increases are modest (new albedo capped at 0.35 in freeways / highways and 0.30 in residential areas) -- essentially similar to some light-colored cement or concrete pavements that already exist in the region (also see Table 5-6, below). It is not being assumed in this study that extremely reflective materials will be used.

5.6.5 Cool pavement materials

This report provides a quantitative assessment of the effects of various modifications to pavement albedo on surface and air temperatures and their impacts on neighboring communities, e.g., AB617 and disadvantaged populations. The effectiveness of pavements / cool roadways is also compared to that of other measures.

However, it was not part of the scope of work in this project to evaluate cost and life-cycle aspects of implementing cool pavements. This is another significant layer of information altogether, which was addressed in other major studies, e.g., Levinson et al. (2017) and Gilbert et al. (2017). Thus, the choice of materials based on cost or construction-related information is not evaluated here, only the selection based on climate criteria and impacts of pavements on urban heat.

To provide some brief information on the possible pavements choices and materials that could be used to attain the cooling goals set forth in this study, e.g., a maximum pavement albedo of 0.30 or 0.35 (see definitions in Section 5.19), some data is provided in Table 5-6, which is a very simplified and abridged version of information from Levinson et al. (2017). The table shows that some pavement materials currently on the market do have sufficiently high albedo to achieve the cooling effects discussed in this report and with minimal glare issues, per discussion above. Table 5-6 lists a small sample of conventional and relatively more reflective surface types for pavements. It also provides information on expected service life for a sample from the larger dataset of Levinson et al. (2017).

Thus, to achieve the target cooling defined by cool-pavement scenarios in this study, surface types with an albedo range of 0.20 to 0.30 in Table 5-6 would be suitable for application in the Capital region per modeling results (discussed in following sections). Such pavement types will also satisfy the above-discussed glare issue by capping pavement albedo to a maximum of 0.30 or 0.35.

Table 5-6: Sample of pavement surface types and treatment materials. Abridged from and simplified based on Levinson et al. (2017).

Pavement surface type	Albedo range	Service-life range (years)
Bonded Concrete Overlay on Asphalt	0.20 - 0.35	10 - 20
Cape Seal	0.05 - 0.15	2 - 15
Chip Seal	0.10 - 0.24	1 - 10
Fog Seal	0.04 - 0.07	1 - 5
Conventional Asphalt Concrete	0.05 - 0.15	5 - 20
Conventional Interlocking Concrete Pavement (Pavers)	0.20 - 0.35	5 - 20
Permeable Asphalt Concrete	0.08 - 0.15	5 - 20
Permeable Portland Cement Concrete	0.20 - 0.30	5 - 20
Permeable Rubberized Asphalt Concrete	0.08 - 0.15	5 - 20
Permeable Asphalt Concrete	0.08 - 0.15	5 - 20
Permeable Portland Cement Concrete	0.20 - 0.30	5 - 20
Permeable Rubberized Asphalt Concrete	0.08 - 0.15	5 - 20
Portland Cement Concrete	0.20 - 0.30	10-60 depending on design
Reflective Coating - Bisphenol A	0.20 - 0.30	-
Reflective Coating - Polyester Styrene	0.20 - 0.30	-
Reflective Coating – Polyurethane	0.20 - 0.30	-
Reflective Coating - Styrene Acrylate	0.20 - 0.30	-
Rubberized Asphalt Concrete (mill and fill)	0.04 - 0.13	5 - 20
Rubberized Asphalt Concrete (overlay)	0.04 - 0.13	5 - 20
Sand Seal	0.07 - 0.10	1 - 6
Slurry Seal	0.07 - 0.10	1 - 10

5.7 IMPACTS OF MITIGATION MEASURES ON WINTERTIME OUTDOOR AIR TEMPERATURE

Before proceeding with the presentation of summertime impacts from UHI-mitigation measures, a brief revisit to the potential wintertime effects on temperature is in order. Among some of the concerns regarding potential negative effects occurring inadvertently from implementing urban-cooling measures, several were discussed in Section 5.6. An additional concern may be the potential penalties in terms of heating needs during the winter season.

Albedo

The purpose of the brief discussion in this section is to demonstrate that during winter, cooling measures such as increased albedo have small or no impacts on air temperature, hence small or no negative effects on heating energy needs. It should be noted, however, that there may be negative effects at the building scale if, for example, a cool roof is applied that can affect the heating energy needs of the space (floor) directly beneath it. Such effects would have to be evaluated on a case-by-case basis, although these impacts have been shown to be small (e.g., Akbari and Konopacki 2005) because of larger air mass (lower sun angle), increased cloudiness, and snow cover in winter. Thus, the net year-round effects of cool roofs are a significant reduction in energy use. Furthermore, in the Sacramento region, winters are not particularly cold compared to other parts of the country.

In this study, the effects of mitigation measures on wintertime ambient urban air temperature were examined briefly. The modeling and analysis indeed show small or non-existent cooling effects in winter (a result of smaller solar altitude angle and larger cloud cover). An example from this analysis is summarized in Figure 5-13 showing results from the Altostratus Inc. AREAMOD / WRF modeling approach for two summer and two wintertime intervals. The temperature differences presented in this example correspond to the cooling effects of case10, a scenario of small increases in albedo, as defined earlier in Section 5.5. The figure shows the impacts on air temperature at the time of the maximum effect from the albedo measures, i.e., around midday.

In this example, whereas case10 decreases the summertime midday temperature by 1 °C or slightly more in large and well-defined areas that are affected by cooling (top two graphs in Figure 5-13), the wintertime effects are either non-existent or small (e.g., up to 0.5 °C) and impacting very small areas that also are not as well-defined as in summer (bottom two graphs). The analysis suggests that the albedo-increase levels proposed in this study would result in no significant negative impacts during the winter. Higher levels of albedo increase (hypothetical and not modeled in this study) might result in negative wintertime effects. As such it is important to constrain the albedo increases to reasonable levels, i.e., as defined in this study.

Canopy cover

In terms of vegetation cover (not shown in Figure 5-13), the same conclusion applies as most trees shed their leaves in winter thus reducing cooling effects from shading and evapotranspiration. For evergreen trees, the lower incoming solar radiation (increased cloudiness and larger air mass) and lower air temperatures reduce the trees' cooling effects via shading and evapotranspiration, respectively. As with the albedo modifications, the results suggest small or no effects during the wintertime, depending on location and scenario.

Figure 5-13: Cooling from case10 (increase in albedo) in summer (top figures) and winter (bottom figures) for random hours as examples.

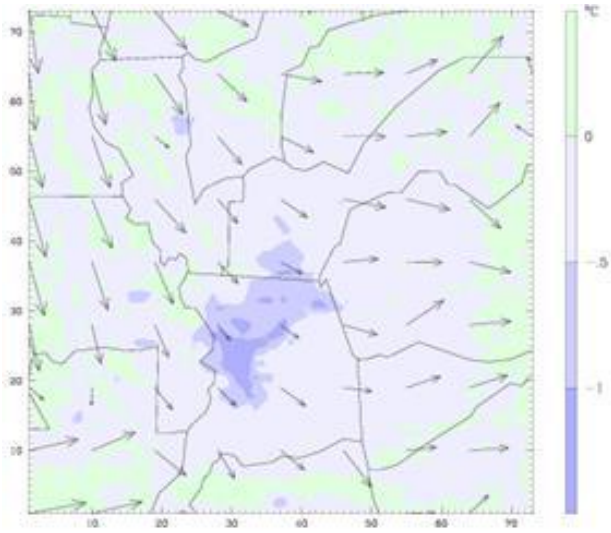

(SUMMER) 1200 PDT, June 3rd, 2013

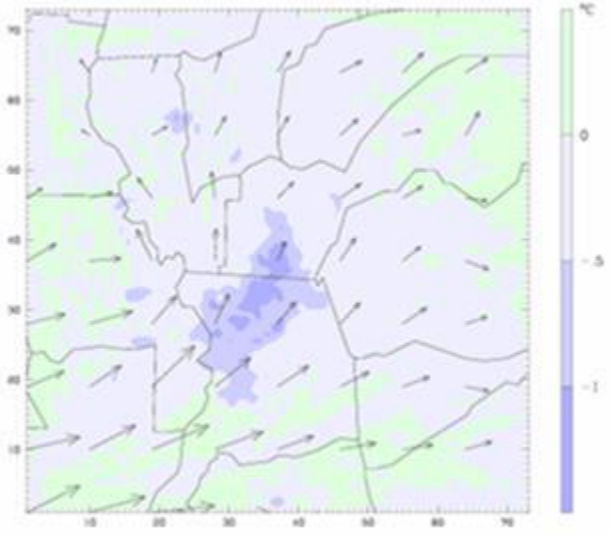

(SUMMER) 1500 PDT, June 4th, 2013

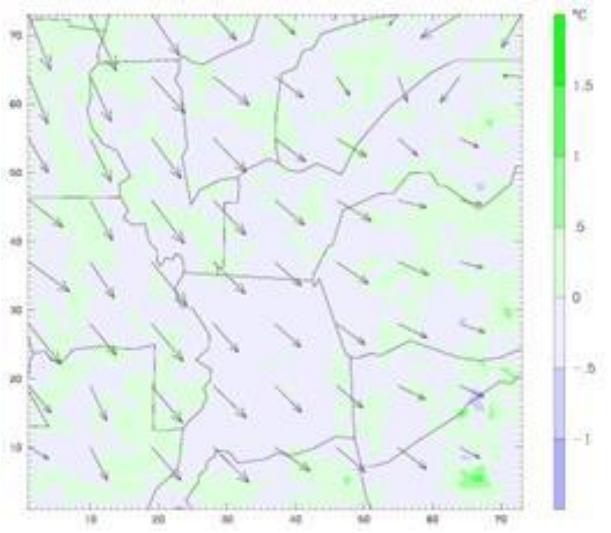

(WINTER) 1500 PST, January 31st, 2016

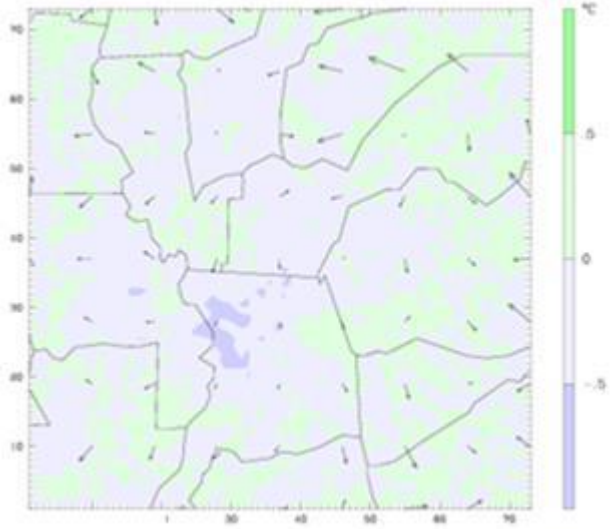

(WINTER) 1300 PST, January 28th, 2016

5.8 COOLING EFFECTS AND WIND: ESTIMATION OF A LENGTH SCALE

Taha (2017) defined four levels of the UHII for characterization, quantification, and modeling, as discussed in Section 1 and shown graphically in Figure 1-1. The third level (Level 3) involves defining a community's "responsibility" for its local UHII, i.e., how much heat is locally generated versus transported from upwind sources. Hence there is interest in estimating a length scale for urban heat transport. Such length scale is also of relevance in the selection of UHI reference points and locating them outside of urban heat plumes (as introduced in Section 5.3).

Thus, in this study, a modeling exercise was undertaken to characterize the fetch or length scale of a reverse effect, i.e., cooling effects from a mitigation measure. A "reverse" Level-3 length scale is an indicator to the impacts of an urban area on a downwind location. As expected, this depends on the level of surface modification, weather conditions, wind speed and direction, the upwind distance over which an air parcel travels over hot or cooled surfaces, and the desired downwind temperature threshold or lifetime, i.e., how large the temperature reduction is relative to an original upwind value, Δ_o, by the time it reaches the downwind point of interest.

To establish a downwind temperature-change threshold, several metrics could be used, for example, e-folding ($1/e\ \Delta_o$) or half lifetime ($\frac{1}{2}\ \Delta_o$), or some other measure. In this discussion, a temperature-reduction half-lifetime ($\frac{1}{2}\ \Delta_o$) is presented, meaning the time or distance downwind where temperature reduction reaches half of the original temperature depression (Δ_o) at the edge of the urban area.

Figure 5-14 shows an example from this analysis for 2-m AGL temperature difference corresponding to case10 at different time intervals. These are results from Altostratus Inc.'s AREAMOD / WRF modeling approach. The sample hours in this figure were selected to show different wind patterns and directions for demonstration purposes. The cool-air plumes are shown for the coincident wind directions in the domain (depicted in the upper-left part of each figure).

The small circles are the grid cells where albedo was actually modified (the darker the circle, the larger the albedo increase, per legend on each figure). The shades of blue are the changes in air temperature (per legend) – the darker blue means larger cooling. As can be seen, there are areas that have become cooler even though no changes in albedo were applied at those locations. Thus, these are areas affected by the transport of cooler air from the modified grid cells.

Averaging over the wind speed range (per each direction), temperature reduction, and albedo change (in this example), the half-lifetime for temperature reduction was found at 2 to 4 km downwind (the "average" qualifier is important to note here, as the fetch can be longer under certain conditions). In other words, for the current-climate summer conditions studied in this effort (MJJAS 2013-2016), an air mass cooled by flowing over an urban area where mitigation measures have been implemented can retain half of its cooling by the time it reaches 2 to 4 km downwind from the edge of the urban area (where temperature depression = Δ_o). The reverse is also true for warming of an air parcel flowing over a hot urban area.

Figure 5-14: Length scales associated with cooling from increased albedo for case10. Examples provided for several time intervals with different flow patterns.

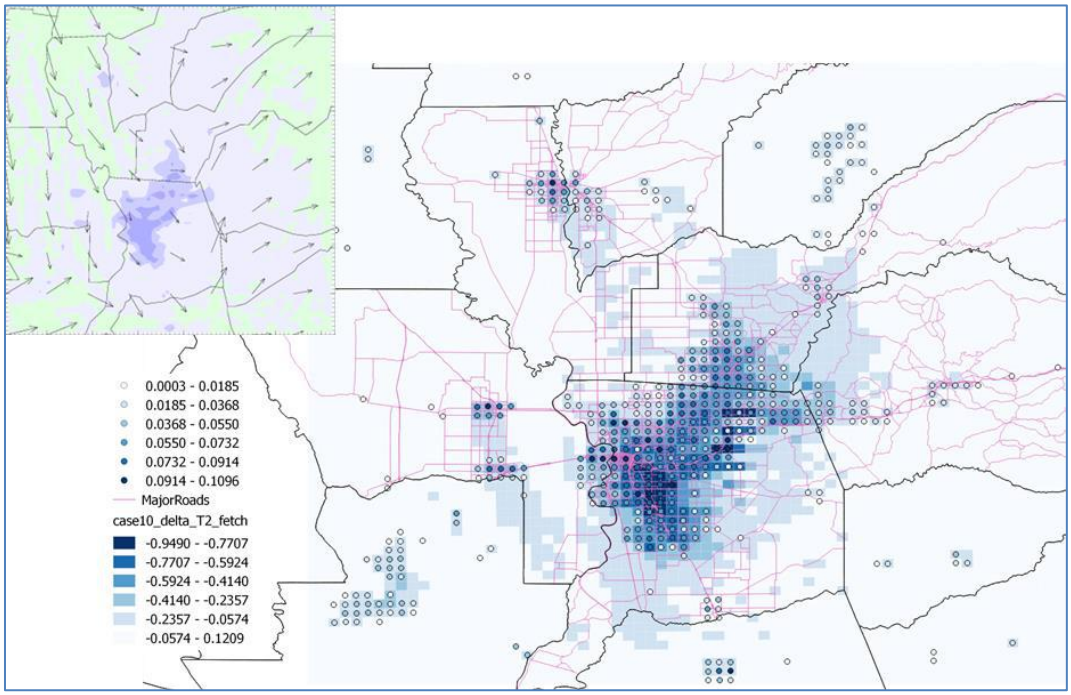

1400 PDT, June 1st, 2013

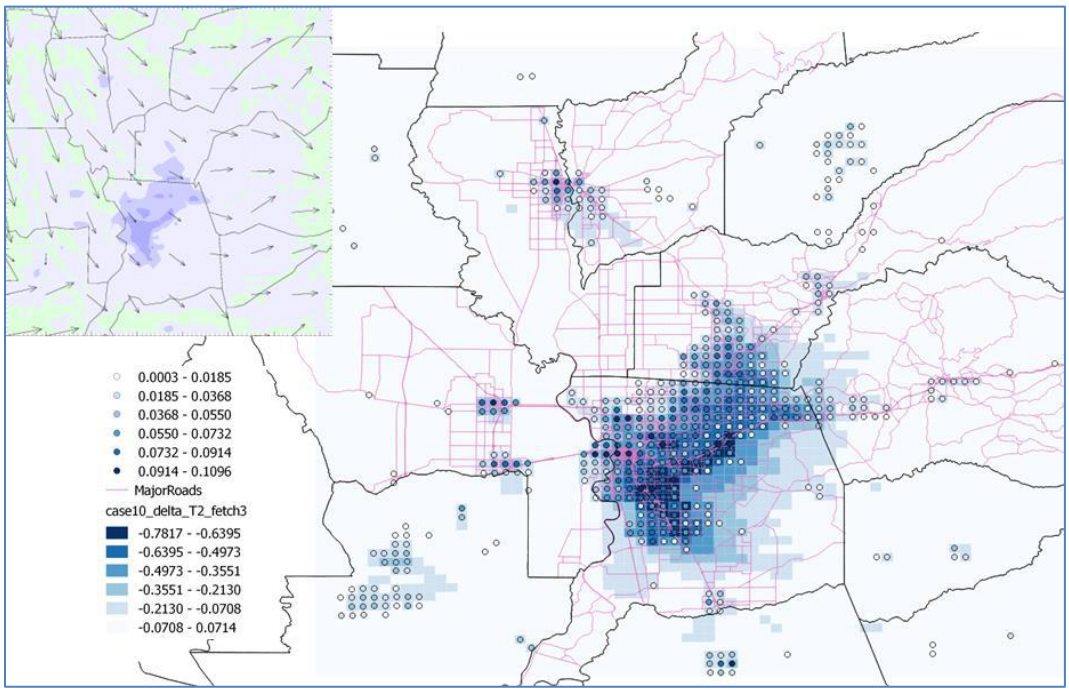

1200 PDT, June 3rd, 2013

Figure 5-14, continued.

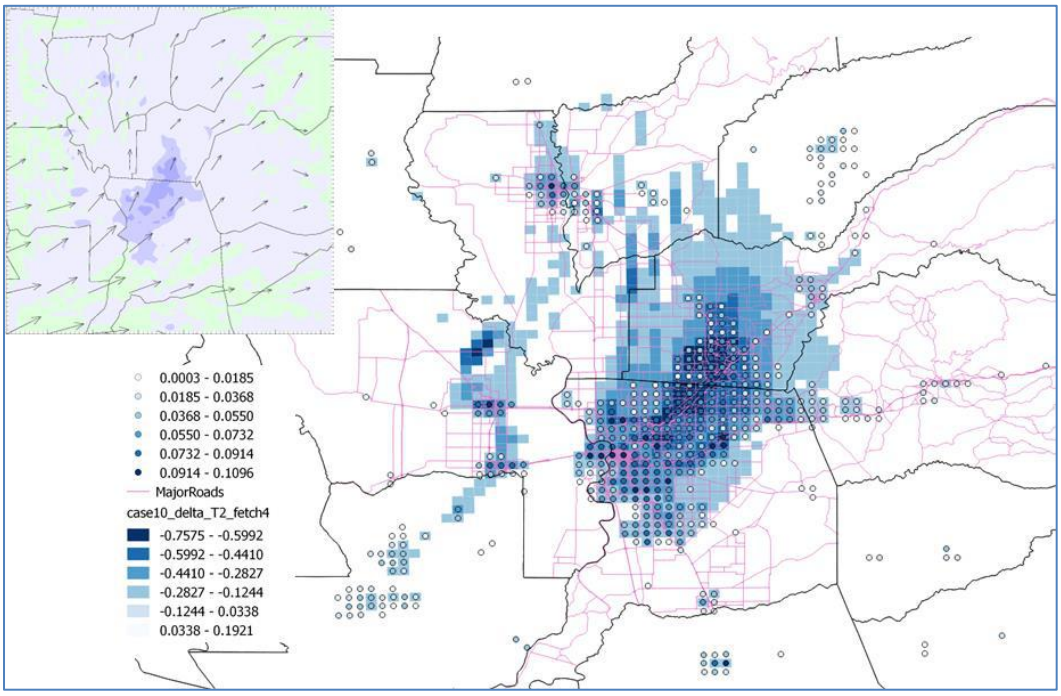

1500 PDT, June 4th, 2013

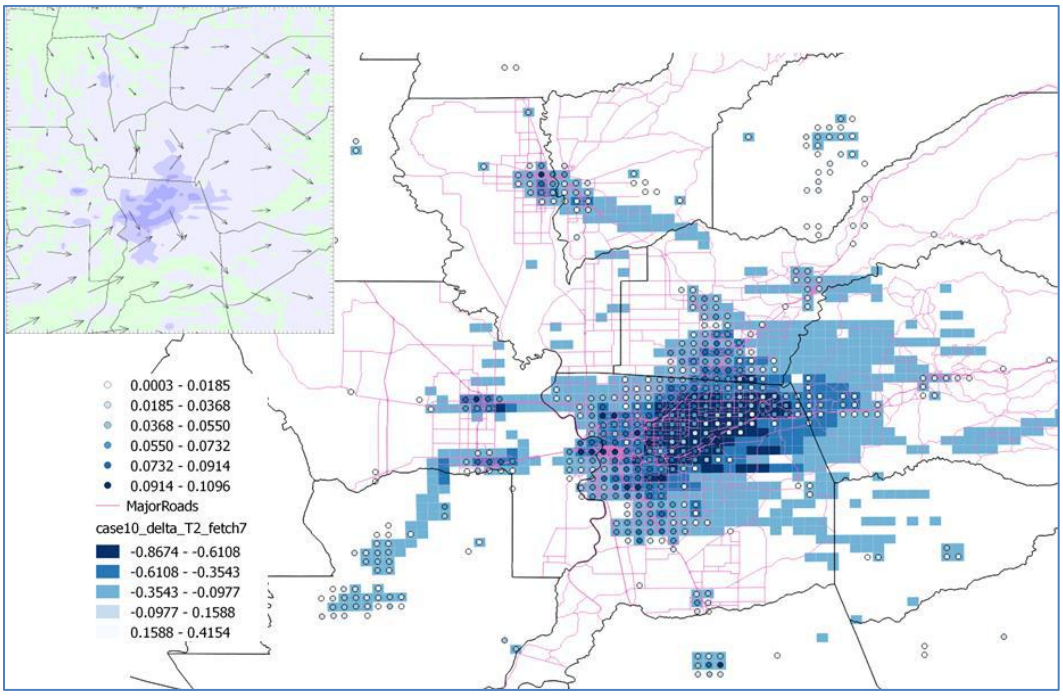

1500 PDT, June 6th, 2013

Figure 5-14, continued.

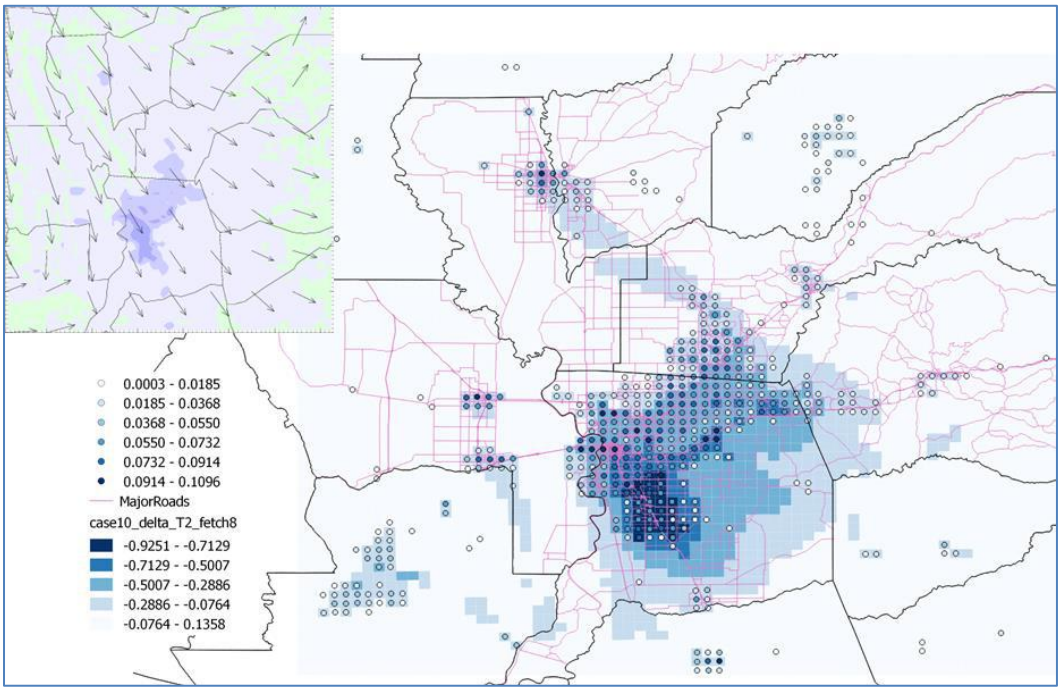

1300 PDT, June 7th, 2013

5.9 METRICS AND THRESHOLDS

To provide an assessment of the urban-heat mitigation potentials of various measures, several metrics and thresholds were defined in consultation with the SMAQMD, LGC, and project TAC:

Metrics at the 2-km level: all hours, all months (MJJAS), all years (2013-2016):

- Instantaneous, 4-dimensional, hourly analysis
- 0600 PDT average 2-km temperature (~minimum temperature)
- 0600 PDT 2-km UHII
- 1300 PDT average 2-km temperature (~solar noon)
- 1400-to-2000 PDT average 2-km temperature
- 1500 PDT average 2-km temperature (~peak temperatures)
- 1500 PDT 2-km UHII
- All-hours 2-km UHII
- All-hours average 2-km temperature
- Degree-hours over 35 °C threshold
- Degree-hours over 38 °C threshold
- National Weather Service Heat Index exceedances
- National Weather Service Heat Index time series

Metrics at the 500-m level (specific locations and roadway projects at community scale):

- ≡ Instantaneous, 4-dimensional, hourly analysis
- ≡ 0600 PDT (daily minima)
- ≡ 1300 PDT (daily peaks)
- ≡ 1500 PDT (daily peaks)
- ≡ All hours / cumulatives
- ≡ 0700 PDT (morning commute peak)
- ≡ 1700 PDT (evening commute peak)

5.9.1 Metrics

In this modeling effort, metrics were computed at each model grid cell or station location for (1) base scenarios (for current and future climates / land use) to characterize urban heat and the UHI / UHII, as well as other indicators, and (2) mitigation scenarios (for current and future climates / land use), per each 2-week interval (from May 30th through September 16th of each year). These metrics include the following (in no particular order):

i. Simple averages (non-UHII), non-threshold:

   a. All-hour averages and all-hour degree-hours (*DH*).
   b. Peak temperature averages (hours between 1400 and 1800 PDT; and 1400 – 2000 PDT, of interest to area utilities).
   c. Daily minimum temperature averages, e.g., at 0600 PDT.

ii. Thresholds-based, non-UHII cumulatives, DH_{TH}:

   Degree-hours (per specified intervals) computed when urban air temperatures exceed certain predefined static or dynamic temperature threshold, *TH* (this is not a UHII).

iii. Level-3 UHII:

   Based on the UHI signal from (i and ii) above, develop a Level-3 UHII estimate. Or, conversely, based on the impacts of mitigation measures (i.e., cooling signal), develop a "reverse" Level-3 UHII as discussed, above, in Section 5.8. Either way, the goal is to characterize the length scale of interest in urban areas within the 6-counties region, so that the UHI / UHII reference points can be selected outside of the heat plume's influence (as was discussed in Section 5.3).

iv. UHI Index (UHII), non-threshold:

   a. All hours UHII (see *UHII; UHII_b* in equations 5-4 and 5-5).
   b. Peaks (see *UHII_d* in equation 5-7), for 1400 – 1800 PDT; through 2000 PDT for utilities.
   c. Minima (see *UHII_d* in equations below) for 0600 PDT.

v. Thresholds-based UHII:

Regardless of date/interval or time of day, this threshold-based UHII (*UHII_c* in Equation 5-6) is computed for each hour the urban air temperature exceeds a certain threshold.

Note that in Equation 5-6 we compute the metrics when urban air temperature is higher than the specified threshold, regardless of whether or not the rural reference temperatures are below or above the threshold. The Cal/EPA proposed an equation where the threshold applied to both urban and non-urban temperatures (which is a more stringent criterion), here, we apply it only to urban temperature because we'd want to quantify the potential for cooling urban areas (i.e., to make them as cool as possible) during a heat event or when temperature is above a certain threshold.

vi. National Weather Service Heat Index (*HI*)

This is defined with Equation 5-8 and the subsequent calculations in Equation 5-9. In addition to computing changes in *HI* with Equation 5-8, the potential "shift down" from one *HI* warning level to a lower one (per NWS– see Figure 5-15) will be assessed and used to demonstrate potential benefits from UHI mitigation techniques, e.g., shifting the *HI* down from "Extreme Danger" to "Danger" level, or from "Danger" to "Extreme Caution". Note that Figure 5-15 is a variant of the *HI* -- it was developed for areas that are generally hot but with relatively lower humidity, which is suitable for the Capital Region.

Note: the NWS Experimental *HeatRisk* index was not used in this study since it relies on climatology (e.g., temperatures from 1985 to 2015) and thus will require an additional, extensive level of effort to produce (climatological analysis is not part of this study). Thus, the NWS *HI* is used instead (practically, the main difference between *HeatRisk* and *HI* is that the former has a climatology context added to it).

Equation 5-4 represents the form used in computing the Level-1 UHI Index (UHII) for the state of California that was developed for Cal/EPA (Taha 2017) to satisfy AB 296 requirements in that the index captured both the *severity* (magnitude) and *extent* (duration) of the urban-nonurban temperature differential. In the following equations, $T_{u(k),h}$ is the urban temperature at time step (hour) *h*, $T_{nu(k),h}$ is the nonurban temperature at time-step *h*, and *H* is the number of time-steps, in this case, the number of hours in the period MJJAS of a given year, or *int#* (interval) per year. Here, *k* is a location index representing a pair of points, one urban and one reference, that is, *u(k)* is the urban point of the pair *k*, and *nu(k)* is the non-urban, reference point of the pair *k*. Note that there is no temperature threshold associated with the UHII definition in Equation 5-4.

In Equation 5-6 the threshold temperature is denoted as $T_{TH,h}$ indicating a dynamic, time-dependent threshold. If the threshold is static (constant across all hours), then the threshold temperature will simply reduce to T_{TH}.

$$UHII = \sum_{h=1}^{H(JJA)} \left[T_{u(k),h} - min\left(T_{u(k),h}, T_{nu(k),h}\right)\right] \qquad (5-4)$$

$$UHII\_b = \sum_{h=1}^{H(int\#)} \left[T_{u(k),h} - T_{nu(k),h}\right] \qquad (5-5)$$

$$UHII\_c = \begin{cases} \sum_{h=1}^{H(int\#)} \left[T_{u(k),h} - T_{nu(k),h}\right], & T_{u(k),h} > T_{TH,h} \\ 0, & T_{u(k),h} \leq T_{TH,h} \end{cases} \qquad (5-6)$$

$$UHII\_d = \sum_{h=1}^{H(int\#)} \left[T_{u(k),h} - T_{nu(k),h}\right], \quad H_{start} \leq h \leq H_{end} \qquad (5-7)$$

Per NWS Technical Attachment (SR 90-23) the Heat Index (*HI*) is given by Equation 5-8, where *T* is temperature in °F and *H* is relative humidity (%):

$$HI = -42.379 + 2.04901523\,T + 10.14333127\,H - .22475541\,T\,H - .00683783\,T^2 - .05481717\,H^2 + .00122874\,T^2\,H + .00085282\,T\,H^2 - .00000199\,T^2\,H^2 \qquad (5-8)$$

Thus, if we partially differentiate *HI* with respect to temperature (*T*), we obtain (per Taha 2015):

$$\frac{\partial HI}{\partial T} = c_2 - c_4\,H - 2c_5\,T + 2c_7\,T\,H + c_8\,H^2 - 2c_9\,T\,H^2 \qquad (5-9)$$

where c_2=2.04901, c_4=0.224755, c_5=0.006837, c_7=0.001228, c_8=0.000852, and c_9=0.00000199, and where *HI* and *T* are in degree °F, in this case, and *H* (relative humidity) is in percent. Thus for example, during relatively mild heat conditions, e.g., 85°F (29.4°C) and 40% relative humidity, $\partial HI/\partial T$ from equation (5-9) is 1.06°F °F^{-1} (1.9°F °C^{-1}) whereas during a relatively more severe

heat episode, say 94°F (34.4°C) and 70% relative humidity, $\partial HI/\partial T$ is 3.53°F °F^{-1} (6.4°F °C^{-1}), showing the relatively different influence of a one degree change in temperature in different weather conditions. This type of dependence was used in this study to evaluate the potential of mitigation measures in alleviating heat stress.

Note that the NWS HI is the only instance in this study and report where degrees F are used. Otherwise, the entirety of the report uses SI units and ºC.

Figure 5-15 shows the NWS Heat Index warning levels developed for areas with generally high temperatures but relatively lower humidity, which is suitable for the Capital Region. In this project, this information was used to evaluate the potential of cooling measures in "shifting down" the HI from one warning level to a lower one.

5.9.2 Thresholds

The following temperature thresholds were used in this analysis and in conjunction with the metrics defined above:

i. 35 °C (95 °F) for DH_{TH}
ii. 38.3 °C (101 °F) for DH_{TH}, per SMUD (extreme heat days)
iii. 35 °C (95 °F) for equation 5-6 (for static T_{TH})
iv. NWS HI 95 °F + humidity (for equations 5-8 and 5-9)
v. NWS HI 105-110 °F exceeded for at least two consecutive days, which is the definition of a heat wave.

Figure 5-15: NWS HI for hot areas with lower humidity. Source: https://www.wrh.noaa.gov/psr/general/safety/heat/heatindex.png

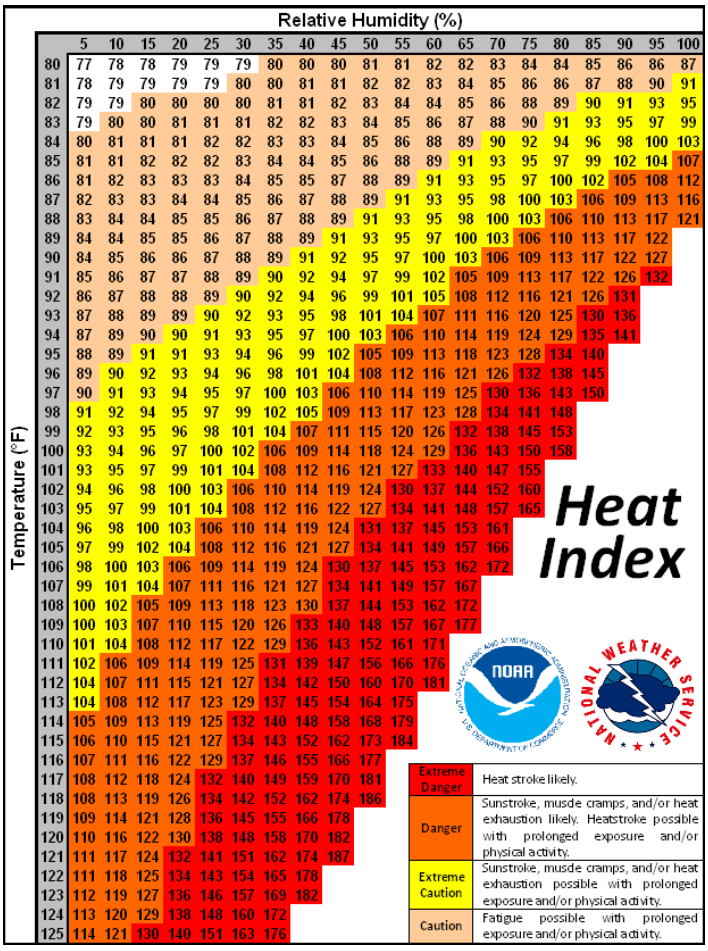

5.10 EFFECTS OF MITIGATION MEASURES IN CURRENT CLIMATES AND LAND USE: INSTANTANEOUS TEMPERATURE DIFFERENCES

To begin the presentation of effects from various mitigation measures, a brief snapshot from the temperature-difference field is provided as an introduction. The examples for a random hour from the studied periods are provided here to help formulate a general idea as to the spatial characteristics of the changes in the temperature field in the Capital region. This is a general sketch of the extent, geographical locations, and levels of changes in temperature that can be expected in the region as a result of implementing UHI-mitigation measures.

Thus, in Figure 5-16, the instantaneous temperature impacts of five mitigation measures are presented for the scenarios defined earlier in Section 5.5 and for a random hour at 1300 PDT, July 28, 2015. These temperature perturbations result from cases 01, 02, 10, 20, and 31.

At this snapshot hour, the temperature reductions reach up to 0.7, 1.4, 1.5, 2.4, and 3.9 °C, respectively, for the measures and scenarios listed above. The spatial pattern of these reductions follows the urban boundaries as well as the downwind transport of cool air, as discussed in Section 5.8. The magnitude of cooling increases with built-up density and the size of the urban area being modified. Of note, the mitigation measures can also cause some warming, generally downwind of the modified urban areas. However, the warming is small compared to the cooling effect both in magnitude and the size of the areas affected.

Furthermore, different measures produce different spatial patterns of cooling. For example, vegetation canopy measures (case01 and case02) produce an effect that is somewhat spatially uniform across the affected urban areas (first two graphs), whereas the albedo measures (case10 and case20, second two graphs in Figure 5-16) produce some more distinguishable or spatially differentiated patterns in the cooling effect. It can be seen, for example, that the American River and surrounding areas (the lighter-colored curved pattern in the middle of the Sacramento region) do not get as much cooling in the albedo scenarios because of the relatively smaller built-up fraction in those areas (i.e., less roofs and paved surface available for modification). Compare the second two graphs in this figure with the impervious fraction characterized earlier in Figures 2-10.C and 2-10.D (in Section 2.3.3).

Figure 5-16**:** Instantaneous differences in air temperature at a random hour and date for five different mitigation scenarios in the 6-counties Capital region. The temperature differences (del01 through del31) were defined in Section 5.5.

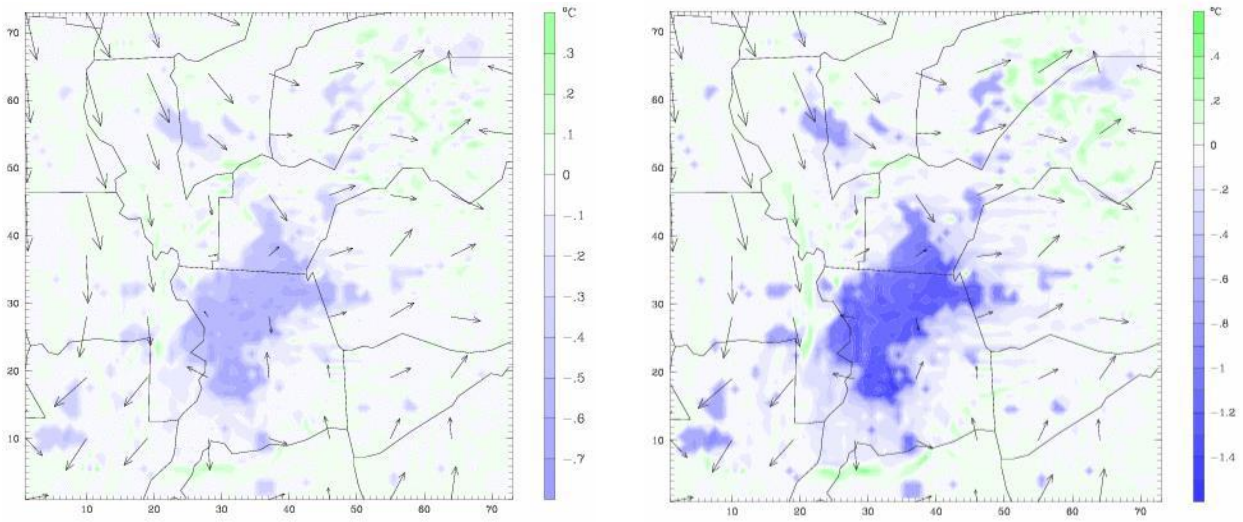

Left: del01:1300 PDT, July 28, 2015, horizontal wind vector (base) at 2 m AGL, maximum change at this hour: -0.7 °C. Right: same but for del02, maximum change at this hour: -1.4 °C.

Figure 5-16, continued.

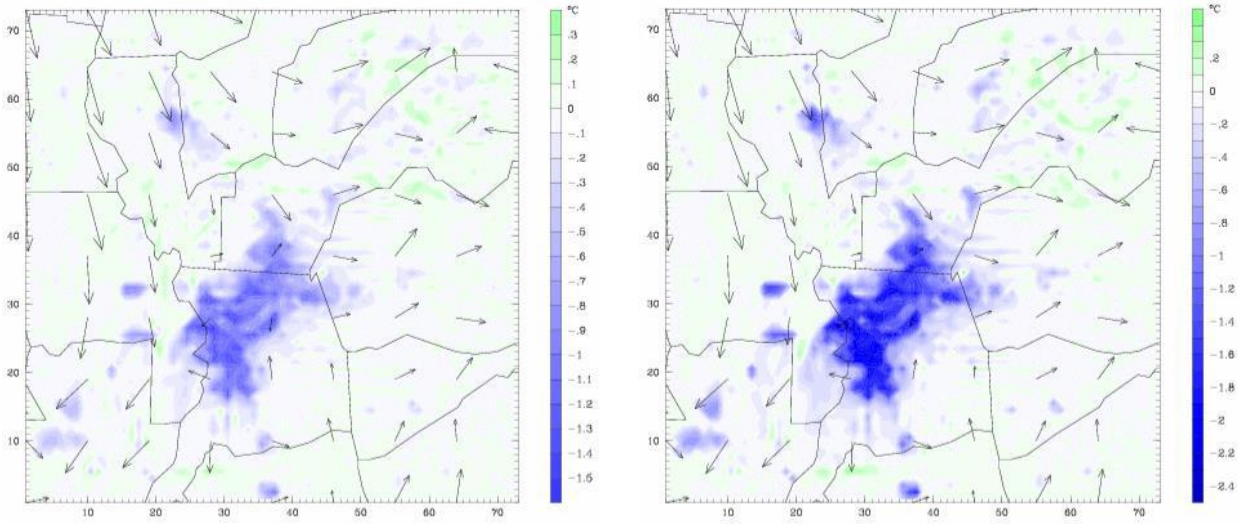

Left: del10: 1300 PDT, July 28, 2015, horizontal wind vector (base) at 2 m AGL, maximum change at this hour: -1.5 °C. Right: same but for del20, maximum change at this hour: -2.4 °C.

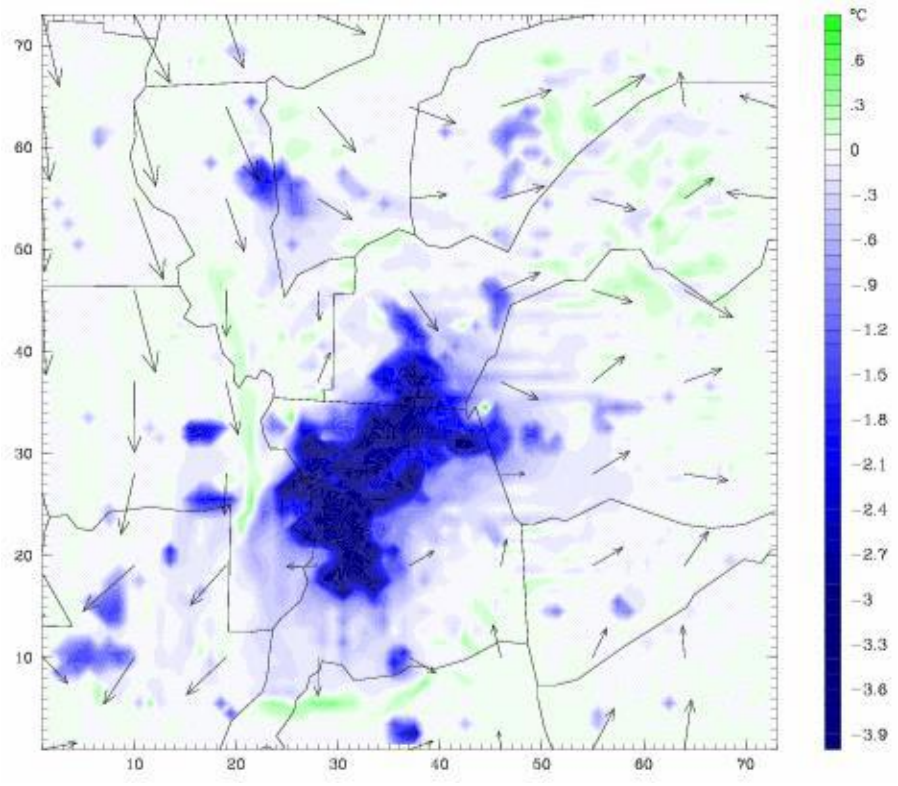

del31:1300 PDT, July 28, 2015, horizontal wind vector (base) at 2 m AGL, maximum change at this hour: -3.9 °C.